

Characterisation of a cyanobacterial nickel sensor and a thermodynamic model of metal sensing

Andrew William Foster, M. Chem.

Thesis submitted for the degree of Doctor of Philosophy

Newcastle University

Faculty of Medical Sciences

Institute for Cell and Molecular Biosciences

May 2013

Memorandum

Parts of this work have been published as:

Foster A. W., Patterson C. J., Pernil R., Hess C. R. & Robinson N. J. (2012) Cytosolic Ni(II) sensor in cyanobacterium: Nickel detection follows nickel affinity across four families of metal sensors. *J. Biol. Chem.* 287: 12142-12151.

Patterson C. J., Pernil R., Dainty S. J., Chakrabarti B., Henry C. E., Money V. A., Foster A. W. & Robinson N. J. (2013) Co(II)-detection does not follow $K_{\text{Co(II)}}$ gradient: Channeling in Co(II)-sensing. *Metallomics*. 5: 352-362.

Additional manuscripts are in preparation.

During the course of these studies the author has additionally contributed to:

Foster A. W. & Robinson N. J. (2011) Promiscuity and preferences of metallothioneins: the cell rules. *BMC Biol.* 9: 25.

Totley S., Patterson C. J., Banci L., Bertini I., Felli I. C., Pavelkova A., Dainty S. J., Pernil R., Waldron K. J., Foster A. W. & Robinson N. J. (2012) A cyanobacterial metallochaperone inhibits deleterious side effects of copper. *Proc. Natl. Acad. Sci. USA*. 109: 95-100.

Declaration

No portion of this work has been submitted in support of an application for another degree or qualification from this or any other University or institute of learning.

Acknowledgements

I would like to thank Professor Nigel Robinson for supervision and support throughout the course of these studies as well as other members of the Robinson group for support, advice and expertise. In particular I would like to thank Dr. Rafael Pernil whose *in vivo* studies of metal homeostasis in *Synechocystis* enabled a deeper understanding of the data presented here, Dr. Carl Patterson for labourious production of CoaR and both Dr. Carl Patterson & Dr. Kevin Waldron for helpful discussions and for providing training.

Abstract

The product of *Synechocystis* PCC 6803 open reading frame *slr0176*, InrS (Internal nickel responsive Sensor) a member of the CsoR-RcnR metalloregulatory family, has been characterised in the course of this work and found to regulate the expression of *nrsD*, encoding a nickel export protein, in a nickel dependent manner. InrS occludes a previously unidentified cryptic promoter in a nickel resistance operon.

In addition to Ni(II) InrS is also competent to bind and respond to Zn(II), Co(II) Cu(II) and Cu(I) *in vitro* as determined by metal binding studies & fluorescence anisotropy. The factors that favour a response to nickel but disfavour responses to zinc and copper *in vivo* have been explored including determining allosteric coupling free energies of Ni(II) and Cu(I) binding. The cognate and non-cognate metal binding affinities of InrS, ZiaR (zinc-sensing SmtB family member), Zur (zinc-sensing Fur family member) and CoaR (cobalt-sensing MerR family) have been determined through competition with a range of metal chelators and infer that selective sensing of zinc and nickel can be dictated by the relative affinities of the metalloregulators but selective cobalt sensing cannot.

The primary metal coordination sphere of InrS has been investigated through a combination of site directed mutagenesis and metal binding studies. Three of four Ni(II) ligands constituting the square planar Ni(II) site have been identified and mutant variants with weakened Ni(II) affinities produced. InrS displays metal binding properties characteristic of the copper sensing sub-branch of this protein family thought to be a consequence of the primary coordination sphere. Results of this work have been used to refine predictions as to the metal(s) sensed by uncharacterised members of this protein family based on the predicted secondary rather than primary coordination sphere. An alternative allosteric network involving a secondary coordination sphere hydrogen bond in nickel sensing CsoR-RcnRs is proposed.

Contents

Memorandum	ii
Acknowledgements	iii
Abstract	iv
Contents	v
Abbreviations	xii
1 Introduction	1
1.1 Biological requirement for metal ions	1
1.2 The challenge of correct protein-metal speciation	2
1.3 Kinetic and thermodynamic control of metal ion availability	3
1.4 Prokaryotic cytosolic metalloregulators	5
1.5 CsoR-RcnR family	6
1.5.1 Discovery of a novel family of metalloregulators	6
1.5.2 Protein assembly, structure and DNA interaction	8
1.5.3 Metal coordination sphere	11
1.5.4 Allosteric linkage of metal binding to DNA dissociation	12
1.5.5 Selectivity in CsoR-RcnR family proteins	14
1.5.6 CsoR-RcnR homologues that do not sense metal stress	15
1.6 ArsR-SmtB family	16
1.6.1 Variety of metal binding motifs on a common scaffold	19
1.6.2 Allosteric linkage of metal binding to DNA dissociation	20
1.6.3 Selectivity of metal sensing in the ArsR-SmtB family	22
1.7 MerR family	24
1.7.1 Selectivity in the MerR family	25

1.8	Fur family	29
1.8.1	Metal binding sites of Fur proteins	29
1.8.2	Regulatory mechanisms of Fur proteins	32
1.8.3	Zur, a zinc sensing member of the Fur family	33
1.8.4	Fur homologues that sense other metals/ non-metal signals	34
1.8.5	Selectivity of metal sensing in Fur family proteins	35
1.9	Other metalloregulatory families	36
1.10	<i>Synechocystis</i> sp. PCC 6803 as a model organism for studying metalloregulation	37
1.10.1	The metal requirements of <i>Synechocystis</i>	37
1.10.2	Metalloregulation in <i>Synechocystis</i>	40
1.11	Project aims	42
2	Methods and materials	46
2.1	Reagents and chemicals	46
2.2	Maintenance of bacterial strains	46
2.2.1	Bacterial strains and growth conditions	46
2.2.2	Production of competent cells	46
2.2.3	Transformation of competent cells to antibiotic resistance	47
2.3	DNA manipulation	47
2.3.1	Amplification of DNA by polymerase chain reaction	47
2.3.2	3'-A tailing of PCR products	51
2.3.3	Agarose gel electrophoresis	51
2.3.4	Ligation of PCR fragments into pGEM-T	51

2.3.5	Identification of transformant cells by blue/ white screening and colony PCR	52
2.3.6	Isolation of plasmid DNA	52
2.3.7	Site directed mutagenesis using the ‘Quikchange’ method	54
2.4	Protein manipulation	54
2.4.1	Overexpression of InrS, InrS mutants, ZiaR and Zur	54
2.4.2	SDS-PAGE analysis	55
2.4.3	Purification of recombinant InrS and mutant variants	55
2.4.4	Purification of recombinant ZiaR	56
2.4.5	Purification of recombinant Zur	56
2.4.6	Quantification of protein stocks	57
2.5	Anaerobic manipulation of proteins	58
2.5.1	Production of O ₂ free chelex treated buffers	58
2.5.2	Production of anaerobic protein samples	58
2.5.3	Quantification of reduced thiol content of anaerobic protein stocks	58
2.5.4	Measurement of the residual metal content of anaerobic protein stocks	59
2.6	Experimental procedures	59
2.6.1	Preparation of metal stocks	59
2.6.2	UV-visible spectroscopy	60
2.6.3	Fractionation of protein-metal complexes by size-exclusion chromatography	60
2.6.4	Analysis of DNA binding by Electrophoretic mobility shift assays	60
2.6.5	Analysis of InrS-DNA stoichiometry by size exclusion chromatography	62

2.6.6	Analysis of DNA binding by fluorescence anisotropy	62
2.6.7	Measurement of the metal binding affinities of InrS, ZiaR, Zur and CoaR	63
2.6.8	Monitoring quenching of intrinsic protein fluorescence upon metal binding	67
2.6.9	Inter-protein nickel exchange	67
2.6.10	Circular dichroism spectroscopy	67
2.7	Bioinformatics	68
3	Identification and functional assignment of InrS: A protein of the CsoR-RcnR metalloregulator family controlling nickel export to the periplasm	70
3.1	Bioinformatic analysis of InrS	70
3.2	Purification of recombinant InrS	73
3.3	Analysis of the metal binding properties of InrS	77
3.3.1	Ni(II) and Cu(II) binding properties	77
3.3.2	Co(II) binding properties	83
3.3.3	Cu(I) binding properties	88
3.4	Identification of the InrS DNA-binding site by EMSA	91
3.4.1	Targets whose promoter regions contain similarity to the <i>B. subtilis</i> CsoR DNA recognition site	92
3.4.2	Targets known to be copper regulated	105
3.4.3	Targets whose promoter regions contain similarity to the <i>E. coli</i> RcnR DNA recognition site	109
3.4.4	Targets whose promoter regions contain similarity to the CsoR consensus sequence	113
3.5	<i>In vivo</i> analysis of the role of InrS	122

3.6	Phenotypic analysis of $\Delta inrS$	124
4	Further characterisation of the DNA- and cognate metal-binding properties of InrS	126
4.1	InrS DNA interactions	126
4.1.1	InrS-DNA stoichiometry	128
4.1.2	Studying InrS-DNA interactions by fluorescence anisotropy	131
4.2	Cognate metal binding affinity of InrS	134
4.2.1	Determination of the Ni(II) affinity of InrS	134
4.2.2	Determination of the Co(II) affinity of InrS	140
4.3	Identification of residues required for Ni(II) and Co(II) binding to InrS	145
4.3.1	Ni(II) coordinating cysteine residues	146
4.3.2	Metal and DNA binding properties of InrS Cys53→Ala	149
4.3.3	Metal and DNA binding properties of InrS Cys82→Ala	152
4.3.4	Metal and DNA binding properties of InrS His78→Leu	158
4.3.5	Metal and DNA binding properties of InrS His21 mutant variants	163
5	Contributions of affinity, access and allostery in favour of cognate and against non-cognate metal selectivity of InrS	172
5.1	Affinity and relative affinity	172
5.2	Purification of recombinant ZiaR, Zur and CoaR	173
5.3	Relative Ni(II) affinities of the metalloregulators of <i>Synechocystis</i>	176
5.3.1	Determination of the Ni(II) affinities of ZiaR, Zur and CoaR	176
5.3.2	Confirmation of the relative Ni(II) affinity hierarchy of the metalloregulators of <i>Synechocystis</i>	185
5.4	Relative Co(II) affinities of the metalloregulators of <i>Synechocystis</i>	189
5.5	Allosteric response of InrS to non <i>in vivo</i> effector metals	195

5.5.1	Disruption of InrS-DNA complexes by non-cognate metals	195
5.5.2	Allosteric coupling of InrS metal (Cu(I) or Ni(II)) binding and DNA binding	198
5.6	Relative Zn(II) affinities of the metalloregulators of <i>Synechocystis</i>	201
5.7	Cu(I) affinity of InrS	205
6	Final discussion and future work	210
6.1	InrS is a Ni(II) sensing member of the CsoR-RcnR metalloregulatory family that regulates expression of <i>nrsD</i> a deduced major facilitator superfamily protein proposed to mediate Ni(II) export to the periplasm	210
6.2	A model of nickel homeostasis in <i>Synechocystis</i>	211
6.3	The primary and secondary metal coordination spheres of InrS	214
6.3.1	Ni(II) coordination by InrS	214
6.3.2	Co(II) coordination by InrS	217
6.3.3	Allostery in CsoR-RcnR	218
6.4	Biological significance of coordination geometry	225
6.5	Selective Ni(II) and Zn(II) sensing can be explained on the basis of relative affinity and access	228
6.6	Selectivity against Cu(I) sensing by InrS cannot currently be explained by allostery, affinity or access	234
6.7	Prediction of metals sensed by CsoR-RcnR family members on the basis of sequence	235
6.8	Affinities and an associative biology in the cell	236
6.9	Future work	238
6.9.1	Opportunities for further study based on bioinformatics results	238
6.9.2	Controlling the buffered intracellular concentration of metal ions by engineering metalloregulators in order to create useful phenotypes	241

6.9.3 Understanding the metalloregulatory circuits of the cell	243
References	248
Appendix A	292
Appendix B	294
Appendix C	299
Appendix D	305
Appendix E	311

Abbreviations

A	adenine
ABC	ATP binding cassette superfamily
Ala	alanine
Arg	arginine
ATP	adenosine triphosphate
BCS	bathocuproine disulfonate
BLAST	basic local alignment search tool
bp	base pair
BSA	bovine serum albumin
C	cytosine
CD	circular dichroism
cDNA	complementary DNA
Cys	cysteine
Da	Dalton
dATP	deoxyadenosine triphosphate
dCTP	deoxycytosine triphosphate
DDM	<i>n</i> -dodecyl β -D-maltoside
dGTP	deoxyguanosine triphosphate
DNA	deoxyribonucleic acid
dNTP	deoxynucleotide triphosphate
DTNB	5,5'-dithiobis-(2-nitrobenzoic) acid
DTT	dithiothreitol
dTTP	deoxythymidine triphosphate
DUF	domain of unknown function
EDTA	ethylenediaminetetraacetic acid
EGTA	ethylene glycol tetraacetic acid

ELISA	enzyme-linked immuno-sorbent assay
EMSA	electrophoretic mobility shift assay
EPR	electron paramagnetic resonance
ESI-MS	electrospray ionisation mass spectrometry
EXAFS	extended X-ray absorption fine structure
FNR	fumarate and nitrate reductase
G	guanine
GFP	green fluorescent protein
Glu	glutamic acid
GSH	reduced glutathione
Hepes	4-(2-hydroxyethyl)-1-piperazineethanesulfonic acid
HEX	hexachlorofluorescein
His	histidine
ICP-MS	inductively coupled plasma mass spectrometry
IPTG	isopropyl β -D-1-thiogalactopyranoside
kb	kilobase
LB	Luria-Bertani growth medium
Leu	leucine
LMCT	ligand to metal charge transfer
Lys	lysine
MACiE	mechanism, annotation and classification in enzymes
MALDI-PMF	matrix-assisted laser desorption/ ionisation peptide mass fingerprinting
mf2	mag-fura-2
M_r	molecular weight
MRW	mean residue weight
N	any amino acid
NTA	nitrilotriacetic acid
OD	optical density

OMC	outer membrane channel
ONPG	o-nitrophenyl- β -D-galactoside
ORF	open reading frame
PAGE	polyacrylamide gel electrophoresis
PCR	polymerase chain reaction
Phe	phenylalanine
PMSF	phenylmethanesulfonyl fluoride
RLM-RACE	RNA ligase mediated rapid amplification of cDNA ends
RND	resistance-nodulation-cell division superfamily
r_{obs}	observed anisotropy
rpm	revolutions per minute
RT-PCR	reverse transcriptase polymerase chain reaction
RuBisCO	Ribulose-1,5-bisphosphate carboxylase oxygenase
SDS	sodium dodecyl sulphate
SOD	superoxide dismutase
T	thymine
TBE	tris/ borate/ EDTA buffer system
TCEP	tris(2-carboxyethyl)phosphine
TNB	2-nitro-5-thiobenzoate
tris	tris(hydroxymethyl)aminomethane
Tyr	tyrosine
UV	ultraviolet
V	volt
Val	valine
Vis	visible
v/v	volume to volume
w/v	weight to volume
XANES	X-ray absorption near edge structure

XAS	X-ray absorption spectroscopy
X-gal	5-bromo-4-chloro-indolyl- β -D-galactopyranoside

Chapter 1. Introduction

1.1 Biological requirement for metal ions

The requirement for metal ions across all three domains of life is well established. In addition to the bulk biological elements sodium, potassium, magnesium and calcium all the elements from the first row of the *d*-block with the exception of scandium and titanium are believed to be trace elements essential for bacteria, plants or animals and in some cases all three (Fraústo DaSilva & Williams. 2002). A systematic bioinformatics survey of proteins, for which the structures are known, suggested that almost 50 % of enzymes require a metal cofactor with 41 % requiring the metal ion at the active site (Andreini *et al.* 2008; Waldron *et al.* 2009). Metals have been recruited for catalysis and structural roles on the basis of their chemical properties, fulfilling varied roles such as acid-base catalysis, electron transfer and maintenance of protein structure (Haas & Franz. 2009) and metalloenzymes are represented in all six Enzyme Commission classes (Andreini *et al.* 2008).

The abundance of available metals has changed over the course of evolutionary time leading to the recruitment of newly available metals for emerging functions. The availability of zinc and copper is low in anoxic, reducing environments such as those believed to be found in the Archean ocean but under these conditions iron, manganese and cobalt are enriched (Dupont *et al.* 2010). Following the advent of oxygenic photosynthesis leading to a large increase in atmospheric molecular oxygen $\sim 2.4 \times 10^9$ years ago (great oxidation event) the Proterozoic ocean remained low in available zinc and copper as increased continental weathering and oceanic sulphate reduction meant these metals were locked away in inorganic sulphides. As the oxygen content of the ocean increased and moved to the modern oxic conditions of the ocean today ($\sim 0.8\text{--}0.5 \times 10^9$ years ago) the availability of copper and zinc would have been greatly increased and this shift in metal availability accompanied the evolution of eukaryotic life (the first eukaryotic fossils are dated to $\sim 1.6 \times 10^9$ years ago) (Dupont *et al.* 2010). As such the availability of these metals is reflected by their eukaryotic utilisation and can be observed in the increased usage of zinc and copper in eukaryotes relative to prokaryotes and archaea. A log-log plot of the sum total zinc containing structural domains versus the sum total of structural domains reveals a slope greater than one for eukaryotes and less than one for prokaryotes and archaea (although the total number of metal binding

domains relative to proteome size scales roughly equally across all three superkingdoms (Dupont *et al.* 2010)) revealing the increased usage of this metal in organisms proposed to have evolved as this metal became more readily available (Dupont *et al.* 2006). The gradient of this slope is steeper in multi-cellular eukaryotes relative to single cell eukaryotes consistent with the role of zinc finger proteins in cell differentiation. Newly available metals have also been substituted into pre-existing roles, for example the use of copper containing plastocyanin in photosynthetic electron transport rather than iron containing cytochrome c_6 (Peers & Price. 2006). Following the transition to a modern oxic ocean the availability of iron plummeted as the readily soluble Fe^{2+} form was oxidised to insoluble hydroxides of the Fe^{3+} form (which have a solubility product of 10^{-18} M at pH 7) (Fraústo DaSilva & Williams. 2002). This is again reflected in eukaryotic versus prokaryotic usage of this metal with a significantly greater proportion of total prokaryotic structural domains being iron binding relative to eukaryotes (Dupont *et al.* 2006). The extensive early use of iron by bacteria has created a dependence on iron and indeed it is now recognised that iron restriction constitutes an important defence mechanism of innate immunity (Haley & Skaar. 2012).

1.2 The challenge of correct protein-metal speciation

In addition to the handful of metals that are biologically essential many metals and metalloids have no known biological role and are regarded as toxic, although the discovery of a cadmium-utilising carbonic anhydrase (Lane & Morel. 2000) suggests that biological roles may exist for metal ions traditionally thought of as toxic, especially in extreme habitats. In excess all metal ions are toxic and it is emerging that a common mechanism of this toxicity is the replacement of native metals at the active sites of enzymes, the differing chemistry of the non-native replacement ion often rendering the enzyme inactive (Ranquet *et al.* 2007; Macomber & Imlay. 2009; Macomber *et al.* 2011). The poisoning of enzymes by non-native metals highlights the challenge for the cell in achieving correct protein-metal speciation. Although variations in metal binding site chemistry can help tune the preference of a binding site for a particular metal, for example employing cysteine ligands for thiophilic metals such as Cu(I), these variations can often not overcome the inherent metal binding preference as defined by the Irving-Williams series and it has been demonstrated *in vitro* that many proteins display a binding preference for an incorrect metal over a correct metal. The Irving-Williams

series (equation 1) defines the divalent metal binding preferences of organic ligands, including proteins (Irving & Williams. 1948).



The origins of the series predominantly lie in the increased nuclear charge and decreased ionic radii on moving across the first *d*-block row although there is a sharp peak in the stability of Cu^{2+} due to Jahn-Teller distortion, which does not occur for the d^{10} ion Zn^{2+} (Haas & Franz. 2009). There is debate as to the exact position of zinc on the series, however experimentally zinc has frequently been observed to displace cobalt from protein sites and can so be considered, for practical purposes, to occupy a position above cobalt. Cu^{+} has also been shown to form tight complexes with proteins and is also frequently shown at the top of the series with Cu^{2+} . Thus in a common cytosol different proteins must somehow be selectively co-factored with highly competitive and more weakly competitive metal ions.

1.3 Kinetic and thermodynamic control of metal ion availability

For some metalloproteins there exist specialised delivery proteins known as metallochaperones, which deliver metals via specific protein-protein contacts. As well as delivery of metals to target proteins these metallochaperones can help prevent the deleterious side effects of mis-location of competitive metals such as Cu^{+} (Tottey *et al.* 2012). For the majority of metalloproteins however, no metallochaperones are known and so presumably these proteins acquire their metals from the cellular milieu, acquisition then is presumably largely under thermodynamic rather than kinetic control. A key conceptual observation is that cells limit the buffered or available concentrations of metal ions several orders of magnitude below the total cellular metal quota such that protein sites compete for a limited supply of metals rather than a surplus of metals competing for protein sites (Fraústo DaSilva & Williams. 2002; Robinson. 2007) (Figure 1.1). Under such a regime the relatively subtle variations in protein metal binding sites may be sufficient to select the correct binding partner (Waldron & Robinson. 2009). The intracellular availability of metal ions is controlled through the actions of the proteins of metal homeostasis including importers, exporters and sequestration proteins (Waldron & Robinson. 2009). Additionally organisms can modulate their metabolism to make use of more abundant metals and spare scarce ones (Merchant & Helmann. 2012). In prokaryotes the regulation of genes of metal

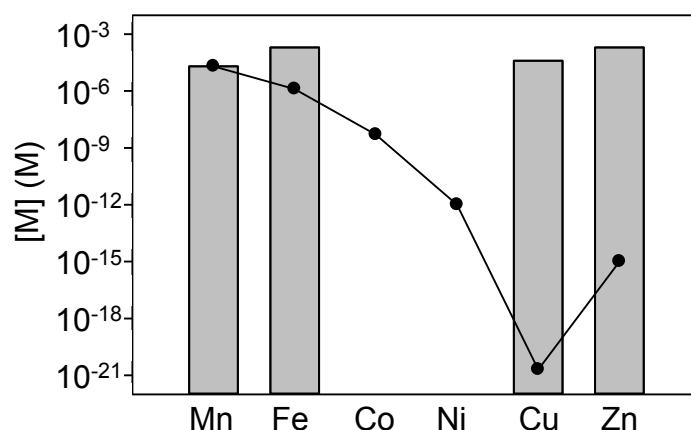


Figure 1.1. Total and predicted buffered levels of transition metal ions in *E. coli*. Total metal concentrations (bars) were taken from Outten & O'Halloran (2001). Total cobalt and nickel contents were reported as below the level of detection and are therefore not shown. The proposed buffered levels (circles) are based on the equilibrium binding affinities of the sensors of each element present in *E. coli* (or *B. subtilis* in the case of MntR where data is unavailable for *E. coli*): MntR (manganese) (Golynskiy *et al.* 2006), Fur (iron) (Mills & Marletta. 2005), RcnR (cobalt) (Iwig *et al.* 2008), NikR (nickel) (Wang *et al.* 2004), CueR (copper) (Changela *et al.* 2003), ZntR and Zur (zinc) (Hitomi *et al.* 2001; Outten & O'Halloran. 2001). The reported Co(II) affinity of RcnR was a minimum estimate (Iwig *et al.* 2008). The buffered level for manganese is set at the same level as the total concentration as the reported Mn(II) affinity of *B. subtilis* MntR is numerically greater than the total manganese content of *E. coli*. This may reflect a greater buffered concentration of manganese in *B. subtilis* relative to *E. coli* and indeed there is evidence that the buffered concentration of manganese in *B. subtilis* may be high (Guedon & Helmann. 2003).

homeostasis is commonly under the control of cytosolic metal-responsive transcriptional regulators (metalloregulators) although alternative mechanisms exist such as the use of two-component sensors and alternative sigma factors (Hobman *et al.* 2007). Cytosolic metallorepressors are considered as one of the most important factors in controlling correct metal speciation within a cell as they control the expression of the other genes of metal homeostasis (which likely in turn coordinates the intracellular availability of metal ions, although this remains to be formally tested) and have been referred to as the ‘arbiters of metal sufficiency’ (Helmann *et al.* 2007).

Metallorepressors (also known as metal sensor proteins) are subject to the same limitations imposed by the Irving-Williams series as other proteins, so how do they selectively sense and respond to their cognate metals? It has been proposed that a combination of allostery, affinity and access (Totterdell *et al.* 2005) control the selective responses of metallorepressors and examples of these concepts are given throughout the following discussion of the various metallorepressor families.

1.4 Prokaryotic cytosolic metallorepressors

Seven major structural families of prokaryotic cytosolic metallorepressors have been identified to date and the majority of prokaryotic genomes encode some complement of these proteins (Ma *et al.* 2009c). In addition to these major families there exist examples of individual, specialised metal sensors such as the molybdenum uptake regulator ModE (Anderson *et al.* 1997; McNicholas *et al.* 1997) and the sensor of iron-sulphur cluster status IscR (Schwartz *et al.* 2001). Some members of transcriptional regulator families not primarily involved in metal sensing function as metallorepressors, for example two zinc sensors from *Streptococcus pneumoniae*, AdcR (Reyes-Caballero *et al.* 2010) and SczA (Kloosterman *et al.* 2007), are members of the MarR and TetR family respectively.

The seven major families of metallorepressors can be arranged into three groups based on broad mode of action similarities. The ArsR-SmtB, CsoR-RcnR and CopY families function as metal-dependent de-repressors and have a weakened affinity for DNA in the metal bound state. The Fur, NikR and DtxR families function as metal-dependent co-repressors exhibiting an increased affinity for DNA in the metal bound state. Finally, the MerR family of proteins function as metal dependent activators of gene expression. These proteins maintain a high DNA binding affinity in both the apo- and metal-bound

states (although there is some weakening of DNA affinity upon metal binding (Parkhill *et al.* 1993)). Conformational changes upon metal binding cause a rearrangement of the local structure of DNA to which the protein is bound converting a sub-optimal promoter to an optimal one.

1.5 CsoR-RcnR family

1.5.1 Discovery of a novel family of metalloregulators

The CsoR-RcnR family represents the most recently discovered family of prokaryotic metalloregulators. RcnR was originally identified via a bioinformatics approach to find the regulator of the nickel/ cobalt inducible resistance gene *E. coli rcnA* (Iwig *et al.* 2006), identified in an earlier study (Rodrique *et al.* 2005). *rcnR* is divergently transcribed from *rcnA* and a BLAST search revealed that homologues are widespread across the prokaryotic kingdom with 51 % of identified homologues being located next to genes encoding putative metal export proteins (Iwig *et al.* 2006). RcnR was confirmed as the nickel/ cobalt dependent regulator of *rcnA* by a β -galactosidase (*lacZ*) reporter gene assay. Briefly, the promoter region of *rcnA* was fused to *lacZ* such that RcnR controlled the expression of *lacZ*. Efficacy of metals at dissociating the RcnR-DNA interaction could then be followed by the conversion of o-nitrophenyl- β -D-galactoside (ONPG) by LacZ to galactose and o-nitrophenol, which has a yellow colour. When the sixth codon of *rcnR* was mutated to a stop codon constitutive expression from the *rcnA* promoter was observed and the nickel/ cobalt responsiveness of this promoter could be restored by the introduction of a plasmid with constitutive low level expression of *rcnR*. It was later shown that the *rcnA* promoter is unresponsive to manganese, iron, zinc, cadmium and crucially copper, at least *in vivo* (Iwig *et al.* 2008). Direct binding of RcnR to the *rcnA* promoter region was observed by electrophoretic mobility shift assay (EMSA) and this interaction could be inhibited by the addition of nickel or cobalt to the binding reaction (Iwig *et al.* 2006).

The existence of a new metalloregulatory family was confirmed by the discovery and structural characterisation of copper sensing *Mycobacterium tuberculosis* CsoR (Liu *et al.* 2007). The gene encoding CsoR, *rv0967 (csoR)*, is located upstream of the copper responsive gene *rv0969 (ctpV)* thought to encode a copper translocating P-type ATPase (with a gene of unknown function, *rv0968*, separating the two) (Liu *et al.* 2007). These genes were shown to be co-transcribed and show a strong induction by copper and so

the operon was named 'copper sensitive operon' (*cso*). Based on bioinformatics analysis, which showed that the protein contained a conserved domain of unknown function (DUF), DUF156, with strongly conserved cysteine and histidine residues (commonly involved in metal ligation), the authors hypothesised that this gene might encode the copper dependent regulator of the *cso* operon. A segment of DNA encompassing the region upstream of *csoR* through to residue 49 of *ctpV* was cloned and transformed into *Mycobacterium smegmatis*. The coding sequence after residue 49 of *ctpV* was replaced with the coding sequence of green fluorescent protein (GFP). *M. smegmatis* transformed with this DNA sequence exhibited strong induction of fluorescence in the presence of exogenous copper and this induction was lost when cysteine 36 (later shown to be a Cu(I) ligand) was mutated to the non-coordinating alanine (Liu *et al.* 2007). Negligible induction was observed with maximum permissive concentrations of other metal ions including nickel and cobalt.

Direct binding of CsoR to the promoter region of *csoR* was observed by EMSA and CsoR was demonstrated to bind specifically to the 28 bp pseudo-palindromic sequence (5'-GTAGCCCACCCCCAGTGGGGTGGGATAC-3') which overlaps the putative -35 and -10 regions of the *cso* promoter. This interaction could be inhibited by the addition of copper and to a lesser extent silver but not by zinc, cadmium, cobalt or lead to the binding reaction.

Copper sensing CsoR homologues have subsequently been described in *Bacillus subtilis* (Smaldone & Helmann. 2007; Ma *et al.* 2009a), *Listeria monocytogenes* (Corbett *et al.* 2011), *Staphylococcus aureus* (Baker *et al.* 2011; Grosseohme *et al.* 2011), *Thermus thermophilus* (Sakamoto *et al.* 2010) and *Streptomyces lividans* (Dwarkanath *et al.* 2012). These proteins all regulate expression of a copper chaperone and copper translocating P-type ATPase in a copper dependent manner. In addition a second copper sensing CsoR homologue has been described in *M. tuberculosis*, RicR (Festa *et al.* 2011). The regulon of RicR appears to be larger than that of other CsoRs encompassing genes only found in pathogenic mycobacteria and includes the copper metallothionein gene *mymT* (Gold *et al.* 2008). Additionally, *ilvD* is found divergent to *M. tuberculosis ricR*. This gene encodes the dehydratase found to be the primary target for copper toxicity in *E. coli* (Macomber & Imlay. 2009) and given that RicR regulates its own expression (Festa *et al.* 2011) may represent an additional member of the RicR controlled regulon. A CsoR-RcnR family member from *Leptospirillum ferriphilum* UBK03, NcrB, was identified during the course of this work as the nickel dependent

regulator of NcrA a major facilitator superfamily protein involved in nickel resistance (Zhu *et al.* 2011). Homologues of the CsoR-RcnR family are widespread in bacteria and based on genetic context may play roles other than in metal homeostasis (Liu *et al.* 2007; Iwig *et al.* 2008).

1.5.2 Protein assembly, structure and DNA interaction

The crystal structure of *M. tuberculosis* Cu(I)-CsoR revealed an all α -helical fold (Liu *et al.* 2007) and this has also shown to be the case for *E. coli* RcnR by circular dichroism (CD) (Iwig *et al.* 2008), although no structure is currently available for *E. coli* RcnR. The asymmetric unit of the *M. tuberculosis* Cu(I)-CsoR protein crystal contained a single monomer and copper ion, application of crystallographic symmetry generated a model of the protein arranged as a homodimer and the authors assigned this as the likely biological assembly (Liu *et al.* 2007). This prediction was later changed to a tetrameric assembly upon the publication of further analytical ultracentrifugation data which suggested CsoR-RcnR family proteins exist as tetrameric assemblies at low micromolar concentrations (Iwig *et al.* 2008; Ma *et al.* 2009a). Later crystal structures of *T. thermophilus* (Sakamoto *et al.* 2010) and *S. lividans* CsoR (Dwarakanath *et al.* 2012) contained four and two monomers in the asymmetric unit respectively and their arrangement supports the multimeric model generated for *M. tuberculosis* Cu(I)-CsoR. Each CsoR monomer consists of three alpha helices, two longer (~ 25 amino acids, $\alpha 1$ and $\alpha 2$) and one shorter (11 amino acids, $\alpha 3$) (Figure 1.2). $\alpha 1$ and $\alpha 2$ from one monomer pack against $\alpha 1'$ and $\alpha 2'$ from the symmetry related monomer to form an antiparallel four helix bundle (Figure 1.2). The revised tetrameric assembly can be thought of as a dimer of dimers and resembles a flat disc with a central cavity (Figure 1.2).

The all α -helical bundle structure lacks a common DNA binding motif, such as winged helix, helix-turn-helix and ribbon-helix-helix found in other prokaryotic metal sensors and therefore represents a novel DNA binding fold. In copper sensing CsoRs surface exposed positive charge is conserved in the form of several lysine and arginine residues and two of these arginine residues were shown to be important for the DNA binding ability of *M. tuberculosis* CsoR (Figure 3.2) (Liu *et al.* 2007). Protection of a number of these lysine residues from chemical modification in the DNA bound form of *B. subtilis* CsoR revealed a patch of positive charge running across the surface of the tetrameric assembly that may represent a DNA interaction surface (Chang *et al.* 2011).

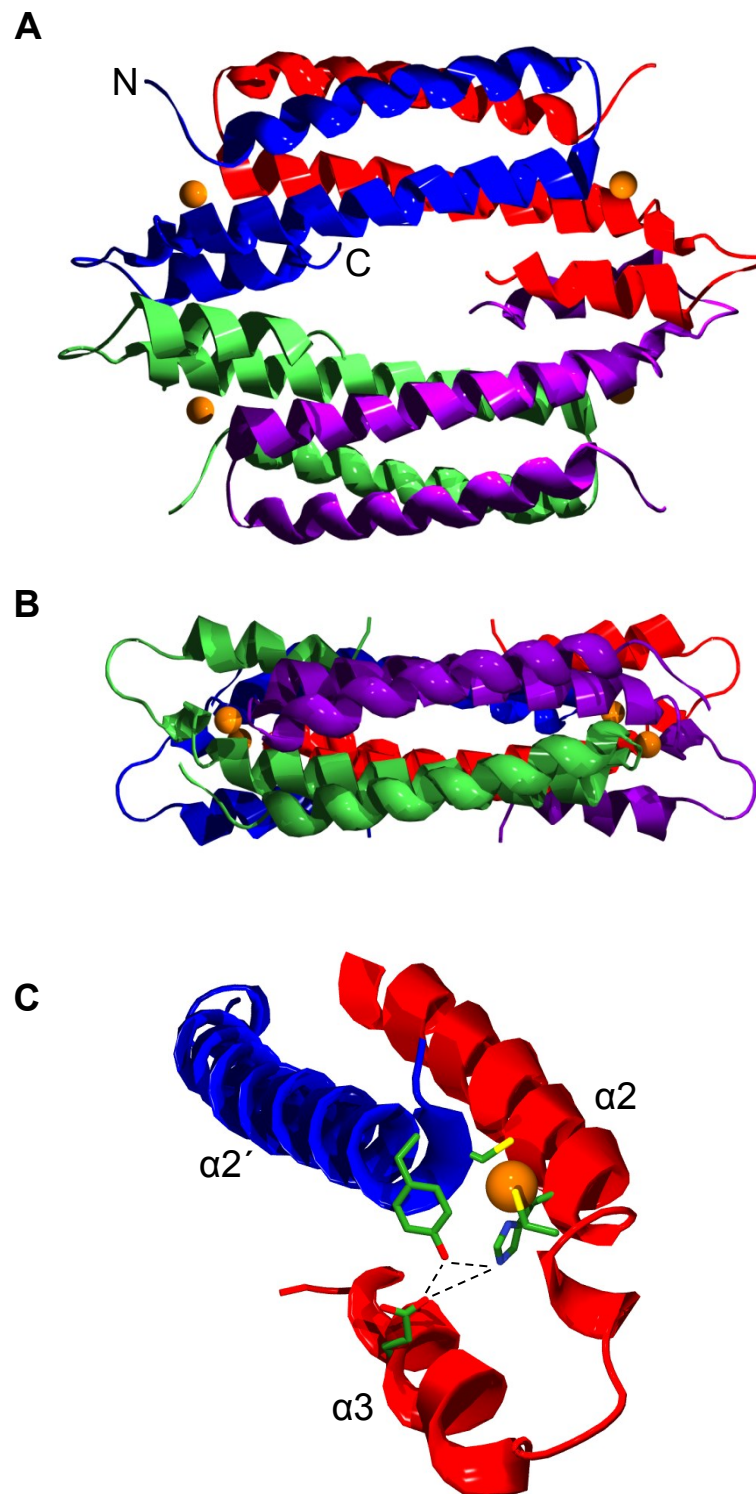


Figure 1.2. *M. tuberculosis* CsoR structure and proposed allosteric network. A. Proposed biological assembly of *M. tuberculosis* CsoR. The individual chains of the tetrameric assembly are differently coloured with the amino (N) and carboxyl (C) terminus of the blue chain labelled. Cu(I) is represented as an orange sphere. B. Rotation through 90° of the structure shown in 'A' in order to emphasise the flat, disc-like nature of *M. tuberculosis* CsoR. C. *M. tuberculosis* CsoR Cu(I) binding site derived from the side chains of His61, Cys65 and Cys36' showing proposed allosteric hydrogen bond network (dashed lines) involving the side chains of His61, Tyr35' and Glu81. Cu(I) is represented as an orange sphere. All models were created using coordinates from the PDB file 2HH7 (Liu *et al.* 2007).

DNA recognition sites of CsoR-RcnR proteins take the form of runs of guanines or cytosines flanked by adenine-thymine rich pseudo-palindromic repeats. Much of the current understanding of the interaction of CsoR-RcnR proteins with DNA has come from study of the DNA binding properties of *E. coli* RcnR. *E. coli* RcnR binds specifically to the *rcnR-rcnA* intergenic region within which is found a pair of guanine rich regions comprising a run of six or seven guanines (Iwig & Chivers. 2009). These ‘guanine tracts’ are flanked by inverted repeats of the sequence TACT (5'-TACTGGGGGG(G)AGTA-3'). By a DNaseI footprinting assay *E. coli* RcnR was shown to protect a core region of ~ 40 bp encompassing the two potential recognition sites but the region of protection additionally extended ~ 60 bp in each direction with hypersensitive sites observed at approximately 10 bp repeats indicative of DNA bending or wrapping (Iwig & Chivers. 2009). These contacts outside the core protected region were shown to be important for high affinity DNA binding with the apparent affinity of *E. coli* RcnR for a DNA probe containing the core recognition site increasing ~ 4 fold as the probe length increased from 80 to 150 bp (Iwig & Chivers. 2009). Additionally, contacts outside the core protected region were shown to be non-specific as a probe where the flanking regions were exchanged for unrelated vector sequence maintained a similar affinity as a probe with wild type sequence (Iwig & Chivers. 2009). A single RcnR tetramer binds to each of the two recognition sites found in the *rcnR-rcnA* intergenic region and binding of a single tetramer is retained using a probe containing only a single site however wrapping of flanking DNA is only observed with a probe containing both recognition sites (Iwig & Chivers. 2009).

A number of recognition sites for copper sensing CsoR proteins have been experimentally validated concurrent with this study. The DNA recognition sites of CsoR-RcnR proteins have been divided into two groups based on the length of the intervening guanine-cytosine rich tract (Iwig & Chivers. 2009). Type 1 sites, such as the RcnR recognition site, have a single guanine-cytosine tract flanked by an adenine-thymine rich inverted repeat whereas the type 2 sites, typically recognised by copper sensing CsoR homologues, have two shorter guanine-cytosine tracts between the adenine-thymine rich inverted repeat separated by adenine-thymine bases (Iwig & Chivers. 2009). The nature of the recognition site is predicted to influence the stoichiometry of protein binding as discussed further in Section 4.1.1. The specific sequence of both the guanine-cytosine rich tract and the flanking adenine-thymine rich regions has been shown to be important for recognition with mutation of the TACT inverted repeat of the *E. coli* RcnR recognition site lowering the affinity with which *E.*

coli RcnR binds DNA (Iwig & Chivers. 2009) and mutation of the *M. tuberculosis* RicR recognition site from 5'-TACCCCTATAGGGTA-3' to 5'-TACCCCTATAGTTTA-3' resulting in loss of binding by RicR (Festa *et al.* 2010). The guanine tract of the *E. coli* RcnR recognition site confers A-DNA features and it has been hypothesised that the A-DNA/ B-DNA junction found between the adenine-thymine rich inverted repeat and the guanine-cytosine rich tract may additionally be an important determinant of DNA recognition by CsoR-RcnR family proteins (Iwig & Chivers. 2009).

1.5.3 Metal coordination sphere

In the modelled homodimer of *M. tuberculosis* CsoR one Cu(I) ion is observed bound at the homodimer interface coordinated with a trigonal geometry by the sulphur atoms of Cys36 and Cys65' (from the opposite subunit) and N^{δ1} of His61' (Liu *et al.* 2007) (Figure 1.2). As the proposed tetrameric assembly can be thought of as a dimer of dimers the primary copper coordination sphere is unchanged. The three coordinate nature of the Cu(I) site was confirmed by X-ray absorption spectroscopy (XAS) and the ligand set of two sulphurs plus one oxygen or nitrogen by extended X-ray absorption fine structure (EXAFS) spectroscopy (Liu *et al.* 2007). Interestingly EXAFS features characteristic of imidazole coordination were not observed in this analysis. The authors suggest that this may be due to the imidazole ring being rotated relative to the Cu-N bond or an alternative coordination of copper in solution (Liu *et al.* 2007). Critically though a His61→Ala mutant gives an XAS spectrum diagnostic of two-coordinate Cu(I) with thiolate ligands strongly suggesting that His61 is a Cu(I) ligand in solution. The EXAFS spectrum of Cys36→Ala suggests the loss of one thiolate ligand. Additionally Cys36→Ala and His61→Ala lost copper responsiveness in EMSA analyses and were less able to compete with the Cu(I) chelator BCS for Cu(I) indicating a weakened copper affinity (Liu *et al.* 2007).

The Cu(I) coordination sphere for copper sensing CsoR homologues is predicted to be the same as that observed for *M. tuberculosis* due to the nearly absolute conservation of the Cu(I) coordinating residues (Figure 3.2). EXAFS has been used to experimentally verify that the Cu(I) coordination environment in *B. subtilis* and *S. aureus* CsoR which in both cases is three-coordinate with two sulphur ligands and one oxygen or nitrogen ligand, additionally, significant outer shell scattering at 3-4 Å is consistent with the presence of a histidine residue in the primary coordination sphere (Ma *et al.* 2009a; Grosseohme *et al.* 2011). Mutation of *S. aureus* CsoR Cys41 or His66 (Grosseohme *et al.* 2011) and *S. lividans* CsoR Cys75 or His100 (Dwarakanath *et al.* 2012) (in both

cases equivalent to *M. tuberculosis* CsoR Cys36 and His61) to alanine results in a weakened Cu(I) affinity and Cys42→Ala (equivalent to *M. tuberculosis* CsoR Cys36) mutation of *L. monocytogenes* CsoR results in a protein non-responsive to exogenous copper in a *lacZ* reporter gene assay (Corbett *et al.* 2011). The nickel and cobalt coordination sphere of *E. coli* RcnR is less well defined but available information suggests a pseudo-octahedral coordination geometry for both metals bound at an equivalent locus to Cu(I) on CsoR (Iwig *et al.* 2008). The metal coordination sphere of *E. coli* RcnR is discussed further in Section 4.3.

1.5.4 Allosteric linkage of metal binding to DNA dissociation

Inspection of the structures of Cu(I)-CsoR (Liu *et al.* 2007) and apo-CsoR (Sakamoto *et al.* 2010; Dwarakanath *et al.* 2012) and CD studies of *E. coli* RcnR (Iwig *et al.* 2008) suggest no gross structural changes occur upon the coordination of metal ions by CsoR-RcnR family proteins prompting studies to understand the mechanism of de-repression in terms of the energetic changes in the DNA bound and unbound forms of these proteins. From the crystal structure of Cu(I) bound *M. tuberculosis* CsoR a hydrogen bond network involving His61, Tyr35', and Glu81, which could propagate an allosteric switch upon copper binding, was proposed (Liu *et al.* 2007). When Cu(I) coordinates N^{δ1} on one face of the His61 imidazole ring N^{ε2} on the opposite face is orientated such that it points towards the side chains of the two conserved second shell residues, Tyr35' from the N-terminal of α2' of the symmetry related monomer and Glu81 located on α3 (Figure 1.2). This could allow the formation of hydrogen bonds and it was hypothesised that this may stabilise the allosterically inhibited (with regards to DNA binding) Cu(I) bound state (Liu *et al.* 2007). An allosteric hydrogen bonding network propagated by orientation of histidine upon metal coordination has also been observed in ArsR-SmtB zinc sensor proteins (Eicken *et al.* 2003). A Glu81→Ala mutant of *M. tuberculosis* CsoR (Liu *et al.* 2007; Ma *et al.* 2009 b) and the equivalent mutant, Glu90→Ala, of *B. subtilis* CsoR (Ma *et al.* 2009a) were both found to be competent to bind Cu(I) however this Cu(I) coordination did not trigger dissociation from DNA. Tyr35 has been shown to tune the extent to which Cu(I) binding drives allostery but is not critical to retain Cu(I) responsiveness (Ma *et al.* 2009b). This has also been shown to be the case for an equivalent mutant of *L. monocytogenes* CsoR *in vivo* (Corbett *et al.* 2011) and the role of this residue in the allosteric switch is discussed further in Section 6.3.3. The importance of His61 in this proposed allosteric coupling mechanism was shown by elegant experiments where His61 was replaced, in a synthetically assembled CsoR, with

unnatural histidine analogues in which N^{δ1} was retained but N^{ε2} was substituted for a methyl or thioether group (Ma *et al.* 2009b). The C-terminal regions, including the unnatural histidine analogue, of these proteins were produced by solid state peptide synthesis. The N-terminal regions were produced by overexpression from the pTBX1 vector which results in a fusion protein with a C-terminal intein domain. Cleavage of the intein resulted in the N-terminal region of CsoR with a C-terminal thioester group which could be ligated to the synthetically produced C-terminal fragment. In these mutant proteins high copper affinity was retained but copper binding was uncoupled from DNA binding as determined by fluorescence anisotropy (Ma *et al.* 2009b).

In the crystal structure of apo-CsoR from *S. lividans* a hydrogen bond network between His100 and Glu122 (equivalent to *M. tuberculosis* CsoR His61 and Glu81) bridged by a water molecule was visualised suggesting that coordination of Cu(I) may not be essential to form this hydrogen bond network (Dwarakanath *et al.* 2012). However this does not necessarily contradict the model proposed from work with *M. tuberculosis* CsoR. The hydrogen bond network may form spontaneously as different conformations are sampled by the protein but upon binding Cu(I) may be locked into this conformation. The cadmium sensor CmtR of the ArsR-SmtB family is known to sample a range of conformations both competent and incompetent to bind DNA but upon binding cadmium the conformations suitable for binding DNA are no longer sampled (Banci *et al.* 2007). A water molecule was not visualised in the putative allosteric hydrogen bond network of *M. tuberculosis* CsoR (Liu *et al.* 2007) and so it is unclear if this water molecule plays a role in metal induced allostery (Dwarakanath *et al.* 2012). The copper coordinating residues Cys75 and His100 in the *S. lividans* apo-CsoR crystal structure were closely aligned with the corresponding residues from copper bound *M. tuberculosis* CsoR (Cys36 and His61) however Cys104 (equivalent to Cys65) is visualised in such a position that it must undergo a large movement in order to complete the copper coordination sphere (Dwarakanath *et al.* 2012). This movement may also play a role in metal mediated allostery.

Little is currently known about the propagation of allostery in *E. coli* RcnR upon metal binding. *E. coli* RcnR does not conserve tyrosine and glutamate residues at equivalent positions to *M. tuberculosis* Tyr35 and Glu81 (Figure 3.2). Additionally His60 (equivalent to His61 of *M. tuberculosis* CsoR) is not implicated in Ni(II) coordination (Iwig *et al.* 2008; Higgins *et al.* 2013) (Section 4.3). These observations suggest the mechanism of allosteric coupling of metal binding to DNA binding must be distinct for

RcnR and suggest that it may be relatively easy to evolve different sensory mechanisms on a common protein scaffold as has been observed for metalloregulators of the ArsR-SmtB family (Osman & Cavet. 2010).

1.5.5 Selectivity in CsoR-RcnR family proteins

The issue of what dictates sensing selectivity in this family of proteins has been addressed in studies using *E. coli* RcnR and *B. subtilis* CsoR. Although the induction by metals other than copper of the *copZA* operon regulated by *B. subtilis* CsoR has not been investigated induction of the *cso* operon of *M. tuberculosis* is only induced in response to copper (Section 1.5.1) (Liu *et al.* 2007). *B. subtilis* CsoR is competent to bind both Zn(II) and Ni(II) with affinities of $1.6 \times 10^8 \text{ M}^{-1}$ and $3.6 \times 10^9 \text{ M}^{-1}$ respectively however the allosteric coupling free energy (Section 5.8.2) associated with coordination of Zn(II) ($1.7 \text{ kcal mol}^{-1}$) and Ni(II) ($1.6 \text{ kcal mol}^{-1}$) is significantly less than that associated with coordination of Cu(I) ($\geq 5.4 \text{ kcal mol}^{-1}$) (Ma *et al.* 2009a). This has been correlated with the adoption of a non-native coordination geometry by Zn(II) (tetrahedral) and Ni(II) (square planar) as inferred from UV-Vis spectroscopy (Ma *et al.* 2009a). These observations are consistent with the notion that adoption of native coordination geometry can help impose selectivity on metalloregulators (Cavet *et al.* 2002; Pennella *et al.* 2003; Phillips *et al.* 2008).

Metal coordination geometry may also be important for selective metal sensing by *E. coli* RcnR. Cognate metals Ni(II) and Co(II) have been shown by XAS to be coordinated with pseudo-octahedral coordination geometry (Iwig *et al.* 2008). Both zinc and copper have been shown by *lacZ* reporter gene assay to be non-cognate metals (Iwig *et al.* 2008) and adopt lower number coordination geometries, four coordinate for Zn(II) and three or four coordinate for Cu(I) depending on buffer constitution (Higgins *et al.* 2012b). A mutant variant of *E. coli* RcnR in which Zn(II) adopts a 6-coordinate geometry has been shown to display some responsiveness to exogenously added zinc in a *lacZ* reporter gene assay (Higgins *et al.* 2012b), thus for *E. coli* RcnR as well as *B. subtilis* CsoR metal selectivity appears to be correlated with the adoption of a native coordination geometry. It should be noted that in both these cases, especially for *E. coli* RcnR where selectivity has only been examined *in vivo*, that factors in addition to allosteric regulation by adoption of the correct coordination geometry may also act to ensure selectivity of these metalloregulators. For example the affinity of RcnR for Zn(II) may not be sufficient for it to compete with other components of the intracellular

Zn(II) buffer, this may explain the modest induction of the *rcnA* promoter by an RcnR mutant which binds Zn(II) with a 6-coordinate geometry (Higgins *et al.* 2012b).

1.5.6 CsoR-RcnR homologues that do not sense metal stress

The observation that some CsoR-RcnR homologues are co-localised with genes other than those involved in metal homeostasis led to the suggestion that some members of this protein family may be responsive to signals other than metal ion stress (Iwig *et al.* 2006; Liu *et al.* 2007; Iwig *et al.* 2008). A second CsoR-RcnR protein is encoded in the genome of *E. coli*, FrmR. *frmR* is co-localised with *frmA* encoding a zinc dependent formaldehyde dehydrogenase and *frmB* encoding a putative S-formylglutathione hydrolase and a decrease in the expression of both these genes is caused by an overexpression of FrmR (Herring & Blattner. 2004). Expression of *frmAB* is induced by formaldehyde (Herring & Blattner. 2004) but it is currently unknown if this induction is regulated by FrmR although this seems likely. Members of the MerR family that regulate genes involved in formaldehyde resistance have been described (Kidd *et al.* 2005; Huyen *et al.* 2009; Potter *et al.* 2010). These proteins all contain a conserved cysteine residue (Kidd *et al.* 2005) and in *B. subtilis* AdhR this cysteine residue has been shown to be essential for induction in response to aldehydes leading to the hypothesis that the sensory mechanism may involve this residue being alkylated by electrophilic carbonyl compounds (Huyen *et al.* 2009). FrmR contains two cysteine residues one of which is in an equivalent position to *M. tuberculosis* CsoR Cys36 and so it is tempting to speculate that alkylation of this residue may be involved in the sensory mechanism.

The genome of *S. aureus* encodes two members of the CsoR-RcnR family one of which is a *bona fide* copper sensing CsoR regulating the expression a copper exporting P-type ATPase and a copper chaperone and the second of which was shown to be a regulator of an operon of genes involved in sulphur metabolism (Grossoehme *et al.* 2011). The regulator of the sulphur metabolism operon, named CstR, retains cysteine residues equivalent to Cys36 and Cys65 of *M. tuberculosis* CsoR but lacks a histidine residue equivalent to H61 of *M. tuberculosis* CsoR (Figure 3.2) (Grossoehme *et al.* 2011). Incubation of CstR with an excess of sodium sulphite results in a mixture of oxidised products with a greatly reduced affinity for DNA whereas *S. aureus* CsoR was shown to be unreactive toward sodium sulphite (Grossoehme *et al.* 2011). Treatment of CstR with the thiol modifying agent methylmethanethiosulphonate also results in a protein with a

weakened DNA affinity. Modification of a conserved cysteine residue may represent a sensory mechanism for non-metal sensing members of the CsoR-RcnR family.

In *Saccharomyces cerevisiae* the expression of two forms of zinc requiring alcohol dehydrogenase are regulated indirectly through the zinc sensing transcriptional regulator Zap1 (Bird *et al.* 2006) and so an alternative possibility for regulation via FrnR-like proteins may involve the direct coordination of zinc analogous to other metal sensing CsoR-RcnR family members.

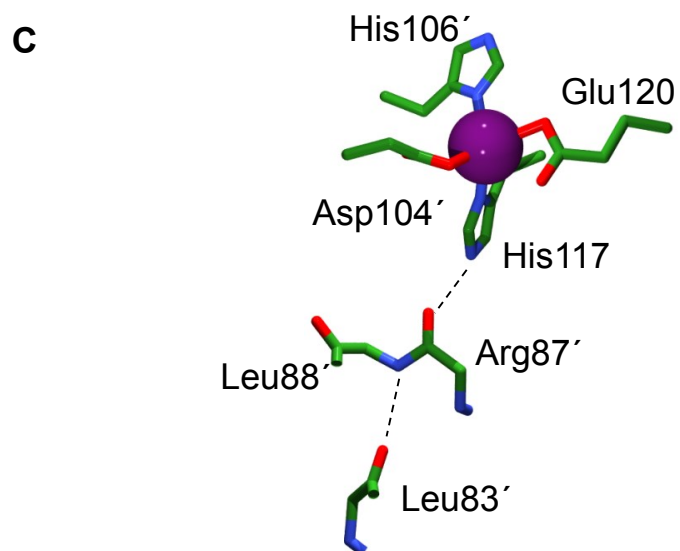
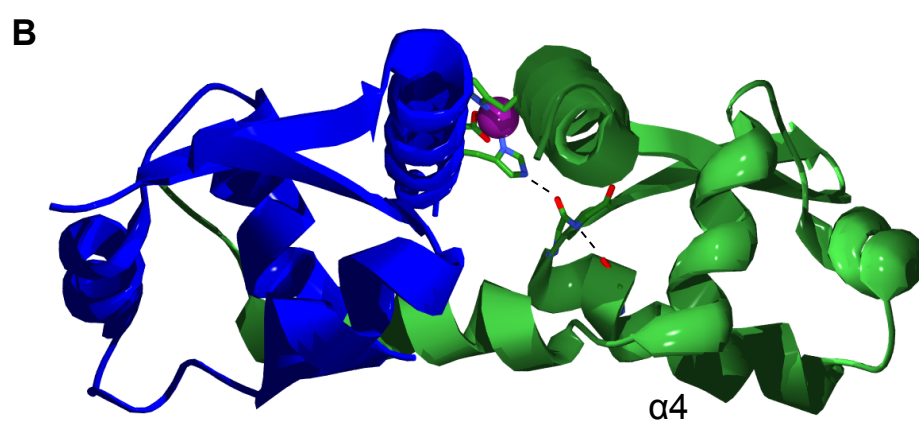
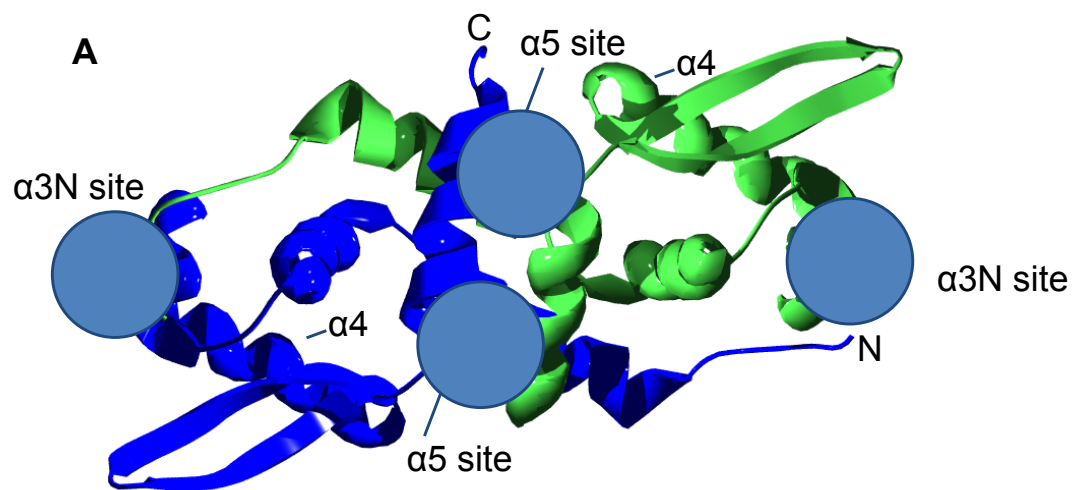
1.6 ArsR-SmtB family

The ArsR-SmtB family metal sensors are widespread across the prokaryotic kingdom with a recent estimate suggesting that there may be in excess of 500 representatives once proteins with low sequence similarity have been excluded (Campbell *et al.* 2007). Some bacteria possess a large number of deduced ArsR-SmtB family proteins, a notable example being *M. tuberculosis* which possesses twelve (Osman & Cavet. 2010).

This family is named for the founding members, the zinc sensor SmtB from *Synechococcus* PCC 7942, repressor of *smtA* which encodes a zinc metallothionein (Huckle *et al.* 1993; Morby *et al.* 1993) and *E. coli* ArsR which regulates the expression of genes involved in resistance to arsenicals and antimonials in response to binding trivalent forms of the group 5 elements arsenic, antimony and bismuth (Kaur & Rosen. 1992; Wu & Rosen. 1993). Members of this family exist predominantly as dimers in solution (Kar *et al.* 1997) and are projected to share a common winged-helix fold ($\alpha 1$ - $\alpha 2$ - $\alpha 3$ - $\alpha 4$ - $\beta 1$ - $\beta 2$ - $\alpha 5$) first structurally characterised in SmtB (Cook *et al.* 1998) and now observed in other family members (Ye *et al.* 2005; Arunkumar *et al.* 2009; Lee *et al.* 2012) (Figure 1.3). Some members of this family have an additional N-terminal α -helix referred to as $\alpha 0$ (Ye *et al.* 2005). The crystal structure of SmtB (Cook *et al.* 2008) confirmed that this family of proteins contains a helix-turn-helix DNA binding motif consisting of $\alpha 3$ and $\alpha 4$ as predicted in earlier studies (Morby *et al.* 1993) (Figure 1.3). This helix-turn-helix motif bears a strong structural resemblance to other bacterial transcriptional repressors including CAP (catabolite activator protein) (Schultz *et al.* 1991) and several other metal sensor families (Giedroc & Arunkumar. 2007).

SmtB recognises an imperfect 12-2-12 inverted repeat within the *smt* operator-promoter region (Morby *et al.* 1993) and similar sequences are also recognised by other ArsR-

Figure 1.3. *Synechococcus elongatus* PCC7942 SmtB structure and proposed allosteric network. A. Structure of *S. elongatus* apo-SmtB. The locations of the $\alpha 5$ and $\alpha 3N$ metal binding sites are shown and the DNA contacting $\alpha 4$ helices annotated. The individual chains of the dimeric assembly are differently coloured with the amino (N) and carboxyl (C) termini of the blue chain labelled. B. Structure of *S. elongatus* Zn_2 -SmtB with one chelate and the blue $\alpha 1$ removed to aid visualisation of the proposed allosteric hydrogen bonding network (dashed line) connecting zinc chelating His117 to Leu83' of DNA contacting $\alpha 4$ via the backbone of residues Arg87' and Leu88'. C. Side chain only representation of the $\alpha 5$ zinc site of *S. elongatus* SmtB with the backbone of residues involved in the proposed hydrogen bonding allosteric network (represented as a dashed line). Models were created using coordinates from PDB file 1R1T (apo-SmtB) and 1R22 (Zn_2 SmtB) (Eicken *et al.* 2003).



SmtB metalloregulators. It has been shown to be possible to successfully predict genes regulated by this family from a consensus sequence of these binding sites (Harvie *et al.* 2006). These motifs usually lie between the transcriptional start site and the -10 promoter element of the regulated gene meaning transcription is repressed while the repressor is associated with DNA. The DNA binding stoichiometry varies between members of this family with only a single dimer binding even under conditions of excess protein for *S. aureus* CadC (Busenlehner *et al.* 2001) whereas multimeric complexes of up to four or five dimers have been reported for *S. aureus* CzcA (Pennella *et al.* 2003).

Since the discovery of ArsR, SmtB and the *S. aureus* cadmium, bismuth, lead and zinc responsive sensor CadC (Endo & Silver. 1995), also identified during early work on this protein family, members have been described displaying responsiveness to a wide variety of metals and metalloids (Osman & Cavet. 2010). Additionally, some members of this family such as *Vibrio cholerae* HlyU and *Xyella fastidiosa* BigR do not regulate the expression of genes involved in metal ion homeostasis but instead regulate the expression of a gene encoding the cytotoxic virulence protein HlyA (Williams & Manning. 1991; Williams *et al.* 1993) and an operon containing genes implicated in biofilm formation (Barbosa & Benedetti. 2007), respectively. Neither HlyU (Campbell *et al.* 2007) nor BigR (Barbosa & Bendetti. 2007) are metal responsive, and the sensory mechanism of BigR has recently been shown to involve oxidation of two conserved cysteine residues (Guimarães *et al.* 2011). For a structural family closely related in sequence terms this family of proteins contains a remarkable variety of sensory sites, discussed further in Section 1.6.1. This variety of metal binding sites has been referred to as the ‘themes and variations’ model (Busenlehner *et al.* 2003) and helps confer selectivity of metal sensing on this family of proteins (Section 1.6.3). Despite the variety of sensory motifs ArsR-SmtB proteins share the same basic mechanism: binding with a high affinity to the operator-promoter region of the regulated gene(s) in the apo-state, upon metal binding the affinity for DNA is weakened and thus allows unhindered transcription. It is currently unclear *in vivo* if metal binding promotes dissociation from DNA by ArsR-SmtB proteins or prevents interaction with DNA.

1.6.1 Variety of metal binding motifs on a common scaffold

Early work with SmtB and ArsR suggested that two distinct sensory motifs may be present in this protein family. In an attempt to discover the metal binding loci of SmtB, protein crystals were soaked with mercuric acetate (Cook *et al.* 1998). The difference

electron density map obtained in this experiment suggested the presence of two symmetry related pairs of metal binding sites per dimer, one pair associated with the $\alpha 3$ helices at the extremities of the dimeric structure and one pair associated with the $\alpha 5$ helices which form part of the dimerization interface (Figure 1.3). Further *in vitro* work confirmed that SmtB does indeed contain two pairs of symmetry related sites per dimer with the non-cysteine containing $\alpha 5$ site ligands derived from both dimer sub-units at the interface and the ligands of the cysteine containing $\alpha 3$ zinc site derived from $\alpha 3$ of one sub-unit and the N-terminus of the other (VanZile *et al.* 2002b; Eicken *et al.* 2003). These metal binding sites have been termed $\alpha 5$ and $\alpha 3N$ and represent two of the metal binding motifs present in this protein family. Interestingly only the $\alpha 5$ site is required for sensing zinc both *in vivo* (Turner *et al.* 1996) and *in vitro* (VanZile *et al.* 2002b) and so the $\alpha 3N$ site of SmtB appears to be vestigial. *S. aureus* CadC also possesses an $\alpha 5$ and a thiol rich $\alpha 3N$ site (Busenlehner *et al.* 2002), however only the $\alpha 3N$ site is required for responsiveness highlighting the interesting observation of the retention of apparently vestigial metal binding sites in this protein family which in some cases actually have tighter metal binding affinities than the allosteric site (VanZile *et al.* 2002b). Of course it remains possible that these apparently vestigial sites have a functional role that remains to be characterised. ArsR binds and senses As(III) in a trigonal coordination geometry with cysteine ligands derived exclusively from the $\alpha 3$ helix (Shi *et al.* 1994; Shi *et al.* 1996) and therefore represents a third type of sensory motif in this family of proteins termed $\alpha 3$. Subsequently further distinct metal sensing motifs have been named for the location of the metal sensing residues on the protein fold (Osman & Cavet. 2010). The categorisation of some of these sensory motifs may require reassessment as, for example, it was recently found that the archetypal $\alpha 5C$ sensor NmtR is more accurately described as $\alpha 5N$ (Reyes-Caballero *et al.* 2011b).

1.6.2 Allosteric linkage of metal binding to DNA dissociation

S. aureus CzcA is a Zn(II) and Co(II) sensing $\alpha 5$ member of the ArsR-SmtB which lacks an $\alpha 3$ metal binding site (Pennella *et al.* 2003) and regulates expression of *czcB* encoding a Zn(II) and Co(II) exporter (Kuroda *et al.* 1999). The Zn(II) loaded crystal structures of both CzcA and $\alpha 5$ SmtB (a mutant protein with abrogated $\alpha 3N$ sites) revealed the presence of a hydrogen bond network (Eicken *et al.* 2003) with analogy to the allosteric hydrogen bond network subsequently discovered in *M. tuberculosis* CsoR (Liu *et al.* 2007; Ma *et al.* 2009b). In SmtB this network originates from the non-coordinating $N^{\epsilon 2}-H^{\epsilon 2}$ from Zn(II) coordinating His117 bonding with the main chain

carbonyl group of Arg87'. The immediately adjacent main chain amide group of Leu88' then forms a hydrogen bond to the main chain carbonyl group of Leu83' located near the C-terminus of the DNA recognition helix (Eicken *et al.* 2003) (Figure 1.3). Slow exchange of the $N^{\epsilon 2}$ -H $^{\epsilon 2}$ hydrogen of SmtB H117 with solvent was additionally observed in NMR experiments with the Zn(II) bound but not apo protein consistent with the existence of a hydrogen bond in the Zn(II) bound state (Eicken *et al.* 2003). This effect is also observed for CzrA His97 (equivalent to SmtB His117) (Eicken *et al.* 2003; Arunkumar *et al.* 2007). Molecular dynamics simulations also show that this network likely only exists in CzrA in the Zn(II) bound but not DNA bound state, additionally a longer and weaker hydrogen bond exists between His97 and His67' (equivalent to SmtB His117 and Arg87') in the apo state (Chakravorty *et al.* 2012). Site directed mutagenesis of CzrA His97 to both metal coordinating (Asp) and non-coordinating (Asn) residues results in a protein in which zinc binding is uncoupled from the allosteric response, however, this effect was also observed for mutants of His86 (another Zn(II) coordinating ligand not thought to be part of an allosteric switch) (Pennella *et al.* 2006). As CzrA mutants at both these positions adopt non-native Zn(II) coordination geometry it was not possible to conclusively assign an allosteric role to the identified hydrogen bond network (Pennella *et al.* 2006). However, in very recently published work utilising unnatural amino acid substitution as employed to probe allostery in *M. tuberculosis* CsoR, replacement of CzrA His97 with methylhistidine ($N^{\epsilon 2}$ replaced with a methyl group) results in a decoupling of zinc binding and DNA binding (a reduction in coupling free energy from 4.9 kcal mol⁻¹ to 1.1 kcal mol⁻¹) demonstrating the importance of this hydrogen bond in the allosteric mechanism (Campanello *et al.* 2013).

Despite a conserved hydrogen bonding network proposed to propagate the allosteric effect of zinc binding the conformational changes associated with this switch appear to vary in SmtB and CzrA. The SmtB homodimer becomes more compact upon Zn(II) binding with significant movement of the DNA binding helix-turn-helix motif and β -hairpin wings in opposing monomer subunits relative to each other (Eicken *et al.* 2003). In contrast the zinc bound form of CzrA reveals small global quaternary structure change relative to the apo form however the internal dynamics of the protein are quenched significantly upon zinc binding (Eicken *et al.* 2003). It was suggested this may have the effect of 'freezing out' those conformations of protein assembly that are competent to bind DNA with a high affinity. Cadmium binding to the cadmium and lead sensing *M. tuberculosis* CmtR also has the effect of dampening the internal dynamics of the protein, rigidifying the structure such that forms competent to bind DNA are

predicted to be excluded (Banci *et al.* 2007). The DNA bound solution structure of CzcA revealed that the quaternary structure of the protein in this state is significantly different to the Zn(II) bound state with a ‘closed’ conformation more suited for binding DNA visualised which is driven to an ‘open’ conformation upon Zn(II) binding (Arunkumar *et al.* 2009). The NMR solution studies of DNA bound CzcA additionally revealed an energetically important interaction between $\alpha 3$ residue Val42 and DNA (Arunkumar *et al.* 2009). The equivalent valine residue in the $\alpha 3$ sensor ArsR is found between two of the As(III) coordinating cysteine residues in a Cys-Val-Cys motif. It is suggested that As(III) coordination to this motif would disrupt the interactions between this valine residue and DNA and thus may underpin the allosteric response of $\alpha 3$ ArsR-SmtB proteins (Arunkumar *et al.* 2009).

1.6.3 Selectivity of metal sensing in the ArsR-SmtB family

ArsR-SmtB proteins and indeed all metal sensors must be able to respond to different metals selectively within a common cytosol. Studies of ArsR-SmtB proteins from *M. tuberculosis* have provided insights into how allostery, affinity and access can help dictate selectivity (Tottey *et al.* 2005; Osman & Cavet. 2010).

NmtR was the first of the twelve ArsR-SmtB proteins of *M. tuberculosis* to be characterised (Cavet *et al.* 2002). In its native host it is responsive to nickel and cobalt but not zinc and regulates the expression of *nmtA*, which encodes a P-type ATPase predicted to export cobalt and nickel (Cavet *et al.* 2002). When the protein was expressed in the cytosol of a heterologous host, cyanobacterium *Synechococcus* PCC 7942, it was responsive only to cobalt, losing responsiveness to nickel. Quantification of the number of nickel atoms per cell in the two host cell types revealed that under growth conditions where the growth medium was not supplemented with additional nickel the two cell types had very similar nickel quotas (0.2×10^5 atoms cell⁻¹), however, when cultured at maximum permissive concentrations of exogenous nickel the cellular nickel quota of the mycobacterial host increased ~40 fold whereas the cellular nickel quota of the cyanobacterial host increased less than four-fold (Cavet *et al.* 2002). This suggested that the lower nickel content of the cyanobacterial cell effectively meant that NmtR did not have access to nickel and was therefore unresponsive to exogenous addition of this element. An analogous phenomenon is observed when the iron sensor from *Corynebacterium diphtheriae* is transferred to *B. subtilis* where it gains the ability to respond to manganese as well as iron (Guedon & Helmann. 2003). These examples highlight how the cellular environment can influence selectivity of metal sensor proteins

and suggest the evolution of properties of these proteins, for example metal affinity, are likely, in part, determined by the cellular environment.

In addition to losing responsiveness to nickel NmtR remained non-responsive to zinc when transferred to the cyanobacterial cell (Cavet *et al.* 2002) despite displaying some allosteric response to zinc *in vitro* (Pennella *et al.* 2003). The zinc sensor SmtB is present in the same cellular environment and does respond to zinc (Huckle *et al.* 1993; Morby *et al.* 1993). Possible explanations for this effect involve affinity and allostery. Both NmtR and SmtB bind zinc with a tighter affinity than nickel or cobalt however a competitive zinc binding experiment revealed that zinc preferentially bound to SmtB over NmtR (Cavet *et al.* 2002). Thus although both proteins display tighter zinc than nickel and cobalt affinities, in accordance with the Irving-Williams series (Section 1.2), it is the relative affinity of the two sensors that may help dictate selectivity. A similar relative affinity gradient has also been observed between NmtR and CmtR with competitive metal binding experiments showing cadmium preferentially binds to CmtR and nickel to NmtR matching the *in vivo* preferences of these two proteins (Cavet *et al.* 2003). In addition to this relative affinity gradient NmtR and SmtB bind their cognate metals in different coordination environments (Cavet *et al.* 2002). Whilst both proteins utilise side chain ligands from the $\alpha 5$ helices NmtR recruits additional ligands to coordinate nickel (and cobalt) with an octahedral geometry (Cavet *et al.* 2002) in contrast to the tetrahedral coordination geometry of zinc on SmtB (VanZile *et al.* 2000; VanZile *et al.* 2002b). NmtR binds zinc with tetrahedral coordination geometry analogous to SmtB and CzrA, which is unsurprising considering the three proteins share nearly identical $\alpha 5$ ligand sets and CzrA (and presumably SmtB) binds nickel in an octahedral coordination environment; however, these non-native coordination geometries are either less effective (in the case of zinc on NmtR) or non-effective (in the case of nickel on CzrA) at driving allostery (Pennella *et al.* 2003). Thus the adoption of native coordination geometry appears to be important for eliciting an allosteric response. The origins of allostery are still currently unclear for NmtR which is predicted to lack an analogous allosteric hydrogen bonding network to SmtB and CzrA (Chakravorty *et al.* 2012). The allosteric coupling free energy of nickel binding to NmtR ($2.8 \text{ kcal mol}^{-1}$) (Reyes-Caballero *et al.* 2011) is substantially smaller than that observed for zinc binding to CzrA (6 kcal mol^{-1}) (Pennella *et al.* 2006) suggestive of a distinct allosteric mechanism.

The variety of metal binding sites exhibited by ArsR-SmtB family proteins help to tune metal selectivity. Borderline hardness metals such as zinc, cobalt and nickel are sensed by $\alpha 5$ sites utilising carboxylate and imidazole ligands whereas soft thiophilic metals such as cadmium and lead are sensed by $\alpha 3$ variants via cysteine ligands (Osman & Cavet. 2010). The coordination number can additionally be varied to select metals with a preference for higher coordination geometries as observed for NmtR (Cavet *et al.* 2002). The $\alpha 3$ site of ArsR is also expanded from a three coordinate to a four coordinate site in the $\alpha 3N$ sensor CadC by recruitment of N-terminal ligands to accommodate the preference for four coordinate coordination geometry of cadmium (Busenlehner *et al.* 2002). Interestingly *Oscillatoria brevis* BxmR which regulates expression of P-type ATPase and a metallothionein (Liu *et al.* 2004) is able to sense Zn(II) via an $\alpha 5$ site and cadmium via an $\alpha 3N$ site, additionally it is able to sense copper which it binds at the $\alpha 3N$ site in a Cu_2S_4 cluster (Liu *et al.* 2008).

1.7 MerR family

The MerR family of transcriptional regulators represents a group of gene activators that share a common DNA binding domain but a variety of effector binding domains that dictate the wide variety of signals sensed by this family. The founding member of this family, MerR, is a component of the mercuric resistance operon *mer* from bacterial transposons Tn501 and Tn21 (Summers. 1992). In addition to MerR the *mer* operon of Tn501 comprises genes encoding a periplasmic mercuric metallochaperone (*merP*), a mercuric transporter (*merT*), a mercuric reductase (*merA*) and a potential co-regulator (*merD*). Hg(II) is proposed to be bound by MerP in the periplasm, delivered to the cytosol via MerT and reduced to Hg(0) by MerA (Hobman *et al.* 2005). The mercury vapour then diffuses from the cell.

The promoter of the *mer* regulon has abnormal spacing (19-20 bp rather than the usual 16-18 bp found in most bacterial promoters) between the -35 and -10 regulatory elements. This displacement of the -10 and -35 sites makes the promoter suboptimal for recognition by RNA polymerase and shortened promoter mutants show constitutive activity (Parkhill & Brown. 1990). MerR homodimers bind to a symmetric inverted repeat located between the -35 and -10 elements which results in the bending of DNA further reducing the suitability for recognition by RNA polymerase (Ansari *et al.* 1995). Coordination of Hg(II) by MerR, which occurs at a high affinity three cysteine

containing trigonal site (Shewchuk *et al.* 1989; Helmann *et al.* 1990), results in a relaxation of the bend in DNA induced by apo-MerR (Frantz & O'Halloran. 1990) and an underwinding of DNA by $\sim 33^\circ$ aligning the -35 and -10 RNA polymerase recognition sites allowing transcription to occur (Ansari *et al.* 1994). MerD is proposed to dissociate the mercury bound form of MerR from DNA allowing its replacement with newly synthesised apo-MerR (Champier. 2004).

MerR homologues that sense other metal ions and signals other than metal ions such as small molecule drugs and oxidative stress have subsequently been described. Notable examples of metal sensing homologues include *E. coli* CueR (Petersen & Møller. 2000; Stoyanov *et al.* 2001) and ZntR (Brocklehurst *et al.* 1999). These proteins, respectively, represent copper and zinc sensing homologues of MerR which regulate the expression of P-type ATPases (CopA and ZntA) involved in the export of Cu(I) (Petersen & Møller. 2000) and in the case of ZntA zinc (Rensing *et al.* 1997), cadmium and lead (Rensing *et al.* 1998; Binet & Poole). CueR is additionally responsive to gold and silver (Stoyanov *et al.* 2001; Stoyanov & Brown. 2003). Other examples of metal sensing homologues of MerR include *Salmonella typhimurium* GolS which was initially shown to respond to gold (Checa *et al.* 2007) (which it is unlikely to encounter in this pathogen) but has subsequently been shown to act as a copper sensor (Osman *et al.* 2013), *Haemophilus influenzae* NimR which responds to nickel via an unusual mechanism (Kidd *et al.* 2011) (Section 6.4) and *Synechocystis* CoaR, the only member of the MerR family shown to be cobalt responsive (Rutherford *et al.* 1999).

Non-metal responsive members of the MerR family include the oxidative stress sensor SoxR of *E. coli*, the drug sensing protein BmrR from *B. subtilis* and formaldehyde sensing homologues mentioned in Section 1.5.6. SoxR regulates the expression of SoxS which in turn regulates the expression of genes involved in the oxidative stress response (Amábile-Cuevas & Demple. 1991; Wu & Weiss. 1991; Nunoshiba *et al.* 1992; Li & Demple. 1994). Oxidative stress is sensed via oxidation of a 2Fe-2S cluster bound to the protein (Gaudu & Weiss. 1996). Direct binding of various dyes to BmrR results in a rearrangement of the promoter of *bmr* (encoding an efflux pump) by BmrR to initiate expression of *bmr* (Heldwein & Brennan. 2001).

1.7.1 Selectivity in the MerR family

Selectivity across the range of sub-groups within the MerR family can primarily be attributed to the C-terminally located effector binding domain. MerR proteins from

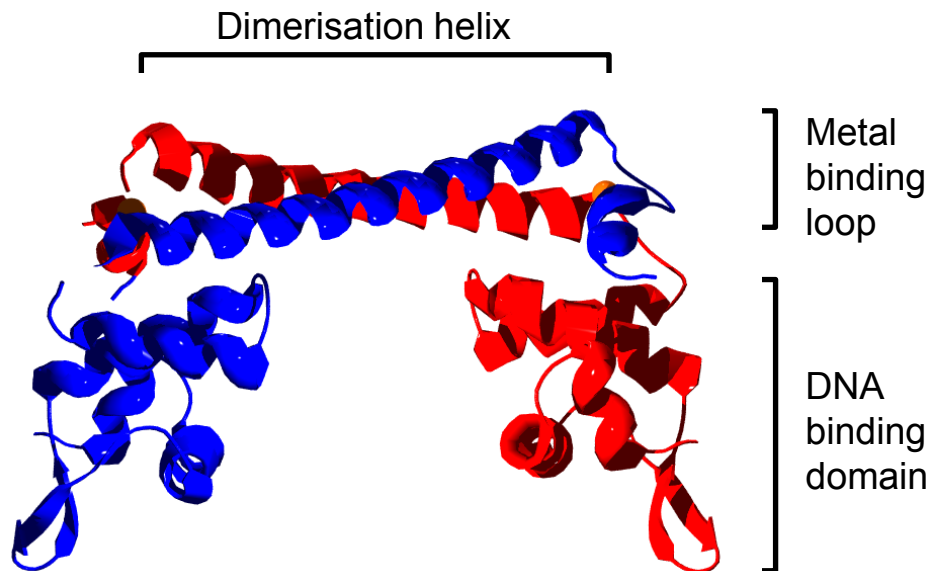


Figure 1.4. *E. coli* CueR structure. A. Structure of Cu(I) bound *E. coli* CueR dimer. Cu(I) is represented as an orange sphere. The individual chains of the dimeric assembly are differently coloured and the location of the N-terminal DNA-binding domain, dimerisation helix and C-terminal effector binding domain, in this case the metal binding loop, are indicated. Model created using coordinates from PDB file 1Q05 (Changela *et al.* 2003).

different sub-groups share considerable sequence and structural similarity in their N-terminal domains which contain the helix-turn-helix DNA binding motif and dimerisation helix (Figure 1.4) but considerable variability has been observed in the C-terminal effector binding domain (Heldwein & Brennan. 2001; Changela *et al.* 2003; Watanabe *et al.* 2008). The multidrug sensor BmrR contains a drug binding domain (Heldwein & Brennan. 2001) whereas a metal binding loop defines the C-terminal regions of metal sensors CueR & ZntR (Changela *et al.* 2003). Clearly the presence of a drug binding region on BmrR distinguishes drug sensing MerRs from metal sensing MerRs but how is metal sensing selectivity achieved among metal sensing MerR proteins?

Insight into how selectivity between divalent Zn(II) ions and monovalent Cu(I) ions may be achieved was obtained through structural studies of the CueR and ZntR proteins of *E. coli* (Changela *et al.* 2003). An *in vitro* transcription assay revealed that Cu(I), Ag(I) and Au(I) were all competent to activate the regulatory mechanism of CueR whereas Zn(II) and Hg(II) were not (Changela *et al.* 2003). Both CueR and ZntR bind their sensed metal within a metal binding loop located between the dimerization helix and domain and C-terminal two turn α -helix but primary sequence differences in these regions are proposed to tune the selectivity of these proteins (Changela *et al.* 2003) (Figure 1.5). Cu(I) bound to CueR is coordinated in a linear geometry between two cysteine ligands which define the ends of the metal binding loop (Figure 1.5). Zn(II) binds to ZntR in an unusual dinuclear site where both zinc atoms are bound tetrahedrally utilising using ligands derived from the metal binding loop and a cysteine residue (Cys79') located at the N-terminal end of the dimerization helix of the opposite monomer (Changela *et al.* 2003) (Figure 1.5). In CueR the residue equivalent to ZntR Cys79 is replaced by a serine (Ser77), this residue extends into the metal binding loop and helps create a shielded environment for Cu(I) (Changela *et al.* 2003) (Figure 1.5). Thus discrimination between monovalent and divalent metals may be partially achieved through the creation of environments that favour binding of monovalent metals through the limited availability of side chain ligands and creation of a shielded environment for divalent metals through the availability of metal coordinating side chains (Changela *et al.* 2003). In CueR the two sulphur copper centre has an overall negative net charge, it is thought this charge is neutralised through side chain interactions and the positioning of Cys120 over the helix dipole created by the C-terminal short α -helix (Changela *et al.* 2003) (Figure 1.5). These interactions would lead to charge neutrality when a monovalent ion is bound but not a divalent ion and this may explain why Hg(II) is not

activatory despite the ability of Hg(II) to adopt a linear geometry in a dithiolate environment (Changela *et al.* 2003). Selective response in the metal regulated sub-group of the MerR family appears to be correlated with the adoption of a native metal chelate however due to a lack of structures of DNA bound protein in both the activated and inactivated form the details of how effector binding controls allostery awaits discovery.

1.8 Fur family

The Fur (ferric uptake regulator) family of proteins represents another widespread family of cytosolic metal sensors with a recent survey suggesting there are ~800 homologues represented across the prokaryotic kingdom (Lee & Helmann. 2007). *E. coli* Fur was first described as an iron dependent repressor of iron uptake genes, first inferred by genetic methods (Hantke. 1981; Bagg & Neilands. 1985) then demonstrated using an *in vitro* coupled transcription-translation system (Bagg & Neilands. 1987). Early studies of Fur led to a model where coordination of Fe(II) by Fur led to DNA binding by Fur at a 19 bp inverted repeat motif termed the ‘Fur box’ typically found in the operator-promoter region of regulated genes, thereby occluding access to the promoter by RNA polymerase (Lee & Helmann. 2007). Later analysis of the ‘Fur boxes’ found in the operator-promoter regions of genes regulated by Fur in *B. subtilis* revealed the presence of two overlapping 7-1-7 inverted repeat motifs in an extended 21 bp binding site and the proposal that two Fur dimers interact with the ‘Fur box’ each binding one of the two 7-1-7 motifs on opposite faces of the DNA helix (Baichoo & Helmann. 2002).

Subsequently it has been discovered that the regulon of Fur proteins often expands beyond simply control of iron uptake and different regulatory mechanisms, both negative and positive, by Fur have been described (Lee & Helmann. 2007) (Section 1.8.2). Additionally, members of this family have evolved to sense metals other than iron and signals other than direct binding of a metal ion (Sections 1.8.3 and 1.8.4). The fold of this family of proteins consists of two domains: an N-terminal DNA binding domain and a C-terminal dimerization domain (Pohl *et al.* 2003) (Figure 1.6).

1.8.1 Metal binding sites of Fur proteins

Despite the discovery of this protein family more than twenty years ago controversy over the number and nature of metal binding sites in this protein family is only just

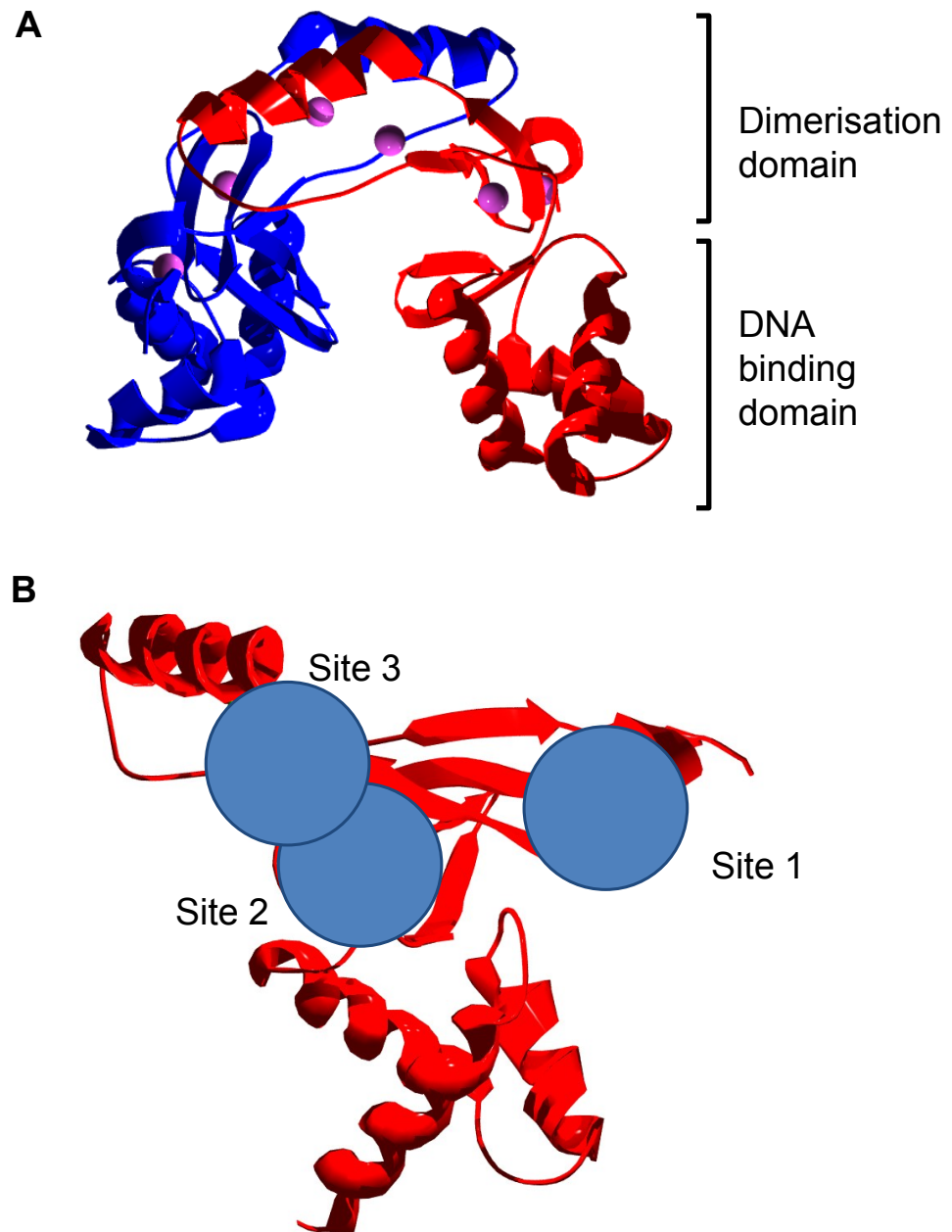


Figure 1.6. *S. coelicolor* Zur structure. A. Structure of *S. coelicolor* Zur dimer with full occupancy of the zinc (represented as purple spheres) binding sites. The individual chains of the dimeric assembly are differently coloured and the location of the N-terminal DNA-binding domain and the C-terminal dimerisation domain are indicated. B. A single monomer of *S. coelicolor* Zur showing the location and amino acid side chains of site 1 (Cys90, Cys93, Cys130, Cys133), site 2 (Asp65, Cys79, His85, His87) and site 3 (His84, His86, Glu105, His122) in order to highlight the proximity of sites 2 and 3. Models were created using coordinates from PDB file 3MWM (Shin *et al.* 2011).

beginning to be resolved. In addition to a regulatory metal binding site it is known that many members of the Fur family, including *E. coli* Fur, contain a structural zinc ion which is required for correct folding (Jacquamet *et al.* 1998; Althaus *et al.* 1999). XAS analysis suggest a $S_2(N/O)_2$ coordination environment for Zn(II) in *E. coli* Zur whereas in some other Fur homologues Zn(II) is coordinated in a S_4 environment (Lee & Helmann. 2006a). The metal binding sites of Fur were first visualised in the crystal structure of *Pseudomonas aeruginosa* Fur which was crystallised coordinated with zinc (Pohl *et al.* 2003). This structure revealed the presence of two metal binding sites, Zn(II) in one of the sites was reported as readily exchangeable with Fe(II) whereas the other was not leading to the assignment of the first site (later named site 3) as the regulatory Fe(II) sensing site and second site (later named site 2) as the structural zinc site (Pohl *et al.* 2003) (Figure 1.6). In fact *P. aeruginosa* Fur lacks a structural zinc site (termed site 1), Zn(II) can readily be removed from site 2 by EDTA and mutation of liganding histidine residues in the proposed sensory site of *P. aeruginosa* results in a protein which retains iron responsiveness whereas mutation of a liganding histidine residue in the proposed structural site abolishes iron responsiveness (Lewin *et al.* 2002). This, combined with the fact that another conserved histidine residue in the proposed structural site of *P. aeruginosa* Fur is required for iron responsiveness in *V. cholerae* (Lam *et al.* 1994), *B. subtilis* (Bsat & Helmann. 1999) and *S. typhimurium* Fur (Hall & Foster. 1996), led to the suggestion that site 2 may represent the sensory site (Lee & Helmann. 2007). The exact roles of site 2 and 3 in metal sensing are only just being elucidated. Site 2 corresponds to the regulatory metal sensing site in *B. subtilis* Fur homologues PerR (Ma *et al.* 2011b) and Zur (Ma *et al.* 2011a) which sense peroxide stress and zinc respectively (Bsat *et al.* 1998; Gaballa & Helmann. 1998). No metal binding to site 3 for either protein was detected (Ma *et al.* 2011a and b). In contrast *B. subtilis* Fur has recently been shown to bind metal ions with a physiologically relevant affinity at both sites 2 and 3 and occupancy of both sites is required for high affinity DNA binding (Ma *et al.* 2012). The close proximity of the metal binding sites observed in the *P. aeruginosa* Fur structure and later structures of this family of proteins (Figure 1.6) combined with the redundancy of site 3 in some homologues and the lack of a structural zinc ion in some homologues, likely explains the difficulty in attempts to identify metal coordinating residues in this protein family (Jacquamet *et al.* 2008).

1.8.2 *Regulatory mechanisms of Fur proteins*

In addition to the classical iron dependent repressor mode of action of Fur, other mechanisms have to come to light which greatly extend the regulatory potential of Fur. Data suggesting a positive regulatory role for Fur was published as early as 1994 with proteomic analysis of a *fur* mutant strain of *V. cholerae* revealing that the expression of some genes was dependent on both iron and Fur (Litwin & Calderwood. 1994). Positive regulation by Fur is known, in a sub-set of cases, to be mediated by the action of anti-sense regulatory small RNAs (sRNA) the best known example of which is RyhB from *E. coli* (Lee & Helmann. 2007). RyhB is a 90 nt sRNA that is repressed by Fur in an iron dependent manner (Massé & Gottesman. 2002). Under conditions where intracellular iron availability is low or in *fur* mutants transcription of RyhB is de-repressed and this down-regulates the production of proteins encoded by the RNA targets of RyhB (Massé & Gottesman. 2002). This is thought to happen via a post-transcriptional mechanism involving RyhB binding to target coding RNAs which encourages degradation (Massé *et al.* 2003). RhyB has a large regulon consisting predominantly of iron containing enzymes and iron storage proteins (Massé *et al.* 2005). Down-regulation of non-essential iron containing enzymes and iron storage proteins under conditions of low iron availability allows *E. coli* to remodel its proteome to make more efficient use of available iron, this is termed the ‘iron sparing response’ and is thought to be important for maintenance of iron homeostasis in both prokaryotic and eukaryotic organisms (Massé & Arguin. 2005; Lee & Helmann. 2007).

Fur also has been shown to act in a directly positive regulatory manner. *Neisseria meningitidis* Fur regulates the expression of some genes in a classical manner of Fur family proteins but additionally appears to act as a positive regulator in other cases (Delaney *et al.* 2004). For positively regulated genes it was proposed that iron bound Fur binds sequences upstream of the RNA polymerase binding site and therefore does not interfere with RNA polymerase promoter interaction (Delaney *et al.* 2004). In fact it has been suggested that activation of transcription in these cases involves direct interaction between iron loaded Fur and RNA polymerase (Delaney *et al.* 2004). There is also evidence for the binding of Fur to DNA in the iron free state. In *Helicobacter pylori* the expression of the iron storage protein ferritin is activated by iron in a Fur dependent manner, expression is constitutive in a *fur* mutant suggesting that Fur directly represses the expression of the gene and this repression is alleviated upon the binding of iron by Fur (Delaney *et al.* 2001). Binding of apo-Fur to the promoter of this ferritin

gene and iron mediated dissociation has also been demonstrated with *in vitro* footprinting assays (Delaney *et al.* 2001).

The wide range of genes shown to be regulated in both negative and positive manners by Fur has led to Fur being referred to as a global regulator of iron homeostasis. In some bacteria Fur has been reported to respond to nitric oxide (D’Autreaux *et al.* 2002; Moore *et al.* 2004; Richardson *et al.* 2006) and a recent study has identified Fur box sequences upstream of genes involved in diverse metabolic pathways such as sulphur metabolism, methane metabolism, sucrose metabolism and lipopolysaccharide biosynthesis (Sridhar *et al.* 2012) suggesting that Fur may play a role as a global regulator beyond iron homeostasis or that iron homeostasis requires global regulation of a diversity of metabolic processes.

1.8.3 Zur, a zinc sensing member of the Fur family

Zur proteins represent perhaps the best characterised sub-branch of the Fur family. The discovery of a Fur homologue responsive to zinc *in vivo* was first reported concurrently in *B. subtilis* (Gaballa & Helmann 1998) and *E. coli* (Patzner & Hantke. 1998). In *E. coli* Zur was first characterised as a regulator of the ATP binding cassette (ABC) type zinc uptake system ZnuACB (Patzner & Hantke. 1998). Under conditions of zinc sufficiency Zur binds the bi-directional promoter region of *znuA* and *znuBC* repressing transcription of this zinc uptake system, under conditions of zinc starvation Zur dissociates from the promoter allowing transcription (Patzner & Hantke. 1998 and 2000). *B. subtilis* Zur was originally shown to regulate the expression of a zinc uptake ABC transporter and an operon encoding three genes of largely unknown function (*yciABC*) (Gaballa & Helmann. 1998; Gaballa *et al.* 2002). Subsequent work has led to the elucidation of a larger Zur regulon in various organisms (Panina *et al.* 2003; Maciag *et al.* 2007; Shin *et al.* 2007; Schröder *et al.* 2010; Napolitano *et al.* 2012) and the suggestion that by analogy to Fur, Zur may act as a global regulator of zinc homeostasis. A key observation, first shown in *B. subtilis* and subsequently in other organisms, is that Zur represses the expression of genes encoding homologues of ribosomal proteins (Panina *et al.* 2003). Under conditions of zinc deficiency *ytiA* is derepressed, this gene encodes a non-zinc containing paralogue of ribosomal protein L31, YtiA replaces RpmE, the zinc containing L31 paralogue making the zinc bound by this protein available to the cell (Akanuma *et al.* 2006; Gabriel & Helmann. 2009). The high abundance of ribosomes in rapidly growing cells means ribosomally bound zinc represents a significant zinc reservoir that can be mobilised under zinc deficiency (Lee & Helmann. 2007). *E. coli*

and *B. subtilis* Zur both contain two physiologically relevant zinc binding sites; site 1 - the structural zinc site which is refractory to removal by EDTA and site 2 - the sensory site which is highly exchangeable (Outten *et al.* 2001; Ma *et al.* 2011a). In contrast it has been shown that zinc occupancy of sites 2 and 3 of *Streptomyces coelicolor* Zur fine tunes the affinity of the protein for different promoters (Shin *et al.* 2011).

1.8.4 *Fur* homologues that sense other metals/ non-metal signals

In addition to the widespread zinc responsive Zur branch of the Fur family, members of the Fur family that sense other metals have been described. A Fur homologue from *Rhizobium leguminosarum* which represses the transcription of an ABC type manganese uptake system under manganese replete but not iron replete conditions was identified and named Mur (manganese uptake regulator) (Diaz-Mireles *et al.* 2004).

Nur represents a nickel responsive member of the Fur family first identified as a nickel dependent repressor of the iron containing superoxide dismutase (SOD) gene *sodF* and the nickel uptake system *nikABCDE* in *Streptomyces coelicolor* (Ahn *et al.* 2006). The upregulation of a nickel containing SOD, *sodN*, occurs concurrently with the repression of *sodF* and so this can be thought of as an iron sparing mechanism.

PerR and Irr represent members of the Fur family that do not respond to metal ions but to peroxide stress and heme respectively (Lee & Helmann. 2007). The PerR regulon protects cells from peroxide mediated damage and includes the major vegetative catalase encoded by *katA* (Chen *et al.* 1995). PerR contains two metal binding sites, a structural zinc site (Lee & Helmann. 2006a) and a sensory site which can bind both iron and manganese but only the iron form of the protein is sensitive to peroxides (Herbig & Helmann. 2001). PerR utilises a metal-catalysed oxidation reaction of two of the histidine residues proposed to coordinate iron (Lee & Helmann. 2006b). This is thought to weaken the iron binding affinity of the sensory site leading to loss of iron from the site and therefore de-repression of the target genes. Irr regulates the expression of a heme biosynthesis enzyme and thus iron utilisation in heme biosynthesis (Hamza *et al.* 1998). Under iron deplete conditions, Irr binds DNA, repressing transcription of its target gene, it is proteolytically degraded in the presence of iron allowing transcription (Qi *et al.* 1999). Heme is proposed to be the actual effector of protein degradation and can be delivered to the heme binding site of Irr through an interaction with ferrochelatase (Qi & O'Brian. 2002). Irr therefore senses iron availability indirectly by monitoring the availability of iron containing heme.

1.8.5 Selectivity of metal sensing in Fur family proteins

Selectivity in Fur family proteins appears to be governed by a combination of allostery, affinity and access. In addition to iron; manganese, cobalt, and zinc have been shown to be competent to activate the binding of DNA by *E. coli* Fur *in vitro* (Mills & Marletta 2005) and both manganese and zinc can also activate *B. subtilis* Fur for DNA binding *in vitro* (Ma *et al.* 2012). However, *in vivo* only iron and manganese are found to be activatory (Hantke. 1987). Iron is thought to bind to Fur in at least one 5 or 6 coordinate site (Jacquamet. 1998). Manganese and cobalt can both readily adopt such coordination geometry but zinc tends to adopt a four-coordinate tetrahedral geometry, although 5 and 6 coordinate zinc has been visualised in the crystal structures of Fur family proteins (Pohl *et al.* 2003; Dian *et al.* 2011). Coordination chemistry alone is unlikely to be the sole determinant of selectivity for Fur.

Comparison of the metal binding constants of Fur with the estimated levels of intracellular metal ions suggested that only iron and manganese may be present at a sufficient level to activate Fur for DNA binding *in vivo* (Mills & Marletta. 2005; Lee & Helmann. 2007). A recent study by Ma *et al* (2012) has provided insight into how a combination of affinity and access may determine metal sensing selectivity of *B. subtilis* Fur. *B. subtilis* Fur requires metal binding at both sites 2 and 3 to be activated for DNA binding; whilst site 3 has a zinc affinity in the picomolar range, site 2 has a zinc affinity in the micromolar range (Ma *et al.* 2012). This means site 2 is unlikely ever to become occupied with zinc as *B. subtilis* Zur, which is presumed to control the buffered intracellular concentration of zinc, has an affinity in the picomolar to femtomolar range (Ma *et al.* 2011a). In *B. subtilis* the buffered concentration of manganese is thought to be controlled by MntR, the manganese affinity of MntR is only marginally tighter than that of Fur and therefore it was proposed that under conditions where manganese homeostasis is perturbed, Fur may respond to manganese (Ma *et al.* 2012). The expression of Fur in *B. subtilis* is regulated by PerR (Faulkner *et al.* 2012) and in a *perR* mutant where Fur levels are elevated Fur was shown to respond to manganese, the mode of action of Fur as a co-repressor meaning mass action can increase the sensitivity of metal detection (Ma *et al.* 2012).

Work with Mur supports the proposal that metal ion availability is a key determinant of selectivity in the Fur family of proteins. *In vitro* it has been shown that in addition to manganese; iron, zinc, and cobalt can all activate Mur to bind DNA (Bellini & Hemmings. 2006) however *in vivo* these metals cannot activate Mur for DNA binding

(Díaz-Mireles *et al.* 2005). When Mur was transferred from *R. leguminosarum* to *fur* deficient *E. coli*, iron but not manganese activated Mur for DNA binding, presumably due to an increased buffered concentration of iron and potentially a buffered manganese level lower than that found in the native host cell (Díaz-Mireles *et al.* 2005). This study has analogy to findings with NmtR (Cavet *et al.* 2002) and DtxR (Guedon & Helmann. 2003) where transfer to heterologous host cell resulted in altered selectivity of metal sensing and exemplify the notion that selectivity evolves in the context and as a result of the cellular environment (Waldron & Robinson. 2009).

As well as the combination of two sensory sites having an effect on the selectivity of *Bacillus subtilis* Fur, residues in an equivalent location to site 3 on *B. subtilis* PerR appear to determine selectivity despite the fact that no metal binding to this site occurs (Ma *et al.* 2011b). Mutation of residues in this region were found to result in a protein which although functional as a repressor was unable to sense peroxide stress, consistent with these mutant proteins using manganese rather than iron as a co-repressor (Ma *et al.* 2011b). These results suggested the iron binding affinity of site 2 had been weakened and could therefore not compete for buffered iron. Consistent with this hypothesis a site 3 mutant with a confirmed weakened affinity for iron regained the ability to sense peroxide stress when transferred to a *fur* mutant strain where the buffered concentration of iron is predicted to be maintained at a higher concentration (Ma *et al.* 2011b).

1.9 Other metalloregulator families

NikR, DtxR and CopY represent the other three major classes of metal sensing transcriptional regulators present in prokaryotes. NikR was first identified as a nickel dependent repressor of the high affinity NikABCDE nickel uptake system in *E. coli* (DePina *et al.* 1999; Chivers & Sauer. 1999 and 2000). Despite the ability to bind several metal ions *in vitro* (Wang *et al.* 2004; Leitch *et al.* 2007), NikR is only responsive to nickel *in vivo* (Leitch *et al.* 2007). This specificity was found to correlate with the coordination geometry adopted by metal ions when bound to NikR, with only Ni(II) and Cu(II) (which is thought to be reduced to Cu(I) in the reducing environment of the cytosol) capable of adopting a square planar geometry (Leitch *et al.* 2007; Phillips *et al.* 2008).

CopY was first identified as a metalloregulator involved in regulation of genes involved in copper homeostasis in *Enterococcus hirae* (Odermatt & Solioz. 1995). The mode of

action of the protein involves acting as a co-repressor of expression when zinc is bound to a C-terminal cluster of cysteine residues and dissociating from DNA upon delivery of copper to this cluster which is mediated by the copper chaperone CopZ (Cobine *et al.* 1999, 2002a and b). Selectivity of metal sensing by this protein is likely enforced by the selective interaction with the copper chaperone.

C. diphtheriae DtxR represents the founding member of a family of metal dependent co-repressors (Schmitt *et al.* 1992). Selectivity in this protein family is related to the ability to form a native metal chelate with iron, cobalt, manganese and nickel, all of which readily adopt octahedral coordination geometries (Spiering *et al.* 2003), all more effective at activating DtxR for DNA binding than Zn(II) (Tao & Murphy. 1992), which does not readily adopt octahedral coordination geometry. As mentioned earlier access to metal is an important determinant of metal sensed by this family and indeed must be an important determinant across all families of metal sensors.

1.10 *Synechocystis* sp. PCC 6803 as a model organism for studying metalloregulation

The cyanobacterium *Synechocystis* sp. PCC 6803 (henceforth referred to as *Synechocystis*) isolated from a fresh water lake in 1968 was one of the first organisms to have its genome completely sequenced, the ~3.6 Mbp genome encodes 3,317 proteins and the total of protein encoding open reading frames is taken to 3,725 when the seven plasmids are considered. The early availability of the genome sequence combined with the natural transformability of *Synechocystis* has made it an ideal model organism for exploring various metabolic processes including metal homeostasis.

1.10.1 *The metal requirements of Synechocystis*

The photosynthetic machinery of *Synechocystis* and other cyanobacteria places an elevated demand on these organisms for metals. The requirement of vast amounts of iron and manganese needed for photosynthesis contributes to an iron quota which is 10 times greater than *E. coli* (Keren *et al.* 2004) and a manganese requirement which is 100 times greater than that of *Rhodobacter captulatus* (Keren *et al.* 2002). The carbon dioxide concentrating mechanism required for efficient function of RuBisCO in carbon fixation relies on carbonic anhydrase (Cannon *et al.* 2010) which is predicted to be a zinc requiring enzyme in *Synechocystis* (Barnett *et al.* 2012). *Synechocystis* has an

unusual prokaryotic cytoplasmic requirement for copper both for the soluble electron carrier plastocyanin (which can be functionally substituted with the iron containing cytochrome *c*₆) and for cytochrome oxidase (Tottey *et al.* 2001). Cobalt is needed for the production of vitamin B₁₂ which may be required for the function of a methionine synthase (Tanioka *et al.* 2009).

Nickel is a rarely utilised element in biology with reported use in enzymes restricted to less than 10 examples and most bacteria utilising less than a handful of these enzymes (Li & Zamble. 2009). The genome of *Synechocystis* encodes potentially three nickel requiring enzymes. *Synechocystis* produces a [NiFe] bidirectional hydrogenase which has a bias toward hydrogen production (McIntosh *et al.* 2011). Although the precise physiological role of the enzyme is still under debate it is proposed to act as an electron valve dissipating surplus reducing potential produced during photosynthesis, this role is further discussed in Section 6.9.2 (Appel *et al.* 2000). *Synechocystis* is a non-nitrogen fixing cyanobacterium and therefore in the absence of a source of nitrate requires ammonium for growth which can be produced by the nickel requiring enzyme urease from urea (Valladares *et al.* 2002). The glyoxalase system is composed of two enzymes, glyoxalase I and II (GlxI and II) which convert harmful α -ketoaldehydes into 2-hydroxycarboxylic acids using an intracellular thiol such as glutathione as a co-substrate (Suttisansanee & Honek. 2011). GlxI from *Pseudomonas putida* was reported as requiring zinc as a co-factor (Saint-Jean *et al.* 1998) in common with GlxI from yeast and mammals (Aronsson *et al.* 1978). However GlxI from *E. coli* (Clugston *et al.* 1998), and subsequently GlxI from other prokaryotic organisms, has been shown to be a nickel (or cobalt) requiring enzyme and it is now thought that the majority of bacterial GlxI enzymes with the exception of those from pseudomonads are likely nickel or cobalt requiring (Suttisansanee & Honek. 2011). A BLAST search of the genome of *Synechocystis* with the sequences of *E. coli* and *P. putida* GlxI as search terms reveals the presence of a GlxI homologue in *Synechocystis* (Slr0381) (Figure 1.7). The length of bacterial GlxI proteins is a good indicator of the metal requirement of the enzyme as zinc requiring GlxI enzymes possess an N-terminal extension and extra loop regions (Suttisansanee & Honek. 2011). At 131 aa Slr0381 fits the criteria for being predicted to require a nickel or cobalt co-factor and the N-terminal extension and loop regions present in zinc requiring *P. putida* GlxI are absent in Slr0381 (Figure 1.7).

```
Slr0381      -----MFLLEMTIRVGDLDKSLQFYCDILGMNLLRKKDYPSPGE   38
P0AC82      -----MRLLLETMLRVGDLQRSIDFYTKVLGMKLLRTSENPEYK   38
Q88GF8      MSLHDLQTLPGVTAQPDAATAQVFVNLTMLRVKDIEKSLDFYTRVLGFRFLVDKKRDFPEAA   60
              : : *:*:* *::*:** :*:. : . : *.

Slr0381      FTLAFVGYGK-----ESENAVIELTHNWGTD----KYDLGN---GFGF   74
P0AC82      YSLAFVGYGP-----ETEEAVIELTYNWGVD----KYLGT---AYGF   74
Q88GF8      FSLYFLALVDPAQIIPADDтарНQMKSIPGVLELTHNHGTENDADFAYHNGNTDPRGFGF   120
              :.* *: .           :: .*.***.* *: .       * . .     :.**

Slr0381      IALGVEDIYSTCDKIRDKGKVVPREPGMPKHGTTVIAFVEDPDGYKIELIQTSKKD---   131
P0AC82      IALSVDNAAEACEKIRQNGGNVTREAGPVKGGTTVIAFVEDPDGYKIELIEEKDAGRGLG   134
Q88GF8      ICISVPDVRAACARFEEL--EVFPQKRQLQDGRMNHLAFVKDPDGYYVEVIQPTLELG---   175
              *.* :    :* ::.:    :* :        . :***:***** :*:. : ..

Slr0381      -
P0AC82      N 135
Q88GF8      -
```

Figure 1.7. Multiple sequence alignment of Slr0381 with the GlxI sequence of *E. coli* and *P. putida*. Slr0381 was identified as a potential glyoxalase I enzyme (GlxI) via a BLAST search with the sequences of *E. coli* and *P. putida* GlxI sequences (Uniprot identifiers P0AC82 and Q88GF8 respectively). The conserved metal binding residues found in *E. coli* and *P. putida* GlxI and additionally Slr0381 are highlighted in red.

1.10.2 Metalloregulation in *Synechocystis*

The genome of *Synechocystis* encodes proteins from five of the major prokaryotic metal sensing families. The ArsR-SmtB family is represented by ArsR and ZiaR. ArsR regulates the expression of the arsenic resistance operon *arsBHC* in response to As(III) both *in vivo* and *in vitro* (López-Maury *et al.* 2003). Based on the retention of a Cys-X-Cys-X-X-Cys motif in the predicted $\alpha 3$ helix *Synechocystis* ArsR is predicted to sense As(III) through an $\alpha 3$ site. ZiaR is a zinc sensor regulating the expression of a zinc exporting P-type ATPase ZiaA (Thelwell *et al.* 1998). ZiaR contains both $\alpha 3N$ and $\alpha 5$ metal binding sites unusually both of which are required to respond to zinc *in vivo* (Thelwell *et al.* 1998) however ZiaR is able to sense zinc through either site *in vitro* (Patterson. 2010).

CoaR is a cobalt responsive member of the MerR family which regulates the expression of CoaT, a cobalt exporting P-type ATPase (Rutherford *et al.* 1999). The *coaT* promoter has a 20 bp spacing between the -10 and -35 regulatory elements and a deletion of 1 or 2 nucleotides within this region enhanced expression from the promoter but resulted in the loss of activation by cobalt mediated by CoaR (Rutherford *et al.* 1999). These observations imply CoaR employs a similar under-winding mechanism to MerR. The N-terminal MerR-like DNA-binding domain of CoaR is fused to a C-terminal precorrin isomerase domain, an enzyme involved in the B₁₂ biosynthesis pathway and it was inferred that an intermediate of this pathway may be inhibitory to sensing of cobalt by CoaR (Rutherford *et al.* 1999). Besides CoaR the genome of *Synechocystis* encodes an additional MerR homologue, the product of ORF *slr0701*. Phylogenetically this protein clusters with other MerR proteins known or predicted to sense Cu(I) (Permina *et al.* 2006) however the presence of two cysteine residues at the start of the predicted dimerisation helix (strongly conserved in zinc sensing MerR homologues (Changela *et al.* 2003)) would argue against this prediction (Figure 1.5). Additionally the metal binding loop appears to start and end with a cysteine and a histidine residue respectively, rather than the usual cysteine (Figure 1.5). A similar motif is observed in MerR regulators of several species of the genus *Vibrio* and these regulators are annotated as ZntR or zinc responsive MerR, however extreme care needs to be exercised with automatically annotated gene functions (Haas *et al.* 2009). A regulatory element corresponding to a MerR-type binding site could not be identified upstream of this gene (Permina *et al.* 2006) which also appears to be genetically unlinked from its target so it is currently unclear what metal (if any) this regulator is responsive to.

There are three Fur-like proteins encoded in the genome of *Synechocystis*. ORF *sll1937* is divergent from the *znuABC* high affinity zinc uptake system and inactivation of this gene resulted in the constitutive expression of the *znuABC* operon (Pakrasi *et al.* 2002). The product of *sll1937* was found to associate with the promoter region of the *znuABC* operon in a zinc dependent manner and was therefore designated Zur (Patterson. 2010; Tottey *et al.* 2012). *Synechocystis* Zur contains one structural zinc atom per monomer and has one sensory site per monomer (Patterson. 2010; Tottey *et al.* 2012). The product of *sll1738* is a PerR homologue and regulates a suite of genes in response to peroxide stress (Kobayashi *et al.* 2004; Li *et al.* 2004). The third Fur homologue encoded in the *Synechocystis* genome (Sll0567) is likely to represent an iron sensing Fur. The protein shares considerable homology to the iron sensing Fur of *Synechococcus* sp. PCC 7942 (Ghassemian & Straus. 1996) and in common with the *fur* gene of *Synechococcus* sp. PCC 7942 a fully segregated mutant strain with a disruption of *sll0567* could not be produced (Kunert *et al.* 2003), suggesting the role played by the product of this gene is indispensable. In spite of not being able to produce a fully segregated mutant the inability of a partially segregated strain to fully repress expression of the iron responsive operon *isiAB*, which contains a putative Fur box in its promoter region, strongly suggests a role for Sll0567 as iron sensing Fur (Kunert *et al.* 2003). One CsoR-RcnR homologue is encoded in the genome of *Synechocystis*, the product of this gene (*sll0176*) was a major focus of this study. A CopY-like protein is encoded in the genome of *Synechocystis* however this is unlikely to function in a manner analogous to CopY, this is discussed further in Section 6.9.1. There are no representatives of the NikR or DtxR families encoded in the genome of *Synechocystis*.

The presence of three two component systems that regulate genes of metal homeostasis in *Synechocystis* is also known. Two component systems are composed of a membrane localised histidine kinase and a response regulator (Gao & Stock. 2009). Upon signal detection in the periplasm the histidine kinase is autophosphorylated, the phosphate group is then transferred to the response regulator which is activated to act as a repressor or activator of transcription (Gao & Stock. 2009). The NrsRS system has been shown to regulate the expression of the *nrs* operon of genes involved in nickel resistance and is discussed in further detail elsewhere in this thesis (Section 3.5, 6.1 and 6.2) (García-Domínguez *et al.* 2000; López-Maury *et al.* 2002). The ManRS system regulates the expression of the *mntCAB* high affinity manganese uptake system in response to manganese deficiency (Ogawa *et al.* 2002; Yamaguchi *et al.* 2002). Recently the characterization of a third metal responsive two component system,

CopRS, was reported which regulates the expression of a putative copper exporting RND-type system (Giner-Lamia *et al.* 2012). Intriguingly this system may sense copper in the thylakoid as well as the periplasm (Giner-Lamia *et al.* 2012). The mechanism by which any of these systems sense metal, or how selectivity of metal sensing is achieved, is currently unknown.

1.11 Project aims

The aims of this project were two-fold:

1). To work toward a complete understanding of the metalloregulatory circuits of *Synechocystis*. The extraordinary demand of *Synechocystis* for metal ions coupled with a complete understanding of the metalloregulatory circuits of this organism would represent a very powerful tool for understanding how a cell coordinates the vast range of processes that ultimately underpin the catalytic chemistry of life. Much effort has been expended to delineate the metalloregulatory circuits of *Synechocystis* particularly in regard to the cytosolic metalloregulatory proteins and the genes they regulate. Therefore characterisation of one or more of the remaining uncharacterised metalloregulators would represent a significant step toward achieving the above stated aim.

Prior to the start of this work there existed, in *Synechocystis*, only three genes encoding proteins belonging to the seven major families of metalloregulatory proteins that remained to be characterised: *slr0176* belonging to the CsoR-RcnR family, *slr0701* belonging to the MerR family and *slr0240* belonging to the CopY family. Due to the more recent discovery of the family CsoR-RcnR proteins are the least studied group of major prokaryotic metalloregulators. This, coupled with the fact that prior to the start of this work *slr0176* had been cloned into an expression vector meant *slr0176* represented the natural candidate to focus efforts on. The most immediate question that needed to be answered with regard to this protein was the metal(s) sensed and the gene(s) regulated. This family of metalloregulators was initially divided into two distinct branches; those that acted as copper sensors and those that acted as nickel and cobalt sensors (Section 1.5). Members of these two sub-branches display distinct spectral properties upon metal binding and it was therefore hypothesised that it may be possible to assign a role for the product of *slr0176* based on these spectral properties.

In *Synechocystis* *coaT* encodes a cobalt exporting P₁-type ATPase for which the regulator, CoaR, is known (Rutherford *et al.* 1999). There is one known determinant of nickel resistance, the operon *nrsBACD* (García-Domínguez *et al.* 2000), expression of which has shown to be under the control of the two component system NrsRS thought to detect periplasmic nickel (and cobalt) (López-Maury *et al.* 2002). The copper exporting P₁-type ATPase PacS and the soluble electron carrier plastocyanin are both likely or known (Section 3.4.2) to be transcriptionally regulated by the presence of copper by an unknown mechanism and therefore the genes encoding these two proteins represented plausible targets of regulation by the product of *slr0176*.

How do closely related proteins selectively respond to different metals? Upon identifying the target regulated by Slr0176 and in response to what metal(s) the next step would be to understand what allows the selective response of this protein. Access, allostery and affinity (Tottey *et al.* 2005) are known to be determinants in the selectivity of metalloregulatory proteins. Prior to this work it had been shown that the copper sensing *B. subtilis* CsoR was less competent to respond to nickel and zinc *in vitro* due to a smaller free energy coupling constant of metal binding and DNA binding (Ma *et al.* 2009a). Could a similar explanation be invoked to explain the selectivity of the protein encoded by *slr0176*? Characterised copper and nickel/ cobalt sensing members of this family of metalloregulators have distinct but overlapping primary metal coordination spheres. Through the use of site directed mutagenesis coupled with spectral analysis and other metal binding studies it was hypothesised that it may be possible to identify primary coordination sphere ligands in the product of *slr0176* and the role these ligands play in determining the selective response of this protein. In addition it may be possible to use these assignments to refine previously proposed methods for predicting the function of uncharacterised members of this family. Access as dictated by the complement of other metalloregulators encoded by a cell has been hypothesised to play an important role in determining the selective response of some metalloregulators and the testing of the relevance of this factor in determining the selective response of the protein encoded by *slr0176* was intimately linked to the second aim of this work.

2). It is a widespread belief that the buffered intracellular concentration of a metal ion is closely correlated with the affinity of the corresponding metalloregulator for that metal. When the ‘set point’ that triggers a transcriptional response is reached (i.e. when the buffered concentration approximates to metalloregulator K_D) the expression (or repression) of genes of metal homeostasis will buffer the intracellular concentration

around this set point (Figure 1.1) accepting that there may be a lag in response due to kinetic effects. A correlation between metalloregulator affinity and buffered metal concentration was observed by electron paramagnetic resonance (EPR) studies of free or loosely buffered iron in *Escherichia coli* (Keyser & Imlay, 1996). Also studies of the *E. coli* Zn(II) sensor ZntR showed that the buffered concentration of Zn(II) at which ZntR activated transcription in an *in vitro* run off assay (Outten & O'Halloran, 2001) closely matched the Zn(II) affinity of ZntR (Hitomi *et al.* 2001). In some instances the metal specificity of metalloregulators has been shown to change upon transfer to a heterologous host (Section 1.6.3), this encouraged the notion that the 'set point' of metal sensors may reflect the cellular environment in which the sensor evolved (Waldron & Robinson, 2009). This suggests that selectivity in metal sensing could be achieved by a given sensor having an affinity tighter than the other sensors in the cell for its cognate element. This would allow intracellular levels of this element to be buffered such that the other sensors in the cell never gain access to it (Waldron & Robinson, 2009). Such a method of regulation would be of particular importance where a non-cognate metal can be activatory, as is the case with *Synechocystis* ZiaR and Zur with Co(II) (Patterson *et al.* 2013). Testing this 'relative affinity hypothesis' represented the second major objective of this work.

Previous pairwise comparisons between metal sensor proteins from the same organism have suggested that the relative order of affinity for metal binding may follow the same order as selectivity. This remained to be tested in earnest across a number of metal sensor proteins from the same organism and across a range of metals. In addition this hypothesis is equally applicable to the acquisition of metals by metallochaperones which deliver metals to a substantial number of targets. Testing the 'relative affinity hypothesis' across a number of metallochaperones from the same organism may help distinguish between a kinetic or thermodynamic model for acquisition of metals by these metallochaperones and therefore their targets. Can these proteins selectively obtain their metal cargos directly from cytosolic metal pools or must selective interaction with metal importers be invoked? Early success with the characterisation of the product of *slr0176* meant the project focussed on relative affinity between metalloregulators rather than metallochaperones.

By determining and comparing the metal affinities of a number of metalloregulators from a common cell, under the same conditions, for both their cognate and non-cognate metals the 'relative affinity hypothesis' was experimentally tested on a larger scale than

previously attempted and allowed identification of cases where alternative explanations must be sought to explain selectivity.

Chapter 2. Methods and Materials

2.1 Reagents and chemicals

All reagents and chemicals were purchased from standard commercial suppliers (Sigma-Aldrich and Melford Laboratories Ltd) unless otherwise stated. Enzymes were obtained from New England Biolabs, Fermentas and Promega. All solutions were prepared using nanopure (double deionised) water.

2.2 Maintenance of bacterial strains

2.2.1 Bacterial strains and growth conditions

The *E. coli* strain DH5 α (Genotype: *supE44* Δ *lacU169* (ϕ 80 *lacZ* Δ M15) *hsdR17* *recA1* *endA1* *gyrA96* *thi-1* *relA1*) was used for all gene cloning steps and the *E. coli* strain BL21(DE3) (Genotype: *hsdS* *gal* (λ cIts857 *ind* 1 *Sam7* *nin5* *lacUV5*-T7 gene *I*) for overexpression of recombinant proteins (Sambrook and Russell. 2001).

E. coli cultures were grown in Luria-Bertani (LB) medium (Sambrook and Russell. 2001) at 37 °C with orbital shaking at approximately 180 rpm for liquid cultures. Plated *E. coli* cultures were incubated overnight to allow formation of colonies. All media for bacterial culturing was sterilised by autoclave prior to use.

Kanamycin (50 μ g ml⁻¹) and carbenicillin (100 μ g ml⁻¹) were used as selectable markers for *E. coli* strains transformed with pET29a and pGEM derivatives respectively.

2.2.2 Production of competent cells

Competent cells were produced using a variation of the CaCl₂/MgCl₂ method (Sambrook and Russell. 2001). All salt solutions used were sterilised by passing through a sterile 0.22 μ m filter prior to use. A previously prepared aliquot of competent cells was streaked on an LB plate and a colony from this plate was used to inoculate 5 ml of LB media which was incubated overnight with shaking. 1 ml of this overnight culture was used to inoculate 100 ml of LB media which was then cultured until an optical density (OD_{600 nm}) of ~0.5 was reached. Cells were pelleted in a Beckman Coulter Avanti J-20 XP centrifuge using a JLA 10.500 rotor (2,500 rpm, 10 min, 4 °C). The supernatant was discarded and the cell pellet was resuspended in 25 ml of ice cold

100 mM MgCl₂ and incubated on ice for 5 min. Cells were then pelleted in sterile 50 ml centrifuge tubes in a Beckman Coulter Allegra X-22R benchtop centrifuge (2,500 rpm, 10 min, 4 °C). The supernatant was discarded and the cell pellet was resuspended in 5 ml of ice cold 100 mM CaCl₂ before addition of a further 45 ml of ice cold 100 mM CaCl₂. The resuspended pellet was incubated on ice for 1 h and cells pelleted in sterile 50 ml centrifuge tubes in a Beckman Coulter Allegra X-22R benchtop centrifuge (2,500 rpm, 10 min, 4 °C). The supernatant was discarded and the pellet was resuspended in 2 ml of ice cold 85 mM CaCl₂ with 15 % v/v glycerol (sterilised by autoclave) solution. This cell suspension was divided into 50 µl aliquots (on ice), flash-frozen in liquid nitrogen and stored at -80 °C until required.

2.2.3 Transformation of competent cells to antibiotic resistance

50 µl of competent cells were incubated with 1 µl (unless otherwise stated) of plasmid DNA (typically produced by ‘miniprep’ see Section 2.3.6) on ice for 30 min. Cells were heat shocked at 42 °C for 1 min using a pre-heated heat block, then returned to ice for further 2 min. Following addition of 500 µl of LB the cells were incubated at 37 °C for 60 min with orbital shaking. Cell cultures were pelleted by centrifugation in a Beckman Coulter Microfuge 18 (14,000 rpm, 10 min). 400 µl of supernatant was removed and the cell pellet was resuspended in the remaining supernatant. These resuspended cells were plated on an LB-Agar plate containing the appropriate antibiotic.

2.3 DNA manipulation

2.3.1 Amplification of DNA by polymerase chain reaction

Polymerase chain reactions (PCR) were prepared to a final volume of 50 µl containing dNTPs (dATP, dTTP, dGTP and dCTP each to a final concentration of 400 µM), 10-100 ng of genomic or plasmid DNA, forward and reverse PCR primers (Table 2.1) both to a final concentration of 0.4 µM, Promega PCR buffer (diluted from a 10 x stock containing 20 mM MgSO₄) and 1.5-3 units of Promega *Pfu* polymerase. All *Synechocystis* genomic DNA used in this work was provided by Dr Kevin Waldron. Reaction volumes were made up to 50 µl with nanopure water. PCR reactions were performed using an appropriate combination of melting, annealing & extension temperatures, cycles and duration using a PCR thermocycler. 95 °C and 72 °C were

Primer name	Description	Sequence (5'-3')
MoeAPro_F	Amplification of <i>moeA</i> upstream region	GAAGTCTACGGTATGCCCATGAAG
MoeAPro_R	Amplification of <i>moeA</i> upstream region and production of <i>moeAPro</i>	GAATGGGCTTGGATAATTTCAACG
MoeAPro+CsoR Box_F	Production of <i>moeAPro</i> and <i>moeAPro+</i>	CGGGTTAAAGTAACGATGAATGG
Ccosu2Pro_F	Amplification of <i>coxB</i> upstream region	GAAATCCCCTTTATCAGCGAAGAC
Ccosu2Pro_R	Amplification of <i>coxB</i> upstream region and production of <i>coxBPro</i>	GAATAGCAAACCTCTATCTCTCGG
CcoPro+CsoR Box_F	Production of <i>coxBPro</i> and <i>coxBPro+</i>	AATTTGGCTGGAGCTTGACCC
T7 Promoter	Production of pGEMCon1	TAATACGACTCACTATAGGG
pGEM-T_rev	Production of pGEMCon1 & 2, <i>moeAPro+</i> and <i>coxBPro+</i>	CAAGCTATGCATCCAACG
pGEMPI_F	Production of pGEMCon2, 3 and 4	ATCACTAGTGCGGCCGCC
pGEMPI_R	Production of pGEMCon3	GATAACAATTTACACAGGAAACA GC
pGEMPI_R2	Production of pGEMCon4	GCTTTACACTTTATGCTTCCGGC
PcPro_F	Production of <i>petEPro</i>	GAATGAGGCTGTATAATCTACGACG GG
PcPro_R	Production of <i>petEPro</i>	GAAACTTCTTGGCGATTGTATCTAT AGGG
PacSPro_F	Production of <i>pacSPro</i>	GAAAGAGTTCCACTGCTGACATCG

Primer name	Description	Sequence (5'-3')
PacSPro_R	Production of <i>pacSPro</i>	GAAGCCATGGTTAATCGTAATACT CAG
slr0750_F	Production of <i>chlNPro</i>	GAATGTTTTACGATTACCAACGAT CAAG
slr0750_R	Production of <i>chlNPro</i>	GAAGGGGCTTGTTGAGCAACAG
nrsDPro_F	Production of <i>nrsDPro</i>	GAAATATTCGATTCAGTACCAAGTA CTATTGCG
nrsDPro_R	Production of <i>nrsDPro</i>	GAATTGTGGGGGTTTGGGGTAG
nrsDProFA_F	Production of <i>nrsDProFA</i> (5' HEX labelled where appropriate)	TCATCAATATCCCCCCTGGGGGCAT AGAATAGA
nrsDProFA_R	Production of <i>nrsDProFA</i>	TCTATTCTATGCCCCCAGGGGGGAT ATTGATGA
H21L_F	InrS His21→Leu 'quikchange' forward primer	GCCCATCCCCATGTCCTGAGCCAAG AATCCTTAC
H21L_R	InrS His21→Leu 'quikchange' reverse primer	GTAAGGATTCTTGGCTCAGGACATG GGGATGGGC
H21E_F	InrS His21→Glu 'quikchange' forward primer	GCCCATCCCCATGTCGAGAGCCAAG AATCCTTAC
H21E_R	InrS His21→Glu 'quikchange' reverse primer	GTAAGGATTCTTGGCTCTCGACATG GGGATGGGC
H21C_F	InrS His21→Cys 'quikchange' forward primer	GCCCATCCCCATGTCTGCAGCCAAG AATCCTTAC
H21C_R	InrS His21→Cys 'quikchange' reverse primer	GTAAGGATTCTTGGCTGCAGACATG GGGATGGGC

Primer name	Description	Sequence (5'-3')
C53A_F	InrS Cys53→Ala 'quikchange' forward primer	GCAGGAAAATCGTCCCGCCCCAGA GGTGTTAATTC
C53A_R	InrS Cys53→Ala 'quikchange' reverse primer	GAATTAACACCTCTGGGGCGGGAC GATTTTCCTGC
H78L_F	InrS His78→Leu 'quikchange' forward primer	GATTAATTTTGGATGACCTGATGA ATGAGTGCATCACCAG
H78L_R	InrS His78→Leu 'quikchange' reverse primer	CTGGTGATGCACTCATTCATCAGG TCATCCAAAATTAATC
C82A_F	InrS Cys82→Ala 'quikchange' forward primer	GACCACATGAATGAGGCCATCACC AGGGCGGGCG
C82A_R	InrS Cys82→Ala 'quikchange' reverse primer	CGCCGCCCTGGTGATGGCCTCATT CATGTGGTC

Table 2.1. Primers/oligonucleotides used in this work

used for melting and extension, respectively. The annealing temperature was dependent on the PCR primer properties. 2 min kb⁻¹ was allowed for extension. All primers were obtained from Sigma-Aldrich and are listed in Table 2.1.

2.3.2 3'-A tailing of PCR products

The pGEM-T plasmid (Promega) was used for the propagation of cloned DNA fragments. In order to allow ligation of blunt ended PCR products into pGEM-T an 'A-tailing' strategy was used to add a single 3'-adenine to complement the single 3'-thymidine present in the pGEM-T vector. Immediately following the PCR strategy described in Section 2.3.1 the PCR reaction was heated to 95 °C for 20 min in order to degrade *Pfu* polymerase. 15 µl of 2 mM dATP was added to the reaction mix along with 5 units of *Taq* polymerase. The reaction was then incubated at 70 °C for 15 min.

2.3.3 Agarose gel electrophoresis

DNA fragments generated by PCR were analysed and separated from the PCR reaction mix by agarose gel electrophoresis. The agarose concentration selected was based on the size of the DNA fragment to be analysed and was dissolved in a Tris/Borate/EDTA (TBE) buffer system which was also used for running the gel (Sambrook and Russell, 2001). Agarose gels were typically run at 90 V and DNA was visualised by the addition of ethidium bromide solution (~0.5 µg ml⁻¹) to the gel prior to setting and the use of UV transilluminator. A Qiaquick gel extraction kit (Qiagen) or GenElute gel extraction kit (Sigma-Aldrich) was used to purify DNA fragments from agarose gels according to manufacturer instructions.

2.3.4 Ligation of PCR fragments into pGEM-T

The pGEM-T vector system (Promega) was used to ligate A-tailed PCR products into the pGEM-T plasmid. A 10 µl ligation reaction was prepared containing 5 µl T4 DNA ligase 2x rapid ligation buffer, 3 µl gel purified PCR product, 1 µl pGEM-T vector (50 ng µl⁻¹ stock) and 1 µl T4 DNA ligase (3 units µl⁻¹ stock). Positive controls using a control DNA insert (2 µl) and negative controls with no DNA insert were also performed, in each case the reaction volume was made up to 10 µl with nanopure water. Ligation reactions were incubated overnight at 4 °C then 2 µl of ligation reaction mix was used to transform DH5α cells as described in Section 2.2.3

2.3.5 Identification of transformant cells by blue/ white screening and colony PCR

The multi-cloning site of pGEM-T is contained within the α -peptide coding region of the enzyme β -galactosidase. The $\phi 80$ *lacZ* Δ M15 mutation present in DH5 α cells allows α -complementation with this peptide to yield the active enzyme. Cells containing the pGEM-T plasmid with desired insert in the multi-cloning site (which disrupts the α -peptide coding sequence) were therefore selected on a loss of ability to convert the colourless substrate 5-bromo-4-chloro-indolyl- β -D-galactopyranoside (X-gal) into the intensely blue coloured 4-chloro-3-bromo-indigo. Prior to the addition of DH5 α cells transformed with pGEM-T derivatives LB-Agar plates containing carbenicillin were streaked with 40 μ l 2 % w/v X-gal and 7 μ l 20 % w/v isopropyl β -D-1-thiogalactopyranoside (IPTG) which was allowed 3-4 h to soak into the plate.

Following incubation overnight the presence of the desired insert in white colonies was further confirmed by the use of a colony PCR screen. PCR reactions were prepared as described in Section 2.3.1 however using NEB Thermopol buffer (diluted from a 10 x stock containing 20 mM MgSO₄) and 5-10 units of *Taq* polymerase. PCR primers were those used to amplify the DNA fragment from genomic DNA. Colonies were first streaked onto a replica plate using a sterile pipette tip then added to the PCR reaction by gentle aspiration. 1 kb min⁻¹ at 68 °C was allowed for extension. Colonies containing the desired insert were identified by analysing the PCR reaction mix by agarose gel electrophoresis (Section 2.3.3). Plasmid DNA was prepared from colonies harbouring the desired PCR product (Section 2.3.6) and sequenced (GATC Biotech and DBS Genomics, Durham University) to validate the integrity of the cloned fragment. Plasmid constructs used as part of this work are listed in Table 2.2.

2.3.6 Isolation of plasmid DNA

E. coli cell cultures transformed with the appropriate plasmid were grown overnight in LB (5 ml for a miniprep and 100 ml for a midiprep (which was only used to produce large quantities of pET29a derived constructs for site directed mutagenesis, Section 2.3.7)). Cells were pelleted by centrifugation in sterile 50 ml centrifuge tubes in a Beckman Coulter Allegra X-22R benchtop centrifuge (4,000 rpm, 10 min, 4 °C). Plasmid DNA was prepared by alkaline-SDS lysis using either a Qiaprep Spin Miniprep Kit (Qiagen) or a GenElute Plasmid Miniprep Kit (Sigma-Aldrich) for minipreps and a Qiagen Plasmid Midi Kit for midipreps according to manufacturer instructions. Confirmation of successful isolation and estimation of the concentration of plasmid

Plasmid	Source	Function
pGEM-T	Promega	Sub-cloning of DNA fragments Template for PCR-amplification of non-specific control DNA fragments for EMSA Analysis
pET29aInrS	Dr. Kevin Waldron	Overexpression of InrS protein Template for 'Quikchange' mutagenesis
pET29aZiaR	Patterson. 2010	Overexpression of ZiaR protein
pET29aZur	Patterson. 2010	Overexpression of Zur protein
pET29aInrSH21C	This work	Overexpression of InrS His21→Cys protein
pET29aInrSH21E	This work	Overexpression of InrS His21→Glu protein
pET29aInrSH21L	This work	Overexpression of InrS His21→Leu protein
pET29aInrSC53A	This work	Overexpression of InrS Cys53→Ala protein
pET29aInrSH78L	This work	Overexpression of InrS His78→Leu protein
pET29aInrSC82A	This work	Overexpression of InrS Cys82→Ala protein

Table 2.2. Plasmids/constructs used in this work

DNA was achieved using a NanoDrop 1000 spectrophotometer (Thermo Scientific) and where necessary by agarose gel electrophoresis (Section 2.3.3).

2.3.7 Site directed mutagenesis using the ‘Quikchange’ method

The ‘Quikchange’ site directed mutagenesis method (developed by Stratagene) used to introduce amino acid changes into the pET29aInrS plasmid (Table 2.2) involves a linear rather than exponential generation of product and therefore midiprep plasmid DNA (Section 2.3.6) rather than miniprep plasmid was used as template. ‘Quikchange’ reaction compositions were essentially the same as those described for amplification of DNA by PCR (Section 2.3.1) however the final concentration of each dNTP was 200 μM and instead of genomic DNA 5 μl of midiprep plasmid DNA was used (stock concentration $\sim 245 \text{ ng } \mu\text{l}^{-1}$). Cycling conditions were as follows: 95 °C for 30 s for the initial denaturation followed by 16 cycles of 95 °C for 30 s (‘melt’), 55 °C for 1 min (‘anneal’) and 72 °C for 14 min (‘extend’). A control reaction with the omission of *Pfu* from the reaction mix was also included. Following the mutagenesis reaction 1 μl of DpnI (20 unit μl^{-1}) was added to the reaction mixture and incubated at 37 °C for 3 h in order to digest the methylated template DNA. 3 μl of each reaction mix was used to transform a 50 μl aliquot of DH5 α cells to kanamycin resistance (Section 2.2.3). Typically the minus *Pfu* control yielded zero colonies. Colonies were transferred to a replica plate and cells from this plate were used to produce a plasmid miniprep (Section 2.3.3) for sequencing (GATC Biotech and DBS Genomics, Durham University) to confirm successful mutagenesis.

2.4 Protein manipulation

2.4.1 Overexpression of InrS, InrS mutants, ZiaR and Zur

The plasmids pET29aInrS, pET29aZiaR and pET29aZur (Table 2.2) were produced prior to this work, the pET29aInrS plasmids harbouring the coding sequence for mutant versions of InrS were produced during this work (Section 2.3.7). Plasmids were used to transform BL21(DE3) competent cells to kanamycin resistance (Section 2.2.3). A single colony was picked and used to inoculate a 5 ml overnight starter culture. 1 ml of the starter culture was used to inoculate 1 l of LB which was cultured at 37 °C to an OD_{600 nm} of 0.5-0.7 before induction with 1 mM IPTG. BL21(DE3) cells transformed with pET29aZur grew more slowly than BL21(DE3) harbouring the other expression

plasmids, presumably due to a combination of leaky expression and interference with normal zinc homeostasis by the overexpressed protein. Following induction cells were cultured for a further 2 h before harvesting using a JLA 8.1000 rotor in a Beckman Coulter Avanti J-20 XP centrifuge (4,000 rpm, 20 min, 4 °C). The cell pellet was resuspended in approximately 30 ml of spent media and pelleted again in 50 ml centrifuge tubes in a Beckman Coulter Allegra X-22R benchtop centrifuge (4,000 rpm, 20 min, 4 °C). The media was discarded and the cell pellet stored at -20 °C until required.

2.4.2 SDS-PAGE analysis

The purity of protein samples both during and post purification was assessed by SDS-PAGE analysis (Sambrook and Russell. 2001). For InrS and mutant versions of InrS 18 % w/v acrylamide gels were used and for ZiaR and Zur 17 % w/v acrylamide gels. Gels were typically run at 180-200 V until the dye front reached the bottom of the gel and then stained with Instant Blue Coomassie stain (Expedeon).

2.4.3 Purification of recombinant InrS and mutant variants

All recombinant proteins produced during this work were native, tag free proteins and so the purification protocols exploited the inherent biochemical properties of the protein molecules. Cell pellets harbouring overexpressed InrS or mutant variants (Section 2.4.1) were resuspended in approximately 8 ml of 50 mM sodium phosphate, pH 7.4, 300 mM NaCl, 5 mM DTT, 1 mM PMSF and 10 mM imidazole (buffer A) and divided into ~700 µl aliquots. Each aliquot was sonicated for 30 sec to lyse the cells. Following sonication the cell debris was pelleted by centrifugation in a Beckman Coulter Microfuge 18 (14,000 rpm, 10 min) followed by centrifugation using a JA-25.50 in a Beckman Coulter Avanti J-20 XP centrifuge (18,000 rpm, 20 min, 4 °C) in order to further clarify the cell lysate. Following sonication and clarification the soluble cell lysate was applied to a 5 ml HisTrap FF column (GE Healthcare) prepared according to manufacturer's instructions and equilibrated into buffer A. Following application of the soluble lysate the column was washed with a minimum of 5 column volumes of buffer A before eluting the bound protein in a single step using buffer A with 300 mM imidazole and no PMSF. The presence of InrS in HisTrap eluate was confirmed by SDS-PAGE analysis (Section 2.4.2) however the reproducible results obtained with this step meant this analysis was sometimes discarded in favour of speed. The HisTrap eluate (~2 ml) was further purified by size exclusion chromatography (HiLoad 26/60 Superdex S75, GE

Healthcare) equilibrated with 10 mM Hepes, pH 7.8, 300 mM NaCl, 10 mM DTT and 10 mM EDTA (buffer B). Fractions containing InrS (as identified by SDS-PAGE analysis (Section 2.4.2)) were pooled and applied to either a 5 ml or a 1 ml Heparin column (GE Healthcare) equilibrated in buffer B. Following a wash with ~10 column volumes of buffer B, bound protein was eluted in a stepwise fashion with buffer B at NaCl concentrations of 0.5, 0.8 and 1 M. InrS eluted predominantly at 0.8 M NaCl.

2.4.4 Purification of recombinant ZiaR

Cell pellets harbouring overexpressed ZiaR (Section 2.4.1) were resuspended in approximately 8 ml of 20 mM sodium phosphate, pH 7.8, 500 mM NaCl, 5 mM DTT and 1 mM PMSF (buffer C) then lysed and clarified as described for InrS (Section 2.4.3). The soluble cell lysate was applied to a 5 ml HisTrap FF column (GE Healthcare) prepared according to manufacturer's instructions and equilibrated into buffer C. Following application of the soluble lysate the column was washed with approximately 10 column volumes of buffer C before eluting the bound protein in a single step using buffer C with 250 mM imidazole and no PMSF. The presence of ZiaR in HisTrap eluate was confirmed by SDS-PAGE analysis (Section 2.4.2) again the reproducible results obtained with this step meant this analysis was sometimes discarded in favour of speed (see Section 2.4.3). The HisTrap eluate (~2 ml) was further purified by size exclusion chromatography (HiLoad 26/60 Superdex S75, GE Healthcare) equilibrated with buffer B. Fractions containing ZiaR (as identified by SDS-PAGE analysis (Section 2.4.2) and the $A_{280\text{ nm}}$ elution profile) were pooled, diluted to 100 mM NaCl and applied to a 1 ml Heparin column (GE Healthcare) equilibrated in buffer B with 100 mM NaCl. Following a wash with ~10 CV of the equilibration buffer the bound protein was eluted in a stepwise fashion with buffer B at NaCl concentrations of 0.3, 0.4, 0.5 and 1 M. ZiaR eluted predominantly at 0.4 M NaCl.

2.4.5 Purification of recombinant Zur

Cell pellets harbouring overexpressed Zur (Section 2.4.1) were resuspended in approximately 8 ml of buffer B with 100 mM NaCl and 1 mM PMSF then lysed and clarified as described for InrS (Section 2.4.3). The soluble cell lysate was applied to either a 5 ml or 2 x 1 ml Heparin columns (GE Healthcare) attached in tandem prepared according to manufacturer's instructions and equilibrated into the lysis buffer. Following application of the soluble lysate the column was washed with approximately 10 column volumes of the lysis buffer before eluting the bound protein in a single step

using buffer B with 500 mM NaCl. The presence of Zur in the heparin column eluate was confirmed by SDS-PAGE as described for the first step in the purifications of InrS and ZiaR (Sections 2.4.2, 2.4.3, 2.4.4). The heparin column eluate (~2 ml) was further purified by size exclusion chromatography (HiLoad 26/60 Superdex S75, GE Healthcare) equilibrated with buffer B with 500 mM NaCl. Fractions containing Zur (as identified by SDS-PAGE analysis (Section 2.4.2) and the $A_{280\text{ nm}}$ elution profile) were pooled and diluted to 100 mM NaCl then further purified on a 1 ml heparin column (GE Healthcare) as described for the third purification step of ZiaR (Section 2.4.4). Zur eluted predominantly at 0.4 M.

2.4.6 Quantification of protein stocks

The concentration of solutions of ZiaR and Zur were estimated by recording $A_{280\text{ nm}}$ values and use of the theoretical extinction coefficients of $5,960\text{ M}^{-1}\text{ cm}^{-1}$ and $7,450\text{ M}^{-1}\text{ cm}^{-1}$, respectively, determined using the ProtParam tool on the ExPASy website (<http://web.expasy.org/protparam/>).

InrS and the mutant variants of InrS used in this work do not contain any fluorescent amino acid residues and so the concentration of protein stocks were estimated via calibrated Bradford assays (Bradford. 1976). Bradford reagent reacts with certain basic amino acids (primarily His, Lys, Arg) therefore an approximation of the relative reactivities of BSA and InrS with Bradford reagent (Coomassie Plus Protein Assay Reagent, Thermo Scientific) was first estimated based on the relative abundance of these residues in the two proteins taking into consideration the difference in M_r . InrS has a total of 21 reactive amino acids and experimentally determined M_r 11,887 Da (Section 3.2). BSA has a total of 103 reactive amino acids and theoretical M_r 69,323.4 Da. Therefore InrS is predicted to be 1.2 times more reactive than BSA per unit mass. An aliquot of InrS quantified by Bradford assay (Bradford. 1976) against BSA (without applying a conversion factor) as $1,300\text{ }\mu\text{g ml}^{-1}$ was submitted for amino acid analysis and determined to be $1,070\text{ }\mu\text{g ml}^{-1}$, verifying InrS as 1.2 times more reactive with Bradford reagent than BSA per unit mass.

2.5 Anaerobic manipulation of proteins

2.5.1 Production of O₂ free chelex treated buffers

In order to remove trace metal contaminants from buffers prior to use buffers were treated with Chelex-100, a styrene-divinylbenzene co-polymer containing metal chelating iminodiacetic acid groups. The Chelex-100 media was packed into a column and prepared according to manufacturer's instructions before passing buffer through the column.

To remove dissolved O₂ from buffers used under anaerobic conditions N₂ was bubbled vigorously into the buffer for a minimum of 2 h before transferring into an anaerobic glove box (Belle Technology).

2.5.2 Production of anaerobic protein samples

In order to study metal binding properties of proteins in the absence of reductant analyses were conducted in an anaerobic glove box (Belle Technology). In order to remove DTT and EDTA prior to analyses proteins were bound to a 1 ml heparin column (GE Healthcare) equilibrated in buffer B with 100 mM NaCl for ZiaR & Zur and 250 mM NaCl for InrS. The column was transferred to the anaerobic glove box and washed with 20 ml of chelex treated and N₂ purged (Section 2.5.1) 10 mM Hepes, pH 7 or 7.8 depending on the pH at which experiments were performed and a 1:4 ratio of NaCl:KCl (buffer D). The total salt content used for this wash step was 100 mM for ZiaR & Zur and 250 mM for InrS. Following the wash step proteins were eluted in a 1 ml fraction with buffer D with a total salt content of 500 mM for ZiaR & Zur and 1 M for InrS.

2.5.3 Quantification of reduced thiol content of anaerobic protein stocks

The reduced thiol content of anaerobic protein stocks was quantified by assay with 5,5'-dithio-bis-(2-nitrobenzoic acid) (DTNB). DTNB reacts with thiols in a 1:1 ratio producing the dianion 2-nitro-5-thiobenzoate (TNB) which absorbs intensely at 412 nm (Ellman. 1959). DTNB was dissolved in 100 mM sodium phosphate, pH 8.0, 1 mM EDTA to a concentration of 4 mg ml⁻¹. Assays were performed by one of two methods. In the first method a standard curve was produced using reduced glutathione (GSH). An approximately 100 mM stock of GSH was prepared anaerobically by dissolving in the buffer D variant used to elute the protein from the heparin column (the exact concentration of the stock was calculated from the mass of GSH used). The stock was serially diluted to produce a range of thiol concentrations (final volume of 1 ml upon

DTNB addition) incorporating the expected value for the protein sample. DTNB was added to each dilution to a final concentration of $72 \mu\text{g ml}^{-1}$. Protein samples were similarly prepared. Typically concentrations of GSH covered the range 0-60 μM . Upon addition of DTNB the reaction was left for 15 min to develop before adding 200 μl of each solution to a 96 well microtitre plate and recording the absorbance at 405 or 412 nm depending on the availability of plate readers at the time.

In the second method a 1 ml solution of protein and DTNB ($72 \mu\text{g ml}^{-1}$) was prepared anaerobically in a gas tight 1 ml quartz cuvette (Hellma) and following incubation of the reaction for 15 min the absorbance at 412 nm was recorded using a Perkin Elmer $\lambda 35$ UV-visible spectrophotometer. The concentration of reduced thiols was calculated via the Beer-Lambert law using the reported extinction coefficient of TNB at 412 nm of $14,150 \text{ M}^{-1} \text{ cm}^{-1}$ (Riddles *et al.* 1979). Both methods produced comparable results.

2.5.4 Measurement of the residual metal content of anaerobic protein stocks

Following the removal of EDTA from purified protein stocks (Section 2.5.2) the residual metal contamination was measured by inductively coupled plasma mass spectrometry (ICP-MS). Proteins were diluted into buffer D with a final salt concentration of 500 mM and then diluted into 2 % nitric acid typically to a final concentration of 2 μM for analysis.

2.6 Experimental procedures

2.6.1 Preparation of metal stocks

All metal stocks other than CuCl were prepared by dissolving the metal salt in nanopure water. Concentrations of metal stocks were assayed by ICP-MS analysis of serially diluted stocks. CuCl was prepared in an anaerobic glovebox by dissolving CuCl in 100 mM HCl and 1 M NaCl. This concentrated stock was serially diluted into the experimental buffer; the pH was also adjusted during the serial dilution. The concentration of copper in solution was verified by ICP-MS analysis and the concentration of Cu^+ by titration against an excess of BCS, a Cu(I) specific chelator. BCS forms a 2:1 complex with Cu(I) with an extinction coefficient of $13,500 \text{ M}^{-1} \text{ cm}^{-1}$ at 483 nm (Barry *et al.* 2011).

2.6.2 UV-visible spectroscopy

Spectra were recorded under anaerobic conditions on either a Perkin Elmer λ 35 or Cary 4E UV-visible spectrophotometer. Proteins were diluted into buffer D, with a total salt concentration of 500 mM at the pH stated in the text, in gas tight quartz cuvettes (Hellma). Metal additions were made either in the anaerobic glovebox followed by mixing by aspiration or using a gas tight syringe followed by mixing by inversion.

2.6.3 Fractionation of protein-metal complexes by size-exclusion chromatography

Protein-metal complexes were separated from unbound metal ions by size-exclusion chromatography using a Sephadex G-25 matrix column (PD10 column, GE Healthcare). The PD10 column was prepared by washing with 2 column volumes of nanopure water followed by addition of 0.5 ml of 0.5 M EDTA followed by a further 2 column volumes of nanopure water. The PD10 column was transferred to an anaerobic glovebox and washed with 2 CV of buffer D containing 500 mM salt at the pH stated in the text. Where stated the equilibration buffer was additionally supplemented with metal salts. 0.5 ml of sample was applied to the PD10 column and 0.5 ml fractions were eluted using the equilibration buffer. Fractions were analysed for metal content by ICP-MS analysis and for protein content by Bradford assay (Bradford, 1976) calibrated against protein stocks of known concentration. Samples resolved in this manner were typically from the end point of UV-visible titrations but where indicated protein was incubated with metal in the experimental buffer for 30 min prior to application to the column.

2.6.4 Analysis of DNA binding by EMSA

Production of probe DNA fragments by PCR

All probe DNA fragments were produced by a common protocol. The protocols detailed in Section 2.3.1-2.3.5 were followed to amplify a region of DNA containing the predicted binding site, ligate it into pGEM-T and propagate the newly constructed plasmid in Dh5 α cells. Isolated plasmids (Section 2.3.6) were sequenced and used as template from which to PCR amplify the probe DNA fragments using Promega *Pfu* polymerase. Alternatively probes were amplified directly from genomic DNA using Promega *Pfu* polymerase. The product of multiple PCR reactions were collected using a single gel extraction column in order to produce a high concentration working stock of probe DNA fragment. The concentration of probe was determined using a NanoDrop

1000 spectrophotometer (Thermo Scientific). The PCR primers used to produce each probe are listed in Table 2.1.

Non-specific control DNA fragments were produced by PCR amplification from re-circularised pGEM using the primers listed in Table 2.1. Again the products of multiple PCR reactions were collected using a single gel extraction column to produce a high concentration working stock.

Monitoring binding of InrS to DNA by EMSA

Purified InrS was buffer exchanged by loading onto a 1 ml heparin column (GE Healthcare) equilibrated in buffer B containing 300 mM NaCl before elution in 40 mM Hepes, pH 7.8, 1.2 M NaCl 8 mM DTT and 8 mM EDTA (buffer E). InrS protein concentration was determined by calibrated Bradford assay (Section 2.4.6). For each analysis, binding reactions at several different concentrations of InrS were prepared. Each binding reaction contained DNA probe and non-specific DNA fragment (concentrations stated in the text) and 2.5 µl of buffer exchanged InrS, buffer E or both to achieve different final concentrations of InrS in the binding reaction which additionally contained 1 µl of 30 % v/v glycerol & 0.5 mM spermidine (10x EMSA buffer additives). Binding reactions were made up to a volume of 10 µl with nanopure water. The final composition of binding reaction buffer was therefore 10 mM Hepes, pH 7.8, 300 mM NaCl, 2 mM DTT, 2 mM EDTA, 3 % v/v glycerol and 0.05 mM spermidine. Binding reactions were incubated at room temperature for 30 min before loading onto a non-denaturing polyacrylamide gel (6 % w/v acrylamide) which was run in a TBE buffer system at 120 V for approximately 70 min at 4 °C (Sambrook and Russell, 2001). Pre-running the gel before loading the binding reaction was found to improve the resolution. Gels were stained by incubation in ethidium bromide solution for 20 min before visualisation using a UV transilluminator.

Analysis of the effect of nickel on DNA binding was performed according to a slightly modified protocol. Purified InrS was buffer exchanged by loading onto a 1 ml heparin column (GE Healthcare) equilibrated in buffer B containing 300 mM NaCl before washing the column with buffer D with a total salt concentration of 250 mM and 1 mM TCEP and eluting with the same buffer with a total salt concentration of 1 M. Each binding reaction contained 100 nM of each probe DNA and non-specific DNA fragment, 1 µl of 10x EMSA buffer additives and 5 µl of buffer exchanged InrS, buffer D with a total salt concentration of 1 M and 1 mM TCEP or both to achieve the desired

final concentrations of InrS in the binding reaction. Binding reactions were made up to a volume of 10 μ l with nanopure water. The final composition of binding reaction buffer was therefore 5 mM Hepes, pH 7.8, 100 mM NaCl, 400 mM KCl 0.5 mM TCEP, 3 % v/v glycerol and 0.05 mM spermidine, where stated NiSO₄ and EDTA were included in binding reactions to final concentrations of 400 μ M and 4 mM respectively. Binding reactions were incubated and resolved as described above.

2.6.5 Analysis of InrS-DNA stoichiometry by size exclusion chromatography

Production of annealed, double stranded DNA probe

Complementary single stranded oligonucleotides containing the identified InrS binding site and flanking nucleotides were obtained from Sigma Aldrich. The oligonucleotides were annealed by heating 50 μ M of each strand in 10 mM Hepes, pH 7.8, 150 mM NaCl to 95 °C and then allowing to cool to room temperature overnight. Successful annealing of the strands was confirmed by Native PAGE analysis using a 12 % w/v gel with a TBE buffer system (Sambrook & Russell. 2001).

Assessment of InrS-DNA stoichiometry by size exclusion chromatography

Various concentrations of InrS were incubated with 10 μ M of the annealed DNA in 10 mM Hepes, pH 7.8, 60 mM NaCl, 240 mM KCl, 5 mM EDTA and 2 mM DTT. 100 μ l of the incubation mix was injected onto a Superdex 75 10/300 GL column (GE Healthcare) equilibrated in the above buffer with a flow rate of 1 ml min⁻¹. The elution position of DNA was monitored by absorbance at 260 nm.

2.6.6 Analysis of DNA binding by fluorescence anisotropy

Production of fluorescently labelled annealed, double stranded DNA probe

For fluorescence anisotropy experiments the same sequence oligonucleotides as used in Section 2.6.5 were employed however the 5' end of one of the strands was labelled with the fluorescent tag hexachlorofluorescein (HEX) during synthesis. The oligonucleotides were annealed as described in Section 2.6.5 although typically at a lower concentration (10 or 20 μ M).

Fluorescence anisotropy experimental procedures

The fluorescently labelled annealed probe was added to a gas tight, 2-way quartz cuvette (Hellma) to a final concentration of 10 nM in buffer D containing a total salt

content of 300 mM. All experiments were performed anaerobically. For association experiments in the absence of metal ions 5 mM EDTA was also included in the buffer. Where stated, InrS was incubated with metal (1.2 molar equivalents of NiCl₂, CuCl (verified to be >95 % Cu⁺ (Section 2.6.1)) or ZnSO₄) prior to the start of the experiment and in some experiments metal was included in the buffer. In these experiments EDTA was omitted from the buffer. Changes in anisotropy were measured using a modified Cary Eclipse Fluorescence Spectrophotometer (Agilent Technologies) fitted with polarising filters. Data were recorded at 25 °C with excitation and emission wavelengths of $\lambda_{\text{ex}} = 530 \text{ nm}$ and $\lambda_{\text{em}} = 570 \text{ nm}$. Upon each addition the cuvette was allowed to equilibrate for 5 min before recording data. Reads were averaged over a 20 s period and replicated 5 times from which a mean anisotropy value was produced.

For dissociation experiments EDTA was omitted from the buffer. InrS-DNA complexes were pre-formed by the addition of 1 μM InrS to 10 nM probe and metal was titrated into the cuvette anaerobically, otherwise the experiment was performed as described for the association experiment.

Δr_{obs} values were calculated by subtracting the r_{obs} value of DNA probe alone which was recorded at the start of each experiment.

2.6.7 Measurement of the metal binding affinities of InrS, ZiaR, Zur and CoaR

All experiments were conducted anaerobically using 1 ml gas tight cuvettes (Hellma). For UV-vis spectroscopy a Perkin Elmer $\lambda 35$ was used and for fluorescence spectroscopy a Cary Eclipse Fluorescence Spectrophotometer. All experiments were carried out in buffer D with a total salt concentration of 500 mM. For experiments with CoaR 0.1 % w/v *n*-dodecyl β -D-maltoside (DDM) (chelex treated) was additionally included in the buffer. For fluorescence experiments involving mag-fura-2 the fluorescence spectrophotometer excitation and emission wavelengths were set to $\lambda_{\text{ex}} = 380 \text{ nm}$ and $\lambda_{\text{em}} = 505 \text{ nm}$. For experiments involving fura-2 the fluorescence spectrophotometer excitation and emission wavelengths were set to $\lambda_{\text{ex}} = 360 \text{ nm}$ and $\lambda_{\text{em}} = 510 \text{ nm}$. Mag-fura-2 was quantified via its extinction coefficient at 369 nm of 22,000 M⁻¹ cm⁻¹ (Golynskiy *et al.* 2006), fura-2 via its extinction coefficient at 363 nm of 28,000 M⁻¹ cm⁻¹ and quin-2 via its extinction coefficient at 261 nm of 37,000 M⁻¹ cm⁻¹ (extinction coefficients for fura-2 and quin-2 were obtained from the supplier).

Determination of the Ni(II) affinity of InrS by competition with NTA, EGTA and EDTA

NTA, EGTA or EDTA was incubated with NiSO₄ before addition to an anaerobic solution of InrS in buffer D (pH 7.8) with a total salt concentration of 500 mM. All experimental concentrations are stated in the text. Nickel transfer from chelator to InrS was monitored by the appearance of the Ni(II)-InrS absorbance feature at 333 nm, scanning every 30 s. The absorbance at 333 nm at equilibrium was used in conjunction with a titration of InrS with NiSO₄ in the absence of chelator (Section 2.6.2) to determine the concentration of Ni(II)-InrS. Equation 2 was used to determine the nickel affinity of InrS:

$$K_D K_A' = \frac{([P]_{\text{total}} / [MP]) - 1}{([L]_{\text{total}} / [ML]) - 1} \quad \text{eq. 2}$$

where K_D is the dissociation constant for metal binding to protein, K_A' is the association constant for metal binding to the chelator, $[P]_{\text{total}}$ is the metal binding site concentration in the assay, $[L]_{\text{total}}$ is the chelator concentration used in the assay, $[MP]$ is the concentration of metallated protein metal binding site and $[ML]$ the concentration of metallated chelator determined by mass balance from $[MP]$ and $[M]_{\text{total}}$ the total concentration of metal present in the assay (Xiao & Wedd. 2010). For InrS the assumption was made that four nickel binding sites (Section 3.3.1) on an InrS tetramer (Section 3.2) interact with negative cooperativity and therefore only the contribution of the ‘tightest site’ was considered. For InrS, which is present as a tetramer under the experimental conditions used here (Section 3.2) this value is $0.25 \times [P]_{\text{monomer}}$. The pH dependent Ni(II) affinity constants of NTA and EGTA were calculated using the Schwarzenbach’s α -coefficient method (equations 3 and 4).

$$K_A' = K_A \alpha_{H-L} \quad \text{eq. 3}$$

$$\alpha_{H-L} = (1 + \beta_{H,1}[H] + \beta_{H,2}[H]^2 + \dots + \beta_{H,n}[H]^n)^{-1} \quad \text{eq. 4}$$

where K_A' is the pH dependent affinity constant, K_A is the absolute affinity constant, α_{H-L} is Schwarzenbach’s α -coefficient, $\beta_{H,1} = 10^{\text{pKa1}}$, $\beta_{H,2} = 10^{\text{pKa1} + \text{pKa2}}$ etc., $[H] = 10^{-\text{pH}}$. The absolute affinity constant of EGTA with Ni(II) is $10^{13.5} \text{ M}^{-1}$ and its sequential

acid dissociation constants $pK_{a1} = 9.40$, $pK_{a2} = 8.79$, $pK_{a3} = 2.70$, $pK_{a4} = 1.9$ (Xiao & Wedd. 2010). The absolute affinity constant of NTA with Ni(II) is $10^{11.51} \text{ M}^{-1}$ and its sequential acid dissociation constants $pK_{a1} = 9.73$, $pK_{a2} = 2.49$, $pK_{a3} = 1.89$ (Xiao & Wedd. 2010).

Determination of the Ni(II) affinity of ZiaR, Zur and CoaR by competition with mag-fura-2 and NTA

Mag-fura-2 was incubated with NiSO_4 before addition to an anaerobic solution of either ZiaR, Zur or CoaR in buffer D (pH 7.8) with a total salt concentration of 500 mM. All experimental concentrations are stated in the text. Nickel transfer from chelator to ZiaR, Zur or CoaR was monitored by the alleviation of mag-fura-2 nickel dependent fluorescence quenching. The equilibrium fluorescence value at 505 nm was used in conjunction with a titration of mag-fura-2 with NiSO_4 in the absence of protein to determine the concentration of Ni(II)-mag-fura-2 and by mass balance the concentration of Ni(II)-protein. Equation 2 was used to determine the nickel affinity of ZiaR and Zur in conjunction with the $K_{A, \text{Ni(II)}}$ for mag-fura-2 determined to be $2 \times 10^7 \text{ M}^{-1}$ at pH 7 by Reyes-Cabellero and co-workers (Reyes-Caballero *et al.* 2011b). The assumption was made that the metal binding sites on ZiaR and Zur dimers interact with negative cooperativity and therefore only the contribution of the ‘tightest site’ was considered ($0.5 \times [\text{P}]_{\text{monomer}}$).

Estimation of the nickel affinity of CoaR was carried out by competition with NTA. The occupancy of CoaR with nickel was monitored via the quenching of the intrinsic fluorescence of CoaR upon nickel binding (Section 2.6.8). NiSO_4 was added to a solution of CoaR or NTA & CoaR (concentrations stated in text) in buffer D (pH 7.8) with a total salt concentration of 500 mM.

Determination of the Co(II) affinity of InrS, ZiaR, Zur and CoaR by competition with fura-2

Competition experiments were carried out as described for competitions with mag-fura-2, above, with substitution of NiSO_4 for CoCl_2 . The affinity of fura-2 for cobalt was determined experimentally (below).

Determination of the Co(II) affinity of fura-2 and the Ni(II) affinity of mag-fura-2 by competition with NTA

CoCl₂ was titrated into a mixed solution of fura-2 and NTA. On each addition the change in fluorescence emission of fura-2 was monitored to equilibrium and the value recorded. Data were fit using the non-linear, least squares regression program Dynafit (Kuzmic. 1996) to a model describing a 1:1 Cobalt-chelator complex for both fura-2 (Grykiewicz *et al.* 1985) and NTA (Xiao & Wedd. 2010). The affinity of NTA for Co(II) was calculated using the Schwarzenbach's α -coefficient method (above) and the absolute affinity constant of NTA with Co(II) is $10^{10.38} \text{ M}^{-1}$ (Xiao & Wedd. 2010).

NiSO₄ was titrated into a mixed solution of mag-fura-2 and NTA. On each addition the change in fluorescence emission of mag-fura-2 was monitored to equilibrium and the value recorded. Due to NTA substantially withholding Ni(II) from mag-fura-2 a Ni(II) affinity for mag-fura-2 could not be calculated.

Both experiments were performed at pH 7.8.

Determination of the Zn(II) affinity of InrS by competition with mag-fura-2 and quin-2

ZnSO₄ was titrated into a solution of either InrS and mag-fura-2 or InrS and quin-2. Upon each addition the reaction was allowed to equilibrate for 5 min for mag-fura-2 competitions and 10 min for quin-2 competitions before recording the absorbance spectra. Zinc binding to mag-fura-2 was monitored by the increase in absorbance at 325 nm and decrease in absorbance at 366 nm (Reyes-Caballero *et al.* 2010) and for quin-2 the decrease in absorbance at 261 nm (Jefferson *et al.* 1990). For competitions with mag-fura-2 data were fit using Dynafit to a model describing a set of four high and four low affinity sites per InrS tetramer with no interaction between sites and for competitions with quin-2 a model describing the high affinity sites only (Kuzmic. 1996). The models are discussed in the text (Section 5.6). The affinities of mag-fura-2 and quin-2 for Zn(II) are $2.2 \times 10^{-8} \text{ M}$ (Reyes-Caballero *et al.* 2010) and $2.70 \times 10^{11} \text{ M}^{-1}$ (Jefferson *et al.* 1990), respectively. Control experiments were performed in an analogous manner in the absence of protein.

Estimation of the Cu(I) affinity of InrS by competition with BCS

CuCl (verified to be >95 % Cu⁺ (Section 2.6.1)) was titrated into a mixed solution of InrS and BCS and absorbance change at 483 nm, which reports on the formation of

Cu(I)BCS₂ was recorded. Data were fit using Dynafit (Kuzmic. 1996) to a model describing a total of eight Cu(I) binding sites per InrS tetramer (Section 5.7).

2.6.8 Monitoring quenching of intrinsic protein fluorescence upon metal binding

Intrinsic protein fluorescence was monitored using a Cary Eclipse Fluorescence Spectrophotometer with the excitation and emission settings $\lambda_{\text{ex}} = 280 \text{ nm}$ and $\lambda_{\text{em}} = 300\text{-}400 \text{ nm}$. Experiments were conducted using a gas tight 2-way cuvette (Hellma) and were typically conducted in buffer D with a total salt concentration of 500 mM.

2.6.9 Inter-protein nickel exchange

Ni(II) exchange from Zur to InrS

Zur was incubated with NiSO₄ at the concentrations indicated in the text in buffer D with a total salt concentration of 500 mM before addition of InrS. The intrinsic protein fluorescence of Zur was measured as described in Section 2.6.8 at each step of the experiment.

Ni(II) exchange from CoaR to InrS

CoaR was incubated with NiSO₄ at the concentrations indicated in the text in buffer D with a total salt concentration of 500 mM (additionally supplemented with 0.1 % DDM) before addition of InrS. The UV-visible absorption spectrum was recorded at each experimental step as described in Section 2.6.2.

Ni(II) exchange from ZiaR to InrS

ZiaR was incubated with NiSO₄ at the concentrations indicated in the text in buffer D with a total salt concentration of 200 mM before addition of InrS. Following addition of InrS the solution was incubated at room temperature for 40 min before binding to a 1 ml heparin column (GE Healthcare) equilibrated in the above buffer. Proteins were eluted from the column sequentially by the use of buffer D with a total salt content of 500 mM then 1 M. Fractions were analysed for protein by SDS-PAGE analysis (Section 2.4.2) and for nickel content by ICP-MS analysis.

2.6.10 Circular dichroism (CD) spectroscopy

CD spectra were collected using a JASCO J810 spectropolarimeter set to high sensitivity (5 mdeg), data pitch of 0.2 nm, continuous scanning at 50 nm min⁻¹ and a band width of 2 nm. The path length of the cuvette was 0.2 cm and each spectrum is an

average of 8 replicates. InrS was buffer exchanged into 300 mM potassium phosphate, pH 7.8, 1 mM DTT and 1 mM EDTA using a PD10 column (GE Healthcare) according to manufacturer instructions immediately prior to experiment. Protein concentrations are stated in the text and are estimated assuming 90 % recovery of protein loaded onto the PD10 column. The spectrum of buffer alone was recorded and subtracted from the protein spectrum. Equation 5 was used to convert the raw data from ellipticity in mdeg to molar ellipticity (Bain *et al.* 2001).

$$\theta = \theta_{\text{obs}} \times \frac{\text{MRW}}{10 \times b \times c} \quad \text{eq. 5}$$

where θ is the molar ellipticity in $\text{deg cm}^2 \text{ dmol}^{-1}$, θ_{obs} is the ellipticity in mdeg, MRW is the mean residue weight (M_r / number of residues), b is the cuvette path length and c is the protein concentration in mg ml^{-1} . N-terminal methionine cleavage (Section 3.2) was taken into account in the calculation of MRW.

2.7 Bioinformatics

BLAST searches were performed using the NCBI Protein BLAST tool (<http://blast.ncbi.nlm.nih.gov/Blast.cgi>). Multiple sequence alignments were produced using ClustalW2 (<http://www.ebi.ac.uk/Tools/msa/clustalw2/>). Protein similarity and amino acid identity were compared using EMBOSS Needle (http://www.ebi.ac.uk/Tools/psa/emboss_needle/). InrS binding site searches were performed using the search pattern tool on the Cyanolist website (<http://genolist.pasteur.fr/CyanoList/>). Alignment of EMSA probe sequences with known CsoR DNA binding sites was performed using LAlign (http://embnet.vital-it.ch/software/LALIGN_form.html). General analysis of the *Synechocystis* genome was performed using the Cynaobase website (Nakamura *et al.* 1998; Nakao *et al.* 2010). The cladogram of CsoR-RcnR family proteins was produced using the ‘one click’ phylogeny analysis tool provided by Centre National de la Recherche Scientifique (http://www.phylogeny.fr/version2_cgi/simple_phylogeny.cgi). Molecular structure images were manipulated and produced using DeepView Swiss-PDBViewer (Guex & Peitsch, 1997) and rendered using POV-ray (<http://www.povray.org/>). Multimeric protein structure coordinates were produced using the ‘Protein interfaces, surfaces and assemblies’ service PISA at the European Bioinformatics Institute

(http://www.ebi.ac.uk/pdbe/prot_int/pistart.html) (Krissinel & Henrick. 2007) from the crystallographic symmetry information contained within the PDB file. Molecular models of InrS were produced using the web server SWISS-MODEL (<http://swissmodel.expasy.org/>) (Arnold *et al.* 2006). Membrane protein topology prediction was performed using the TMHMM server version 2.0 (<http://www.cbs.dtu.dk/services/TMHMM/>).

Chapter 3. Identification and functional assignment of InrS: A protein of the CsoR-RcnR metalloregulator family controlling nickel export to the periplasm

3.1 Bioinformatic analysis of InrS

The genome of *Synechocystis* contains one gene, ORF *sll0176*, predicted to encode a protein (designated here InrS for Internal nickel responsive sensor, see Section 3.5) with 38.6 % similarity and 19.3 % identity to *M. tuberculosis* CsoR and 45.4 % similarity and 26.9 % identity to *E. coli* RcnR, the copper and nickel/cobalt sensing founder members of the CsoR-RcnR metalloregulator family (Section 1.5). Based on the sequence similarity to members of this metalloregulator family it was hypothesised that this ORF could encode a metalloregulator. A bioinformatics approach was taken to try to predict what gene(s) may be regulated by InrS and in response to what metal(s).

In prokaryotes metalloregulators are often genetically linked with the genes they regulate and indeed three metal sensors from *Synechocystis* previously characterised by this research group ZiaR (Thelwell *et al.* 1998), CoaR (Rutherford *et al.* 1999), Zur (Tottey *et al.* 2012)) are divergently transcribed from the genes they regulate. Inspection of the genetic context of *inrS* (Figure 3.1) did not reveal any obvious potential targets of metalloregulation by InrS such as a gene encoding a metal export protein. The genes in the vicinity of *inrS* are discussed further in Section 6.9.1.

It has been suggested that the metal sensed by CsoR-RcnR like proteins can be predicted from the identity of amino acids in positions corresponding to metal binding residues in the founder members of this family (Iwig *et al.* 2008), these positions are referred to as W-X-Y-Z (Ma *et al.* 2009c) and are marked in Figure 3.2. Copper sensing CsoR-like proteins are predicted to contain the X-Y-Z motif (no ligand in W position as Cu(I) is coordinated in a trigonal geometry) Cys-His-Cys and nickel/cobalt RcnR-like proteins the W-X-Y-Z motif His-Cys-His-His, although CsoR from *T. thermophilus* has a histidine residue in the Z position (Sakamoto *et al.* 2010). Alignment of InrS with previously characterised CsoR-RcnR like proteins (Figure 3.2) reveals InrS contains the W-X-Y-Z motif His-Cys-His-Cys making it intermediate to the two paradigm ligand sets.

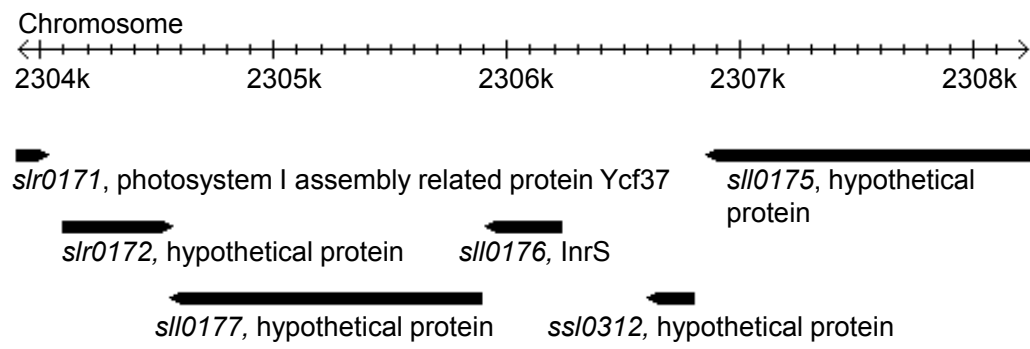


Figure 3.1. Genetic context of *inrS*. Scale representation of the immediate genetic context of *inrS* (produced using image generated from Cyanobase).

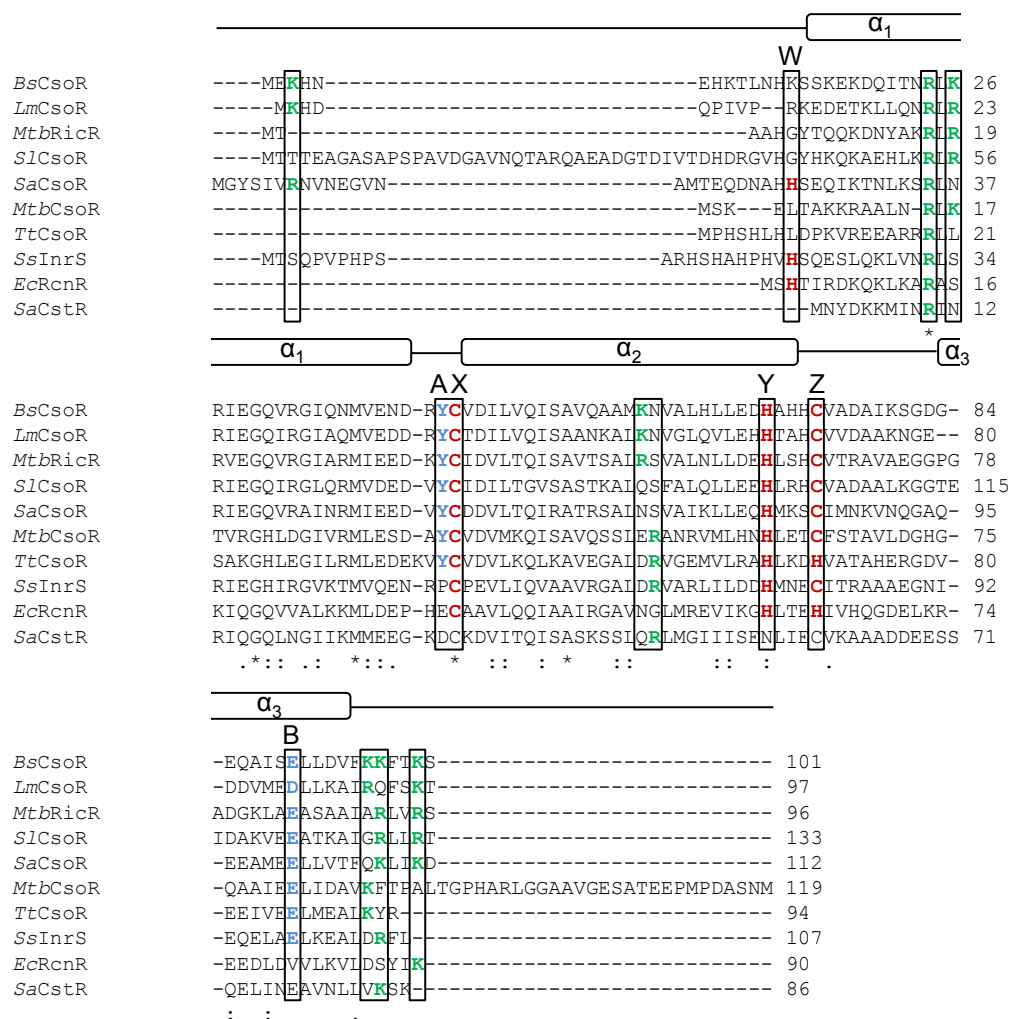


Figure 3.2. Multiple sequence alignment of characterised CsoR-RcnR proteins. Alignment of sequences of CsoR homologues from *B. subtilis* (Bs), *L. monocytogenes* (Lm), *M. tuberculosis* (Mtb) (CsoR and RicR), *S. lividans* (Sl), *S. aureus* (Sa), *T. thermophilus* (Tt) with *E. coli* (Ec) RcnR, *Synechocystis* (Ss) InrS and *S. aureus* (Sa) CstR. Highlighted residues are known or predicted to be metal ligands (red), involved in the allosteric switch (blue) or involved in DNA binding (green). The annotated secondary structure features are based on those of *M. tuberculosis* CsoR (Liu *et al.* 2007).

Of the residues thought to propagate the allosteric switch upon copper binding to CsoR InrS retains the histidine and glutamate equivalent to *M. tuberculosis* CsoR His61 (position Y) and Glu81 (position B) but lacks the tyrosine equivalent to Tyr35 (position A) containing a proline residue instead at this position (Figure 3.2). InrS also contains many conserved positively charged residues shown to be protected by DNA binding of *B. subtilis* CsoR (Chang *et al.* 2011), whereas *E. coli* RcnR shows less conservation in these positions (Figure 3.2).

From the bioinformatics analysis presented here it was not possible to predict what gene(s) InrS regulates and what metal(s), if any, it senses. InrS appears closer to copper sensing CsoRs in some conserved features (metal binding residues, residues important for interaction with DNA) though lacks one of the conserved residues thought to be important, although not critical (Ma *et al.* 2009b), for copper mediated allostery. In addition InrS has an N-terminal extension (relative to *M. tuberculosis* CsoR and *E. coli* RcnR) that is rich in histidine residues (Figure 3.2). *S. aureus* (Grossoehme *et al.* 2011) and *S. lividans* CsoR (Dwarakanath *et al.* 2012) also have N-terminal extensions but these are not His-rich. This combination of features predicts that InrS is likely to function at least partially differently from the literature paradigms of the CsoR-RcnR family.

3.2 Purification of recombinant InrS

As bioinformatics analysis proved inconclusive as to the metal(s) sensed or gene(s) regulated by InrS it was decided to study the *in vitro* metal binding properties of the protein in order to gain clues as to the most likely metal effector of the protein. UV-Vis spectroscopy is often used to probe the metal coordination sites of metalloproteins as absorption of energy in the UV-Vis range can cause promotion of metal ion *d* orbital electrons into higher energy orbitals or transfer of an electron from a ligand centred orbital into a metal ion *d* orbital. This is commonly observed for proteins that utilise the cysteine thiol side chain, which utilises a high energy lone pair of electrons as a metal ligand. Metal to ligand charge transfer is also possible although it has not been compellingly demonstrated in protein-metal complexes (Holm *et al.* 1996). *E. coli* RcnR (Iwig *et al.* 2008) and *B. subtilis* CsoR (Ma *et al.* 2009a) display distinctly different UV-Vis absorption spectra upon binding of nickel and cobalt (whereas the Cu(I) dependent spectra are highly similar (Higgins *et al.* 2012b)) and it was

hypothesised that it may be possible to deduce the metal effector of InrS based on analysis of these spectra.

InrS was overexpressed in *E. coli* as a recombinant, tag-free protein and purified based on its inherent biochemical properties (metal & DNA binding and size). Crude cell lysate was loaded onto a nickel affinity column and eluted in a single step with a high concentration of imidazole (Figure 3.3). This elution fraction was confirmed to contain a high abundance of a protein with the expected mass of InrS (Figure 3.3) and was further purified by size exclusion chromatography (HiLoad 26/60 Superdex S75 GE Healthcare) (Figure 3.3). Finally size exclusion fractions found to be enriched for InrS were subjected to a final purification and concentration step on a small heparin affinity column (Figure 3.3). The heparin affinity column was eluted with a step wise gradient of increasing NaCl concentration with InrS of >95 % purity (as assessed by SDS-PAGE analysis) routinely found in the 800 mM NaCl elution fraction (Figure 3.3).

The elution volume of InrS from a size exclusion column calibrated with standards of known molecular weight (Figure 3.4) (peak fraction volume = 140 ml) corresponds to an assembly of molecular weight 54,954 Da most consistent with InrS existing as a tetrameric complex in solution (theoretical M_r = 12,019.7 Da). This is consistent with the literature on *E. coli* RcnR (Iwig *et al.* 2008) and various CsoRs (Ma *et al.* 2009a; Sakamoto *et al.* 2010; Dwarakanath *et al.* 2012) which are reported to form tetrameric assemblies. The identity of purified InrS was confirmed by MALDI-PMF (Pinnacle, Newcastle University) and the molecular weight determined by ESI-MS (performed by Dr David Dixon). The molecular weight determined (11,887 Da) corresponds to the full length protein with the N-terminal methionine cleaved.

Thiols from cysteine side chains are often used as ligands in metalloproteins but commonly used reductants such as DTT can interfere with metal binding analyses due to their high capacity for metal chelation (Xiao *et al.* 2011), therefore to assess the metal binding properties of InrS in the absence of competitor, but to retain reduced thiols, the protein was transferred into a nitrogen atmosphere anaerobic glovebox and DTT (along with EDTA) removed by buffer exchange into chelex treated, N₂ purged buffer. As InrS lacks any fluorescent residues the protein concentration was estimated by a calibrated Bradford assay (Bradford. 1976) (Section 2.4.6). The concentration of reduced thiols (from cysteine side chains) in protein samples was assessed by DTNB assay and InrS was typically found to be >90 % reduced. Residual metal content of protein samples was assessed by ICP-MS analysis and InrS was typically found to be >95 % apo.

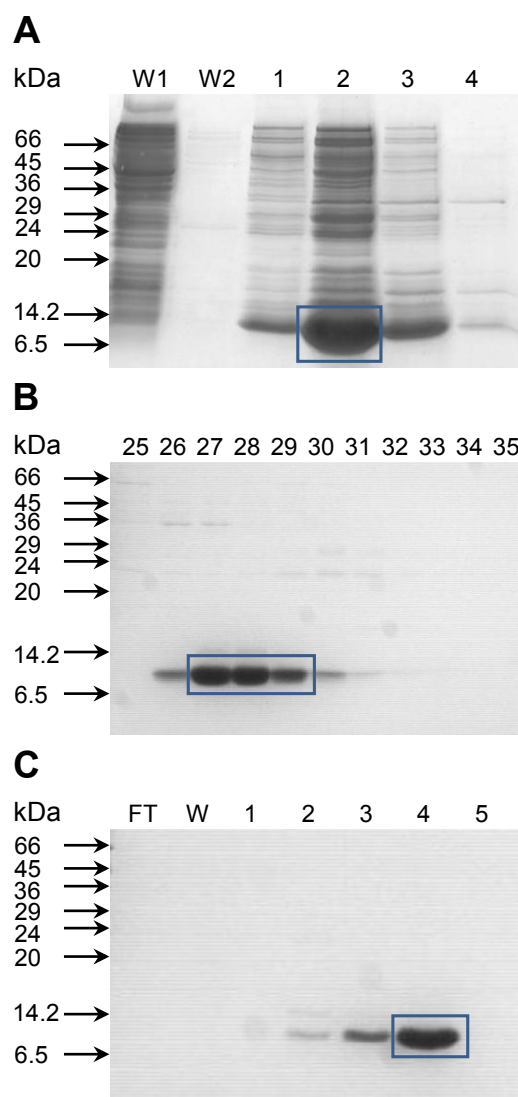


Figure 3.3. Purification of recombinant InrS. A. SDS-PAGE analysis of fractions eluted from a nickel affinity column loaded with soluble lysate from 1 l of cells overexpressing InrS. Fraction W1 contains the unbound material and a 6 column volume wash with buffer A and W2 contains an 8 column volume wash with buffer A. Fractions 1-4 were collected upon elution with buffer A with 300 mM imidazole and no PMSF. Fraction 1 is the lag fraction (i.e. containing the buffer displaced from the column upon the addition of new buffer) (4.5 ml), fractions 2 and 3 the peak protein elution fractions (3 and 2 ml respectively) and fraction 4 is a 2 column volume wash. B. SDS-PAGE analysis of fractions eluted from a Superdex S75 column loaded with 2 ml of fraction 2 from the nickel affinity step 'A'. Fractions are 5 ml in volume. C. SDS-PAGE analysis of fractions eluted from a heparin affinity column loaded with pooled Fraction 27-29 from the size exclusion step 'B'. FT and W contain the flowthrough and wash (with 10 column volumes of buffer B) respectively. Fractions 1-4 contain lag and peak elution fractions upon increasing the NaCl concentration in buffer B. Fraction 4 is the peak elution fraction upon elution with buffer B containing 0.8 M NaCl. Fraction 5 is a 10 column volume wash with buffer B containing 1 M NaCl. The blue boxes show the presence of InrS in fractions which were pooled and carried forward to the next purification step or used in experiments.

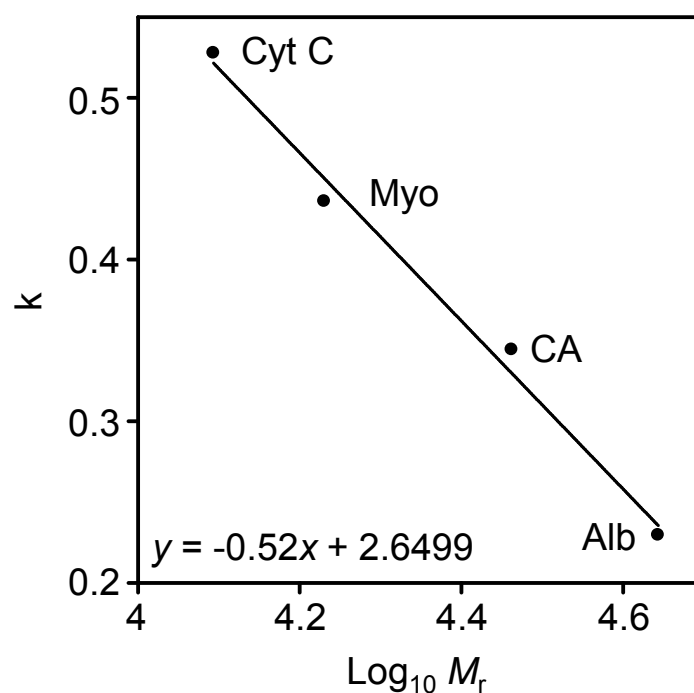


Figure 3.4. Calibration of size exclusion chromatography column. Aliquots (0.4 mg) of albumin (Alb) ($M_r \sim 44$ kDa), carbonic anhydrase (CA) ($M_r \sim 29$ kDa), myoglobin (Myo) ($M_r \sim 17$ kDa) and cytochrome c (Cyt C) ($M_r \sim 12.4$ kDa) were resolved by gel filtration chromatography (HiLoad 26/60 Superdex S75, GE Healthcare) with buffer containing 10 mM Hepes, pH 7.8, 100 mM NaCl, 400 mM KCl, 1 mM DTT and 1 mM EDTA and fractions analysed by SDS-PAGE. k , the gel phase distribution coefficient, was calculated from the formula $k = (V_e - V_0) / (V_t - V_0)$ where V_e = elution volume of protein, V_0 = void volume of column (100 ml) and V_t = total volume of column (318 ml).

Circular dichroism analysis of purified InrS (Figure 3.5) suggests the protein has significant α -helical content (Kelly *et al.* 2005) and is broadly similar to CD spectra for other members of the CsoR-RcnR family (Iwig *et al.* 2008; Dwarakanath *et al.* 2012) suggesting it adopts a similar all α -helical fold.

3.3 Analysis of the metal binding properties of InrS

3.3.1 Ni(II) and Cu(II) binding properties

Upon titration of InrS with NiSO₄ several UV-Vis features are evident from which inferences about the nature of the Ni(II) binding site can be made (Figure 3.6). Firstly two intense features centred at 238 and 333 nm are immediately apparent. The feature at 333 nm increases linearly and saturates cleanly upon addition of approximately one molar equivalent of Ni(II) suggesting a stoichiometry of one nickel atom per protein monomer, analogous to both *E. coli* RcnR (Iwig *et al.* 2008) and *B. subtilis* CsoR (Ma *et al.* 2009a). Although the feature at 238 nm does not increase in a perfectly linear manner it does saturate upon addition of approximately one molar equivalent of nickel. In support of a 1:1 Ni(II) binding stoichiometry InrS migrated with approximately one molar equivalent of nickel when a sample of the completed titration shown in Figure 3.6 was resolved on Sephadex G25 media (Figure 3.7). This stoichiometric binding allows a minimum estimate of Ni(II) binding affinity of InrS of $<10^{-7}$ M. The presence of intense absorbance bands at high energy wavelengths, attributable to ligand to metal charge transfer (LMCT), is generally indicative of the presence of sulphur (from cysteine) in the metal binding site (VanZile *et al.* 2000). In addition to the intense LMCT features there is also an absorbance band centred at roughly 480 nm which, when the contribution of baseline lift has been removed, has an intensity of $\sim 200 \text{ M}^{-1}\text{cm}^{-1}$, characteristic of Ni(II) bound in a square planar geometry (Chen *et al.* 2000). The Ni(II) bound InrS spectrum is remarkably similar to that of Ni(II) bound NikR from both *E. coli* (Wang *et al.* 2004) and *H. pylori* (Abraham *et al.* 2006) both of which exhibit an intense LMCT centred at 302 nm and a weak absorbance band centred around 475 nm attributed to Ni(II) bound in a square planar environment. Interestingly the intensity of the 302 nm feature observed upon Ni(II) binding to these NikR proteins, which each contain one thiolate ligand in their nickel coordination site, is roughly half the intensity of the 333 nm peak observed for InrS upon Ni(II) binding (Figure 3.6). The correlation between the number of sulphur ligands and LMCT intensity is less well defined for Ni(II) sites than Co(II) sites but this increased intensity along with the red shift of this

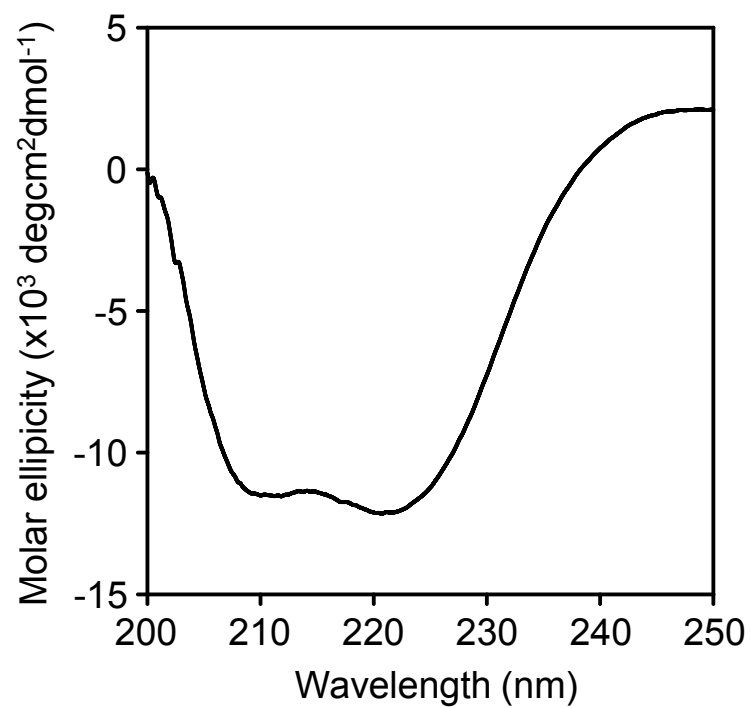


Figure 3.5. Far UV CD spectra of apo-InrS. Recorded with $\sim 2.7 \mu\text{M}$ InrS.

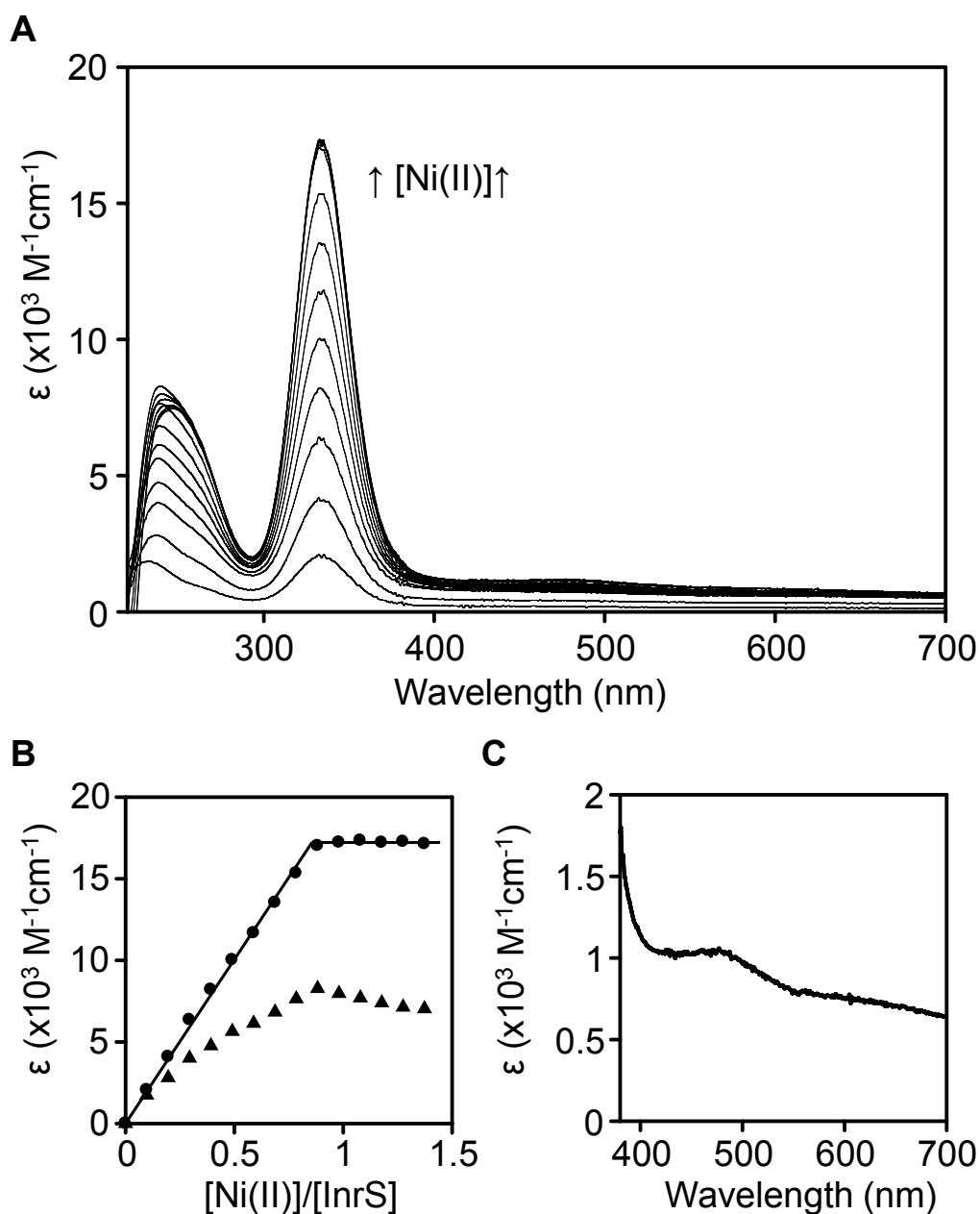


Figure 3.6. UV-Vis spectra of InrS upon titration with NiSO₄. A. Apo-subtracted difference spectra of InrS (10.4 μM) upon titration with NiSO₄ (recorded anaerobically at pH 7.8). B. Binding isotherm depicting the Ni(II) dependent spectral feature at 333 nm (circles) and 238 nm (triangles). C. Enlargement of the InrS UV-Vis spectrum upon addition of ~ 1 molar equivalent of Ni(II) to highlight the small peak with an absorbance maximum of ~ 480 nm, characteristic of Ni(II) bound in a square planar geometry.

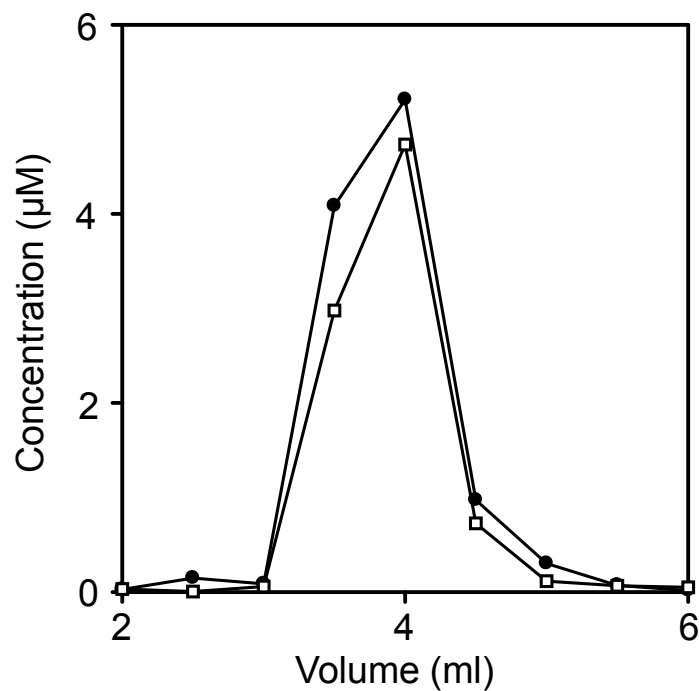


Figure 3.7. InrS migrates with approximately one molar equivalent of nickel by size exclusion chromatography. Following titration of InrS with NiSO₄ (Figure 3.6) an aliquot (0.5 ml) was applied to a Sephadex G25 (PD10 column, GE Healthcare) then eluted with the same buffer under anaerobic conditions (pH 7.8). Fractions (0.5 ml) were analysed for protein (filled circles) by Bradford assay calibrated against a quantified stock of InrS and nickel (open squares) by ICP-MS.

feature (which can report on a more sulphur rich binding site (VanZile *et al.* 2002b)) may be consistent with the Ni(II) binding site of InrS containing two thiolate ligands as one would predict from the sequence alignments (Figure 3.2). Ni(II) bound to *E.coli* NikR has been shown crystallographically to be bound in a square-planar geometry (Schreiter *et al.* 2003; Phillips *et al.* 2008) so the assignment of a square planar Ni(II) coordination geometry for InrS seems reasonable based on the similarity of the spectra.

Cu(II)-InrS has an intense yellow colour caused by the absorbance at 435 nm (Figure 3.8) which may be attributable to sulphur to copper charge transfer similar to that observed in type 2 copper-cysteinate proteins (Lu *et al.* 1996). This feature saturates upon addition of approximately one equivalent of Cu(II) suggesting a Cu(II) binding stoichiometry of 1:1. The spectra additionally displays an intense feature at 233 nm which, although clearly Cu(II) dependent, does not increase in a smoothly linear manner or saturate over the concentration range used in the assay. In support of the assignment of a square planar coordination geometry for Ni(II)-InrS the UV-Vis spectrum of Cu(II)-InrS is also highly similar to that of Cu(II)-NikR from both *E. coli* (Wang *et al.* 2004) and *H. pylori* (Abraham *et al.* 2006). Cu(II) has been shown crystallographically to be coordinated in a square planar geometry by *E. coli* NikR however with slightly longer metal-ligand distances than in the Ni(II) bound structure (Phillips *et al.* 2008). Again the intense probable LMCT feature (centred at 435 nm for InrS) is of a greater intensity and red shifted relative to those observed for the *E. coli* and *H. pylori* NikR proteins consistent with a more sulphur rich binding site (VanZile *et al.* 2002b).

The UV-Vis spectrum of *E. coli* Ni(II)-RcnR displays intense features at 231 and 280 nm with no absorbance at the wavelengths indicative of square planar coordination geometry (Iwig *et al.* 2008). Additionally the XANES pre-edge transitions are diagnostic of a six-coordinate pseudo-octahedral Ni(II) centre (Iwig *et al.* 2008). The UV-Vis spectrum of Ni(II)-CsoR displays intense features at 240 and 338 nm as well as a weak absorbance band centred at 480 nm which was attributed to square planar coordination geometry (Ma *et al.* 2009a). Upon comparison of the UV-Vis spectra of Ni(II)-InrS with those of *E. coli* Ni(II)-RcnR and *B. subtilis* Ni(II)-CsoR it is immediately apparent that they bear more resemblance to those of *B. subtilis* Ni(II)-CsoR than those of *E. coli* Ni(II)-RcnR, sharing both the intense LMCT and 480 nm centred features.

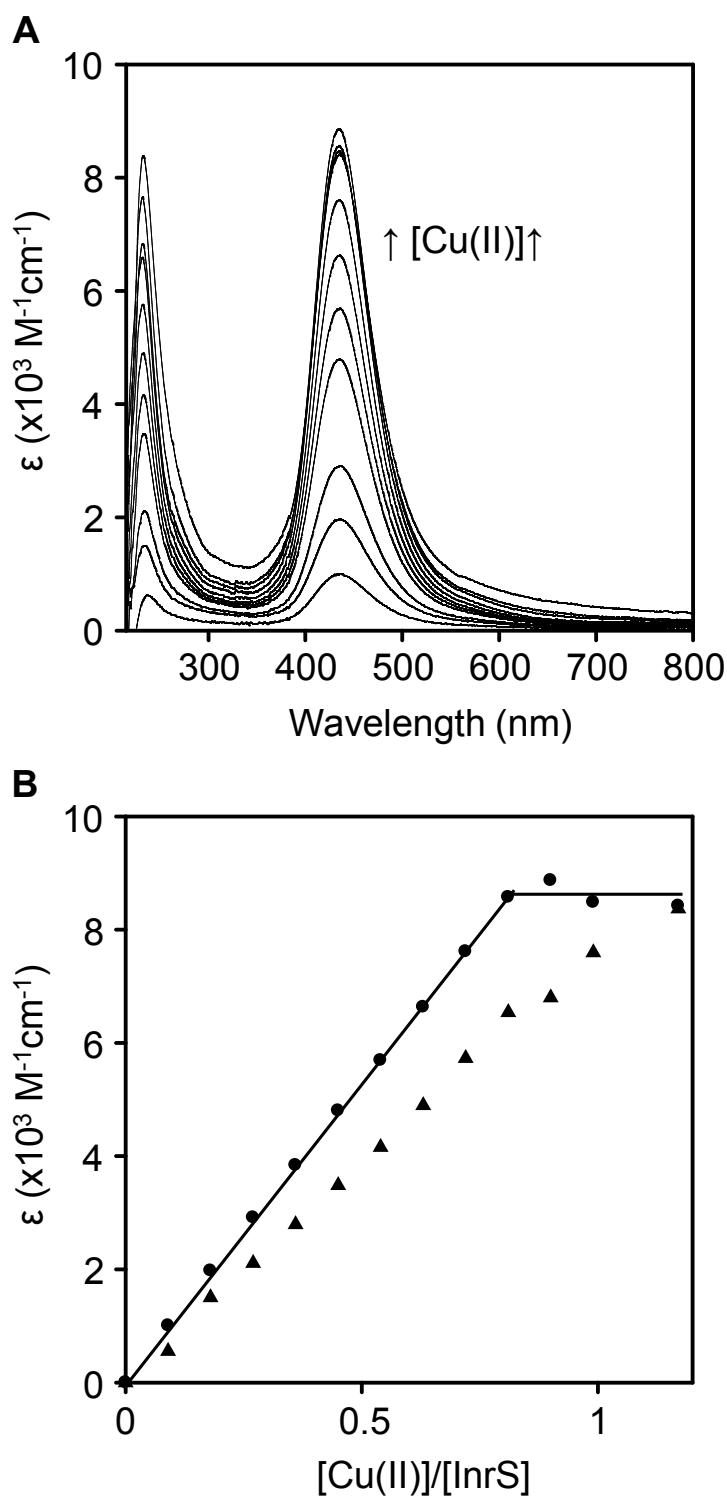


Figure 3.8. UV-Vis spectra of InrS upon titration with CuSO₄. A. Apo-subtracted difference spectra of InrS (10 μM) upon titration with CuSO₄ (recorded anaerobically at pH 7.8). B. Binding isotherm depicting the Cu(II) dependent spectral features at 233 nm (triangles) and 435 nm (circles).

3.3.2 Co(II) binding properties

Upon titration of InrS with CoCl_2 a broad increase in absorbance lacking specific features and covering low energy wavelengths where features that report on metal protein interactions are not usually observed was often apparent. This was likely due to non-specific light scattering due to protein precipitation or aggregation which could sometimes be visualised as ‘cloudiness’ in the protein solution. Figure 3.9 shows InrS cobalt dependent UV-Vis difference spectra up to the addition of 1.47 molar equivalents of CoCl_2 . Above this concentration of CoCl_2 the non-specific light scatter started to mask specific features. A high energy feature centred at 228 nm is apparent along with a broad LMCT envelope containing two peaks and a pronounced shoulder feature. The lower energy peak (341 nm) starts to gain definition on CoCl_2 additions greater than \sim one molar equivalent (each spectrum represents an addition of 0.18 molar equivalents of CoCl_2). A similar phenomenon has previously been observed with cobalt substituted metallothionein (Vašák & Kägi, 1981). Here this was interpreted as cysteine thiolates that coordinate a single cobalt ion in less saturated metallothionein become bridging ligands as the protein is saturated (Vašák & Kägi, 1981). This cobalt-thiolate cluster was later visualised by NMR (Bertini *et al.* 1993). In a separate experiment InrS was titrated with CoCl_2 up to higher stoichiometries and the contribution of non-specific light scatter to these UV-Vis spectra removed by the subtraction of absorbance at 800 nm (Figure 3.10). It should be noted that non-specific light scatter may not be equal at all wavelengths and so care must be taken in making firm conclusions from these data. The cobalt dependent UV-Vis spectral features saturate upon the addition of approximately two molar equivalents of cobalt (Figure 3.10A) and the Co(II)-InrS UV-Vis spectrum upon the single addition of 2.5 molar equivalents of cobalt is shown in Figure 3.10B. The intensity of these features upon saturation is consistent with two thiol ligands coordinating Co(II), with a molar absorbance coefficient of 800-1200 $\text{M}^{-1} \text{cm}^{-1}$ reporting on each cobalt-thiolate bond (VanZile *et al.* 2000). In addition to the LMCT features Co(II)-InrS also displays a broad *d-d* transition envelope centred at \sim 580 nm, which is only evident after removal of the absorbance contribution of non-specific light scatter (Figure 3.10B), the intensity of which is consistent with one Co(II) ion bound in a tetrahedral or pseudo-tetrahedral coordination environment (VanZile *et al.* 2002b). The LMCTs saturate upon addition of approximately two molar equivalents of Co(II) but the binding isotherm for these features is curved rather than a straight line suggesting either the Co(II) is being shared between two distinct protein sites, one sulphur containing and one not or else the binding affinity of the protein for Co(II) is

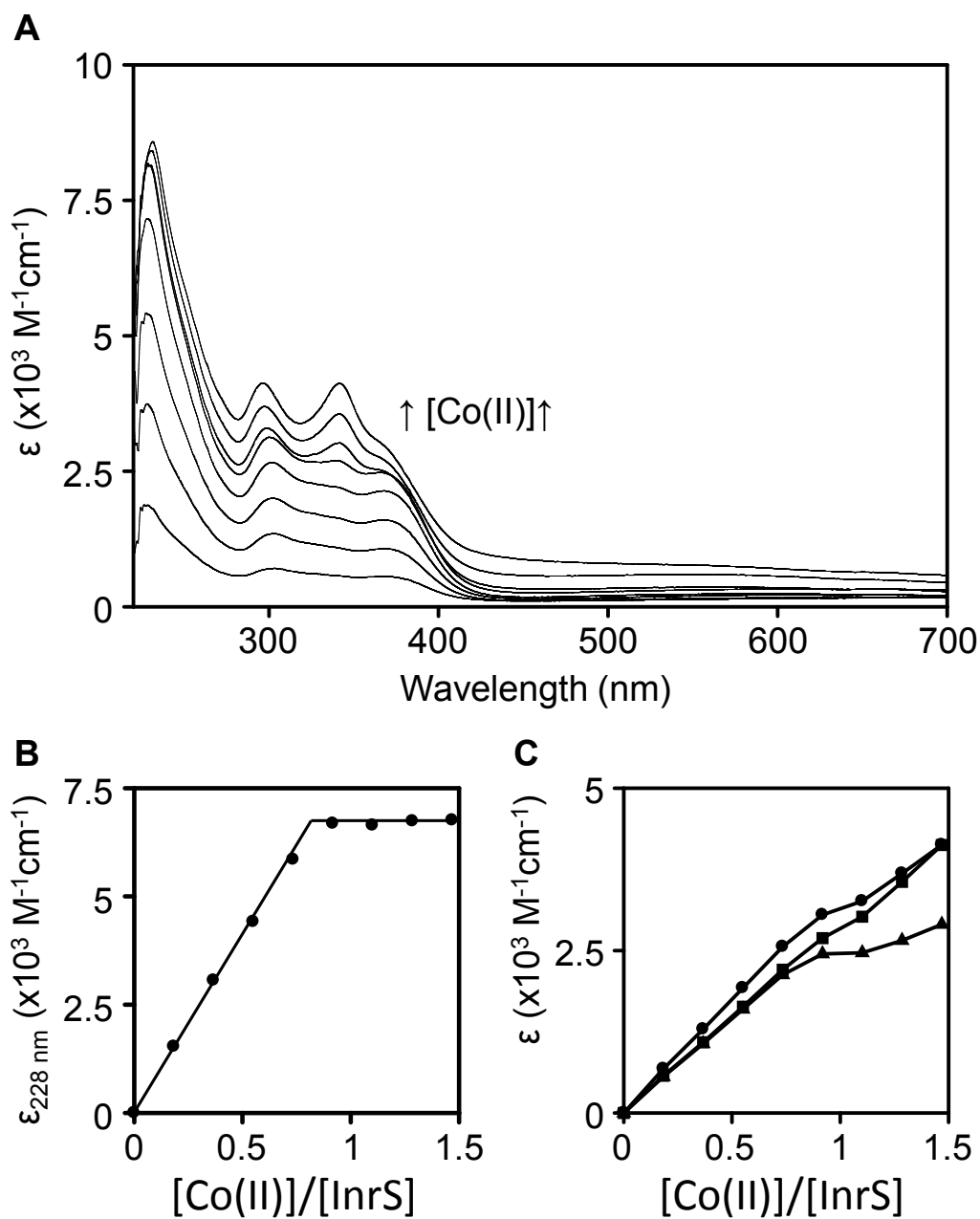


Figure 3.9. UV-Vis spectra of InrS upon titration with CoCl_2 . A. Apo-subtracted difference spectra of InrS ($32.7 \mu\text{M}$) upon titration with CoCl_2 (recorded anaerobically at pH 7.8). B. Binding isotherm depicting Co(II) dependent spectral features at 228 nm. C. Binding isotherms depicting LMCT features at 296 nm (circles), 341 nm (squares) and 370 nm (triangles).

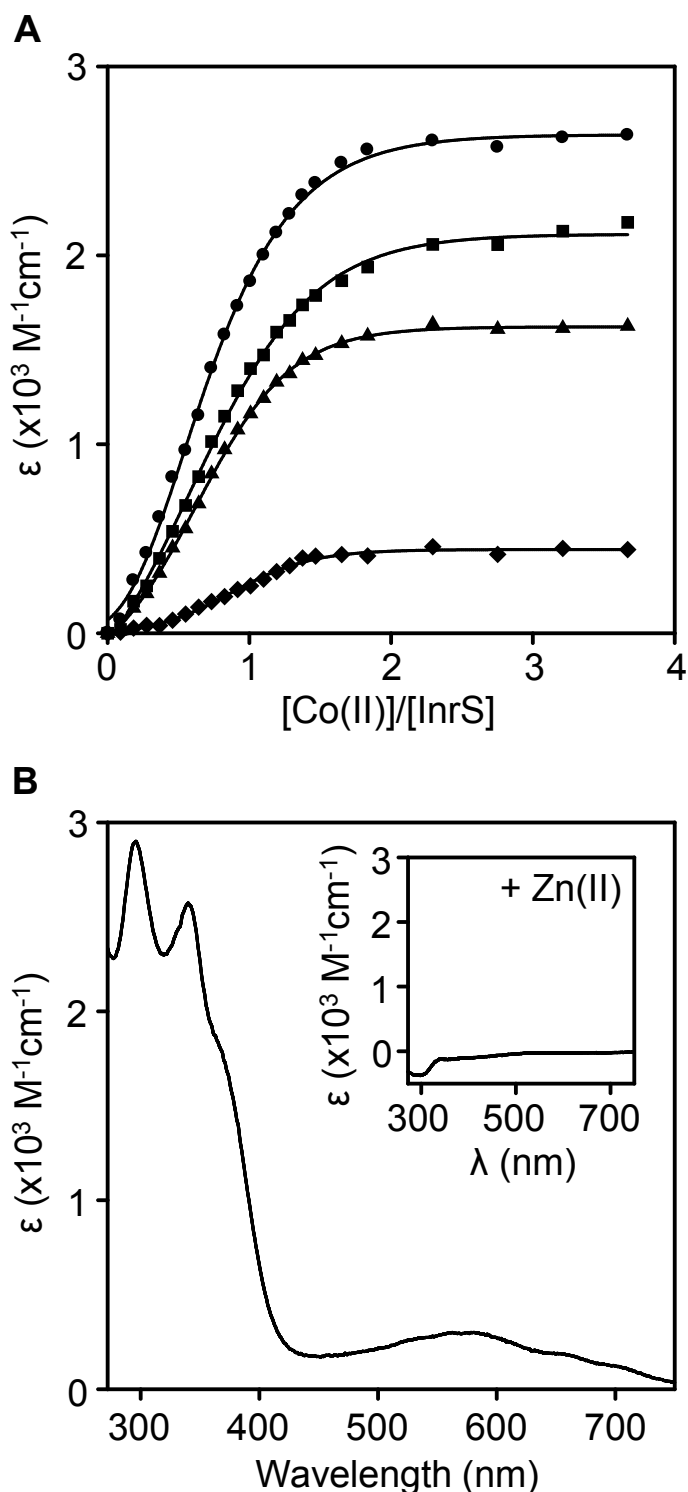


Figure 3.10. Spectral analysis of Co(II) and Zn(II) binding to InrS. A. Binding isotherms depicting the cobalt dependent LMCT and *d-d* transition features at 296 nm (circles), 341 nm (squares), 370 nm (triangles) and 600 nm (diamonds) of InrS (10 μM) upon titration with CoCl_2 , recorded anaerobically at pH 7.8. Absorbance values at 800 nm have been subtracted to attempt to remove the contribution of non-specific light scatter to the extinction coefficient values (see Section 3.3.2). B. Apo-subtracted, $A_{800 \text{ nm}}$ subtracted (see 'A') difference spectra of InrS (30 μM) upon addition of 2.5 molar equivalents of CoCl_2 in order to saturate the cobalt binding sites, recorded anaerobically at pH 7. *Inset* spectrum upon addition of one molar equivalent of ZnSO_4 to the Co(II) saturated protein shown in 'B'.

sufficiently weak that it requires the addition $\sim 20\ \mu\text{M}$ of Co(II) to saturate the site. The interpretation of these data provides a model for Co(II) binding to InrS however the previously mentioned caveat regarding non-specific light scatter subtraction means further analysis such as protein crystallography or XAS will be needed to confirm these predictions.

Zinc is generally considered to be spectrally silent due to its d^{10} electronic structure (although $d-d$ transitions are certainly not possible for a d^{10} ion there are examples in the literature of d^{10} ions exhibiting LMCTs in thiolate containing complexes (see Section 3.3.3 for further discussion)) and therefore cobalt, which is capable of adopting a tetrahedral coordination geometry like zinc, can be used as a spectral probe (VanZile *et al.* 2000). Due to its position on the Irving-Williams series (Equation 1) zinc can often bleach cobalt dependent spectral features (VanZile *et al.* 2000; Ma *et al.* 2011a). Upon addition of one molar equivalent of ZnSO_4 to InrS saturated by the addition of 2.5 molar equivalents of CoCl_2 the cobalt dependent spectral feature is completely quenched (Figure 3.10B *inset*). This could suggest there is only one weak cobalt binding site on InrS, rearrangement of ligands upon zinc binding means that cobalt binding to two sites is lost or that zinc preferentially replaces cobalt at a spectrally active site. In support of the latter models when InrS is applied to and eluted from Sephadex G25 media that has been equilibrated in buffer additionally supplemented with $20\ \mu\text{M}$ CoCl_2 InrS migrates with two molar equivalents of cobalt consistent with a cobalt binding stoichiometry of 2:1 (Figure 3.11).

The cobalt dependent UV-Vis spectra of InrS are complex. The available data suggests two cobalt atoms are bound per InrS monomer with two cysteine residues acting as ligands and pseudo-tetrahedral character to one of the cobalt binding sites. The most parsimonious model given the data described and the presence of two cysteine residues in the protein is two Co(II) binding sites per monomer one of tetrahedral and one of octahedral geometry one or both of which contains cysteine residues (with a total of two cysteine ligands per monomer). As Co(II) appears to be shared between the two sites (given the shape of the binding curve) the Co(II) affinities must be in a similar range. Additionally, there is some evidence that at higher stoichiometries a di-nuclear cobalt site with bridging thiolate ligands rather than two distinct mononuclear sites exists, although this is highly speculative. The cobalt dependent precipitation observed in these titrations may be consistent with the formation of a non-discrete binding site with adventitious ligands being recruited from multiple InrS tetramers.

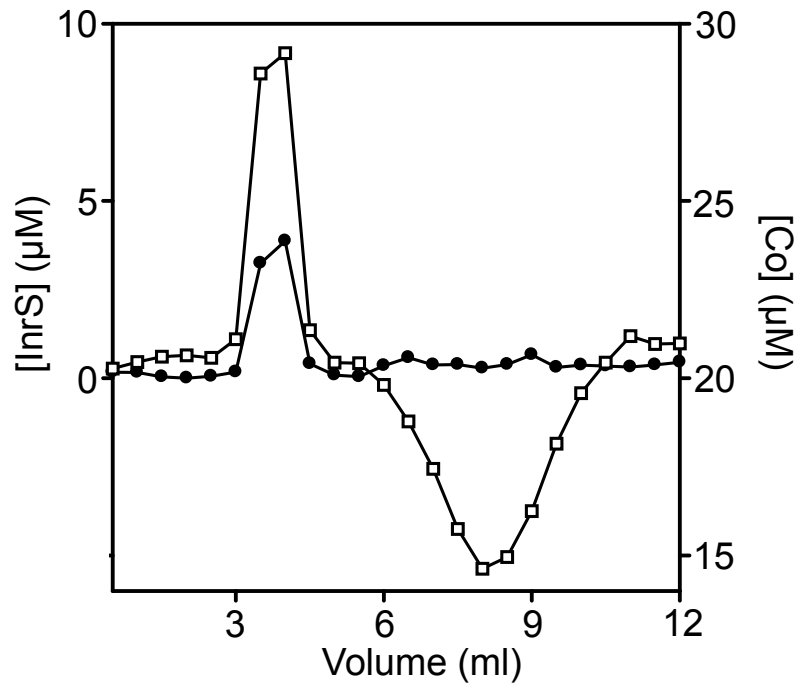


Figure 3.11. InrS migrates with approximately two equivalents of cobalt by size exclusion chromatography when micromolar concentrations of cobalt are present in the buffer. 10 μM InrS was applied to a Sephadex G25 (PD10 column, GE Healthcare) equilibrated in buffer additionally supplemented with 20 μM CoCl_2 then eluted with the same buffer under anaerobic conditions (pH 7.8). Fractions (0.5 ml) were analysed for protein (filled circles, left y axis) by Bradford assay and cobalt (open squares, right y axis) by ICP-MS.

The spectrum of *E. coli* Co(II)-RcnR displays a single LMCT transition peak at 314 nm and no *d-d* transitions, features which are consistent with the XANES pre-edge transitions diagnostic of a six-coordinate, distorted octahedral geometry (Iwig *et al.* 2008). The spectrum of *M. tuberculosis* Co(II)-CsoR displays LMCT features at 290 and 335 nm akin to those of Co(II)-InrS although the longer wavelength LMCT is more akin to a shoulder of the higher energy peak unlike Co(II)-InrS (Ma *et al.* 2009a). *M. tuberculosis* Co(II)-CsoR also displays a *d-d* transition envelope consistent with Co(II) bound in tetrahedral coordination geometry. Two molar equivalents were also needed to saturate the spectral features of *M. tuberculosis* Co(II)-CsoR however here this was taken to mean that there was one site with a weak binding affinity (Ma *et al.* 2009a). Although the Co(II)-InrS spectrum is not highly similar to the *M. tuberculosis* Co(II)-CsoR spectrum it is clear that the spectrum of Co(II)-InrS with its split LMCT feature and *d-d* transitions indicative of tetrahedral Co(II) is more akin to that of *M. tuberculosis* Co(II)-CsoR (Ma *et al.* 2009a) than that of *E. coli* Co(II)-RcnR (Iwig *et al.* 2008).

3.3.3 Cu(I) binding properties

CuCl was prepared in a rigorously anaerobic environment and verified by ICP-MS and BCS assay to be >95 % Cu⁺ (Figure 3.12). Upon titration of InrS with CuCl a single feature with wavelength maximum of 240 nm is observed (Figure 3.13). The binding isotherm for this Cu(I) dependent feature shows an inflection at approximately one molar equivalent suggesting a stoichiometry of one Cu(I) atom per protein monomer, however continues to rise after this inflection point and in a repeat experiment continued to rise even after the addition of four molar equivalents of Cu(I) (Appendix Figure A1). A very subtle feature centred at 435 nm is visible; this is likely due to trace amounts of Cu²⁺ present in the CuCl solution used for the titration (Figure 3.13A *inset*). The low intensity of this feature can be used to confirm the reduced status of the copper used in the experiment.

CsoR homologues from *B. subtilis* (Ma *et al.* 2009a), *S. lividans* (Dwarakanath *et al.* 2012), *M. tuberculosis* (Liu *et al.* 2007) and *S. aureus* (Grossoehme *et al.* 2011) along with *E. coli* RcnR (Higgins *et al.* 2012b) all display similar spectra of similar intensity when titrated with Cu⁺, additionally the CsoR homologue from *T. thermophilus* displays absorbance at 240 nm upon Cu⁺ titration presumably due to a similar feature (Sakamoto *et al.* 2010). Trigonal planar coordination geometry has been experimentally confirmed for Cu(I) bound *M. tuberculosis* (Liu *et al.* 2007), *B. subtilis* (Ma *et al.* 2009a) and *S*

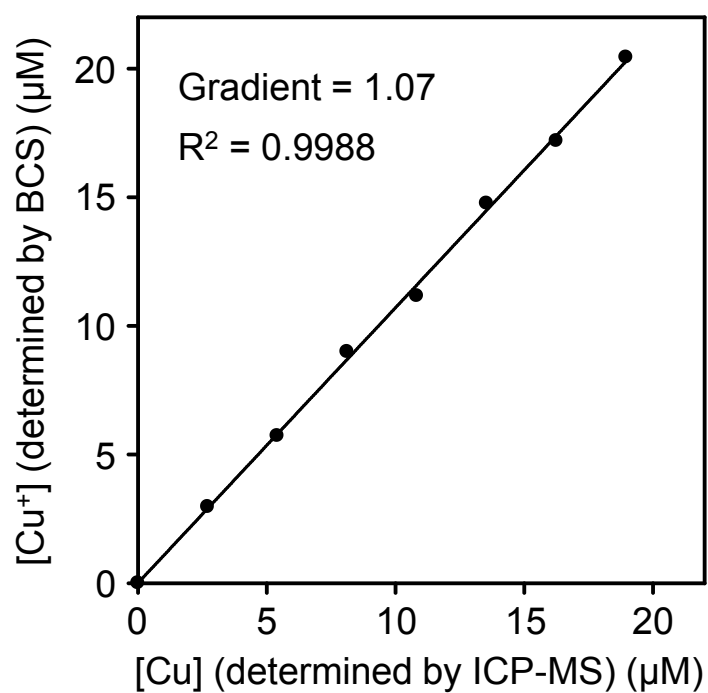


Figure 3.12. Validation of the reduced status of Cu^+ stocks by ICP-MS and BCS assay. Cu^+ stocks were prepared anaerobically and analysed for total dissolved copper by ICP-MS. The proportion of Cu^+ was verified to be close to 100 % by titration against BCS.

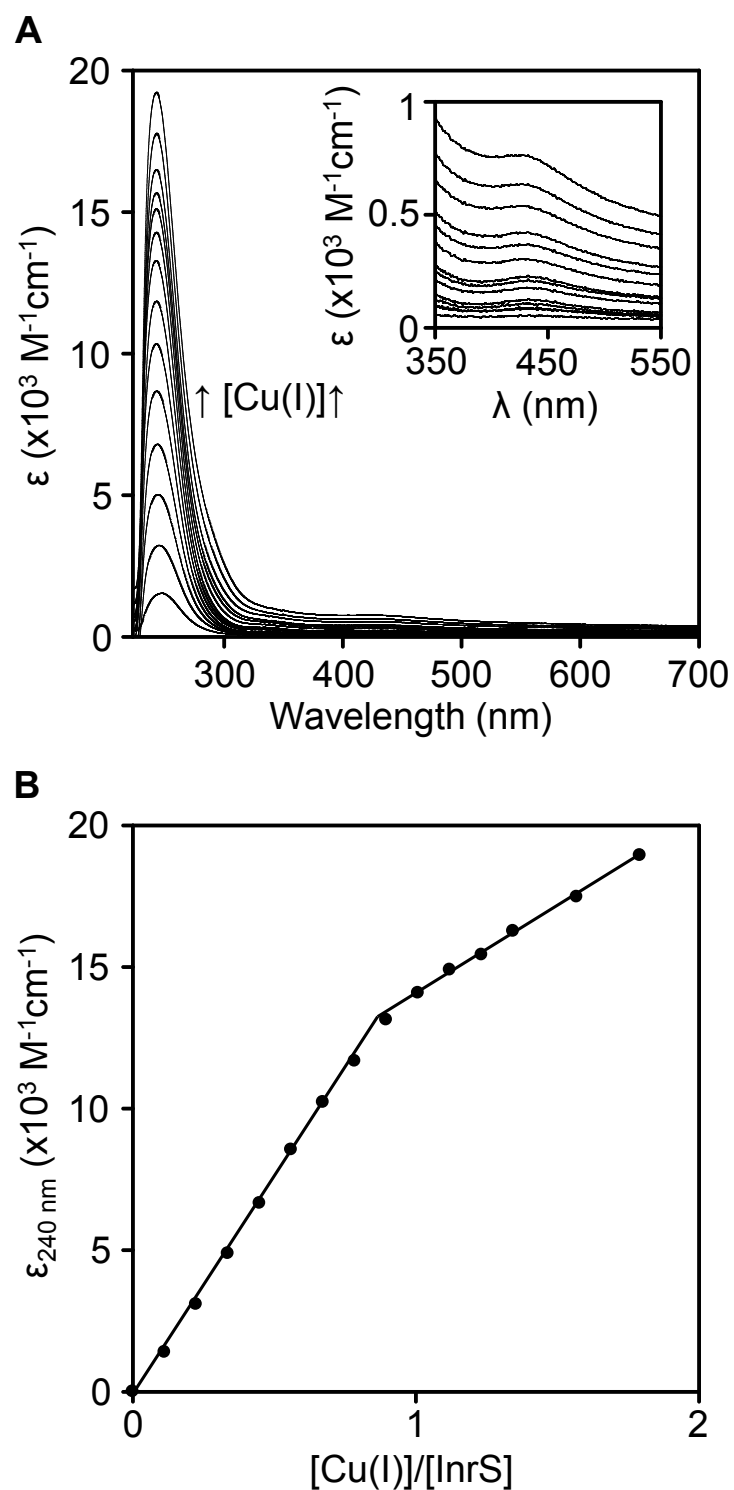


Figure 3.13. UV-Vis spectra of InrS upon titration with CuCl. A. Apo-subtracted difference spectra of InrS (40 μM) upon titration with CuCl (oxidation state verified as Cu^+) (recorded anaerobically at pH 7.8). *Inset*, expansion of the 350-550 nm region of the spectra. B. Binding isotherm depicting the Cu(I) dependent spectral feature of InrS at 240 nm.

aureus CsoR (Grossoehme *et al.* 2011). The coordination geometry of Cu(I) bound *E. coli* RcnR appears to be dependent on the nature of the anion present in the buffer with RcnR forming a trigonal planar Cu(I) complex in NaCl containing buffer and a tetrahedral Cu(I) complex in NaBr containing buffer (Higgins *et al.* 2012b). The UV-Vis spectrum of Cu(I) bound RcnR was recorded in buffer containing NaBr and so this universal Cu(I) dependent feature appears not to be reporting on the coordination geometry of the Cu(I) site. This is consistent with work on model Hg(II) (a d^{10} ion like Cu(I)) complexes which showed that spectral features similar to those being discussed here for Cu(I) protein complexes and previously attributed to a distorted tetrahedral coordination geometry were also observed in a trigonal planar complex (Watton *et al.* 1990). An absorbance feature at ~240 nm has been observed for Cu(I) (Liu *et al.* 2008), Hg(II) (Watton *et al.* 1990) and Pb(II) (Payne *et al.* 1999; Wang *et al.* 2005 & 2010), all d^{10} ions, in thiolate containing binding sites of proteins and peptides and has been attributed to LMCTs. As the d orbitals are full in these ions presumably the charge transfer is into higher energy s and p orbitals and this likely explains the blue shifted nature of these features when compared with, for example, $S^- \rightarrow Co$ LMCTs. Interestingly the Cu(I) dependent UV-Vis spectra of *S. lividans* CsoR contains additional complexity not seen in other homologues currently characterised (Dwarakanath *et al.* 2012). In addition to the intense feature centred around 240 nm there is a peak of lesser intensity centred at 320 nm. These UV-Vis spectra are highly similar to the spectra of Pb(II) substituted CmtR (from both *M. tuberculosis* and *Streptomyces coelicolor*) (Wang *et al.* 2005 & 2010) and Pb(II) substituted peptide analogues of zinc finger domains (Payne *et al.* 1999; Magyar *et al.* 2005). The origin of this longer wavelength band was attributed to intra-atomic electronic transitions. Why this feature is observed for Cu(I) binding to *S. lividans* CsoR and no other homologues remains to be discovered.

3.4 Identification of the InrS DNA-binding site by EMSA

Taken together the above spectral analysis of the metal binding properties of InrS suggested the protein has a metal coordination site with more similarity to copper sensing CsoR than to nickel/ cobalt sensing RcnR. This led to the working hypothesis that InrS might be a cytosolic copper sensor akin to the copper sensing CsoRs however the target regulated by InrS was still unknown. To determine the gene(s) regulated by

InrS a bioinformatics coupled to EMSA screening approach was used to find promoter elements that might represent InrS binding sites.

3.4.1 Targets whose promoter regions contain similarity to the *B. subtilis* CsoR DNA recognition site

The *Synechocystis* genome was searched for promoters with similarity to the DNA binding site of *B. subtilis* CsoR. It has been shown that *B. subtilis* CsoR binds specifically to DNA containing the imperfect palindromic sequence TACCCTACGGGGGTATGGTA (Smaldone & Helmann. 2007; Ma *et al.* 2009a). The genome of *Synechocystis* was searched, using the pattern search tool of the website ‘Cyanolist’, for a two part pattern: 1st part = TACCCTAC, 2nd part = GTATGGTA with a 3-4 nucleotide spacing between the parts. Two mismatches were allowed in either part and only patterns located within a region covering 100 bp immediately prior to a translational start codon were reported. This search strategy returned eight hits (Figure 3.14). Of the eight returned targets two had links to copper homeostasis, *moeA* and *coxB*. In *E.coli* MoeA is required for chelation of molybdenum by molybdopterin to create the molybdenum co-factor (Nichols & Rajagopalan. 2002). Copper plays a role in the assembly of this co-factor, possibly keeping thiols reduced prior to the insertion of molybdenum (Schwarz *et al.* 2009). Additionally, the molybdopterin biosynthesis operon of *E. coli* is up-regulated by CueR in response to copper (Yamamoto & Ishihama. 2005a). *coxB* encodes a sub-unit of cytochrome c oxidase and contains a dinuclear Cu_A site providing a clear link to copper metabolism (Alge & Peschek. 1993).

In some prokaryotes adenylate kinase (encoded by *adk*) has been found to contain a structural metal ion. Zinc, cobalt and most recently iron forms of this protein have been described (Gavel *et al.* 2008; Mukhopadhyay *et al.* 2011) however as copper forms have not been described and because copper is not utilised as a structural ion *sll1059* was excluded from the analysis. The apparent role of InrS as cobalt responsive transcriptional regulator (Section 3.5) perhaps argues that this target should be reassessed. Adk is an essential enzyme required for growth in all organisms, *Synechocystis* encodes two homologues of Adk (*sll1815* and *sll1059*) and so it is tempting to speculate that perhaps one of these enzymes substitutes for the other under conditions where cobalt availability is scarce. However both homologues of Adk from *Synechocystis* belong to the ‘short’ sub-family of adenylate kinases which are relatively rare in prokaryotes (Munier-Lehmann *et al.* 1999). These ‘short’ Adk proteins lack the so called lid domain in which the metal ion is bound in some examples of ‘long’ Adk

TACCCTACGGGGGTATGGTA →.....←	<i>B. subtilis copZ</i>
TACCCTACAAGAA ATGGTA →.....←	<i>moeA (slr0900)</i>
TACCCTGTAGGGG ATTGTA →.....←	<i>coxB (slr1136)</i>
TACTCTAGTCACTTAGGGTA →.....←	<i>adk (slr1059)</i>
TAACCTCCCTAAA ATGGTA →.....←	<i>dnaN (slr0965)</i>
TACGCAACTTAG TCAGGTA →.....←	hypothetical (<i>slr1640</i>)
AACCCACATCACCATGGTA →.....←	<i>purC (slr1226)</i>
CACCCTGCAGAG TTTGGGA →.....←	<i>comM (slr0904)</i>
TGCCATACTCCGCTGTGGTA →.....←	<i>fraH (slr0298)</i>

Figure 3.14. Identification of potential InrS DNA binding sites by analogy to the *B. subtilis* CsoR DNA binding site. Sequences (upstream of gene coding regions) with analogy to the *B. subtilis* CsoR DNA recognition site, identified by a Cyanolist pattern search as described in Section 3.4.1. Nucleotides of the returned sequence matching the *B. subtilis* CsoR DNA recognition site are shown in red. Symmetry elements are underlined with an arrow with breaks in symmetry represented by a dotted line.

proteins and so lack the conserved residues to which these metals bind (Gavel *et al.* 2008). The potential binding site upstream of *sll1059* is also a poor match to the *bona fide* InrS binding site subsequently identified in the promoter region of *nrsD* (Section 3.4.4). Thus on this reanalysis there remains no clear rationale to assess InrS binding to the promoter region of *sll1059*.

The sequence immediately upstream of the translational start codons of *moeA* and *coxB* was amplified by PCR, ligated to pGEM-T and the newly constructed plasmid was propagated in *E. coli* DH5 α . The DNA probes to be used in the EMSA analyses were then PCR amplified from these plasmids and designated *moeA*Pro (110 bp) and *coxB*Pro (96 bp) (Figure 3.15). A non-specific DNA probe (pGEMCon1, 136 bp) was PCR amplified from re-circularised pGEM plasmid using primers homologous to either side of the multi-cloning site (Figure 3.16) and this probe was included in the EMSA analyses to control for non-specific protein-DNA binding.

Inclusion of InrS in the *coxB*Pro EMSA experiment binding reactions caused the appearance of low mobility (shifted DNA band) InrS:DNA complex (Figure 3.17). As the concentration of InrS included in these binding reactions was increased a decrease in the intensity of the free pGEMCon1 but not the *coxB*Pro probe was observed (Figure 3.17). This indicates that InrS displays more specificity for the control fragment than the fragment containing the identified site. In an analogous experiment using the *moeA*Pro probe the low mobility InrS:DNA complex is observed but InrS appears to display no specificity for the *moeA*Pro over pGEMCon1, inferred from the roughly equal intensity of free *moeA*Pro and pGEMCon1 in each lane (Figure 3.18). As InrS appeared to display equal specificity for *moeA*Pro and pGEMCon1 and a greater specificity for pGEMCon1 than *coxB*Pro it was reasoned that InrS should display greater specificity for *moeA*Pro than *coxB*Pro. This was found to be the case in a competitive EMSA using these two probes (Figure 3.19).

The preference of InrS for the DNA sequence amplified from pGEM was unexpected. In order to identify the origin of this effect the sequence of pGEMCon1 was examined. The nucleotide 'lAlign' program was used to look for regions of similarity to the *B. subtilis* CsoR DNA binding site in the pGEMCon1 fragment (along with *coxB*Pro and *moeA*Pro) and to calculate a Waterman-Eggert score to rank the best alignments (Waterman & Eggert. 1987). The highest scoring alignments of the *B. subtilis* CsoR binding site with the pGEMCon1, *moeA*Pro and *coxB*Pro fragments are shown in Figure 3.20. The nucleotide sequences in the *moeA*Pro and *coxB*Pro probes identified in the

A

TTTTATGAGATCATGCAGGTCTACGGTATGCCCATGAAG
MoeAPro_F
GAAGTAATCCATGAGAAATTTGGGGACGGTATCATGAGT
GCCATCGACTTCACCTTAGACATTGAGAAGGAAGCAGAC
CCTAAAGGCGATCGGGTTAAAGTAACGATGAATGGTAAG
MoeAPro+CsoRBox_F
TTTTTACCCTACAAGAAATGGTAATGGGGGACCAACCGAA
ATGATTTCCGTTGCCGCCGCCGTTGAAATTATCCAAGCC
MoeAPro_R
CATTGGCCCAATTTTGGTGAT

B

GTAGAAATCCCCCTTTATCAGCGAAGACAATGATTGCCAT
Ccosu2Pro_F
AGAACAAATTTATCATAAAAACAGGCACAGAAGGAGACG
GCAAGATTGTTAAAGAACTCTGAAGAATTTGGCTGGAGC
CcoPro+CsoRBox_F
TTGACCCCGCTCTGGAGAATTGCTTTACCCTGTAGGGGA
TTGTAATTTTTTGTGTTTCCGAGAGATAGAGGTTTGCT
Ccosu2Pro_R
ATGAAAATTCCCGGTAGTGTTCATAACCCTTCTCA

Figure 3.15. Design of *moeA*Pro and *coxB*Pro EMSA probes. A. Nucleotide sequence of the start of the coding region and upstream region of *moeA*. The translational start codon (red box) and the potential InrS binding site (blue box) are highlighted. Primers homologous to the regions labelled MoeAPro_F and MoeAPro_R were used to amplify this sequence from *Synechocystis* genomic DNA for cloning into pGEM-T and primers homologous to the regions labelled MoeAPro+CsoRBox_F and MoeAPro_R to amplify the probe designated *moeA*Pro from the constructed plasmid for use in EMSAs. B. Nucleotide sequence of the start of the coding region and upstream region of *coxB*. The translational start codon is highlighted in the red box and the potential InrS binding site highlighted in the blue box. Primers homologous to the regions labelled Ccosu2Pro_F and Ccosu2Pro_R were used to amplify this sequence from *Synechocystis* genomic DNA for cloning into pGEM-T and primers homologous to the regions labelled CcoPro+CsoRBox_F and Ccosu2Pro_R were used to amplify the probe designated *coxB*Pro from the constructed plasmid for use in EMSAs.

```

          T7 Promoter
          >
GGCCAGTGAATTGTAATACGACTCACTATAGGGCGAATTGGGCC
  AatII   SphI   BstZI   NcoI   SacII   Apal
CGACGTCGCATGCTCCCGGCCGCCATGGCCGCGGGATACTACTA
  NotI   PstI   SalI   NdeI   SacI   BstXI
GTGCGGCCCGCCTGCAGGTCGACCATATGGGAGAGCTCCCAACGC
pGEMPI_F  NsiI
GTTGGATGCATAGCTTGAGTATTCTATAGTGTACCTAAATAGC
pGEM-T_rev
TTGGCGTAATCATGGTCATAGCTGTTTCCTGTGTGAAATTGTTA
pGEMPI_R
TCCGCTCACAATTCCACACAACATACGAGCCGGAAGCATAAAGT
pGEMPI_R2
GTAAAGCCTGGG

```

Figure 3.16. Design of pGEM derived EMSA control probes. Nucleotide sequence of the multiple cloning sequence of recircularised pGEM-T vector and adjacent regions. Restriction enzyme sites are indicated to provide a point of reference. The site where cloned fragments are inserted is marked with an arrow. The sequence with homology to the *M. tuberculosis* CsoR DNA binding site is indicated in the blue box. pGEMCon1 was amplified using primers homologous to the regions labelled T7 Promoter and pGEM-T_rev. pGEMCon2 was amplified using primers homologous to the regions labelled pGEMPI_F and pGEM-T_rev. pGEMCon3 was amplified using primers homologous to the regions labelled pGEMPI_F and pGEMPI_R. pGEMCon4 was amplified using primers homologous to the regions labelled pGEMPI_F and pGEMPI_R2.

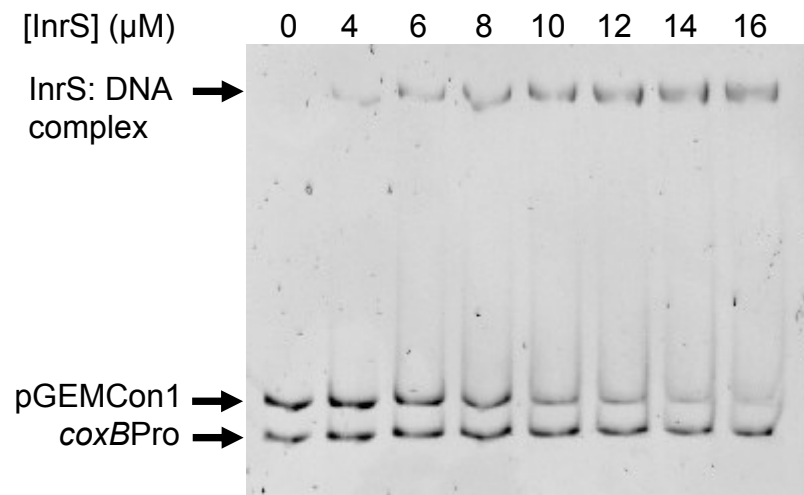


Figure 3.17. Competitive EMSA assessing InrS binding to *coxBPro*. Competitive EMSA with 96 bp *coxBPro* (50 nM) and 136 bp non-specific DNA probe pGEMCon1 (50 nM) incubated with the concentrations of InrS indicated before resolving by native PAGE.

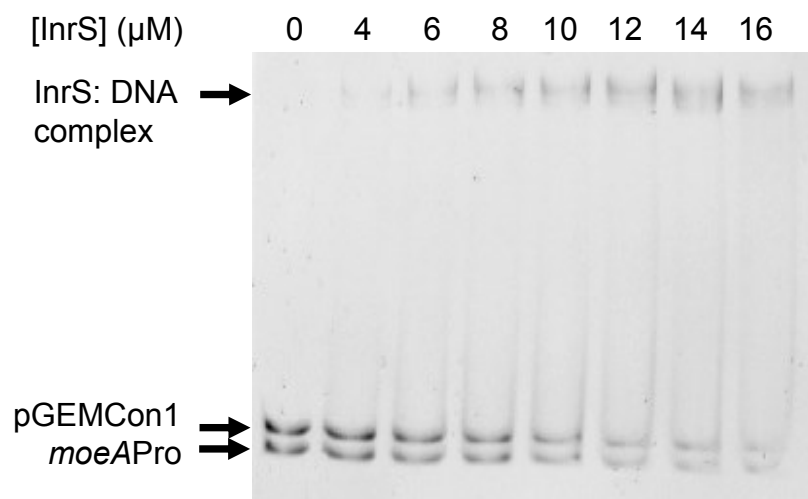


Figure 3.18. Competitive EMSA assessing InrS binding to *moeAPro*. Competitive EMSA with 110 bp *moeAPro* (50 nM) and 136 bp non-specific DNA probe pGEMCon1 (50 nM) incubated with the concentrations of InrS indicated before resolving by native PAGE.

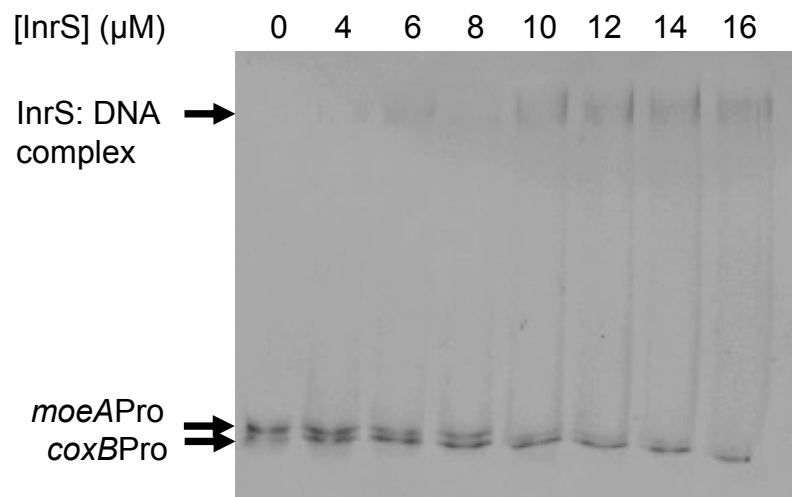


Figure 3.19. Competitive EMSA to assess InrS binding preference for the probes *moeAPro* and *coxBPro*. Competitive EMSA with 110 bp *moeAPro* (25 nM) and 96 bp *coxBPro* (25 nM) incubated with the concentrations of InrS indicated before resolving by native PAGE.

moeAPro

Waterman-Eggert score: 43

```
BsubCs  TACCCTACGGGGGTATGGTA
          ::::: : :::::
moeAPr  TACCCTACAAGAA-ATGGTA
```

coxBPro

Waterman-Eggert score: 43

```
BsubCs  TACCCTACGGGGGTATGGTA
          ::::: : : : :
coxBPr  TACCCTGTAGGGG-ATTGTA
```

pGEMCon1

Waterman-Eggert score: 33

```
BsubCs  ACCCTACGGGGG
          : : : :
pGEMCo  ACCATATGGGAG
```

Figure 3.20. Alignment of *moeAPro*, *coxBPro* and pGEMCon1 with the *B. subtilis* CsoR DNA recognition site. Best scoring alignments of *moeAPro* (moeAPr), *coxBPro* (coxBPr) and pGEMCon1 (pGEMCo) with the *B. subtilis* CsoR DNA recognition sequence (BsubCs) (Section 3.4.1); the Waterman-Eggert score is also shown.

genome pattern search are, as would be expected, the best matches to the *B. subtilis* CsoR binding sites present in those probes and are both better matches than the best match identified in pGEMCon1 (Figure 3.20). At the time of these experiments the only other experimentally validated CsoR binding site was that of *M. tuberculosis* CsoR (Liu *et al.* 2007). Alignment of the DNA recognition site of *M. tuberculosis* CsoR (GTAGCCCACCCCCAGTGGGGTGGGATAC) with pGEMCon1, *moeA*Pro and *coxB*Pro revealed that the pGEMCon1 contains sequence with greater similarity to this recognition site than the other two probes and this may explain why InrS appears to display a preference for pGEMCon1 (Figure 3.21).

The region of pGEMCon1 containing the site identified in Figure 3.21 as containing similarity to the *M. tuberculosis* CsoR recognition site is located immediately 5' to the region of pGEM-T where 3'-A tailed cloned products are ligated and encompasses the BstZI, NcoI and SacII restriction sites (Figure 3.16). Therefore, a new control fragment was produced containing DNA sequence 3' of this region (pGEMCon2, 68 bp, essentially a truncated version of pGEMCon1) (Figure 3.16). Although pGEMCon2 lacks the sequence with the best match to the *M. tuberculosis* CsoR binding site it still contains a region with a slightly better match to the *M. tuberculosis* CsoR recognition site than both *moeA*Pro and *coxB*Pro (Figure 3.21). Therefore longer versions of *moeA*Pro and *coxB*Pro were produced using primer pairs MoeAPro+CsoRBox_F & pGEM-T_rev and CcoPro+CsoRBox_F & pGEM-T_rev respectively (Figures 3.15 and 3.16). These probes, designated *moeA*Pro+ (179 bp) and *coxB*Pro+ (165 bp), contain both the sequence of the original probes and the sequence of pGEMCon2. Thus any specificity of InrS binding observed for either *moeA*Pro+ or *coxB*Pro+ over pGEMCon2 should be due to sequence from the promoter region of the respective gene.

InrS displays a clear preference for both *moeA*Pro+ and *coxB*Pro+ over pGEMCon2 (Figure 3.22 and 3.23) with apparent complete retardation of these probes observed with only a minimal reduction in pGEMCon2 intensity. This could be taken to mean that InrS binds specifically to the sequences identified upstream of *moeA* and *coxB*, however DNA binding by *E. coli* RcnR has been shown to be at least partly dependent on the length of DNA (Section 1.5.2). To test if the observed apparent specificity of InrS binding to *moeA*Pro+ and *coxB*Pro+ was due to length rather than specific sequence, two new control fragments were produced; pGEMCon3 and 4 (141 and 190 bp respectively, essentially extended versions of pGEMCon2) (Figure 3.16).

*moeA*Pro

Waterman-Eggert score: 31

```
mtbCso  ACTGGGGG
        :  :::::
moeAPr  AATGGGGG
```

*coxB*Pro

Waterman-Eggert score: 33

```
mtbCso  ACCCCACTGGGG
        :::::  ::  ::
coxBPr  ACCCGCTCTGG
```

pGEMCon1

Waterman-Eggert score: 43

```
mtbCso  CCCACCCCCAGTGGGGTGGGATA
        ::  ::  ::  :  :  :::::
pGEMCo  CCGGCCGCCATGGCCGCGGGATA
```

pGEMCon2

Waterman-Eggert score: 34

```
mtbCso  TCCCACCCCACTGG
        :::::  :  :  ::
pGEMC2  TCCCAACGCGTTGG
```

Figure 3.21. Alignment of *moeA*Pro, *coxB*Pro, pGEMCon1 and pGEMCon2 with the *M. tuberculosis* CsoR DNA recognition site. Best scoring alignments of *moeA*Pro (*moeA*Pr), *coxB*Pro (*coxB*Pr), pGEMCon1 (pGEMCo) and pGEMCon2 (pGEMC2) with the *M. tuberculosis* CsoR DNA recognition sequence (mtbCso) (Section 3.4.1), the Waterman-Eggert score is also shown.

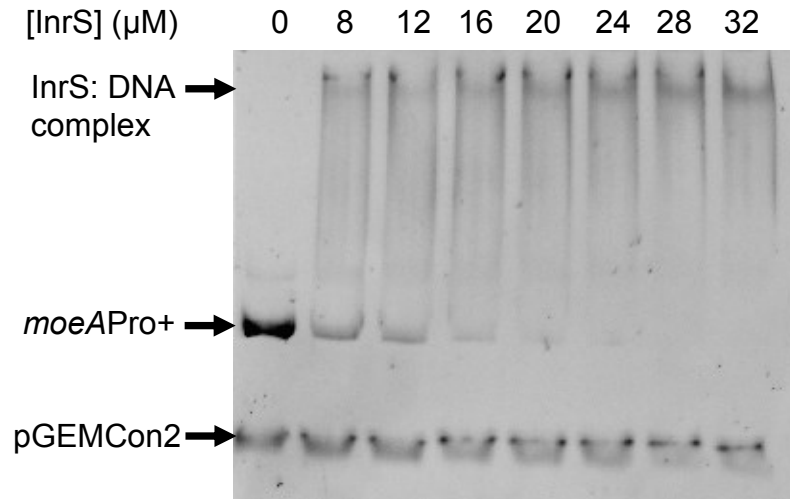


Figure 3.22. Competitive EMSA assessing InrS binding to *moeAPro+*. Competitive EMSA with 165 bp *moeAPro+* (100 nM) and 68 bp non-specific DNA probe pGEMCon2 (100 nM) incubated with the concentrations of InrS indicated before resolving by native PAGE.

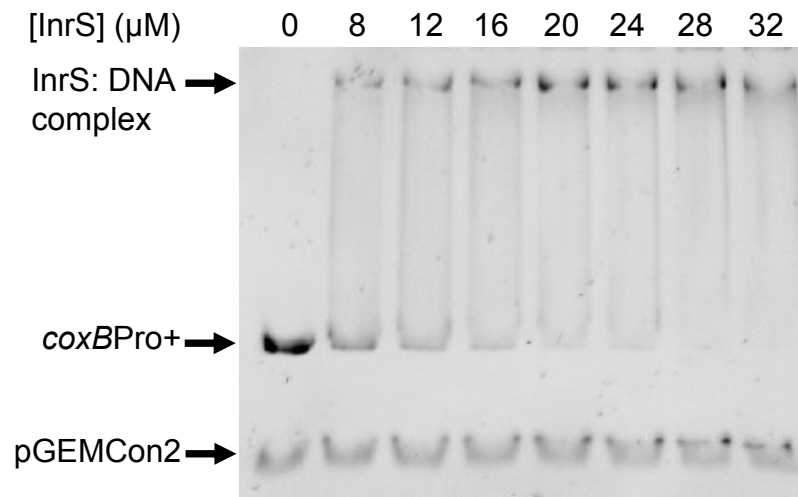


Figure 3.23. Competitive EMSA assessing InrS binding to *coxBPro+*. Competitive EMSA with 179 bp *coxBPro+* (100 nM) and 68 bp non-specific DNA probe pGEMCon2 (100 nM) incubated with the concentrations of InrS indicated before resolving by native PAGE.

InrS shows specificity of binding to *MoeA*Pro+ over pGEMCon3 and this specificity is retained even when the longer pGEMCon4 is used as the competitor (Figure 3.24). The same is true of *coxB*Pro+ (Figure 3.25). InrS displays an apparent affinity for these probes of $K_{\text{DNA, app}} \sim 8 \mu\text{M}$.

The optimised experimental design gives confidence that InrS is specifically recognising a DNA element from the promoter regions of *moeA* and *coxB*; however specificity for these DNA sequences *in vitro* does not prove that InrS regulates these genes, especially given the weak $K_{\text{DNA, app}}$. This experimental approach was therefore applied to other potential targets with the hope of either identifying a target for which InrS showed very clear specificity or building a consensus sequence from DNA elements for which InrS displays some specificity with which to identify the true target(s).

3.4.2 Targets known to be copper regulated

In *Synechocystis* the expression of *petE*, encoding the copper-containing electron carrier protein plastocyanin, is regulated in response to copper (Zhang *et al.* 1992) and in the closely related cyanobacterium *Synechococcus* sp. PCC7942 the copper translocating ATPase encoded by *pacS* is also copper regulated (Kanamaru *et al.* 1994), both by unknown mechanisms. In *Synechocystis* the PacS protein is required for delivery of copper to proteins in both the thylakoid and the periplasm (Waldron *et al.* 2010). Inspection of the region upstream of these genes revealed the presence of a GC rich tract (Figure 3.26), a feature thought to be important for DNA recognition by CsoR-RcnR family proteins (Iwig & Chivers. 2009; Grosseohme *et al.* 2011) (Section 1.5.2). The other copper transporting ATPase of *Synechocystis*, CtaA, is not known to be regulated in response to copper. Given the originally assigned role of CtaA as a copper importer (Tottey *et al.* 2001) CtaA would not be expected to be regulated (at least by a de-repressor) in response to copper. However given more recent data that suggests CtaA may export rather than import copper (Raimunda *et al.* 2012) perhaps this should be addressed. Inspection of the region upstream of *ctaA* does not reveal the presence of a GC rich tract (Appendix Figure A2). Given the hypothesised role of InrS as a cytosolic copper sensor, *petE* and *pacS*, which are both copper regulated and are located downstream of a possible InrS binding sites, represent plausible targets for regulation by InrS. The ability of InrS to bind to the promoter regions of these two genes was tested by EMSA. DNA probes of the upstream regions of *petE* and *pacS*, designed such that the GC rich tracts were located approximately in the middle of the DNA fragment were

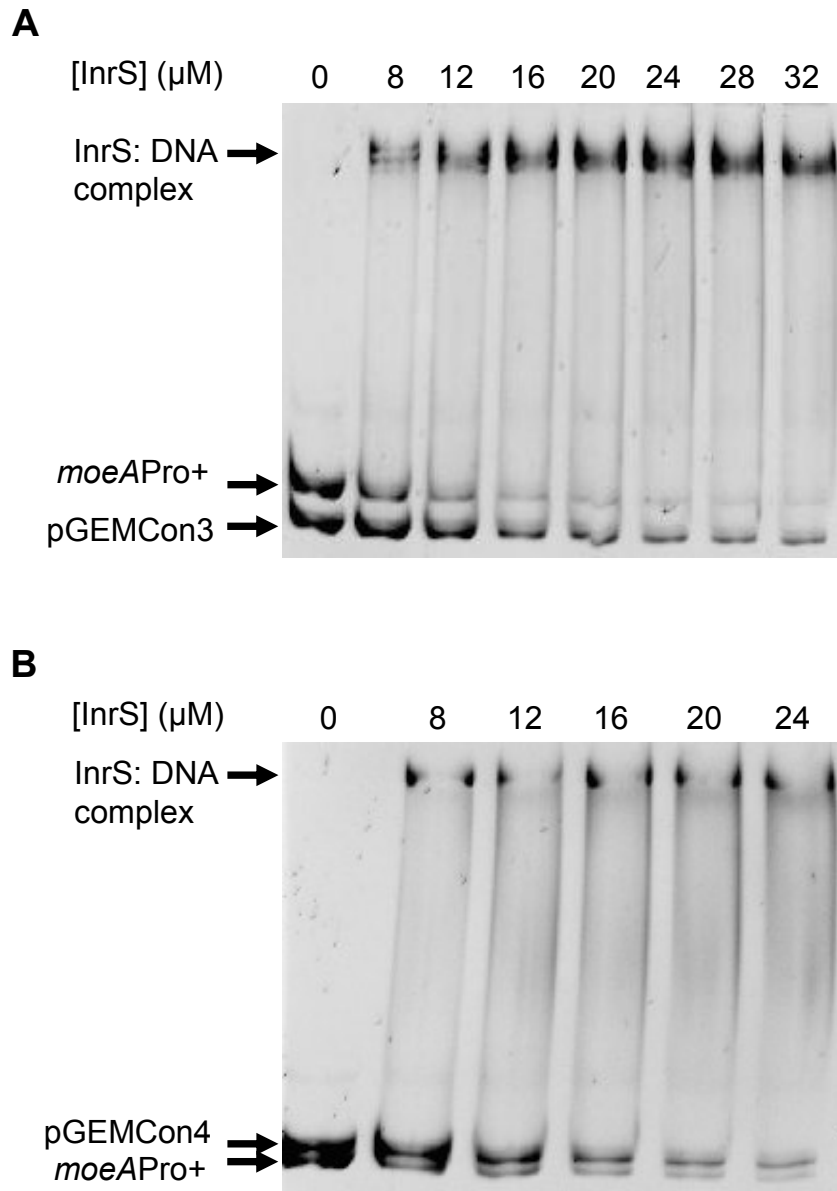


Figure 3.24. Competitive EMSA to assess the role DNA probe length plays in specific recognition of *moeA*Pro+. A. Competitive EMSA with 179 bp *moeA*Pro+ (100 nM) and 141 bp non-specific DNA probe pGEMCon3 (100 nM) incubated with the concentrations of InrS indicated before resolving by native PAGE. B. Competitive EMSA with *moeA*Pro+ (100 nM) and 190 bp non-specific DNA probe pGEMCon4 (100 nM) incubated with the concentrations of InrS indicated before resolving by native PAGE.

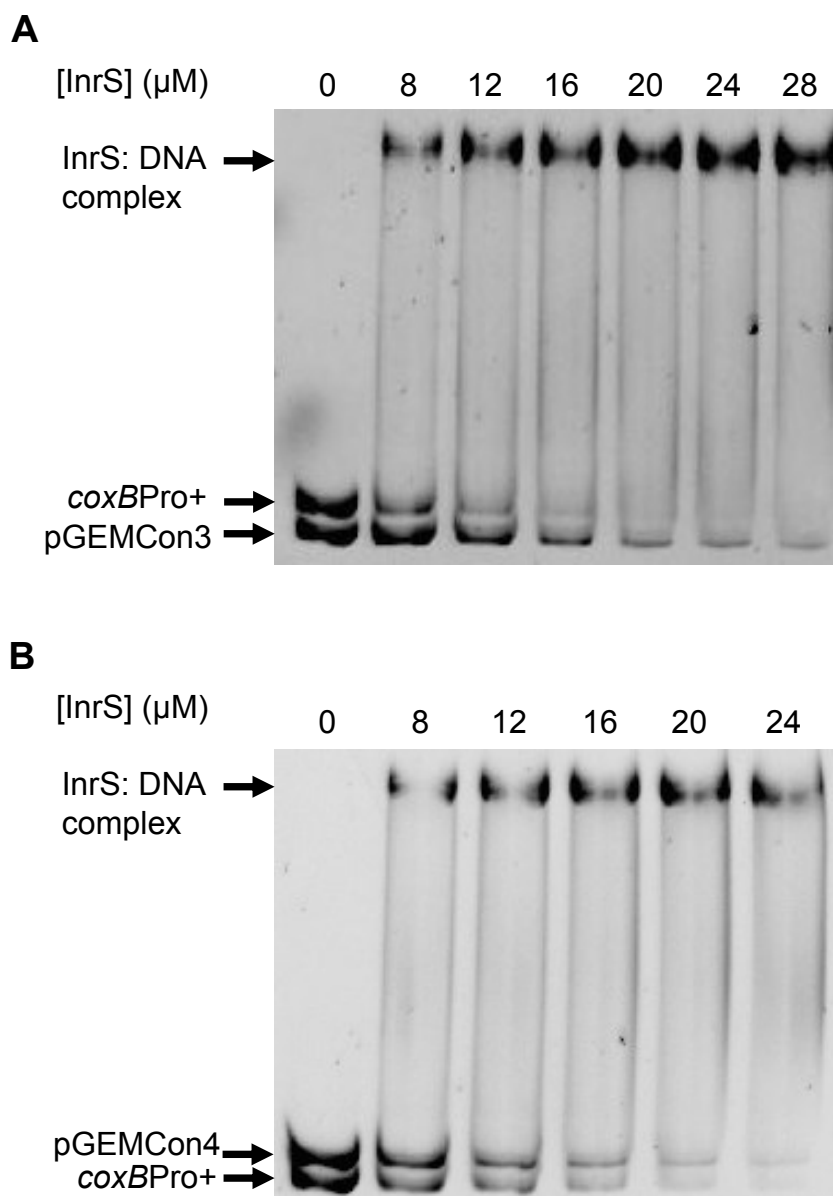


Figure 3.25. Competitive EMSA to assess the role DNA probe length plays in specific recognition of *coxBPro+*. A. Competitive EMSA with 165 bp *coxBPro+* (100 nM) and 141 bp non-specific DNA probe pGEMCon3 (100 nM) incubated with the concentrations of InrS indicated before resolving by native PAGE. B. Competitive EMSA with *coxBPro+* (100 nM) and 190 bp non-specific DNA probe pGEMCon4 (100 nM) incubated with the concentrations of InrS indicated before resolving by native PAGE.

A

GGCTGAGGCTGTATAATCTACGACGGGCTGTCAAACATT
 GTGATACCATGGGCAGAAGAAAGGAAAAACGTCCCTGAT
 CGCCTTTTTGGGCACGGAGTAGGGCGTTA CCCCGGCCCCG
 TTCAACCACAAGTCCCTATAGATACAATCGCCAAGAAGT
ATGTCTAAAAAGTTTTTAACAATCCTCGCTGGCCTTCTG

PcPro_F PcPro_R

B

TTTGGTCACTGCCAAAGAGTTCCACTGCTGACATCGTCC
 GTCTTTAGCTAGGCAATTATACCAAGGC GGCGGGGCCCGGAG
CTATTTCCTGAGCTTGCCAATGGGCGGTGGCTAAAATTGA
 AGGTAAGCTTTTCTTTGTACTGAGTATTACCGATTAAACC
ATGGCCCAAACCATCAATCTGCAACTAGAGGGAATGCGC

PacSPro_F PacSPro_R

Figure 3.26. Design of *petE*Pro and *pacS*Pro EMSA probes. A. Nucleotide sequence of the start of the coding region and upstream region of *petE*. The translational start codon (red box) and a GC-rich tract (blue box) are highlighted. Primers homologous to the regions labelled PcPro_F and PcPro_R were used to amplify this sequence from *Synechocystis* genomic DNA producing the probe designated *petE*Pro for use in EMSAs. B. Nucleotide sequence of the start of the coding region and upstream region of *pacS*. The translational start codon (red box) and a GC-rich tract (blue box) are highlighted. Primers homologous to the regions labelled PacSPro_F and PacSPro_R were used to amplify this sequence from *Synechocystis* genomic DNA producing the probe designated *pacS*Pro for use in EMSAs.

amplified from genomic DNA using primers homologous to the indicated regions in Figure 3.26. These probes were designated *petEPro* (153 bp) and *pacSPro* (146 bp).

InrS appears to show a slight preference for *petEPro* over pGEMCon3 in that the intensity of free *petEPro* is comparatively less than that of pGEMCon3 at the same concentration of InrS (this is best observed in the lanes with [InrS] = 28 and 32 μ M) (Figure 3.27A). However, this order of preference appears to be reversed when pGEMCon4 is used as the control probe (Figure 3.27B), indicating no specific binding of InrS to the region of *petE* promoter used here. Additionally, this result emphasises the importance of using a non-specific DNA probe of a longer length than the specific probe to prevent false positives.

In an analogous experiment using the *pacSPro*, no preference for the *pacSPro* over pGEMCon3 is observed and indeed a greater preference for pGEMCon4 over the *pacSPro* is observed (Figure 3.28). These results suggest that InrS does not regulate expression of either *petE* or *pacS*, at least not by binding directly to their promoter regions.

3.4.3 Targets whose promoter regions contain similarity to the *E. coli* RcnR DNA recognition site

E. coli RcnR specifically recognises the sequence TACTGGGGGGNAGTA (Iwig & Chivers. 2009), two repeats of which are found in the *rcnR/rcnA* intergenic region. The genome of *Synechocystis* was searched for promoter regions with similarity to this sequence. The Cyanolist search pattern tool was used to identify a 2 part pattern; 1st part = TACT, 2nd part = AGTA with a 6-7 nucleotide spacing between the two parts of the pattern. Given the low complexity of the pattern search no mismatches were allowed. Only patterns located within a region 100 bp immediately prior to a translational start codon were reported. This search strategy produced four hits (Figure 3.29). Of these four hits a sequence found upstream of *chlN* displayed a GC rich tract between the inverted repeat elements. *chlN* encodes a subunit of light independent protochlorophyllide reductase which catalyses the penultimate step of chlorophyll *a* biosynthesis (Vavilin & Vermaas. 2002). Deletion of one of the other enzyme subunits, *chlL*, results in a strain which is incapable of synthesising chlorophyll *a* in the dark (Wu & Vermaas. 1995). Rationale for why chlorophyll biosynthesis may be regulated by copper was perhaps weak: perhaps under conditions where there is not enough copper for plastocyanin cells would need less chlorophyll due to the lack of an

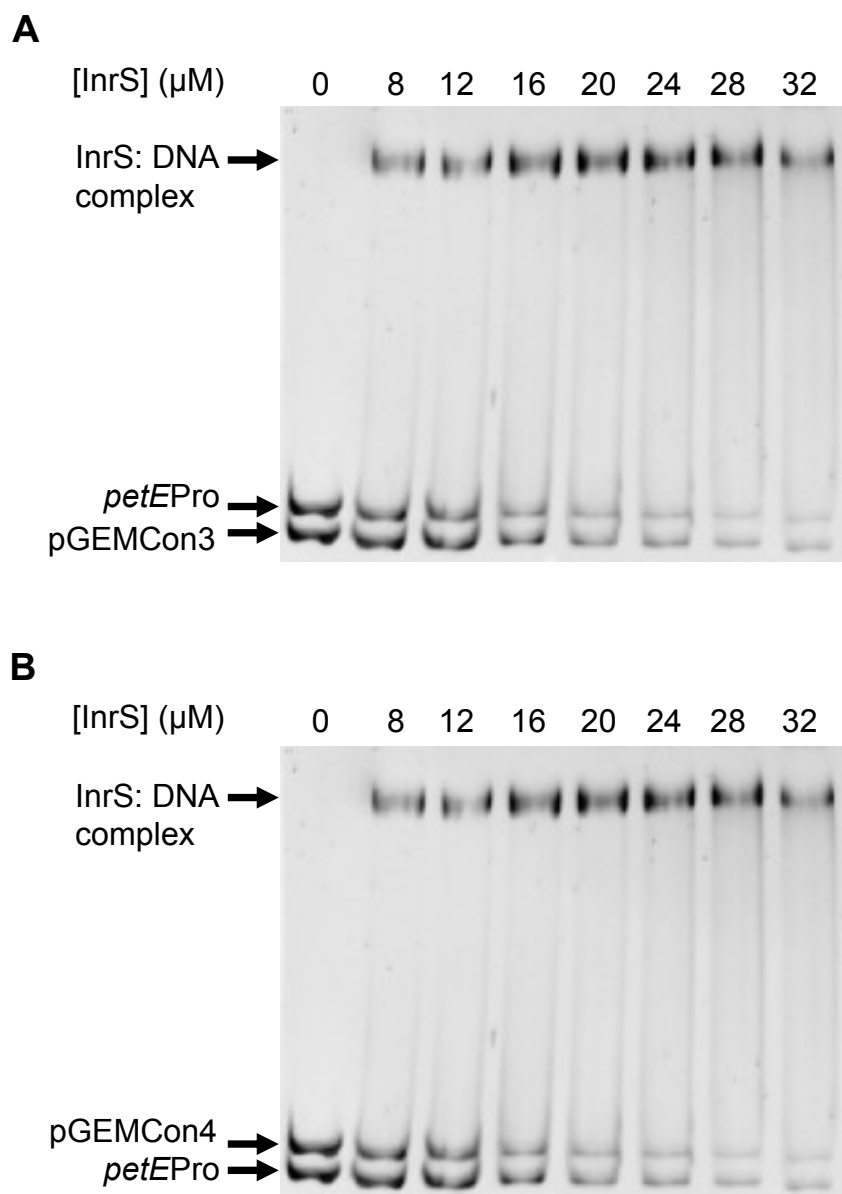


Figure 3.27. Competitive EMSA assessing InrS binding to *petEPro*. A. Competitive EMSA with 153 bp *petEPro* (100 nM) and 141 bp non-specific DNA probe pGEMCon3 (100 nM) incubated with the concentrations of InrS indicated. B. Competitive EMSA with *petEPro* (100 nM) and 190 bp non-specific DNA probe pGEMCon4 (100 nM) incubated with the concentrations of InrS indicated before resolving by native PAGE.

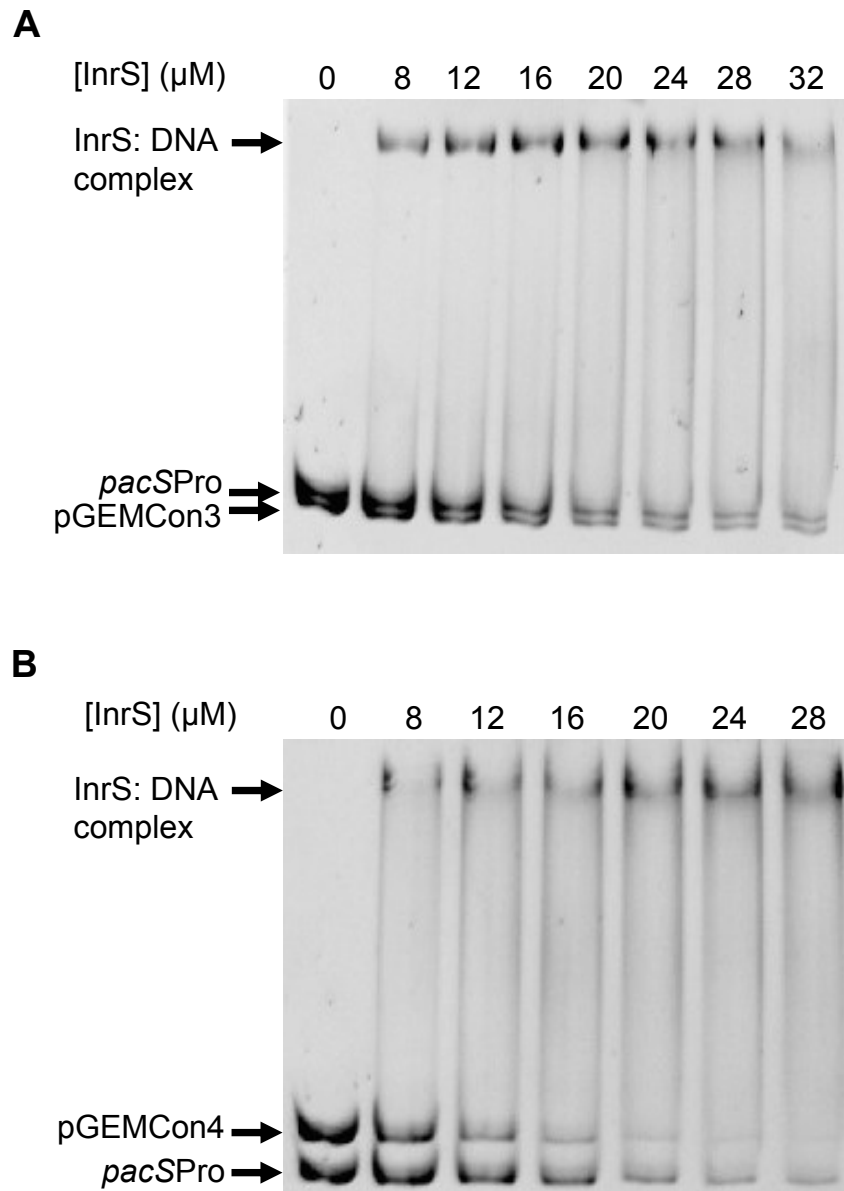


Figure 3.28. Competitive EMSA assessing InrS binding to *pacSPro*. A. Competitive EMSA with 146 bp *pacSPro* (100 nM) and 141 bp non-specific DNA probe pGEMCon3 (100 nM) incubated with the concentrations of InrS indicated before resolving by native PAGE. B. Competitive EMSA with *pacSPro* (100 nM) and 190 bp non-specific DNA probe pGEMCon4 (100 nM) incubated with the concentrations of InrS indicated before resolving by native PAGE.

TACTGGGGGGNAGTA	<i>E. coli rcnA</i>
→ ←	
TACTCCCCC AGTA	<i>chlN (slr0750)</i>
→ ←	
TACTGAGATA AGTA	<i>fabD (slr2023)</i>
→ ←	
TACTACATCGTAGTA	<i>unknown (sll1562)</i>
→ ←	
TACTGACAAA AGTA	<i>hypothetical (sll0072)</i>
→ ←	

Figure 3.29. Identification of potential InrS DNA binding sites by analogy to the *E. coli* RcnR DNA binding sites. Sequences (upstream of gene coding regions) with analogy to the *E. coli* RcnR DNA recognition site, identified by a Cyanolist pattern search as described in Section 3.4.3. Symmetry elements are underlined with an arrow.

electron shuttle. This explanation however ignores the existence of the alternative electron shuttle, c_6 , and that the cell can still produce chlorophyll in the light. In spite of this, because of the similarity of the identified target to the *E. coli* RcnR DNA recognition site the ability of InrS to bind a DNA fragment containing this sequence was tested by EMSA.

The 168 bp *chlN*Pro probe was produced in a manner analogous to that described for *petE*Pro and *pacS*Pro (Figure 3.30). InrS shows specificity of binding to *chlN*Pro over both pGEMCon3 and 4 (Figure 3.31). The experimental design allows an apparent DNA affinity estimation for this probe of $K_{\text{DNA, app}} \sim 8 \mu\text{M}$ to be made.

3.4.4 Targets whose promoter regions contain similarity to the CsoR consensus sequence

During the course of this work a paper in which the sulphite sensing CsoR homologue CstR was characterised was published (Grossoehme *et al.* 2011). This paper contained a consensus DNA binding sequence for *B. subtilis* and *S. aureus* CsoRs, *M. tuberculosis* RicR, *S. aureus* CstR and *Geobacillus thermodenitrificans* CsoR (ATACCCNNNgGGGGTAT, lower case characters representing less conservation at these positions). The Cyanolist search pattern tool was used to identify a 2 part pattern; 1st part = ATACC, 2nd part = GGGGTAT with a 5 nucleotide spacing between the two parts of the pattern. One mismatch was allowed in either part and only patterns located within a region 100 bp immediately prior to a translational start codon were reported. Of the eight hits returned by this search one hit very closely matches the consensus sequence, a near perfectly symmetrical inverted repeat the terminal 3' nucleotide of which is found 36 bp upstream of the start codon of *nrsD* (Figure 3.32). *nrsD* has been shown to be induced by nickel and cobalt and is thought to be a plasma membrane localised exporter required for resistance to nickel but not to cobalt (García-Domínguez *et al.* 2000), thus there is a very clear link between metal homeostasis and the target potentially regulated by InrS. The sequence identified upstream of *nrsD* additionally overlaps a potential Pribnow box sequence (TAGAAT) which matches the consensus for this organism (TA_AAT) (Mitschke *et al.* 2011) (Figure 3.33). This would allow InrS to repress transcription of *nrsD* by occluding access to this promoter element.

TTTGTTCATTATGTTTTACGATTACCAACGATCAAGTT
 slr0750Pro_F
 ATTGATAATTTACCAAAGTTTTAGAAAAATTACTCAG
 ACAACACAAACTCTACTCCCCCAGTATTGGGGGGTTAG
 GAAGGCAAAATAAAAACCTATACCTAGGAGAACCTAAACT
 ATGACTGTTGCTCAACAAGCCCCTTCTGCCCTTAACTTT
 slr0750Pro_R

Figure 3.30. Design of *chlN*Pro EMSA probe. Nucleotide sequence of the start of the coding region and upstream region of *chlN*. The translational start codon is highlighted in the red box and the potential InrS binding site highlighted in the blue box. Primers homologous to the regions labelled slr0750_F and slr0750_R were used to amplify this sequence from *Synechocystis* genomic DNA producing the probe designated *chlN*Pro for use in EMSAs.

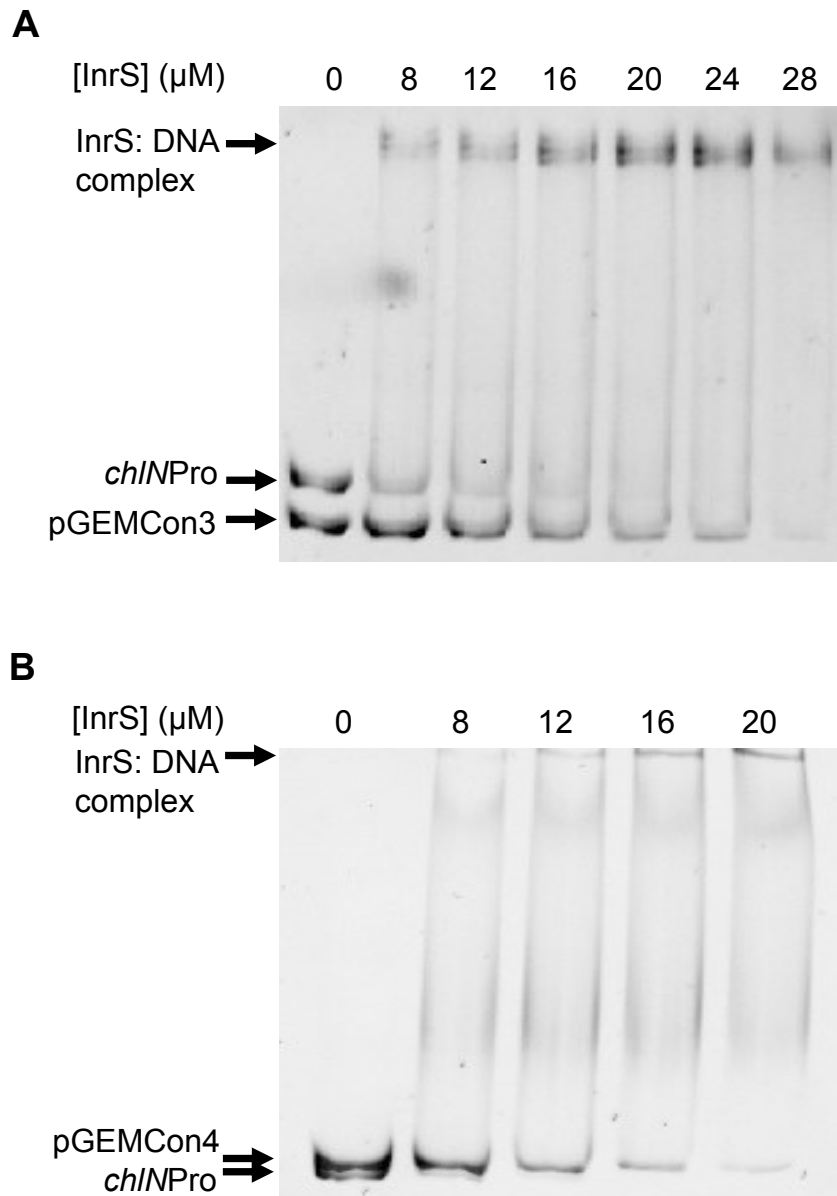


Figure 3.31. Competitive EMSA assessing the competence of InrS to bind *chlN*Pro.
 A. Competitive EMSA with 168 bp *chlN*Pro (100 nM) and 141 bp non-specific DNA probe pGEMCon3 (100 nM) incubated with the concentrations of InrS indicated before resolving by native PAGE. B. Competitive EMSA with *chlN*Pro (100 nM) and 190 bp non-specific DNA probe pGEMCon4 (100 nM) incubated with the concentrations of InrS indicated before resolving by native PAGE.









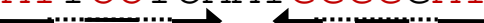
ATACCCNNNGGGGGTAT	consensus CsoR/ CstR binding site
	
TATCCCCCTGGGGCATA	<i>nrsD</i> (<i>slr0796</i>)
	
ATACTCCGCTGTGGTAT	<i>fraH</i> (<i>slr0298</i>)
	
ATATCAAGATTGGGTAT	glutamyl-tRNA (Gln) amidotransferase sub-unit C (<i>slr0033</i>)
	
AAACCTTTCTGGGGTAG	hypothetical (<i>slr1340</i>)
	
AAACCTAGCTAGGGTAT	hypothetical (<i>ssl0312</i>)
	
CTACCACTGAGGGGTAA	hypothetical (<i>slr0954</i>)
	
AAACCTAGATGGGGCAT	<i>nhaS4</i> (<i>slr1595</i>)
	
ATTCTCAATGGGGGAT	<i>pdxA</i> (<i>slr0660</i>)
	

Figure 3.32. Identification of potential InrS DNA binding sites by analogy to a CsoR/ CstR consensus DNA binding site. Sequences (upstream of gene coding regions) with analogy to a CsoR/ CstR consensus DNA recognition site as identified by a Cyanolist pattern search described in Section 3.4.4. Nucleotides of the returned sequence matching the consensus recognition site are shown in red. Symmetry elements are underlined with an arrow with breaks in symmetry represented by a dotted line.

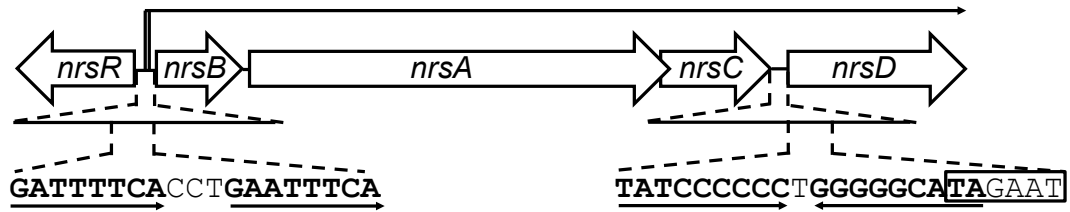


Figure 3.33. Genetic organisation of the *nrs* operon. Representation of the *nrs* operon (to scale). The deduced NrsR binding site between *nrsR* and *nrsB* and the putative InrS binding site located between *nrsC* and *nrsD*, are shown along with an overlapping Pribnow box (*boxed*). Known transcriptional start sites of the *nrsBACD* transcript are also shown (López-Maury *et al.* 2002).

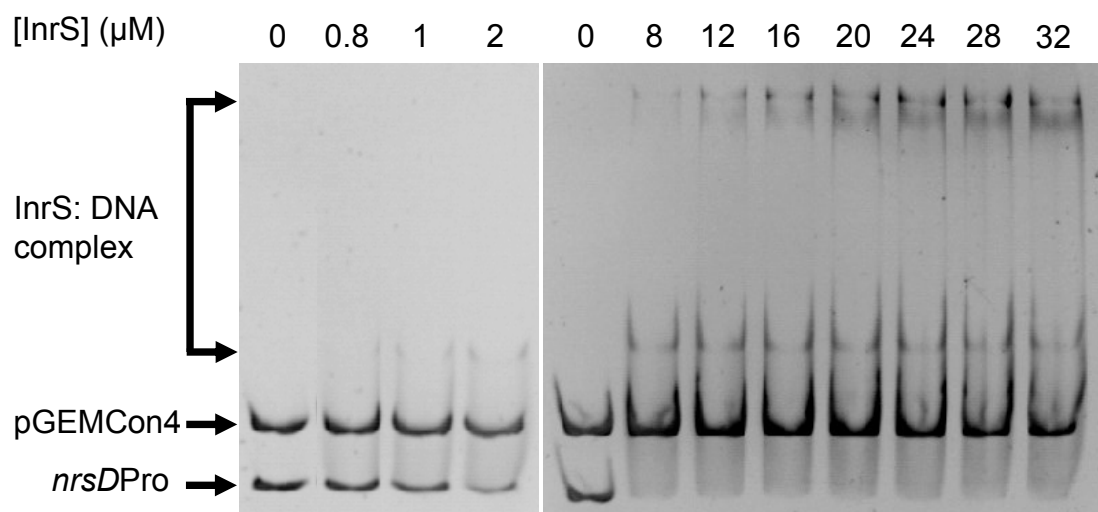


Figure 3.35. Competitive EMSA assessing InrS binding to *nrsDPro*. Competitive EMSA with 116 bp *nrsDPro* (100 nM) and 190 bp non-specific DNA probe pGEMCon4 (100 nM) incubated with the concentrations of InrS indicated before resolving by native PAGE.

EMSA analysis using the entire *nrsCD* intergenic region (*nrsDPro*, 116 bp (Figure 3.34)) reveals that InrS shows a very clear preference for this probe over pGEMCon4 (Figure 3.35) (pGEMCon3 was not used in this analysis due to the initial success with pGEMCon4). Upon addition of 8 μM InrS to the EMSA binding reaction the entire population of *nrsDPro* has been retarded whereas there is no visible retardation of the control fragment and indeed the appearance of a shifted band is visible upon the addition of as little as 0.8 μM InrS (Figure 3.35). The apparent affinity of InrS for this *nrsDPro* is $K_{\text{DNA, app}} \sim 2 \mu\text{M}$, at least four fold tighter than the other probes for which some specificity was shown (Figures 3.24, 3.25, 3.31). This semi-quantitative value is still weak for a specific protein-DNA interaction and this likely reflects the non-equilibrium nature of this assay. A quantitative estimate of the DNA affinity of InrS determined by an equilibrium assay is presented in Section 4.1.2 and is found to be substantially tighter than the estimate from the EMSA. In EMSA analyses using the *nrsDPro* DNA probe two retarded bands were visible (Figure 3.35) whereas with the other DNA probes used throughout this series of EMSA experiments only one high molecular weight retarded band was observed. Multiple retarded bands have also been observed in EMSA analyses using *M. tuberculosis* (Liu *et al.* 2007) and *L. monocytogenes* CsoR (Corbett *et al.* 2011). This phenomenon may be physiologically relevant and may represent a mechanism of gene regulation by this protein family by the formation of multimeric complexes. Alternatively the lower mass retarded band may represent a specific interaction of InrS with DNA whereas the higher mass band may represent non-specific InrS-DNA interactions. This could be the reason why the lower mass retarded band is not observed for probes other than *nrsDPro*. However these explanations are not mutually exclusive.

As *nrsD* has previously been shown to be induced by exogenous nickel, the ability of nickel to inhibit the formation of InrS-DNA complexes was tested. Addition of NiSO_4 to the *nrsDPro* EMSA binding reaction results in the loss of retarded bands (Figure 3.36). Inclusion of NiSO_4 and EDTA in the binding reaction results in the reappearance of the retarded bands (Figure 3.36). These results show that nickel is capable of inhibiting InrS-DNA interactions and show that EDTA is a more effective competitor for Ni(II) at the molar excess used in this assay.

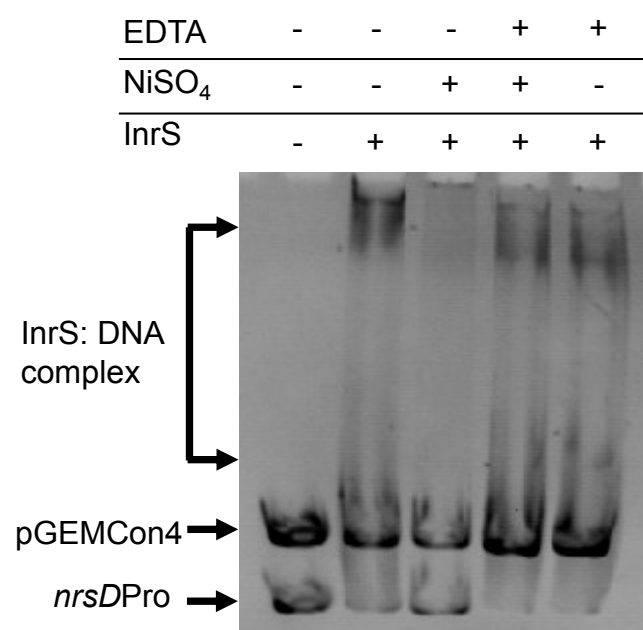


Figure 3.36. Inhibition of InrS DNA binding by Ni(II). Competitive EMSA with 116 bp *nrsDPro* (100 nM) and 190 bp non- specific DNA probe pGEMCon4 (100 nM) incubated with combinations of InrS (8 μ M), NiSO₄ (400 μ M) and EDTA (4 mM) as indicated above gel image before resolving by native PAGE.

3.5 *In Vivo* analysis of the role of InrS

The data discussed in the following sections (Sections 3.5 and 3.6) were collected by Rafael Pernil and the figures are presented in Appendix B to reflect this. The experiments were planned by both Rafael Pernil and the author and the following represents the author's analysis of the data.

In vitro EMSA analysis suggested that InrS might regulate *nrsD* (Figure 3.35), the last gene in the *nrsBACD* operon (Figure 3.33), in response to nickel (Figure 3.36). In order to test this hypothesis, first a mutant deficient in *inrS* was produced by replacement of the majority of *inrS* with a chloramphenicol resistance cassette by homologous recombination. The integration and segregation of this gene disruption to all copies of the chromosome was confirmed by PCR analysis, which demonstrated a loss of the product amplified from the wild type strain (a fragment of 4.3 kb) and the appearance of a larger fragment (4.9 kb) indicative of insertion of the chloramphenicol resistance cassette (Appendix Figure B1A). The abundance of *nrsD* transcripts in this strain was then assessed by reverse transcription PCR (RT-PCR). Previous northern blot analysis of *nrsD* expression suggested the gene was transcribed as part of a polycistronic message along with *nrsBAC* (García-Domínguez *et al.* 2000) expression of which was later shown to be under the control of a two component histidine kinase and response regulator system thought to sense nickel and cobalt in the periplasm (López-Maury *et al.* 2002). Therefore the abundance of *nrsB* (the first gene of the operon (Figure 3.33)) transcript was also assessed (Appendix Figure B1B). *nrsD* transcript abundance is far greater in the $\Delta inrS$ strain than the wild type strain whereas *nrsB* transcript abundance is not increased (it is actually slightly lower than in the wild type analysis for unknown reasons) (Appendix Figure B1B). These data may indicate there is a promoter located upstream of *nrsD*, access to which is occluded by InrS when cells are cultured in standard medium (BG11). This could allow differential expression of *nrsD* from the rest of the *nrs* operon allowing detection and efflux of cytosolic nickel (and potentially cobalt) excess.

To identify the *in vivo* metal effector of InrS the transcript abundance of *nrsD* was assessed in wild type *Synechocystis* cells following a 48 h exposure to maximum non-inhibitory concentrations of nickel, zinc, cobalt and copper salts. These metals were chosen as there is strong evidence for regulation of the CsoR-RcnR family by copper, nickel and cobalt and some evidence that *T. thermophilus* CsoR may be competent to respond to zinc (Sakamoto *et al.* 2010). No increase in transcript abundance was

observed in cells exposed to zinc and copper salts whereas an increase was observed following exposure to both nickel and cobalt salts (Appendix Figure B2A). However *nrsB* transcript abundance also increased in response to the same metal supplementation, confirming the pattern of gene expression previously observed by García-Domínguez *et al* (2000). Close inspection of the northern blot analysis performed by García-Domínguez *et al* (2000) reveals that the probe hybridised to *nrsB* displays a doublet whereas the probe hybridised to *nrsD* only displays a single band. This suggests that there may be transcripts of two different lengths initiated from the promoter upstream of *nrsB*, with perhaps the shorter of the two corresponding to a polycistronic message lacking *nrsD* due to termination of the transcript following *nrsC* possibly due to physical obstruction by InrS. With the probe hybridised to *nrsD* only full length transcripts would be observed because transcripts of *nrsD* alone would not be visualised due to the scale of the blot focussing on products of a size corresponding to a transcript of the full operon. A precedent for transcriptional termination by a transcriptional regulator exists for the *lac* operon in *E. coli* where LacI binding upstream of *lacZYA* prevents read through of the *lacI* transcript into *lacZYA* in the absence of inducer (Sellitti *et al.* 1987). Although analysis of *nrsD* and *nrsB* expression in the Δ *inrS* strain suggests the presence of a promoter allowing independent expression of *nrsD* from the rest of the *nrs* operon (Appendix Figure B1B), the RT-PCR data presented in Appendix Figure B1B and B2A does not formally prove the presence of a promoter or show that transcripts initiated from this promoter accumulate in response to nickel and cobalt *in vivo*. The expression pattern of *nrsD* in response to metal treatment is mirrored by *nrsB* and therefore expression of *nrsD* could be due to read through from transcripts initiated at the *nrsB* promoter.

In order to formally determine the presence of an *nrsD* promoter and to determine if the *nrsD* promoter is metal responsive an RLM-RACE experiment was carried out. Briefly, this method involves treating extracted RNA with Calf Intestinal Alkaline Phosphatase to remove free 5'-phosphates from ribosomal RNA, degraded transcripts, tRNA and contaminating DNA. The sample was then treated with Tobacco Acid Pyrophosphatase (TAP) to remove the 5'-phosphate cap from intact transcripts before ligation of a unique RNA adapter to the exposed free 5'-phosphate. This is followed by reverse transcriptase treatment and PCR using primers specific to the gene of interest and the introduced adapter. Products of a size diagnostic of transcripts initiated from the *nrsD* promoter accumulate in response to nickel and cobalt treatments in a TAP dependent manner, formally showing that the presence of *nrsD* promoter and that this promoter is nickel

and cobalt responsive *in vivo* (Appendix Figure B2B and C). These fragments were cloned into pGEM-T and sequenced revealing (in repeat analyses) two transcriptional start points upstream of the *nrsD* translation start codon and 10-14 bp downstream of the mid-point of a candidate Pribnow box that overlaps the deduced InrS binding site (Figure 3.33 and Appendix Figure B2D). Given these results and those of García-Domínguez *et al* (2000) it seems likely that the observed expression of *nrsD* is due to both expression from its own promoter and read through of transcripts initiated at the *nrsB* promoter. Models of regulation of the *nrs* operon are discussed further in Section 6.2.

In EMSA analyses InrS displayed a degree of preference for the upstream regions of *moeA*, *coxB* and *chlN* over the non-specific control probes (Figures 3.24, 3.25 and 3.31). Strong links to metal ion homeostasis were suggested for *moeA* and *coxB* and therefore the abundance of these transcripts was also assessed in the Δ *inrS* strain. An increase in transcript abundance of *moeA* was observed in Δ *inrS* cells (although not of the same magnitude of the increased abundance of *nrsD* transcripts) (Appendix Figure B3A). However following 48 h exposure of wild type cells to maximum permissive concentrations of nickel and copper salts there is no change in *moeA* transcript abundance, showing that *moeA* is not a target for metalloregulation by InrS and therefore the increased transcript abundance observed in the Δ *inrS* strain is likely indirect (Appendix Figure B3B).

3.6 Phenotypic analysis of Δ *inrS*

The role of InrS in nickel homeostasis was investigated further by assaying the nickel content of Δ *inrS* & wild type cells and the growth of both strains when exposed to nickel (Appendix Figures B4A and B5). Attention was focussed on nickel rather than cobalt as *nrsD* has previously been shown to be dispensable to cobalt resistance (García-Domínguez *et al.* 2000). Δ *inrS* cells constitutively express *nrsD* and therefore it was predicted they would have decreased cytosolic nickel. A reduction in whole cell nickel content from 0.13 million atoms per cell in wild type cells to 0.091 million atoms per cell in Δ *inrS* cells when cultured in standard BG11 media and from 1.0 to 0.64 million atoms per cell in BG11 media additionally supplemented with the maximum non-inhibitory concentration of nickel (for wild type cells) is observed (Appendix Figure B4A). Δ *inrS* cells additionally showed a slight but reproducible increase in

nickel tolerance consistent with a nickel exporter being constitutively expressed (Appendix Figure B5). The modest increase in nickel resistance suggests that *nrsD* may not be the main nickel resistance determinant of *Synechocystis* and it should be remembered that *Synechocystis* has a small complement of nickel requiring enzymes (Section 1.10.1) so a nickel content reduction could also be expected to be inhibitory to growth.

Cultures of $\Delta inrS$ displayed a chlorotic appearance (Appendix Figure B4B *inset*) prompting a series of experiments to try and understand the origin of this colouration. Chlorosis is characterised by a degradation of chlorophyll and phycobilisomes (Luque & Forchhammer, 2008). The major peaks in the absorbance spectrum of a suspension of *Synechocystis* cells can be assigned as chlorophyll *a* (442 and 680 nm) and phycocyanin (630 nm) (Govindjee & Shevela, 2011). The phycocyanin and 680 nm chlorophyll *a* peaks are unaltered in $\Delta inrS$ compared with wild type however the 442 nm chlorophyll *a* peak is elevated in $\Delta inrS$ strain indicative of an increase in other pigments that also absorb in this region such as carotenoids (Appendix Figure B4B) (Bullerjahn & Sherman, 1986). Pigment extraction and quantification revealed that the concentration of carotenoids had indeed increased from 8.02 in wild type cells to 9.51 $\mu\text{g ml}^{-1}$ in $\Delta inrS$ cells whereas the chlorophyll *a* content displayed a very modest decrease (2.92 to 2.78 $\mu\text{g ml}^{-1}$) (Appendix Figure B4C). In *Synechocystis* the orange carotenoid protein, the gene product of *slr1963*, which binds the keto carotenoid 3'-hydroxyechineone (Wu & Krogmann, 1997), interacts with the phycobilisome and dissipates excess energy as heat under high light conditions (Wilson *et al.* 2006). This decreases the amount of energy reaching the reaction centres of the photosystems where an excess can cause the formation of damaging reactive oxygen species and thus carotenoids play a photoprotective role. Energy harvested by the phycobilisome antennae is transferred via chlorophyll to the photosystems (Govindjee & Shevela, 2011). A decrease in the fluorescence emission of chlorophyll following excitation of whole cells at 442 nm is consistent with a decrease in energy reaching chlorophyll due to an increased abundance of photoprotective pigments (Appendix Figure B4D). Why the $\Delta inrS$ strain would display an increase in photoprotective pigments presumably due to a decrease in availability of cytosolic nickel, and the implications for future work, are discussed further in Section 6.9.2.

Chapter 4. Further characterisation of the DNA- and cognate metal-binding properties of InrS

4.1 InrS:DNA interactions

The apparent affinity of InrS for *nrsD*Pro, a 116 bp probe comprising the entire *nrsCD* intergenic region and containing the inverted repeat predicted to be the InrS recognition site, was estimated from the EMSA gel image to be $K_{\text{DNA, app}} \sim 2 \mu\text{M}$ (Section 3.4.4). This is likely to be an overestimate (numerically large, therefore a weak interaction) due to the relatively high concentration of DNA needed for an EMSA experiment with non-radioactively labelled probes and the non-equilibrium nature of EMSA experiments. In order to study the interactions of InrS with DNA in a more quantitative manner fluorescence anisotropy was employed. Fluorescence anisotropy has been used to study metalloregulator-DNA interactions with affinities in the high nanomolar to sub nanomolar range (VanZile *et al.* 2002a; Harvie *et al.* 2006; Campbell *et al.* 2007; Ma *et al.* 2009a). This assay measures the rate of tumbling of a fluorescent molecule in solution based on the intensity of emission of horizontally and vertically polarised light following excitation with vertically polarised light and can therefore be used to report on the size and shape of molecules in solution (Grossoehme & Giedroc. 2012). The anisotropy value (r_{obs}) is calculated via equation 6.

$$r_{\text{obs}} = \frac{(I_{\text{VV}} - I_{\text{VH}})}{(I_{\text{VV}} + 2I_{\text{VH}})} \quad \text{eq. 6}$$

where I_{VV} and I_{VH} are the intensities of emission in the vertical and horizontal planes respectively and therefore a greater r_{obs} indicates a more slowly tumbling molecule as a greater proportion of the emitted light is in the same plane as the incident light (Harvie *et al.* 2006). Interaction of a DNA-binding protein with a fluorescently labelled DNA probe results in an increase in anisotropy due to a reduction in tumbling rate of the DNA.

Complementary oligonucleotides containing the predicted InrS binding site (Figure 3.33) and seven flanking nucleotides either side of the motif were obtained commercially and annealed by heating followed by slow cooling to produce the 33 bp probe *nrsD*ProFA (Figure 4.1). Annealing was confirmed by native PAGE analysis

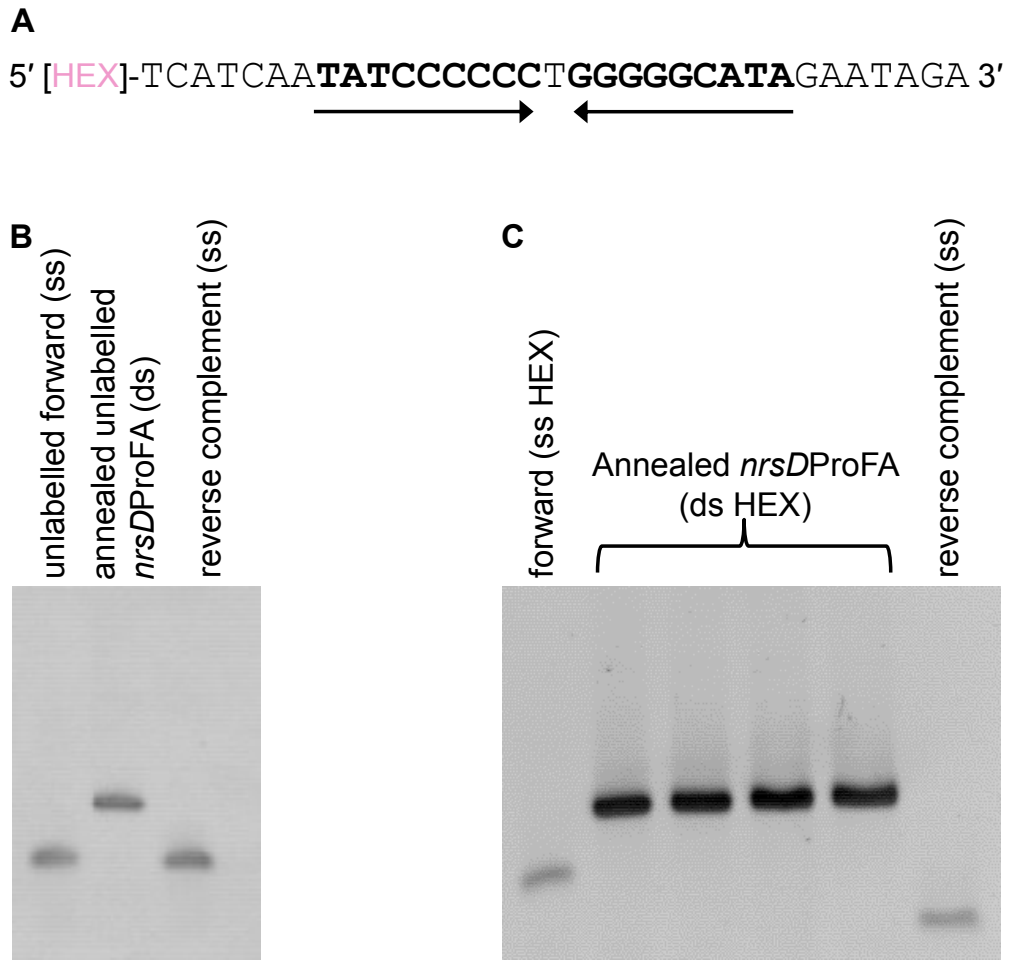


Figure 4.1. Production of a double stranded, oligonucleotide containing the InrS recognition site for use in analytical size exclusion chromatography and a HEX-labelled version for use in fluorescence anisotropy. A. 33 nucleotide DNA sequence composed of the identified InrS recognition site and flanking nucleotides. The oligonucleotide shown (Hex-labelled or unlabelled) was annealed with its unlabelled reverse complement. B. Native PAGE analysis to confirm successful annealing of oligonucleotides to produce double stranded (ds) unlabelled *nrsDProFA*. Un-annealed single stranded (ss) oligonucleotides were included in the analysis to confirm the size difference of annealed ds *nrsDProFA*. C. As 'B' to confirm successful annealing of ds HEX-labelled *nrsDProFA*.

(Figure 4.1). The 5' end of one of the complementary strands was labelled with hexachlorofluorescein (HEX) during synthesis. Additionally an unlabelled version of this probe was produced in the same manner.

4.1.1 *InrS*:DNA stoichiometry

It has been shown that two *B. subtilis* CsoR tetramers interact with a single recognition site (Ma *et al.* 2009a) whereas for *E. coli* RcnR the stoichiometry is one RcnR tetramer per DNA recognition site (Iwig & Chivers 2009). In order to determine the stoichiometry of the InrS:DNA complex varying amounts of InrS were incubated with the unlabelled version of *nrsD*ProFA before resolving by gel filtration chromatography (Figure 4.2), with absorbance at 260 nm used to observe the elution of the DNA probe from the column. Upon incubation with InrS an elution peak at a lower volume is observed consistent with DNA complex of greater mass (Figure 4.2). Upon the addition of a four times molar excess of InrS over probe (i.e. one protein tetramer per DNA molecule as InrS exists as a tetramer in solution (Section 3.2)) the A_{260 nm} peak is essentially completely shifted to the lower volume elution and no further increase in peak intensity is observed upon the addition of higher InrS concentrations. This result shows that the stoichiometry of InrS:DNA interaction is 4:1 or one InrS tetramer per DNA molecule (which contains one recognition site), although it should be noted that lower affinity binding events may not be detected in this assay. It also shows that the predicted InrS binding site is very likely the element of the *nrsCD* intergenic region recognised by InrS in EMSA analyses.

It has been hypothesised that the spacing between the centres of each AT-rich inverted repeat is important in determining the protein-DNA stoichiometry for CsoR-RcnR family proteins (Iwig & Chivers. 2009). The spacing between the centres of the inverted repeat of the *E. coli* RcnR recognition site is 9 bp whereas the spacing for *B. subtilis* CsoR is 13 bp. This places the inverted repeats roughly on the same face of the DNA molecule for the *E. coli* RcnR recognition site but on the opposite faces of the DNA molecule for the *B. subtilis* CsoR recognition site (assuming a rotation per bp of ~ 36°). It was postulated that this would stop a single tetramer, in the case of *B. subtilis* CsoR, from being able to interact simultaneously with both inverted repeat sequences leading to two tetramers interacting with DNA (Ma *et al.* 2009a) whereas *E. coli* RcnR would be able to simultaneously interact with both inverted repeat sequences on one face of the DNA and therefore only one tetramer binds per recognition sequence (Iwig & Chivers. 2009) (Figure 4.3).

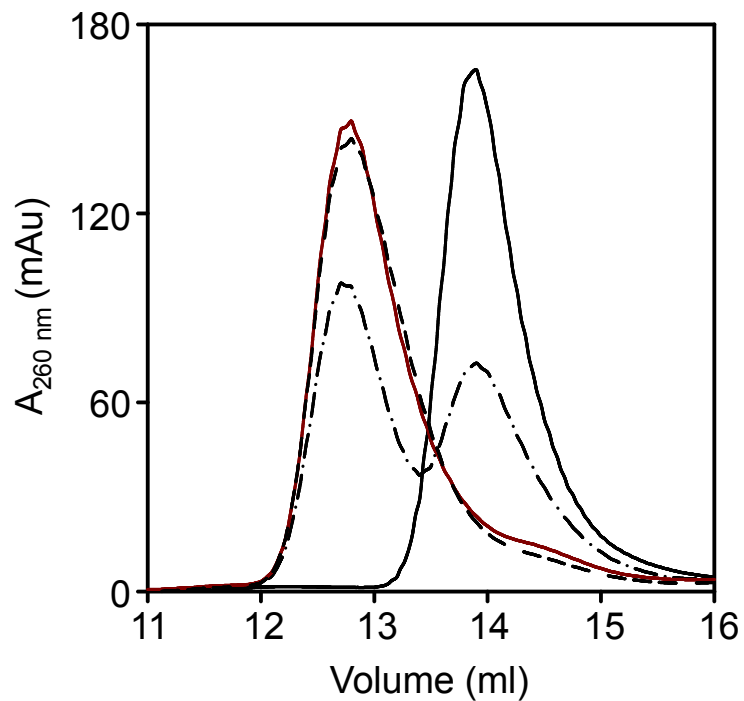


Figure 4.2. Assessment of InrS-DNA stoichiometry by size exclusion chromatography. Elution profile obtained from a Superdex 75 10/300 GL column used to resolve 10 μM unlabelled *nrsD*ProFA pre-incubated with 0 (solid black line), 20 (dot-dashed line), 40 (solid red line) or 80 μM (dashed line) InrS (all concentrations refer to protein monomer).

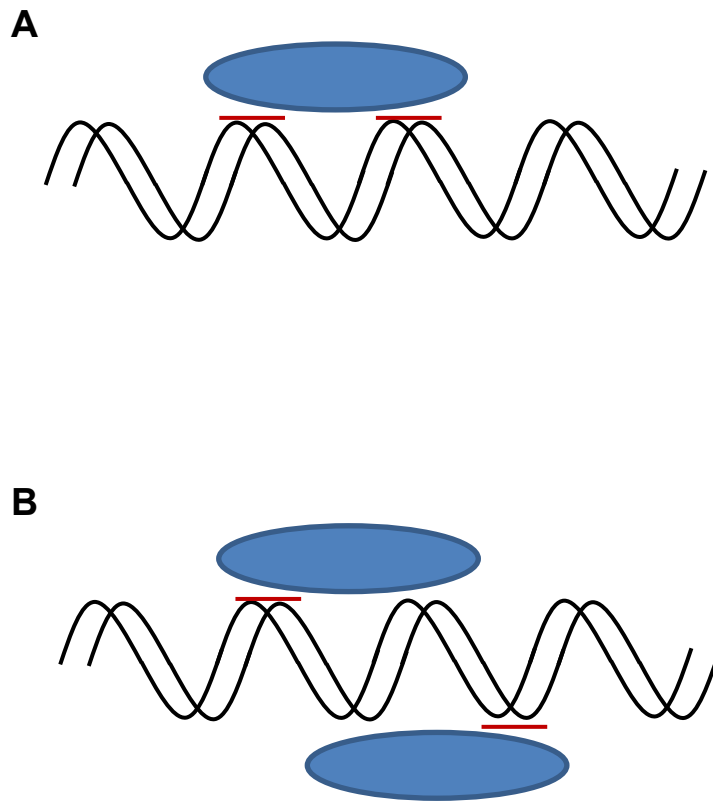


Figure 4.3. Proposed model explaining the stoichiometry of DNA:protein interactions of the CsoR-RcnR family. Interaction of *E. coli* RcnR (A) and *B. subtilis* CsoR (B) with DNA. Protein assemblies are represented by the blue ovals, DNA by the black helix and the symmetric repeats of recognition sites by red lines. The spacing between the symmetric repeats of the *B. subtilis* CsoR recognition site is postulated to prevent a single CsoR tetramer interacting with both halves of the symmetric repeat simultaneously.

The InrS recognition site has a 15 bp spacing between the centres of each inverted repeat, placing them on opposite faces of the DNA molecule. This suggests, given the 1:1 stoichiometry of InrS tetramer:DNA interaction, that factors in addition to spacer length may determine the protein-DNA stoichiometry for CsoR-RcnR like proteins. It is currently unclear if InrS interacts simultaneously with both halves of the inverted repeat of the recognition sequence and if so how.

4.1.2 Studying *InrS*:DNA interactions by fluorescence anisotropy

Fluorescently labelled *nrsD*ProFA (Figure 4.1) was titrated with InrS in the presence of EDTA and the change in anisotropy upon each addition was monitored (Figure 4.4). The data was fit to a simple model describing binding of one InrS tetramer to one DNA molecule (Figure 4.4) (protein:DNA stoichiometry determined in Section 4.1.1, Figure 4.2). The affinity of InrS for the probe was found to be $K_{\text{DNA}} = 56.6(\pm 7.8)$ nM (note this affinity is based on the monomer rather than tetramer protein concentration as per literature precedent). Fitting these data to a model based on a tetramer concentration of InrS yields $K_{\text{DNA}} = 9.39(\pm 2.0)$ nM. This tight binding confirms the specificity of interaction between InrS and this DNA sequence and is comparable to the DNA affinities for *B. subtilis* CsoR (32 nm) (Ma *et al.* 2009a) and *E. coli* RcnR (120 nm at 8 °C and 136 nM at 34 °C for binding to the tightest of the two recognition sites present in the *rcnR/rcnA* intergenic region) (Iwig & Chivers. 2009). These constants were all calculated based on protein monomer concentration.

In vivo the expression of *nrsD* is regulated in response to both nickel and cobalt (Appendix Figure B2A). Therefore the ability of nickel and cobalt to disrupt preformed InrS:DNA complexes was assessed. *nrsD*ProFA (10 nM) was incubated with InrS (1 μ M) to pre-form the InrS:DNA complex before titration with nickel or cobalt salts. Figure 4.5 shows that both nickel and cobalt are able to disrupt preformed InrS:DNA complexes. A decrease in Δr_{obs} (indicating dissociation of the protein:DNA complex) is observed upon addition of ~ 0.25 -0.5 molar equivalents of nickel, suggesting that InrS is titrated off DNA as the second metal binding site on a tetramer is filled. This result implies negative metal binding co-cooperativity between sensory sites on the InrS tetramer as some sites must be filled with nickel in preference to others. The metal-protein stoichiometry required to titrate InrS off DNA was more variable for cobalt with between 0.5-1 molar equivalents being required to observe the maximum decrease in Δr_{obs} . This may be due to the weaker affinity of InrS for Co(II) than Ni(II) (Sections

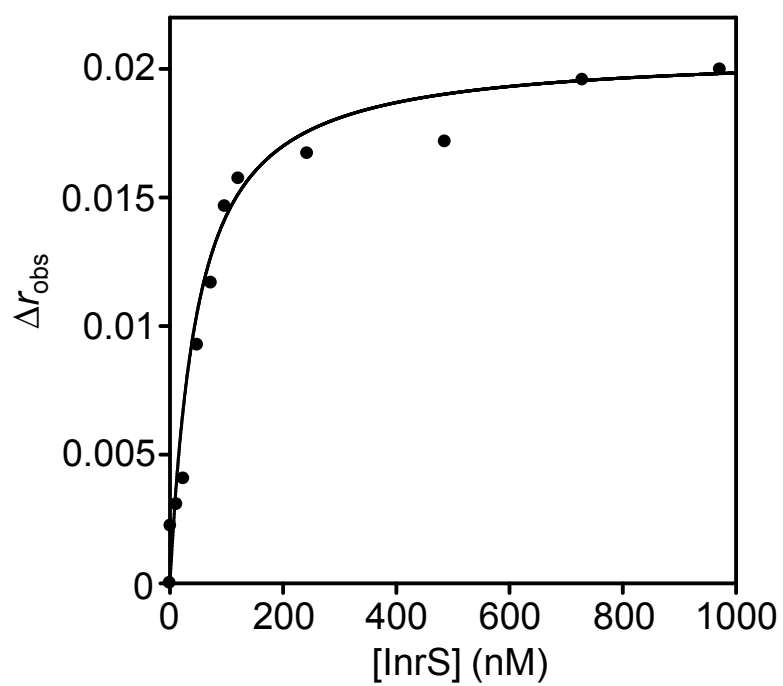


Figure 4.4. Titration of *nrsD*ProFA with apo-InrS. *nrsD*ProFA (10 nM) was titrated with InrS in the presence of 5 mM EDTA, DNA binding was monitored by fluorescence anisotropy. Experiment performed anaerobically at pH7.

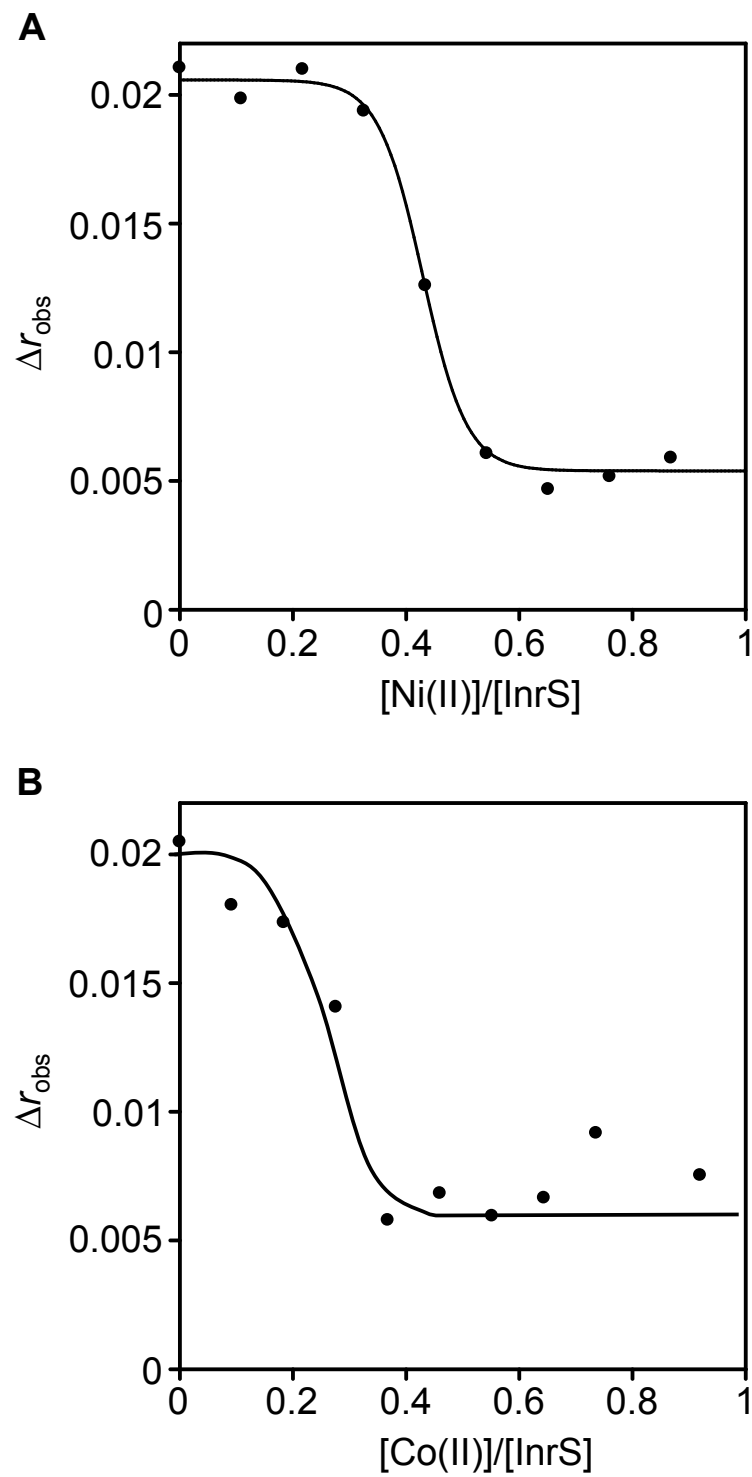


Figure 4.5. Titration of pre-formed InrS:DNA complexes with NiCl_2 and CoCl_2 . *nrsD*ProFA (10 nM) was pre-incubated with InrS (1 μM) before titration with A. NiCl_2 and B. CoCl_2 . Dissociation of protein:DNA complexes was observed by fluorescence anisotropy. Experiments were performed anaerobically at pH7.8.

4.2.1 and 4.2.2). This is consistent with greater than stoichiometric concentrations of cobalt being required to titrate InrS off DNA when these experiments were carried out at pH 7 rather than pH 7.8 (Appendix Figure C1). At the lower pH the metal affinity of the protein is expected to be weaker due to ligand protonation.

4.2 Cognate metal binding affinity of InrS

A key parameter in understanding the metal selectivity of InrS, and the wider implications this has for selectivity of other metalloregulators in the cell, is the affinity with which it binds its cognate metals, thought to be nickel & cobalt (Appendix Figure B2A).

4.2.1 Determination of the Ni(II) affinity of InrS

Direct titration of nickel into a solution of InrS resulted in stoichiometric binding of Ni(II) as judged by the saturation of the LMCT feature and co-migration with ~ 1 molar equivalent of nickel upon resolution using a PD10 column (Figures 3.6 and 3.7). Due to the stoichiometric nature of the binding event only a minimum estimate of Ni(II) binding affinity of $<10^{-7}$ M was able to be made. Therefore, in order to determine the Ni(II) affinity of InrS the protein was competed against chelators of known Ni(II) affinity (Xiao & Wedd. 2010). InrS was competed against chelators with increasing tight Ni(II) affinities; NTA $K_{D, Ni(II)} = 2.66 \times 10^{-10}$ M, EGTA $K_{D, Ni(II)} = 1.36 \times 10^{-11}$ M and EDTA $K_{D, Ni(II)} = 1.00 \times 10^{-16}$ M. These Ni(II) affinity values are all pH corrected using Schwarzenbach's α -coefficient protocol (Xiao & Wedd. 2010) (Section 2.6.7). NTA, EGTA and EDTA are all spectrally silent therefore the intensity of the Ni(II) dependent LMCT displayed by InrS (Figure 3.6) was used as a readout of nickel occupancy of InrS.

Initial experiments suggested that Ni(II) exchange between InrS and chelators may be slow to come to equilibrium and so experiments were designed to ensure equilibrium was reached. Ni(II) was pre-incubated with chelator before the addition of InrS. Upon addition of InrS the increase in absorbance at 333 nm was monitored until an equilibrium value was reached. When InrS was competed with a roughly equimolar concentration of NTA virtually all the Ni(II) partitioned from NTA to InrS (as judged by $A_{333\text{ nm}}$ equilibrium value compared against a control titration of InrS with Ni(II)) however the kinetics of exchange are slow (Figure 4.6A) as suggested by preliminary

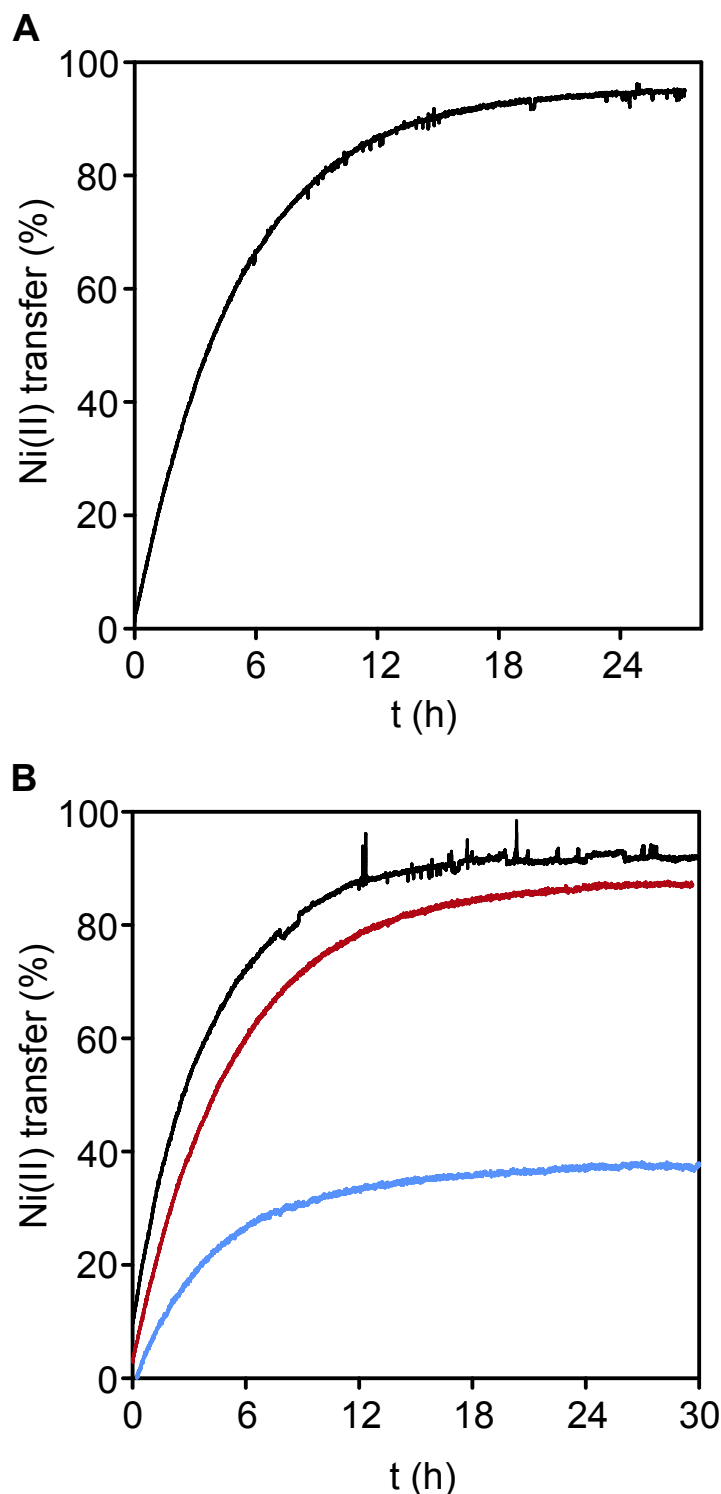


Figure 4.6. Competition with NTA and EGTA to determine the Ni(II) affinity of InrS. A. InrS (10.4 μM) was added to a solution of NTA (10 μM) and NiSO_4 (2.55 μM) (pH 7.8). Absorbance at 333 nm was monitored every 30 s to equilibrium. Percentage Ni(II) transfer was calculated by determining $\epsilon_{333 \text{ nm}}$ at equilibrium and use of the binding isotherm for the 333 nm feature shown in Figure 3.6B. B. InrS (10.4 μM : black and red lines, 10.3 μM : blue line) was added to a solution of EGTA (10 μM : black line, 100 μM : red line, 1 mM: blue line) and NiSO_4 (2.55 μM) (pH 7.8). Absorbance at 333 nm was monitored every 30 s to equilibrium. Percentage Ni(II) transfer was determined as described in part 'A'. The competition between InrS and 1 mM EGTA was carried out with a different stock of InrS to the other competitions shown and so percentage Ni(II) transfer was determined from a calibration curve produced with the same stock.

work. This may be indicative of nickel exchange occurring via free solution rather than being handed directly from chelator to protein via ligand exchange, however it should be noted that nickel exchange from four coordinate sites is thought to usually occur via associative mechanisms (Helm & Merbach. 2005). Next InrS was competed against an increasing molar excess of EGTA (Figure 4.6B). At roughly equimolar concentrations of InrS and EGTA virtually all the Ni(II) partitions to InrS. However, at a 10 and 100 fold molar excess of EGTA Ni(II) partitioned between InrS and EGTA (Figure 4.6B). This allowed a Ni(II) affinity for InrS to be calculated via equation 2 using the equilibrium concentrations of Ni(II)-InrS and Ni(II)-EGTA which were determined using the extinction coefficient of the Ni(II)-InrS complex determined in a control titration of InrS with nickel and mass balance (Table 4.1). In the calculation it is assumed the Ni(II) binding sites of InrS interact with negative cooperativity, which is reasonable assumption as this is implied by the sub-stoichiometric ratios of nickel required to drive allostery (Figure 4.4) and given that negative copper binding cooperativity has been demonstrated for *M. tuberculosis* CsoR (Liu *et al.* 2007). The experiment was also designed such that there was only enough nickel present in the assay to fill one monomer site. A mean average of $K_{D, Ni(II)} = 2.05(\pm 1.5) \times 10^{-14}$ M was obtained from one replicate with an approximately 10 fold molar excess of EGTA and two replicate experiments with an approximately 100 fold molar excess of EGTA (Table 4.1) (all experiments were conducted at pH 7.8). Incubation of EDTA with Ni(II) before addition of InrS resulted in no exchange of Ni(II) from EDTA to InrS as determined by the lack of increase in absorbance at 333 nm even after 24 h (Figure 4.7).

The Ni(II) affinity of InrS obtained by competition with EGTA is tighter than those determined for the square planar Ni(II) sites of *E. coli* NikR (9.4×10^{-13} M at pH 7.6 (Wang *et al.* 2004) and 6.8×10^{-12} M at pH 7.5 (Chivers & Sauer. 2002)) and *H. pylori* NikR (3.5×10^{-12} M at pH 7.6 (Abraham *et al.* 2006)) determined by similar methodology to that used here. The slightly different ligand set (predicted to be 2 Cys/ 2 His for InrS (Section 4.3) versus 1 Cys/ 3 His for NikR) may tune the Ni(II) affinity of InrS to be poised at a lower nickel concentration than that of *E. coli* and *H. pylori* NikR and this may reflect the different bioavailable nickel regimes of these organisms. Indeed it was previously shown that bioavailable nickel in a cyanobacterial cell is buffered substantially lower than that of a mycobacterial cell (Cavet *et al.* 2002). The Ni(II) affinity of InrS is also substantially tighter than *E. coli* RcnR, the nickel sensing paradigm of the CsoR-RcnR family. Although only a lower limit could be placed on the Ni(II) affinity of *E. coli* RcnR by competition with mag-fura-2 (Iwig *et al.* 2008), Iwig

[InrS] ^a (μM)	10.4	10.3	10.3
[EGTA] (μM)	100	1000	1000
[Ni(II)] (μM)	2.56	2.56	2.56
A _{333 nm} ^b	0.0467	0.0192	0.0262
ε _{333 nm} ^c (M ⁻¹ cm ⁻¹)	21,100	20,000	20,000
[Ni(II)-InrS] ^b (μM)	2.21	1.6	1.31
[Ni(II)-EGTA] ^b (μM)	0.35	0.96	1.25
K _{Ni} (M)	8.3x10 ⁻¹⁵	3.67x10 ⁻¹⁴	1.65x10 ⁻¹⁴
Average K _{Ni} (M)	2.05(±1.5 ^d)x10 ⁻¹⁴		

^a monomer concentration, the concentration of 'tight site' is taken to be a quarter of this value. ^b equilibrium values. ^c for a 1:1 Ni(II)-InrS complex. Determined empirically for the protein preparation used in the competition. ^d standard deviation.

Table 4.1. Statistics for the determination of InrS Ni(II) binding affinity through competition with EGTA.

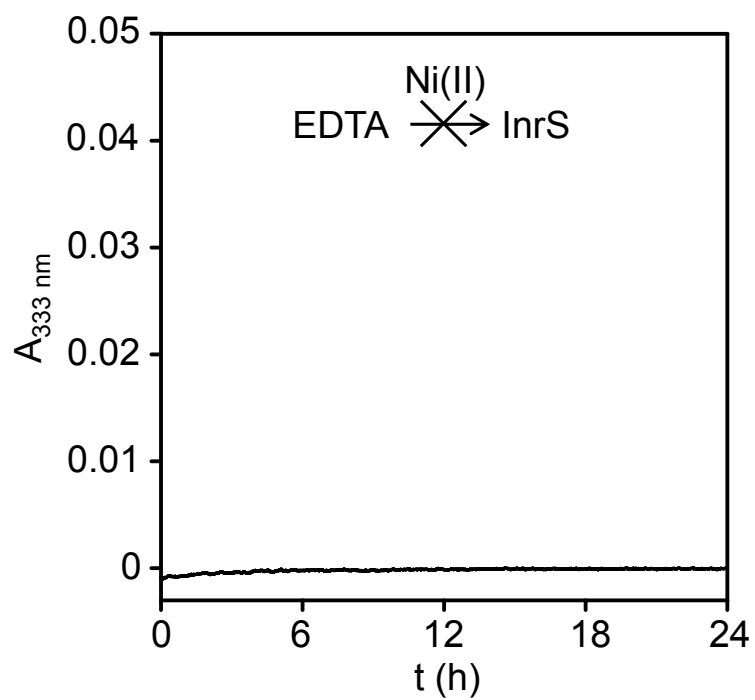


Figure 4.7. EDTA outcompetes InrS for Ni(II). InrS (24.2 μM) was added to a solution of EDTA (50 μM) and NiSO_4 (25 μM) (pH 7.8). Absorbance at 333 nm was recorded every 60 s for 24 h.

and Chivers have observed that RcnR does not compete with EGTA for Ni(II) suggesting a lower limit for the $K_{D, \text{Ni(II)}}$ of 10-20 nM (Iwig & Chivers. 2010). Differences in Ni(II) affinity between InrS and *E. coli* RcnR are likely to be at least partly explained by differences in the coordination geometry (octahedral versus square planar) however the Ni(II) binding affinity of *B. subtilis* CsoR, which is also predicted to bind Ni(II) in a square planar geometry with a similar predicted ligand set (as inferred from bioinformatics and the similarity of the Ni(II) dependent UV-Vis spectrum) has been estimated as 2.56×10^{-10} M (Ma *et al.* 2009a). This is discussed further in Section 6.3.1.

Weaker Ni(II) affinities for *E. coli* and *H. pylori* NikR have also been reported although these studies used either direct titration of the protein with nickel in conjunction with UV-Vis spectroscopy (Diederix *et al.* 2008) or isothermal titration calorimetry (ITC) (Zambelli *et al.* 2007) to determine Ni(II) affinity. Use of UV-Vis to determine a binding constant is necessarily limited by the micromolar concentrations of protein required to obtain a reliable signal and ITC can reliably measure binding constants in the range 1 mM – 10 nM (Grossoehme *et al.* 2010) thus the micromolar and nanomolar Ni(II) binding constants obtained in these studies are likely upper limits (numerically great, therefore a weaker interaction) imposed by the sensitivities of these techniques (Iwig & Chivers *et al.* 2010). The study of Diederix *et al.* (2008) used additional techniques (filter binding assay and stopped flow kinetics) to verify the micromolar binding constant obtained from UV-Vis spectroscopy (Diederix *et al.* 2008), however the non-equilibrium nature of these techniques makes their use challenging for measuring an equilibrium constant.

The Ni(II) affinity of InrS was also found to be pH dependent with the Ni(II) affinity of InrS determined as $K_{D, \text{Ni}} = 7.82(\pm 5.5) \times 10^{-13}$ M when experiments were conducted at pH 7 (Appendix Figure C2). This is likely indicative of a dependence on ligand deprotonation for metal coordination. The pKa of the cysteine side chain is 8 and the first pKa of the histidine side chain is 6, meaning that variations of $K_{D, \text{Ni(II)}}$ should be expected for InrS around physiological pH and these may be more pronounced than those observed for NikR due to the predicted presence of two cysteine residues within the nickel coordination site of InrS (Section 4.3) as opposed to one in NikR.

4.2.2 Determination of the Co(II) affinity of InrS

The Co(II) binding affinity of InrS was determined by competition with the fluorescent metal chelator fura2 which has previously been used to estimate the Co(II) binding affinity of *E. coli* RcnR (Iwig *et al.* 2008).

The Co(II) binding affinity of fura2 was first determined in a competitive binding assay calibrated against the chelator NTA as described by others for the calibration of the Ni(II) binding affinity of mag-fura-2 (Reyes-Caballero *et al.* 2011). Co(II) was titrated into a mixed solution of fura2 and NTA and the fluorescence emission of fura2 (which is quenched upon Co(II) binding) recorded at equilibrium (Figure 4.8). The binding isotherm was fit using the software package ‘DynaFit’ (Kuzmic. 1996) to obtain a Co(II) binding constant for fura2 at pH 7.8 of $K_{D, Co(II)} = 7.03 \times 10^{-9}$ M. The Co(II) binding affinity of NTA used in the calculation was 3.59×10^{-9} M and had been pH corrected using Schwarzenbach’s α -coefficient protocol (Xiao & Wedd. 2010) (Section 2.6.7). This calculated value of fura2 Co(II) affinity is in good agreement with previously published value of 8.64×10^{-9} M at pH 7.0 determined by a similar chelator competition method (Kwan & Putney. 1990) but tighter than that of 2.01×10^{-7} M at pH 7.0 determined by direct titration (Iwig *et al.* 2008). The reason for this discrepancy is unclear as, although the method of Iwig *et al.* used direct titration of cobalt onto fura2 to determine the binding constant, the shape of the binding curve suggests non-stoichiometric binding (Iwig *et al.* 2008). Crucially though the binding constant was obtained here under the same experimental conditions as used for the competition between chelator and protein.

The experimental design of the competition experiments between InrS and fura2 for Co(II) was similar to that described for competitions between InrS and EGTA for Ni(II) in Section 4.2.1. Fura2 was incubated with Co(II) before the addition of InrS. Upon InrS addition the fluorescence emission of fura2 was monitored until an equilibrium value was reached (Figure 4.9A). This equilibrium fluorescence value was used to determine the Co(II)-fura2 concentration using a calibration curve produced by titration of fura2 with Co(II) in the absence of protein (Figure 4.9B). This then allowed the equilibrium Co(II)-InrS concentration to be determined by mass balance and the InrS $K_{D, Co(II)}$ to be calculated via equation 2. Experiments were designed such that there was only enough Co(II) present in the assay to fill one monomer site. UV-Vis and gel filtration experiments to probe the Co(II) binding properties of InrS revealed that InrS binds two molar equivalents of Co(II) ions (Figures 3.10 and 3.11). Although the exact nature of

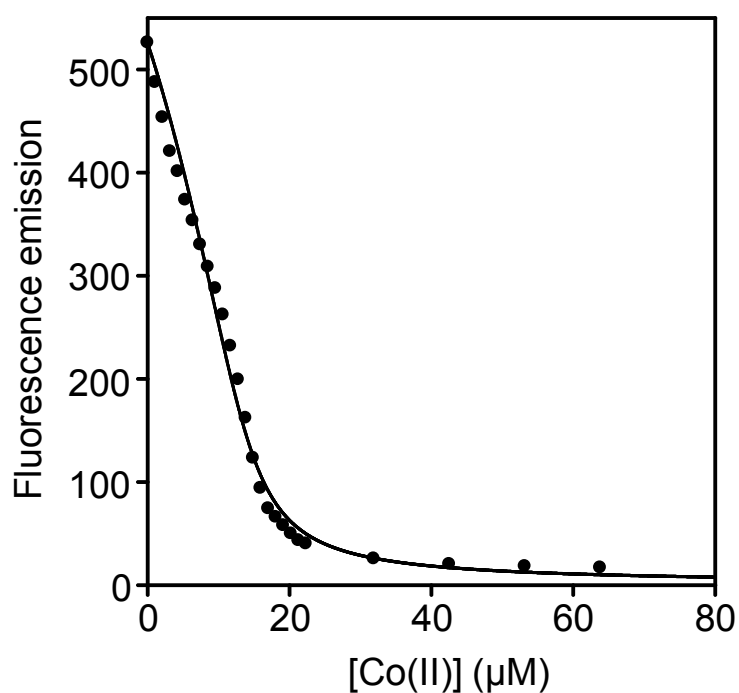


Figure 4.8. Determination of the Co(II) binding affinity of fura-2 by competition with NTA. CoCl₂ was titrated into a mixed solution of fura-2 (4.27 μM) and NTA (10 μM) (pH 7.8). Following excitation at 360 nm fluorescence emission at 510 nm was monitored until equilibrium was reached before recording the fluorescence emission value. The line represents a fit to a model describing one Co(II) binding event to fura-2, NTA and Hepes (present at 10 mM in the buffer) using Dynafit (Kuzmic. 1996) to obtain a Co(II) binding affinity for fura-2.

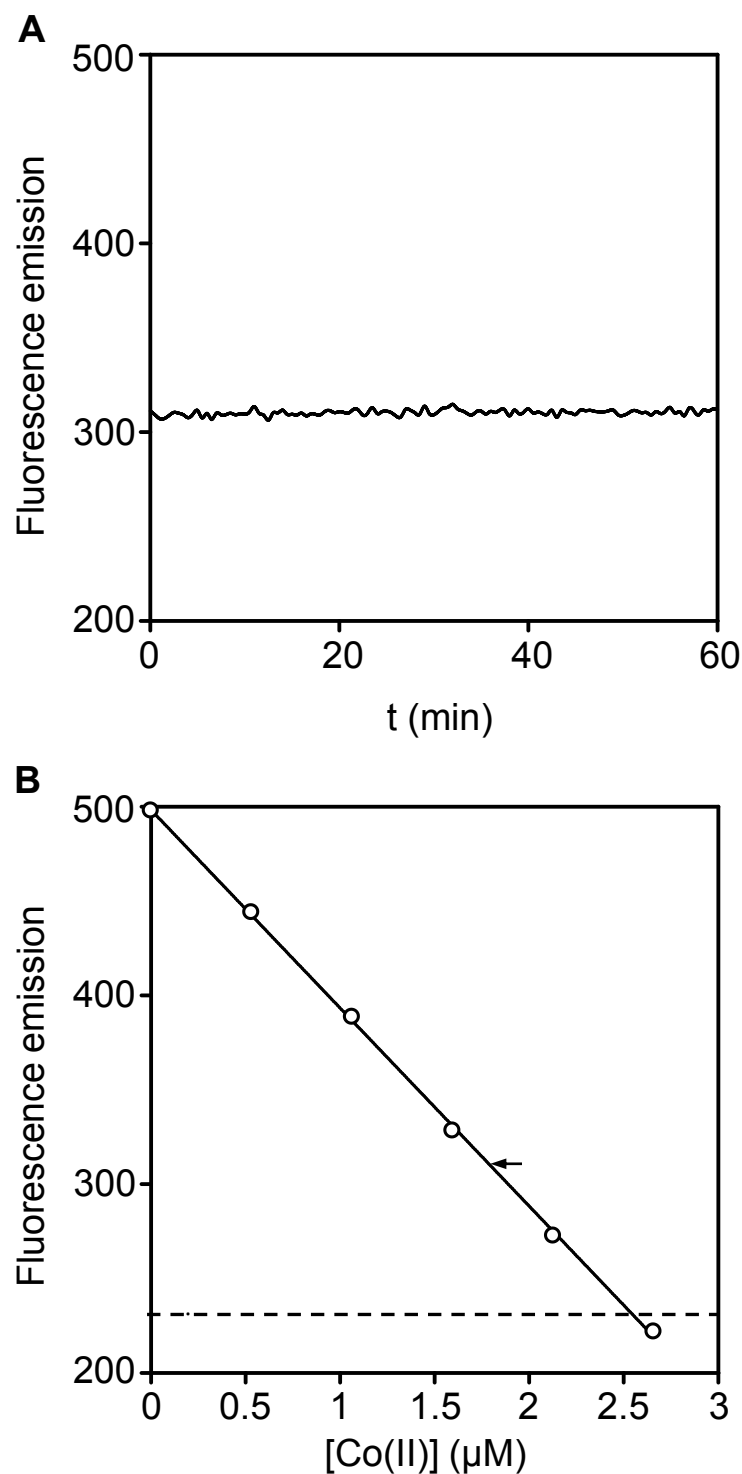


Figure 4.9. Determination of the Co(II) binding affinity of InrS by competition with fura-2. A. InrS ($10.3 \mu\text{M}$) was added to a solution of fura-2 ($5.14 \mu\text{M}$) and CoCl_2 ($2.55 \mu\text{M}$) and fluorescence emission at 510 nm following excitation at 360 nm was monitored for 1 h. B. Fura-2 ($5.14 \mu\text{M}$) was titrated with CoCl_2 in the absence of protein (circles) and fluorescence emission at 510 nm following excitation at 360 nm recorded. The arrow marks the equilibrium fluorescence value of the competition between InrS and fura-2 shown in 'A'. The dotted line represents the fluorescence value expected if fura-2 completely withheld Co(II) from InrS in the experiment described in 'A'.

the two sites is unclear there appeared to be sharing of cobalt between the two sites suggesting relatively closely matched affinities (Section 3.3.2). However, experiments examining the ability of Co(II) to dissociate InrS-DNA complexes revealed that sub-stoichiometric concentrations of Co(II) were required to titrate InrS off DNA suggesting negative cooperativity between cobalt binding sites (Figure 4.5B). Therefore in analysing the competition data two models were employed; the first, model A, assumes a single site on a tetramer has a substantially tighter affinity for Co(II) than the other binding sites on the protein and therefore competition with this site is the only protein Co(II) binding event considered in the analysis. The second, model B, assumes that the allosteric site and the additional site observed for Co(II) binding have similar affinities but that they display negative Co(II) binding cooperativity with respect to the corresponding sites on other monomer subunits. These models were reflected in the analysis as the total protein concentration entered into equation 2. Co(II) affinities calculated using these models were; model A $K_{D, Co} = 7.69(\pm 1.1) \times 10^{-9}$ M and model B $K_{D, Co} = 1.90(\pm 0.23) \times 10^{-8}$ M (Table 4.2).

The partitioning of Co(II) between InrS and fura2 reveals that the Co(II) affinity of InrS is weaker than that observed for *E. coli* RcnR where only a lower limit of <5 nM could be obtained due to RcnR substantially outcompeting fura2 for Co(II) (Iwig *et al.* 2008). Greater than stoichiometric amounts of Co(II) were required to saturate Co(II) binding to *B. subtilis* CsoR and this was taken to infer a weak Co(II) binding affinity of $\leq 10^5$ M⁻¹ (Ma *et al.* 2009a). A similar interpretation of UV-Vis data following Co(II) binding to InrS could have been made but size exclusion experiments showed a Co(II) binding stoichiometry of 2:1 (Figures 3.10 and 3.11). Later experiments with Zn(II) using size exclusion chromatography and a definitive experiment to observe zinc binding stoichiometry by monitoring the zinc withheld from a spectrally active chelator confirmed an InrS Zn(II) binding stoichiometry of 2:1 supporting a 2:1 stoichiometry for Co(II) (Section 5.6). It remains to be determined if *B. subtilis* CsoR has a Co(II) binding stoichiometry of 2:1 or 1:1 but a similar experiment to the one mentioned above for monitoring Zn(II) binding stoichiometry revealed the presence of only one Zn(II) binding site of substantial affinity on *B. subtilis* CsoR (Ma *et al.* 2009a) suggesting that this may also be the case for Co(II). In this case the Co(II) binding affinity of InrS is substantially tighter than that of *B. subtilis* CsoR. Additionally both InrS and *E. coli* RcnR display significantly tighter Co(II) affinities than those estimated for the nickel/cobalt sensors NmtR (Cavet *et al.* 2002) and KmtR (Campbell *et al.* 2007) from *M. tuberculosis*, 1.4 and 6.9 μ M respectively. Both NmtR (Cavet *et al.* 2002; Reyes-

[InrS] ^a (μM)	10.3	10.3	10.3
[fura2] (μM)	5.14	5.14	5.14
[Co(II)] (μM)	2.55	2.55	2.55
F _{510 nm} ^b	310.37	319.39	319.58
m ^c	-104.96	-104.96	-104.96
c ^c	498.26	498.26	498.26
[Co(II)-InrS] ^b (μM)	0.76	0.85	0.85
[Co(II)-fura2] ^b (μM)	1.79	1.7	1.7
Model A K _{Co} (M)	8.92x10 ⁻⁹	7.09x10 ⁻⁹	7.06x10 ⁻⁹
Model A average K _{Co} (M)	7.69 (±1.1 ^d) x10 ⁻⁹		
Model B K _{Co} (M)	2.16x10 ⁻⁸	1.77x10 ⁻⁸	1.76x10 ⁻⁸
Model B average K _{Co} (M)	1.90(±0.23 ^d)x10 ⁻⁸		

^a monomer concentration, the concentration of ‘tight’ site depends on the model used to assess the data (Section 4.2.2). ^b equilibrium values. ^c gradient (m) and intercept (c) of fura-2 cobalt titration standard curve produced concurrently with competition experiment. ^d standard deviation.

Table 4.2. Statistics for determination of InrS Co(II) binding affinity through competition with fura-2.

Caballero *et al.* 2011) and KmtR (Campbell *et al.* 2007) lack cysteine residues in their metal binding sites and perhaps the preference of Co(II) for the soft S⁻ ligand (Fraústo da Silva & Williams. 2002) is part of the explanation.

4.3. Identification of residues required for Ni(II) and Co(II) binding to InrS

InrS represents a novel addition to the CsoR-RcnR family. Despite being functionally analogous to RcnR (appearing to regulate an exporter in response to nickel and cobalt (Appendix Figure B2A)) it displays biochemical properties reminiscent of copper sensing CsoRs (metal binding spectra (Section 3.3) and DNA recognition site (Figure 3.33)) however it has a WXYZ motif intermediate to that of CsoR and RcnR (Figure 3.2) and lacks one of the key residues thought to be important for the propagation of the allosteric switch in *M. tuberculosis* CsoR (Section 3.1).

The crystal structure of CsoR from *M. tuberculosis* revealed Cu(I) bound in a trigonal planar geometry by a X-Y-Z motif consisting of Cys-His-Cys (Liu *et al.* 2007) (Figure 1.2). Subsequently this motif has shown to be required for tight copper binding in numerous CsoR homologues (Section 1.5.3). *B. subtilis* CsoR binds Ni(II) in what is deduced to be a four coordinate square planar geometry (Ma *et al.* 2009a). Ma *et al* commented that the intense LMCT feature observed likely means there are cysteine residue(s) in the binding site. Additionally Ni(II) is capable of driving allostery on binding to *B. subtilis* CsoR (albeit this is an attenuated response when compared to Cu(I) (Ma *et al.* 2009a)) and so His70 (in the Y position) is also predicted to be a Ni(II) ligand of *B. subtilis* CsoR given its essential nature in propagating the allosteric switch in response to Cu(I) binding (Ma *et al.* 2009b). The ligand(s) which complete the Ni(II) coordination sphere of *B. subtilis* CsoR were not identified. Similarly, cysteine residue(s) are implicated in a tetrahedral coordination of Co(II) by *B. subtilis* CsoR (Ma *et al.* 2009a). *E. coli* RcnR Cys35 (X position) plays a role in coordinating Ni(II) but does not appear to be obligatory for sensing (Iwig *et al.* 2008). A Cys35→Ala mutation (the only cysteine residue present in the protein) results in a loss of a UV-Vis LMCT feature indicative of S→Ni(II) coordination and an XAS spectrum diagnostic of a five coordinate, square pyramidal Ni(II) coordination centre rather than the six coordinate, pseudo-octahedral centre observed for wild type RcnR (Iwig *et al.* 2008). However, this mutant retains responsiveness to nickel in a *lacZ* reporter gene assay (Iwig *et al.* 2008). Only when the Cys residue is changed to a bulky Leu residue is Ni(II) responsiveness

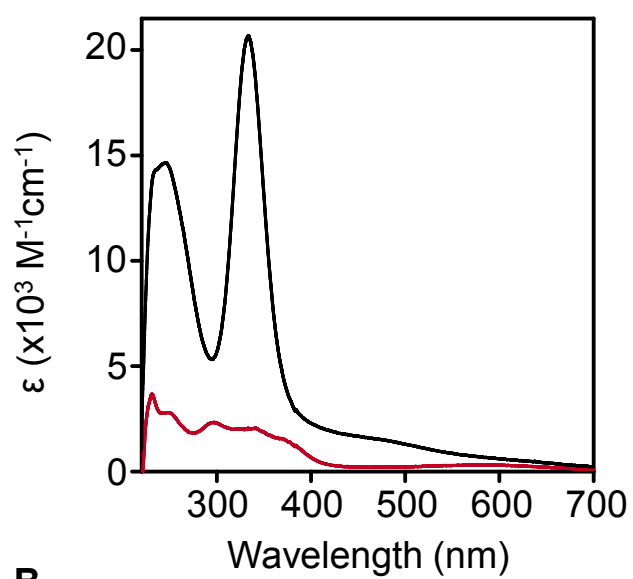
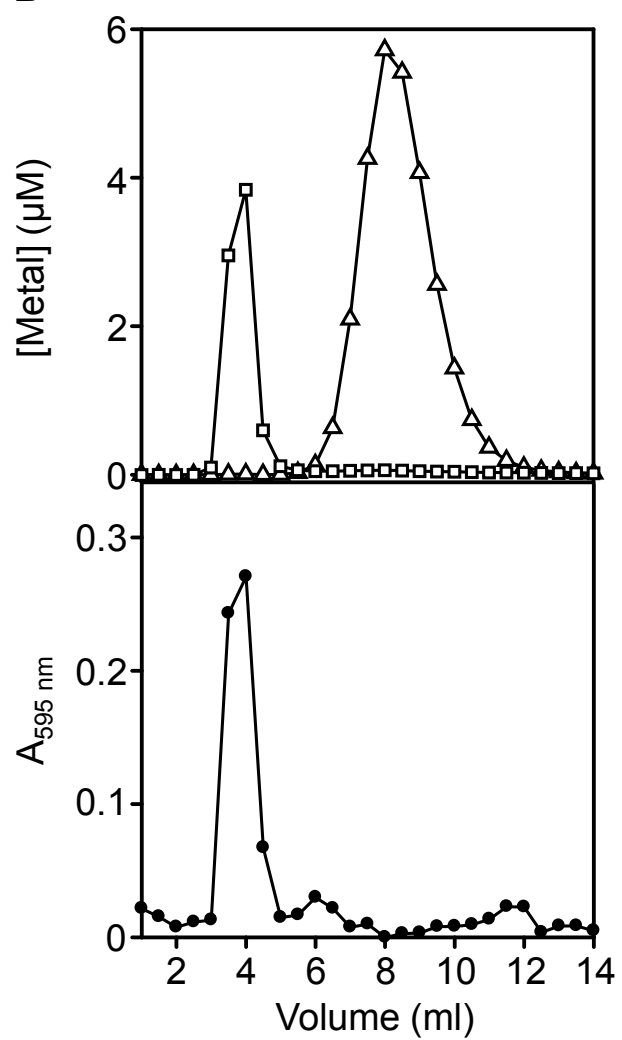
lost (Iwig *et al.* 2008). In contrast this Cys residue is essential for both Co(II) coordination (as revealed by UV-Vis) and responsiveness (in a *lacZ* reporter gene assay) (Iwig *et al.* 2008). *E. coli* RcnR His60 (Y position) is not implicated in Ni(II) coordination or responsiveness, as inferred from UV-Vis spectroscopy and a *lacZ* reporter gene assay, and so the propagation of the allosteric mechanism upon Ni(II) binding is predicted to be distinct from that upon Cu(I) binding to CsoR (Iwig *et al.* 2008). Again in contrast His60 both appears to be a Co(II) coordinating residue and to be essential for responsiveness (Iwig *et al.* 2008). UV-Vis spectra implicate His64 (Z position) in the coordination of both Ni(II) and Co(II) by *E. coli* RcnR (Iwig *et al.* 2008). A His64→Leu mutant displays no responsiveness to Co(II) whereas Ni(II) response is reduced by ~50 % (Iwig *et al.* 2008). His3 (W position) was shown to be required for Ni(II) and Co(II) binding by *E. coli* RcnR *in vitro*, with a His3→Leu mutation altering the Co(II) coordination geometry to five coordinate and causing a loss of all spectral features for Ni(II), and also for Ni(II) and Co(II) responsiveness *in vivo* (Iwig *et al.* 2008). More recent XAS data suggest that His3 may only be a ligand for Co(II) and not Ni(II) and so the exact role of this residue remains unclear (Higgins *et al.* 2012b). The N-terminal amino group (following cleavage of methionine) has been shown to be an obligatory ligand for responsiveness to both Ni(II) and Co(II) by UV-Vis spectroscopy, XAS and *lacZ* reporter gene assay (Iwig *et al.* 2008; Higgins *et al.* 2012b). By analogy coordination of Ni(II) by His3 and the N-terminal amino group following methionine cleavage has also now been shown for *M. tuberculosis* NmtR (Reyes-Caballero *et al.* 2011).

A combination of site directed mutagenesis coupled with a comparison of biochemical and biophysical properties was used to attempt to identify the Ni(II) and Co(II) ligands of InrS. Initially cysteine residues were mutated to alanine and histidine residues to leucine in order to lose metal coordination properties but retain relatively similar steric bulk.

4.3.1 Ni(II) coordinating cysteine residues

Addition of Ni(II) to Co(II) saturated InrS results in the appearance of spectral features indicative of Ni(II) saturated InrS (Figure 4.10A). Resolution of this protein-metal solution by size exclusion chromatography reveals that only Ni(II) is bound to the protein with Co(II) migrating as a free peak (Figure 4.10B). These data suggest that Ni(II) has displaced Co(II) from a binding site containing two cysteine ligands (Section 3.3.2) and therefore is potentially coordinated by two cysteine ligands itself as predicted

Figure 4.10. InrS binds Ni(II) in a site implicated to contain two cysteine ligands.
A. Apo-subtracted UV-Vis difference spectra of InrS (10 μ M) upon addition of 2.5 molar equivalents of CoCl₂ (red line) followed by the addition of 1.1 molar equivalents of NiCl₂ (black line) (spectra recorded ~90 min post nickel addition) (pH 7). Values at 800 nm have been subtracted to attempt to remove the contribution of non-specific light scatter to the extinction coefficient values (see Section 3.3.2). B. Following 'A' an aliquot (0.5 ml) of the reaction was applied to a PD10 column then eluted under anaerobic conditions (pH 7). Fractions (0.5 ml) were analysed qualitatively for protein (filled circles) by Bradford assay and quantitatively for nickel (open squares) and cobalt (open triangles) by ICP-MS.

A**B**

from sequence alignment (Figure 3.2) and comparison of the UV-Vis spectra of Ni(II)-InrS with those of Ni(II)-NikR (Section 3.3.1).

There are two cysteine residues in InrS (Cys53 and Cys82) in the X and Z positions of the CsoR-RcnR WXYZ motif (Figure 3.2); these residues were individually replaced with alanine by site directed mutagenesis to assess the effect on the metal and DNA binding properties of the protein. All site directed mutants were purified (Appendix D) as described for wild type InrS and subject to the same assays for reduced status of cysteine residues and metal contamination (Section 2.5.3 and 2.5.4).

4.3.2 Metal and DNA binding properties of InrS Cys53→Ala

First, the Ni(II) binding properties of InrS Cys53→Ala were assessed by UV-Vis spectroscopy. Upon titration of InrS Cys53→Ala with Ni(II) it is apparent that the coordination environment is substantially altered (Figure 4.11A). The LMCT feature at 333 nm is still present however is of a much reduced intensity to that observed in the wild type protein (Figure 3.6). Additionally, substantial non-specific light scattering due to precipitation is evident (Figure 4.11A). The presence of non-specific light scatter on additions subsequent to 0.194 equivalents of Ni(II) (the first addition) makes it difficult to quote an extinction coefficient for the $A_{333\text{ nm}}$ feature of Ni(II)-InrS Cys53→Ala, however extrapolation of the $A_{333\text{ nm}}$ value obtained on the first Ni(II) addition, where non-specific light scatter is minimal, suggests an extinction coefficient of $1,962\text{ M}^{-1}\text{ cm}^{-1}$ for fully Ni(II) occupied InrS Cys53→Ala (this approximation assumes stoichiometric binding of Ni(II) by InrS Cys53→Ala in this assay, which may not be the case as this mutant has a weakened Ni(II) affinity (Figure 4.11B)). This value is approximately 10 fold lower than the value for wild type InrS (Figure 3.6). The retention of the LMCT feature, albeit of a greatly reduced intensity, suggests that Cys53→Ala may still be capable of binding Ni(II). The non-specific light scattering caused by precipitation could be indicative of an adventitious ligand being recruited to fill the open coordination position left on the Ni(II) centre due to the loss of Cys53. InrS Cys53→Ala displays a weaker Ni(II) affinity than wild type InrS, migrating with ~0.28 equivalents of nickel when resolved on a PD10 column (Figure 4.11B).

To ensure the change in Ni(II) binding properties was not due to misfolding of InrS caused by mutation, the ability of InrS Cys53→Ala to bind *nrsD*ProFA was assessed by fluorescence anisotropy (Figure 4.12). The DNA binding affinity of C53A was found to be $K_{\text{DNA}} = 38.9\text{ nM}$ in good agreement with the value for wild type InrS (56.6 nM

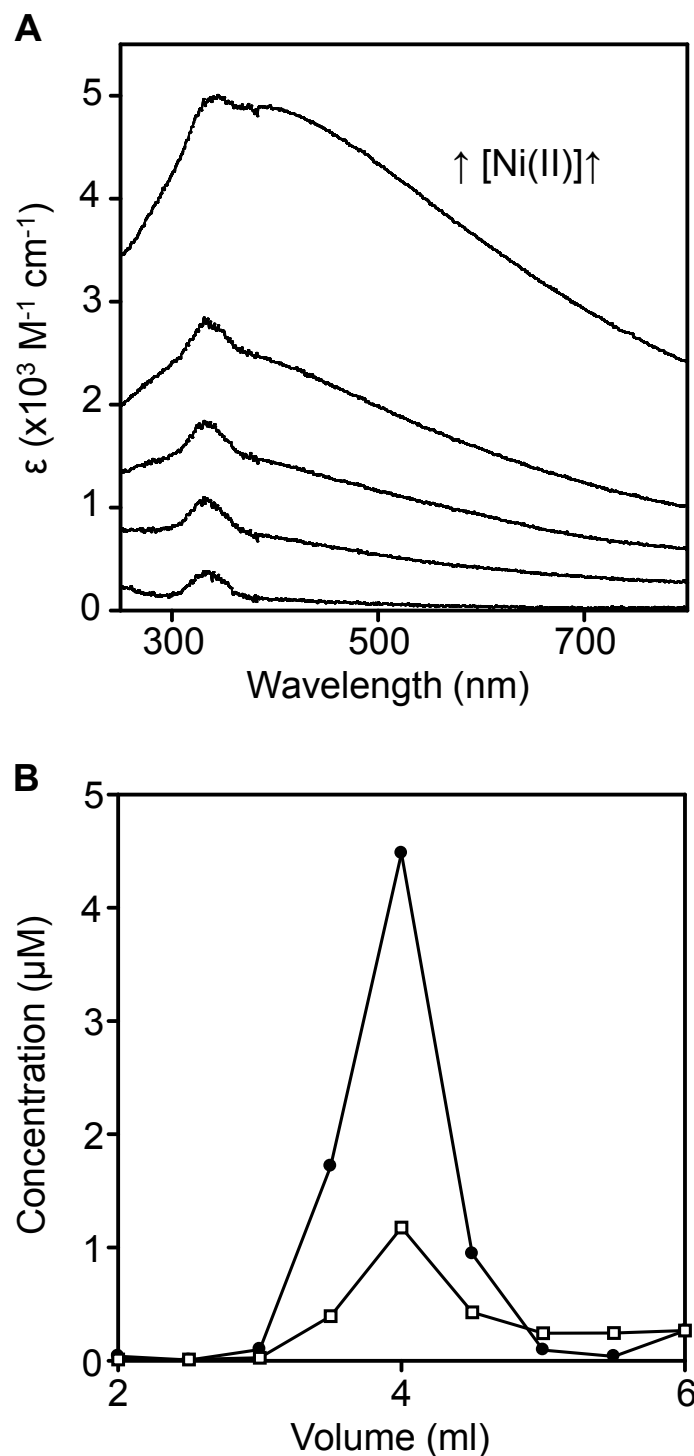


Figure 4.11. Ni(II) binding properties of InrS Cys53→Ala. A. Apo-subtracted UV-Vis difference spectra of InrS Cys53→Ala (10 μ M) upon titration with 5 x 0.194 molar equivalent additions of NiCl₂. B. 10 μ M InrS Cys53→Ala was incubated with 15 μ M NiCl₂ and resolved on a PD10 column. Fractions (0.5 ml) were analysed for protein (filled circles) by Bradford assay calibrated against a quantified stock of InrS Cys53→Ala and nickel (open squares) by ICP-MS. Both experiments performed anaerobically at pH7.

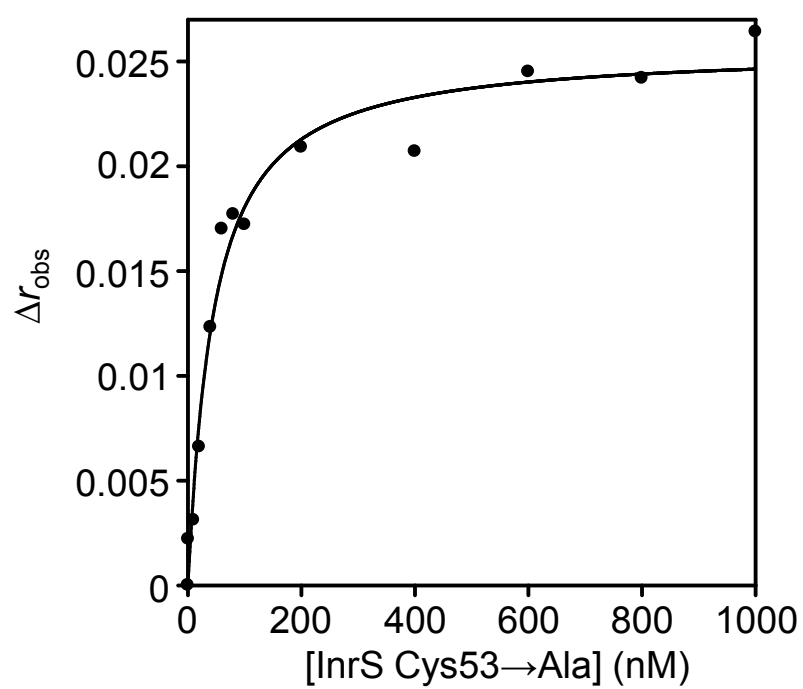


Figure 4.12. Titration of *nrsD*ProFA with InrS Cys53→Ala. *nrsD*ProFA (10 nM) was titrated with InrS Cys53→Ala in the presence of 5 mM EDTA and DNA binding was monitored by fluorescence anisotropy. Experiment performed anaerobically at pH 7.

(Figure 4.4)) suggesting this mutant retains a native fold (at least sufficient to maintain a tight DNA affinity) and therefore changes in metal binding properties are unlikely to be due to misfolding.

Titration of InrS Cys53→Ala with Co(II) results in the appearance of broad featureless spectra likely due to non-specific light scattering caused by protein precipitation (Figure 4.13). Again loss of Cys53 likely encourages the recruitment of adventitious ligands exacerbating the non-specific light scatter already observed in wild type InrS upon cobalt titration (Figure 3.9). The lack of specific features in these spectra suggests that the Co(II) site is completely abrogated by this mutation.

4.3.3 Metal and DNA binding properties of InrS Cys82→Ala

An absorbance feature at 285 nm, which shows an inflection at ~ one molar equivalent, along with some non-specific light scattering is evident upon titration of InrS Cys82→Ala with Ni(II) (Figure 4.14A and B). These spectra are substantially different from those of wild type InrS (Figure 3.6) suggesting a dramatically altered Ni(II) binding site. *E.coli* RcnR also display a Ni(II) dependent feature at a similar wavelength and lacks cysteine coordination at the position equivalent to Cys82 (Iwig *et al.* 2008). However the non-specific light scattering observed in these titrations (Figure 4.14A) makes it impossible to make inferences on coordination geometry based on the presence or absence of *d-d* transitions. This non-specific light scattering due to precipitation may be indicative of recruitment of adventitious ligands. InrS Cys82→Ala migrates with approximately 0.2 molar equivalents of nickel when resolved by PD10 chromatography indicating a severe weakening of Ni(II) binding in this mutant (Figure 4.14C).

Again the interaction of this mutant with DNA was checked by fluorescence anisotropy. Although InrS Cys82→Ala does interact with the InrS recognition site it displays a reduced affinity relative to wild type, $K_{\text{DNA}} = 286 \text{ nM}$, suggesting this residue may additionally play a role in maintaining DNA affinity (Figure 4.15).

The Co(II)-InrS Cys82→Ala (Figure 4.16) spectra display a more pronounced and better defined *d-d* transition envelope than wild type InrS (Figure 4.15) (Figure 3.9 and 3.10) suggesting that the tetrahedral Co(II)-binding site of InrS Cys82→Ala is less distorted than that of wild type InrS (Guo & Giedroc. 1997) and the reduced LMCT intensity is suggestive of a binding site with a lower sulphur content. The splitting of the LMCT feature observed with wild type Co(II)-InrS (Figures 3.9 and 3.10) is not observed with this mutant, consistent with a less distorted Co(II) coordination site.

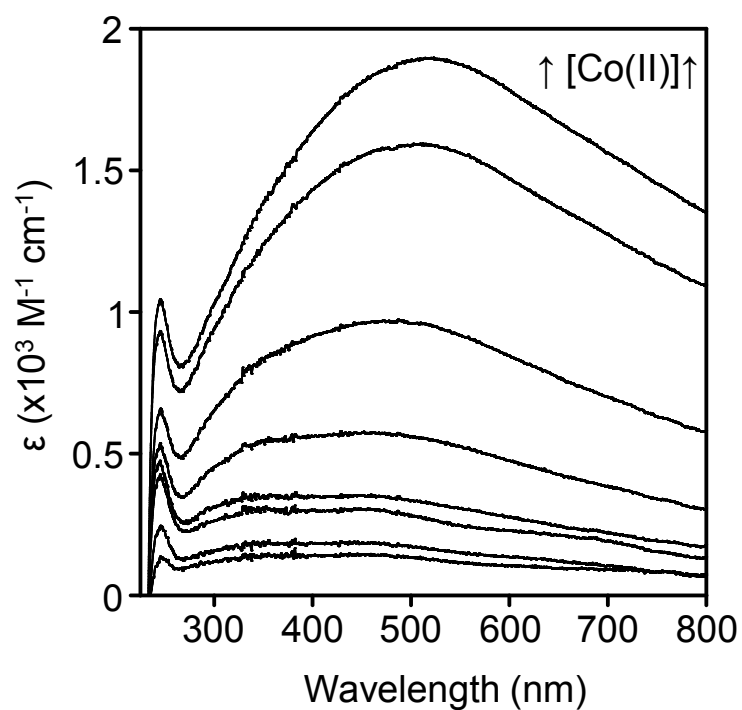
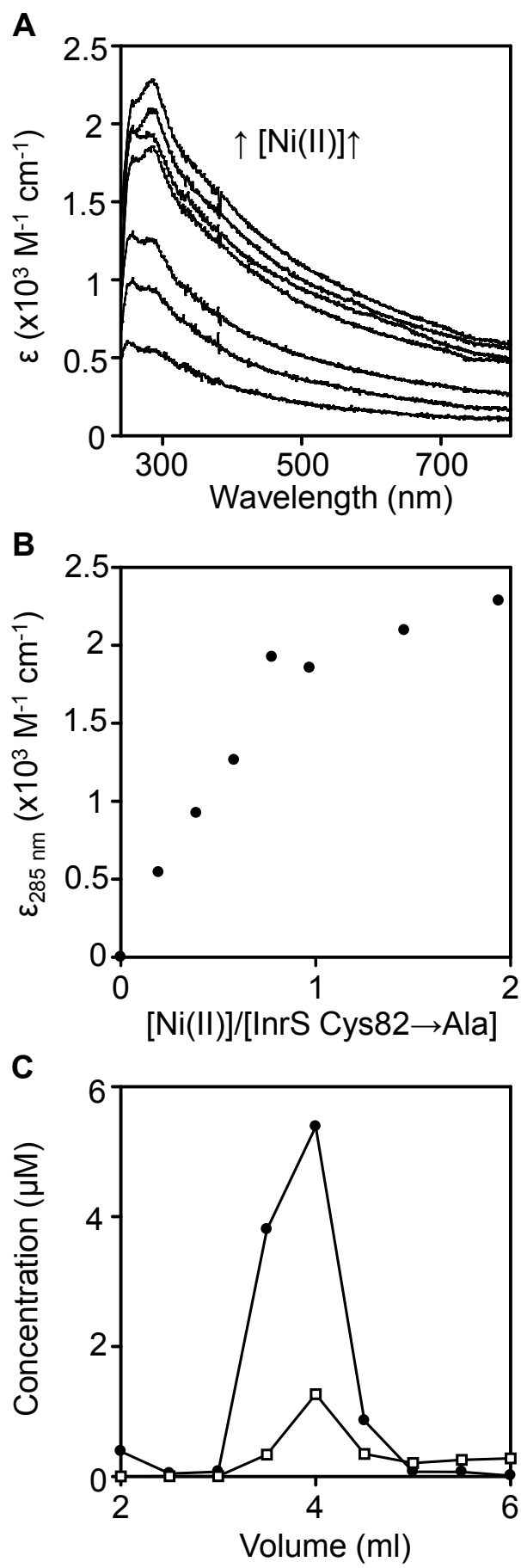


Figure 4.13. UV-Vis difference spectra of InrS Cys53→Ala upon titration with CoCl₂. Apo-subtracted UV-Vis difference spectra of InrS Cys53→Ala (30 μM) upon titration with CoCl₂ (recorded anaerobically at pH 7). Each spectrum represents a 0.184 molar equivalent addition of CoCl₂ other than the uppermost spectrum which represents a 0.368 molar equivalent addition.

Figure 4.14. Ni(II)-binding properties of InrS Cys82→Ala. A. Apo-subtracted UV-Vis difference spectra of InrS Cys82→Ala (10 μ M) upon titration with NiCl₂. B. Binding isotherm of the 285 nm Ni(II) dependent feature shown in 'A'. C. 10 μ M InrS Cys82→Ala was incubated with 15 μ M NiCl₂ and resolved on a PD10 column. Fractions (0.5 ml) were analysed for protein (filled circles) by Bradford assay calibrated against a quantified stock of InrS Cys82→Ala and nickel (open squares) by ICP-MS. Both experiments performed anaerobically at pH7.



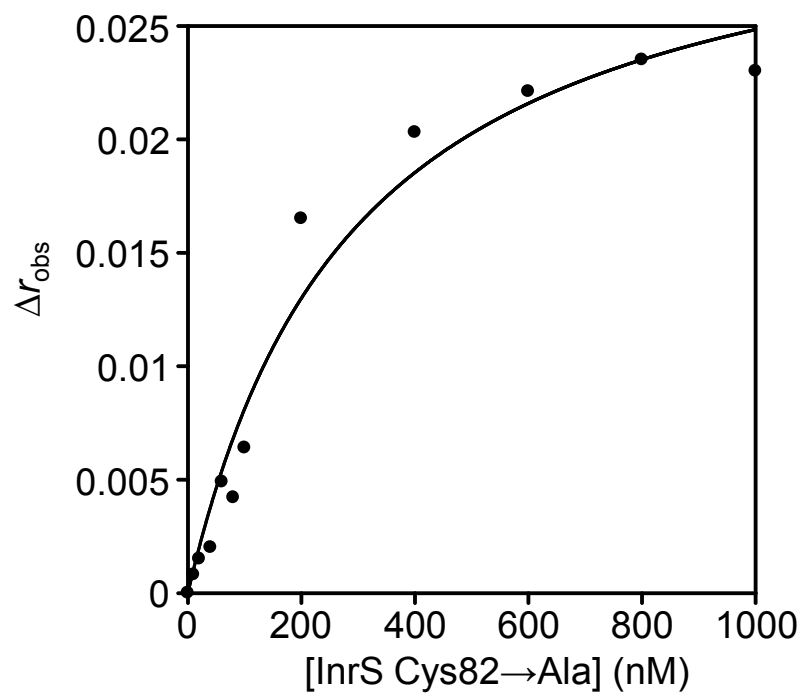


Figure 4.15. Titration of *nrsD*ProFA with InrS Cys82→Ala. *nrsD*ProFA (10 nM) was titrated with InrS Cys82→Ala in the presence of 5 mM EDTA and DNA binding was monitored by fluorescence anisotropy. Experiment performed anaerobically at pH 7.

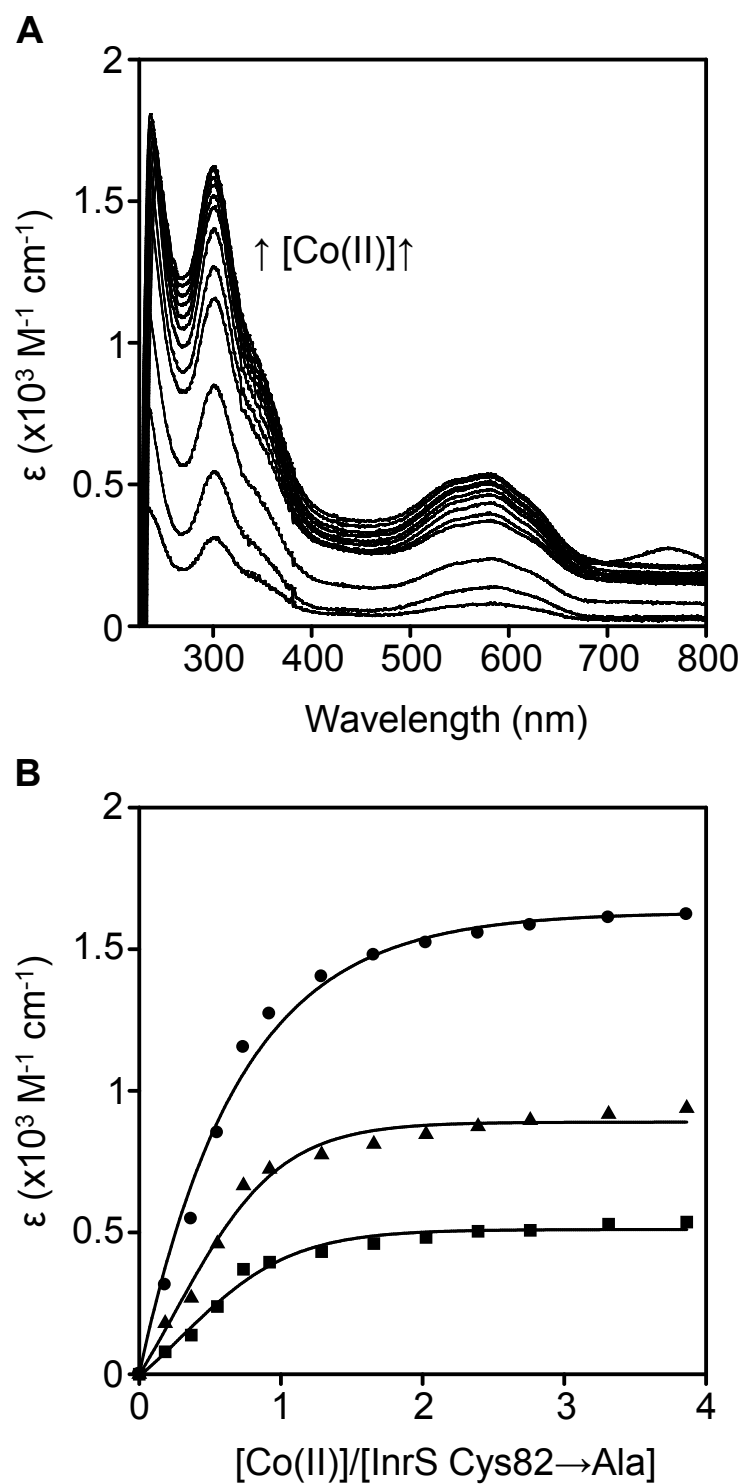


Figure 4.16. UV-Vis difference spectra of InrS Cys82→Ala upon titration with CoCl₂. A. Apo-subtracted UV-Vis difference spectra of InrS Cys82→Ala (30 μ M) upon titration with CoCl₂ (recorded anaerobically at pH 7). B. Binding isotherm of the Co(II) dependent spectral features at 300 nm (circles), 346 nm (triangles) and 582 nm (squares) shown in 'A'.

Interestingly the spectrum of Co(II)-InrS Cys82→Ala is very similar to that of *B. subtilis* Co(II)-CsoR, in terms of shape and wavelength, and intensities of features (Ma *et al.* 2009a). This suggests that the equivalent residue to InrS Cys82 in *B. subtilis* CsoR (Cys74) may not be involved in Co(II) coordination. How this coordination could be avoided by *B. subtilis* CsoR is unclear although perhaps it relates to the second Co(II) coordination event observed with InrS (Figures 3.10 and 3.11). Future experiments should address the Co(II) binding stoichiometry of the InrS Cys82→Ala mutant.

4.3.4 Metal and DNA binding properties of InrS His78→Leu

InrS His78 occupies the Y position of the CsoR-RcnR WXYZ motif and therefore corresponds to the histidine residue essential for the propagation of the allosteric switch upon copper binding in *M. tuberculosis* CsoR (Section 1.5.4) and required for Co(II) but not Ni(II) binding and response in *E. coli* RcnR (Section 4.3).

There are no absorbance features evident upon titration of InrS His78→Leu with nickel and the protein migrates with less than 0.1 molar equivalents of nickel when resolved by PD10 chromatography (Figure 4.17). This suggests that unlike *E. coli* RcnR H60 InrS His78 is essential for binding Ni(II).

Like InrS Cys82→Ala, InrS His78→Leu retains the ability to bind Co(II) although here the spectra are different again (Figure 4.18). The *d-d* transition envelope is more pronounced relative to that observed in wild type Co(II) spectra (Figure 3.9 and 3.10) again suggesting the binding site is less distorted and closer to true tetrahedral geometry. Consistent with this is the observation that the LMCT feature does not show the splitting associated with distorted geometries (Figure 4.18). The LMCT feature is also reduced relative to wild type suggesting a less sulphur rich binding site although it is unclear why this would be the case for this mutant. The more defined, less broad *d-d* transition envelope is also consistent with a less sulphur rich coordination site (Guo & Giedroc. 1997).

Titration of *nrsD*ProFA with InrS His78→Leu shows that InrS His78→Leu interacts with the InrS DNA recognition site with InrS His78→Leu displaying a similar DNA affinity to wild type InrS, $K_{\text{DNA}} = 76.2 \text{ nM}$ (Figure 4.19). As the equivalent residue is essential for allostery in *M. tuberculosis* CsoR the ability of Ni(II) to dissociate preformed DNA:InrS His78→Leu complexes was assessed. Ni(II) cannot titrate InrS His78→Leu off DNA even at a 100 fold molar excess of nickel over protein (Figure 4.20). The explanation for this is likely primarily due to the severe inhibition of Ni(II)

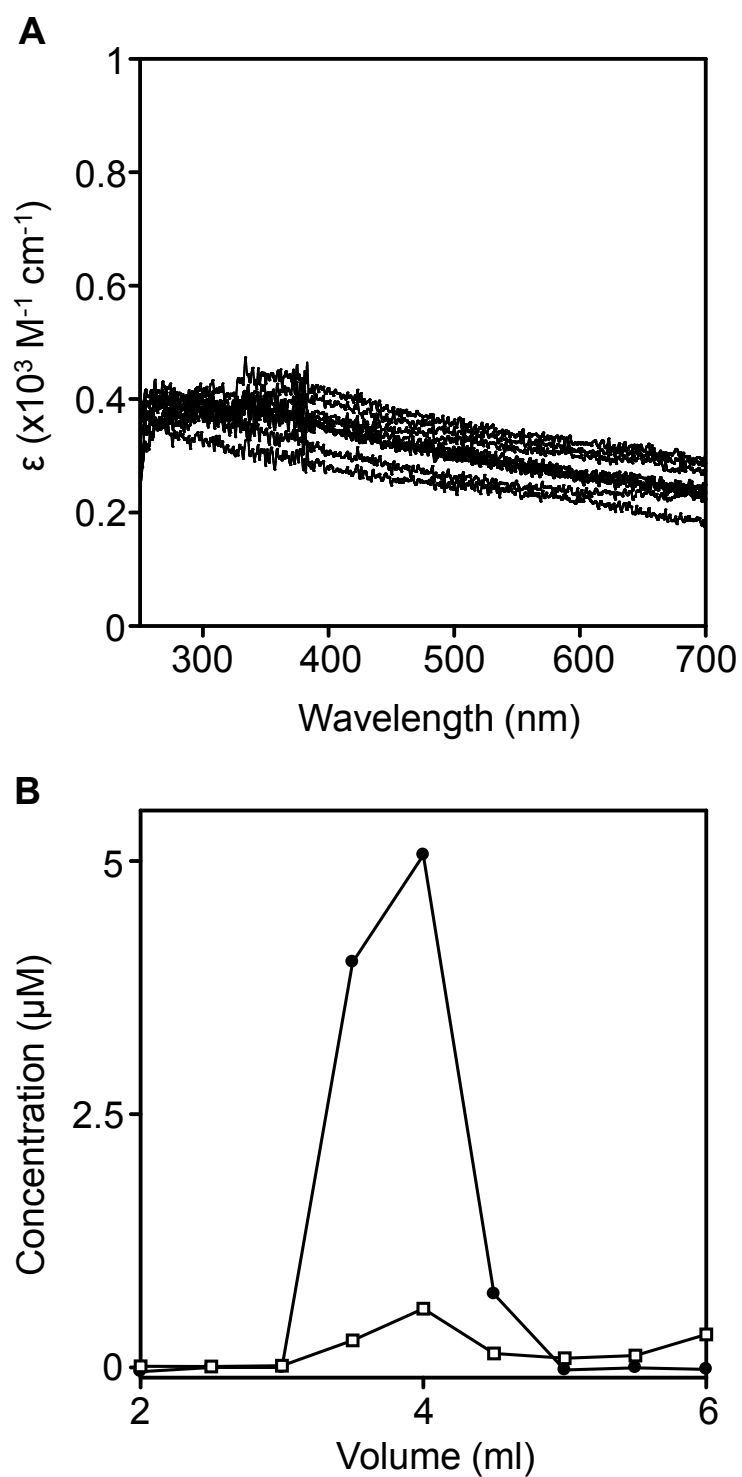


Figure 4.17. Ni(II) binding properties of InrS His78→Leu. A. Apo-subtracted UV-Vis difference spectra of InrS His78→Leu (10 μM) upon titration with up to 1.94 molar equivalents of NiCl_2 . B. 10 μM InrS His78→Leu was incubated with NiCl_2 (19.4 μM). Fractions (0.5 ml) were analysed for protein (filled circles) by Bradford assay calibrated against a quantified stock of InrS His78→Leu and nickel (open squares) by ICP-MS. Both experiments performed anaerobically at pH7.

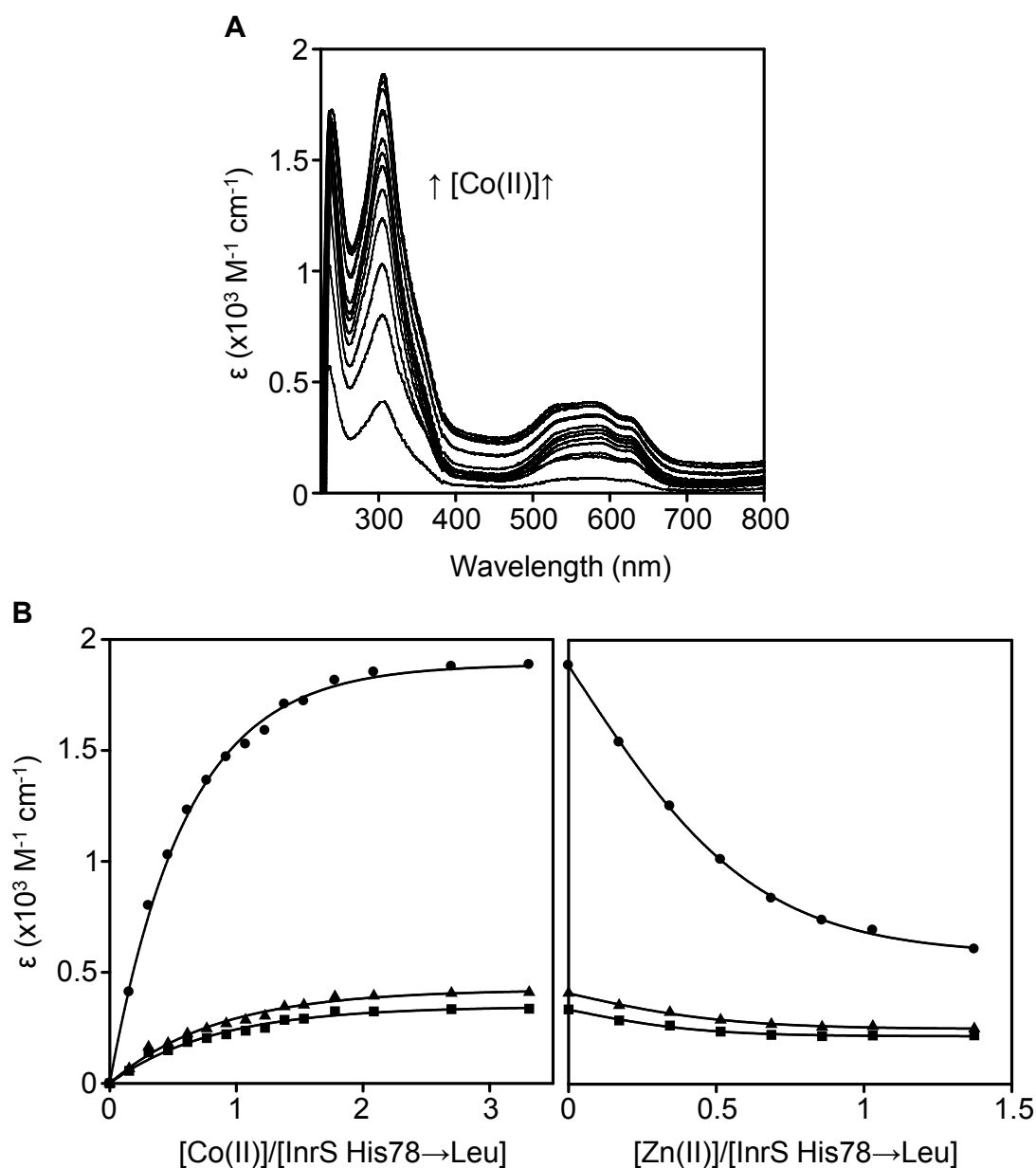


Figure 4.18. UV-Vis difference spectra of InrS His78→Leu upon titration with CoCl₂. A. Apo-subtracted UV-Vis difference spectra of InrS His78→Leu (30 μM) upon titration with CoCl₂ (recorded anaerobically at pH 7). B. *Left panel* - binding isotherm of the Co(II) dependent spectral features at 305 nm (circles), 580 nm (triangles) and 628 nm (squares) shown in 'A'. *Right panel* – the same spectral features upon titration of the end point solution in left panel with ZnSO₄.

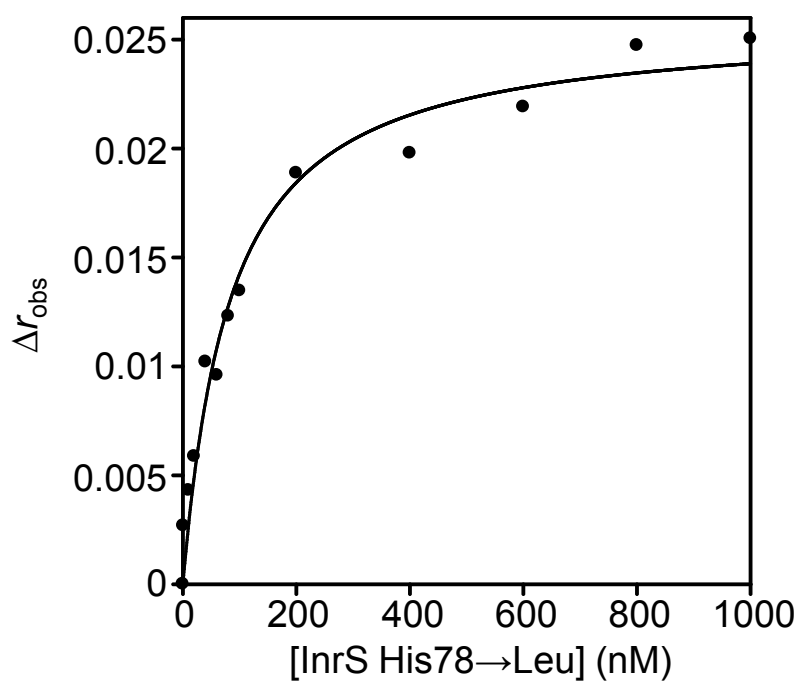


Figure 4.19. Titration of *nrsD*ProFA with InrS His78→Leu. *nrsD*ProFA (10 nM) was titrated with InrS His78→Leu in the presence of 5 mM EDTA and DNA binding was monitored by fluorescence anisotropy. Experiment performed anaerobically at pH 7.

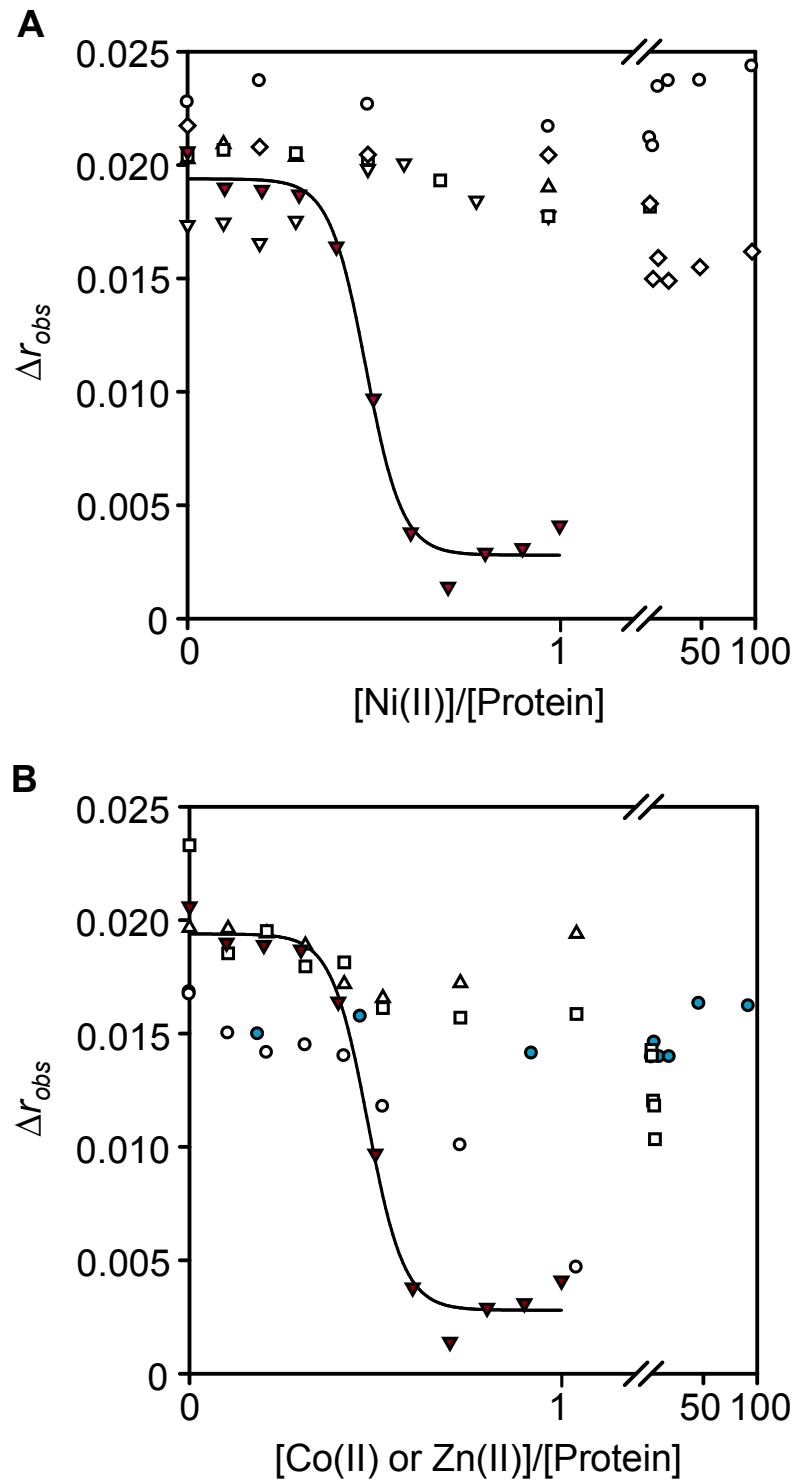


Figure 4.20. Loss of metal mediated allostery in *InrS* His78→Leu. A. Multiple titrations of *nrsD*ProFA (10 nM) pre-incubated with *InrS* His78→Leu (1 μ M) with $NiCl_2$ (open symbols) performed anaerobically at pH7. Dissociation of protein:DNA complexes was monitored by fluorescence anisotropy. B. As 'A' but performed with $CoCl_2$ (blue symbols) or $ZnSO_4$ (open symbols). Shown for comparison in both panels is an analogous experiment performed with wild type *InrS* and $NiCl_2$ (red symbols) (pH 7.8).

binding by this mutant protein (Figure 4.17) and so further experiments will be needed to conclusively determine the function of this residue in InrS Ni(II) driven allostery. The ability of Co(II) and Zn(II) to dissociate preformed DNA:InrS His78→Leu complexes was also investigated. Zn(II) binds InrS His78→Leu, likely at a site which at least partially overlaps with that of Co(II) as shown by Zn(II) bleaching of Co(II) dependent spectral features (Figure 4.18B). Zn(II) is also capable of dissociating wild type DNA:InrS complexes (Figure 5.14). Both Co(II) and the more tightly binding Zn(II) (which is predicted to adopt the same coordination geometry) both appear to be incapable of dissociating preformed DNA:InrS His78→Leu complexes (Figure 4.20B) showing that for Co(II) (and Zn(II)) His78 may be required for allostery. However the nature of the Co(II) complex formed by InrS His78→Leu (Figure 4.18) is clearly distinct from that formed by wild type InrS (Figure 3.9 and 3.10) and this may be the explanation for the loss of allostery.

4.3.5 Metal and DNA binding properties of InrS His21 mutant variants

InrS His21 occupies the W position of the CsoR-RcnR WXYZ motif corresponding to His3 in *E. coli* RcnR (Section 4.3). A residue in this position is not thought to be a ligand for copper in copper sensing CsoRs characterised thus far although *S. aureus* CsoR does contain a histidine residue in this position (Figure 3.2). Additionally the other characterised CsoRs compared in Figure 3.2 with the exception of *L. monocytogenes* CsoR contain a histidine (or glutamate in the case of *M. tuberculosis*) in the position immediately preceding the W position perhaps suggesting an important role for a metal liganding residue in this area of the protein.

Upon titration of InrS His21→Leu with NiCl₂ it is immediately evident that the absorbance spectra is unaltered from that of the wild type protein (Figure 3.6) with LMCT and square planar diagnostic features in identical positions and of similar intensity (Figure 4.21A-C). In addition InrS His21→Leu co-migrates with one molar equivalent of nickel by size exclusion chromatography (Figure 4.21D). The mutant protein interacts with the InrS recognition site ($K_{\text{DNA}} = 120 \text{ nM}$) and is titrated off DNA by Ni(II) at a Ni(II) stoichiometry akin to the wild type protein (Figure 4.22). However, the Co(II) binding absorbance spectra are distinct from wild type InrS (Figure 4.23).

Co(II) bound InrS His21→Leu displays a *d-d* transition envelope that is red shifted (Figure 4.23) relative to those of wild type (Figures 3.9 and 3.10), His78→Leu (Figure 4.18) & Cys82→Ala (Figure 4.16) variants of InrS. A shift to lower energy wavelengths

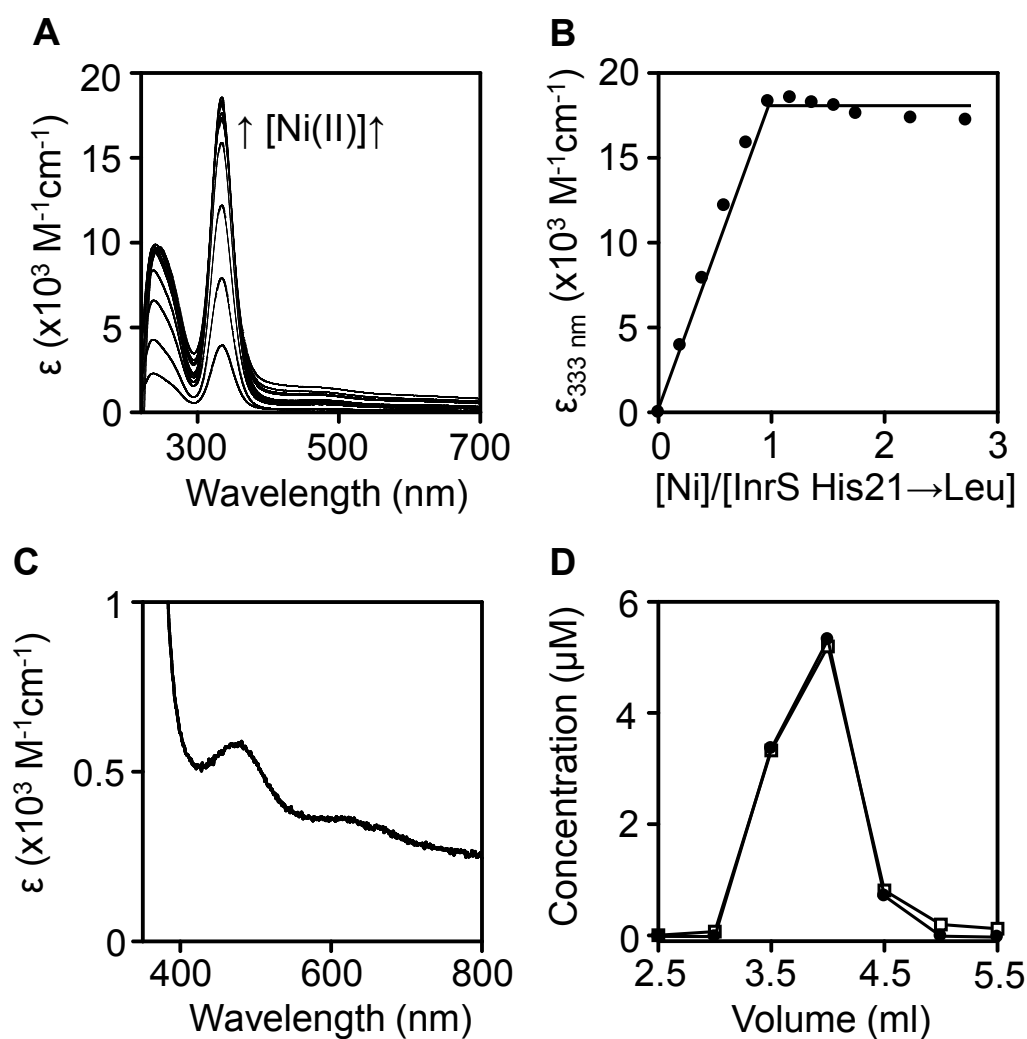


Figure 4.21. Ni(II) binding properties of InrS His21→Leu. A. Apo-subtracted UV-Vis difference spectra of InrS His21→Leu (10 μM) upon titration with NiCl_2 (recorded at pH 7). B. Binding isotherm depicting the Ni(II) dependent spectral feature at 333 nm in ‘A’. C. Enlargement of the InrS His21→Leu UV-Vis spectrum upon addition of 1 molar equivalent of NiCl_2 to highlight the small peak with an absorbance maxima of $\sim 480 \text{ nm}$, characteristic of Ni(II) bound in a square planar geometry. D. H21L migrates with one molar equivalent of nickel by size exclusion chromatography. H21L (10 μM) was incubated with ~ 1.5 molar equivalents of NiCl_2 and after 30 min incubation at room temperature an aliquot (0.5 ml) was applied to and eluted from a PD10 column. Fractions (0.5 ml) were analysed for protein (filled circles) by Bradford assay calibrated against a quantified stock of InrS His21→Leu and nickel (open squares) by ICP-MS. All experiments were performed anaerobically.

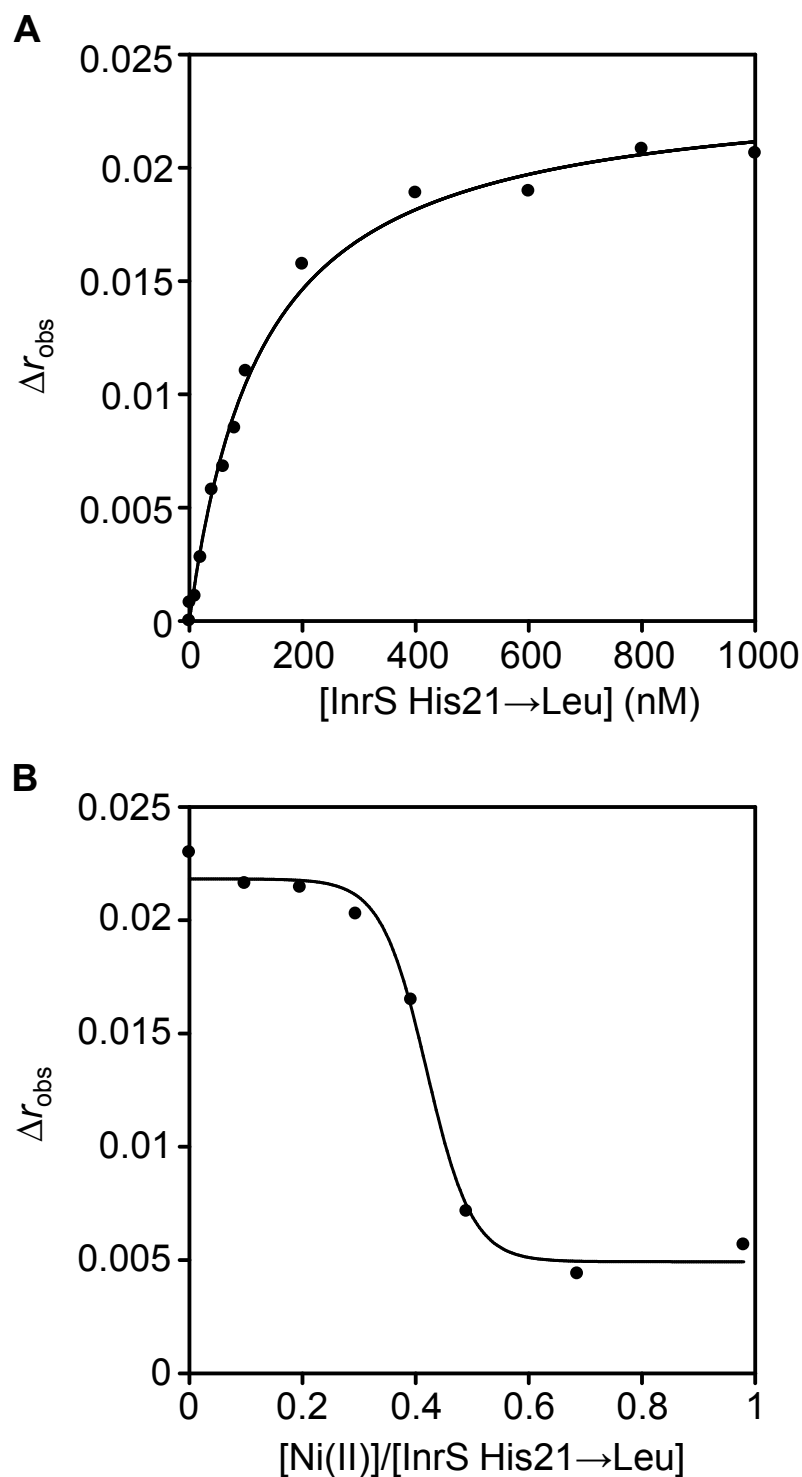


Figure 4.22. DNA binding properties of InrS His21→Leu. A. *nrsDProFA* (10 nM) was titrated with InrS His21→Leu in the presence of 5 mM EDTA and DNA binding was monitored by fluorescence anisotropy. B. Titration of *nrsDProFA* (10 nM) pre-incubated with InrS His21→Leu (1 μ M) with NiCl_2 . Dissociation of protein:DNA complexes was observed by fluorescence anisotropy. Both experiments were performed at pH7.

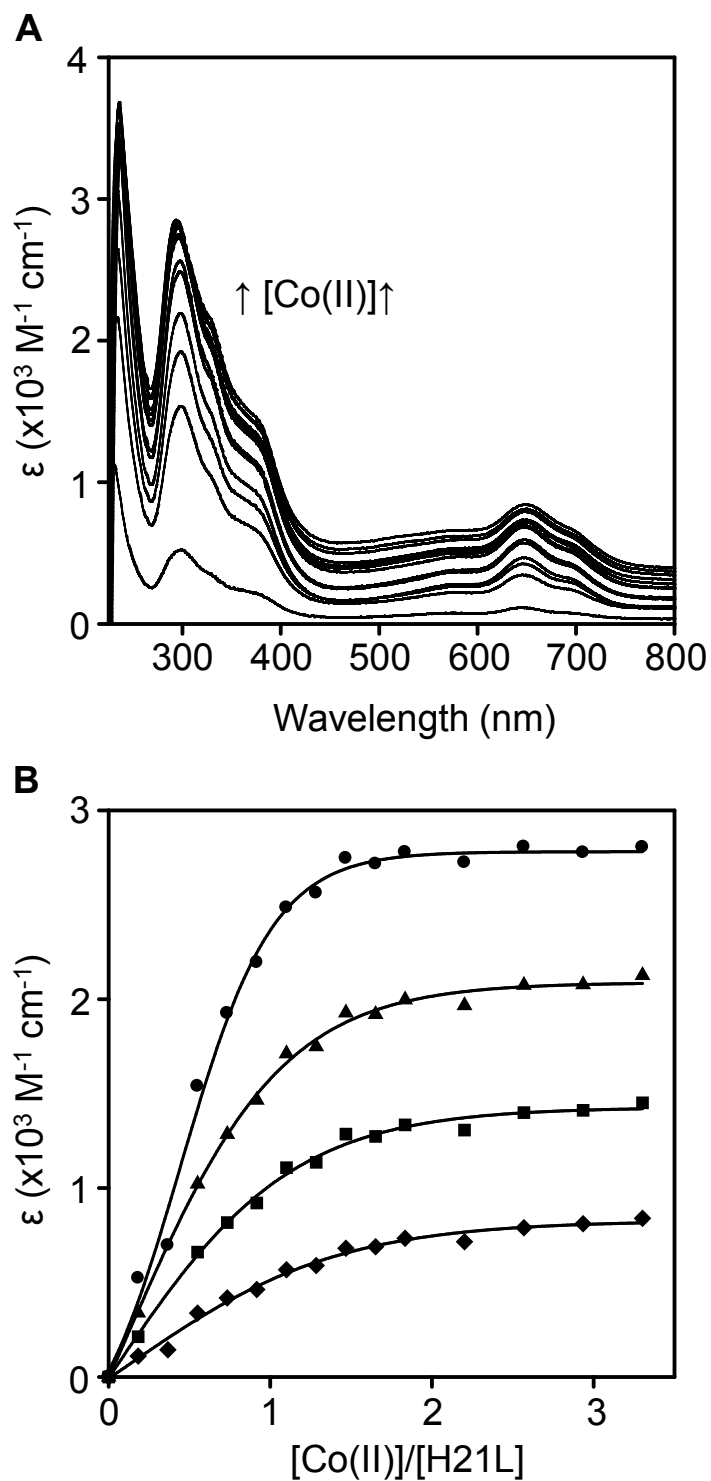


Figure 4.23. UV-Vis difference spectra of InrS His21→Leu upon titration with CoCl_2 . A. Apo-subtracted UV-Vis difference spectra of InrS His21→Leu (30 μM) upon titration with CoCl_2 (recorded anaerobically at pH 7). B. Binding isotherm of Co(II) dependent spectral features at 298 nm (circles), 330 nm (triangles), 375 nm (squares) and 650 nm (diamonds) shown in 'A'.

of Co(II) *d-d* transition envelopes has previously been correlated with the increased presence of sulphur in the binding site (Krizek *et al.* 1993) although it is not clear why this should be the case for this mutant. Splitting of the LMCT feature remains although this effect is less distinct than in wild type InrS suggesting a less distorted coordination geometry.

H21 is clearly a ligand for Co(II) although a role in coordination of Ni(II) is not clear from these data. The presence of sulphur in a binding site may be correlated with nickel dependent LMCT intensity (Section 3.3.1) and therefore it was hypothesised that the mutation His21→Cys may result in increased LMCT intensity if His21 is part of the Ni(II) coordination sphere. However, no significant increase in LMCT intensity above that observed for wild type Ni(II)-InrS was observed upon titration of InrS His21→Cys with Ni(II) (Figure 4.24) (Table 4.3).

These data strongly suggest that InrS His21 is not involved in Ni(II) binding. However the possibility remained that although His21 may not be essential for Ni(II) binding or Ni(II) mediated allostery under the conditions used here, it may modulate the Ni(II) affinity of InrS. To assess this possibility 20 μM of each of wild type, His21→Leu and His21→Cys InrS variants were all competed against 100 μM EGTA for 4.85 μM Ni(II) allowing sufficient time for equilibrium to be reached as described earlier (Section 4.2.1). The end point spectra of these competitions show that wild type InrS acquired more Ni(II) than InrS His21→Cys which acquired more Ni(II) than InrS His21→Leu based on the intensity of the Ni(II) dependent LMCT feature at 333 nm (Figure 4.25). In a separate experiment with InrS His21→Glu, which displays similar Ni(II) binding characteristics to wild type InrS (Appendix Figure C3), InrS His21→Glu acquired an amount of Ni(II) intermediate to that obtained by His21→Leu and His21→Cys (Appendix Figure C4) (fractional Ni(II) occupancies of the tightest site on a tetramer were wt = 0.95, InrS His21→Leu = 0.19, InrS His21→Glu = 0.31 and InrS His21→Cys = 0.64). Fractional occupancies were calculated by determining the concentration of Ni(II)-InrS His21 variant based on the equilibrium $A_{333\text{ nm}}$ value and the $\epsilon_{333\text{ nm}}$ value determined for each of the His21 InrS variants (Table 4.3), as there was 4.85 μM Ni(II) and 5 μM of tightest InrS site in these assays the maximum fractional occupancy value obtainable was 0.97. The presence of a metal liganding residue in the W position increases the ability of InrS to compete with EGTA for Ni(II). Furthermore, the Ni(II) occupancy of the proteins correlates with the preference of Ni(II) for the donor atom supplied by the residue in position 21 (W position) (Fraústo da Silva & Williams. 2002)

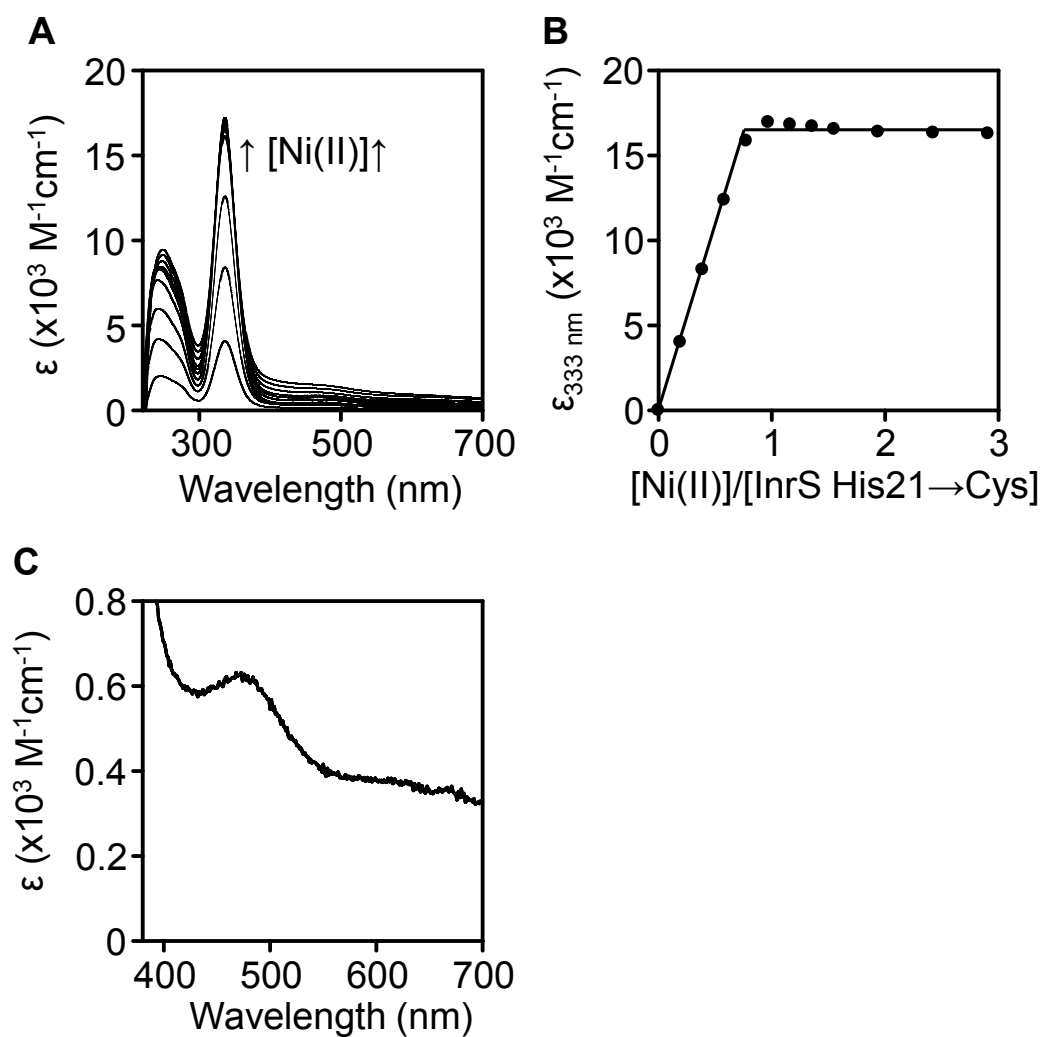


Figure 4.24. Ni(II) binding properties of InrS His21→Cys. A. Apo-subtracted UV-Vis difference spectra of InrS His21→Cys (10 μM) upon titration with NiCl_2 (recorded anaerobically at pH 7). B. Binding isotherm depicting the Ni(II) dependent spectral feature at 333 nm in 'A'. C. Enlargement of the InrS His21→Cys UV-Vis spectrum upon addition of 1 molar equivalent of NiCl_2 to highlight the small peak with an absorbance maxima of $\sim 480 \text{ nm}$, characteristic of Ni(II) bound in a square planar geometry.

InrS variant	$\epsilon_{333\text{ nm}} (\text{M}^{-1}\text{cm}^{-1})$
wild type	20,152 ^a ($\pm 467^b$)
His21→Leu	20,686 ^a ($\pm 144^b$)
His21→Glu	19,934 ^c
His21→Cys	21,590 ^a ($\pm 363^b$)

^a mean average of n=3 replicates. ^b standard deviation. ^c n=1.

Table 4.3. Extinction coefficients of the Ni(II) dependent 333 nm feature of His21 InrS variants. Values determined empirically through titration of InrS His21 variants with NiCl₂. Titrations performed at pH 7.

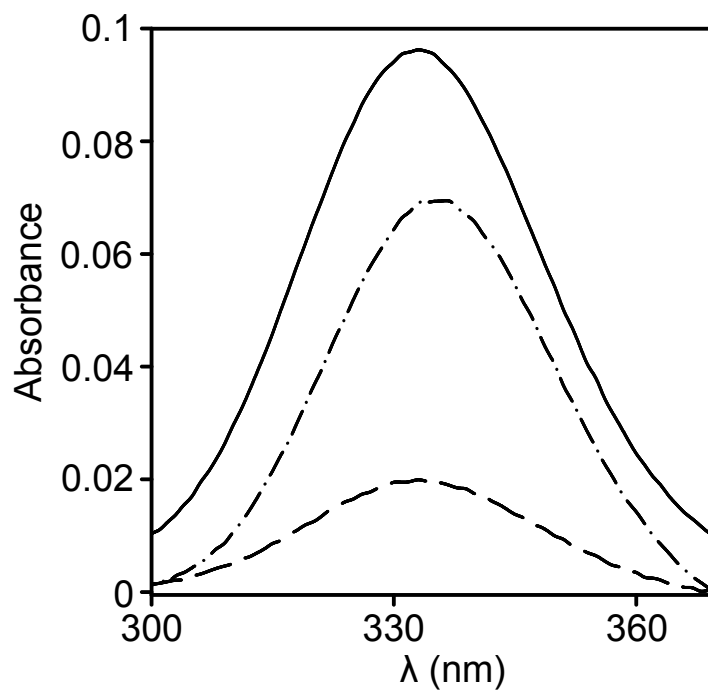


Figure 4.25. Relative Ni(II) affinity of InrS His21 mutants. A pre-incubated mix of EGTA and NiCl_2 was added to wild type (solid line), His21→Leu (dashed line) and His21→Cys (dot-dashed line) InrS to a final concentration of $[\text{protein}] = 20 \mu\text{M}$, $[\text{EGTA}] = 100 \mu\text{M}$ and $[\text{NiCl}_2] = 4.85 \mu\text{M}$. Ni(II) exchange between EGTA and protein was allowed to come to equilibrium before recording the UV-Vis spectrum.

with His21 (nitrogen) and Cys21 (sulphur) containing InrS variants displaying greater Ni(II) occupancies than a His21→Glu (oxygen) variant. Additionally the peak intensity of the Ni(II) dependent InrS His21→Cys LMCT feature is slightly though perceptibly red shifted relative to both wild type InrS and InrS His21→Leu (Figure 4.25). As mentioned previously red shift of spectral features is consistent with a more sulphur rich binding site (VanZile *et al.* 2002).

In order to quantitatively define the nickel binding affinity of these His21 mutants an approach analogous to that taken to determine the nickel affinity of wild type InrS (Section 4.2.1) was used to determine the nickel affinity of the His21 mutants. His21 mutants were competed against varying concentrations of EGTA for Ni(II) sufficient to fill less than one site on a tetramer (Appendix Figure C5). Ni(II) affinities were found to be InrS His21→Leu $K_{D, Ni(II)} = 6.73(\pm 5.0) \times 10^{-11}$ M, InrS His21→Cys $K_{D, Ni(II)} = 1.10(\pm 0.97) \times 10^{-11}$ M, InrS His21→Glu $K_{D, Ni(II)} = 2.65(\pm 2.5) \times 10^{-11}$ M making these mutants 86, 14 and 34 fold weaker nickel binders than wild type InrS respectively (these experiments were performed at pH 7 and therefore the affinities are compared with the wild type InrS nickel affinity determined at pH 7 (Appendix Figure C2)).

Taken together these data suggest that Cys53, His78 and Cys82 are absolutely required for Ni(II) binding and all at least modulate Co(II) binding with His78 required to propagate the allosteric switch upon Co(II) binding. Cys82 may also play a role in determining the DNA binding affinity of InrS. The identity of His21 as the forth ligand is debatable. It appears to be dispensable for both nickel binding and nickel mediated allostery although clearly has an effect on the affinity of the nickel binding site. Putative roles for His21 are discussed in Section 6.3.1.

Chapter 5. Contributions of affinity, access and allostery in favour of cognate and against non-cognate metal selectivity of InrS

As the ‘arbiters of metal sufficiency’ metal sensor proteins are proposed to control the availability of metals within a cell by regulating mechanisms of metal homeostasis (Helmann *et al.* 2007). They are proposed to create a regime in which, at least for the most competitive ions, metalloproteins compete for a limited pool of metal ions rather than an excess of metal ions competing for a limited number of protein binding sites. This is thought to influence the correct occupancy of metalloproteins as the differences between binding sites in metalloproteins may now become sufficient to select the correct element (Robinson. 2007). However, this raises the question of how metalloregulators correctly respond only to their cognate metals as they are subject to the same limitations imposed by the Irving-Williams series as other metalloproteins (Irving & Williams. 1948; Waldron & Robinson. 2009).

In order to address selectivity in favour of nickel and cobalt sensing by InrS the nickel and cobalt affinities of a representative sub-set of metalloregulators from *Synechocystis* were determined. The allosteric response of InrS to non *in vivo* effector metals was assessed and the affinity of InrS for these metals determined in order to elucidate the factors against detection of these metals *in vivo*.

5.1 Affinity and relative affinity

Studies of metalloregulators have largely focussed on individual proteins in isolation but by considering the entire complement of metalloregulators in a cell as an integrated set it becomes possible to build new models for explaining the *in vivo* responses of these proteins. As mentioned above, metalloregulators are not free of the constraints of the Irving-Williams series. However, when a cell’s complement of metalloregulators is considered as an integrated set it becomes apparent that, given the role of metalloregulators in controlling the expression of genes of metal homeostasis, the absolute affinity of a metalloregulator for a metal ion may be less important than the relative affinity of the cell’s complement of metalloregulators for any given element.

InrS has a very tight affinity for Ni(II) ($2.05(\pm 1.5) \times 10^{-14}$ M at pH 7.8) (Section 4.2.1). This raised the possibility that Ni(II) sensing within *Synechocystis* could operate on the basis of relative affinity; that is, InrS may be able to sense Ni(II) and initiate export via NrsD at intracellular concentrations of nickel below the K_D , Ni(II) of the cell's other metalloregulators preventing them aberrantly responding or becoming inhibited by Ni(II) binding. In order to address this hypothesis the Ni(II) affinities of characterised representatives from each of the major cytosolic metal sensor protein families represented in the *Synechocystis* genome were determined. The *Synechocystis* genome contains characterised representatives from four (Fur, ArsR-SmtB, MerR, CsoR-RcnR) of the seven major metal sensing families (Section 1.10.2). *Synechocystis* does not contain a NikR or DtxR homologue however does contain a gene coding for a protein with homology to CopY (ORF *slr0240*) (Section 1.10.2). This protein is unlikely to sense metal directly (Section 5.2) and so a comparison of Zur (Zn(II) dependent co-repressor) (Tottey *et al.* 2012), ZiaR (Zn(II) dependent de-repressor) (Thelwell *et al.* 1998), CoaR (Co(II) dependent activator) (Rutherford *et al.* 1999) and InrS (Ni(II)/Co(II) dependent de-repressor) (Foster *et al.* 2012 & this work) represents each of the major cytosolic metalloregulatory protein families found in *Synechocystis*.

5.2 Purification of recombinant ZiaR, Zur and CoaR

ZiaR and Zur were purified according to previously published protocols (Dainty *et al.* 2010; Tottey *et al.* 2012) by a combination of nickel affinity, size exclusion and heparin affinity chromatography (Figures 5.1 and 5.2). The peak elution volumes of ZiaR (160 ml) (Figure 5.1) and Zur (165 ml) (Figure 5.2) from a calibrated size exclusion column (Figure 3.4) correspond to assemblies of molecular weight 36,908 Da and 33,334 Da, respectively, consistent with both ZiaR (theoretical $M_r = 15,083.2$ Da) and Zur (theoretical $M_r = 15,421.8$ Da) existing as dimers under the conditions used here. CoaR was purified by Dr. Carl Patterson according to protocols that have been published during the course of this work (Foster *et al.* 2012). Briefly, CoaR is predicted to have surface exposed hydrophobic regions and therefore inclusion of the non-ionic detergent DDM allowed purification using a combination of nickel, cation and heparin affinity chromatography. Due to the inclusion of non-ionic detergent in the purification buffers a size exclusion chromatography step was not included in the purification; however, by analogy to structurally characterised MerR family proteins (Heldwein & Brennan. 2001; Godsey *et al.* 2001; Changela *et al.* 2003; Watanabe *et al.* 2008) CoaR is predicted to exist as a dimeric assembly. As with InrS and InrS variants the purity of

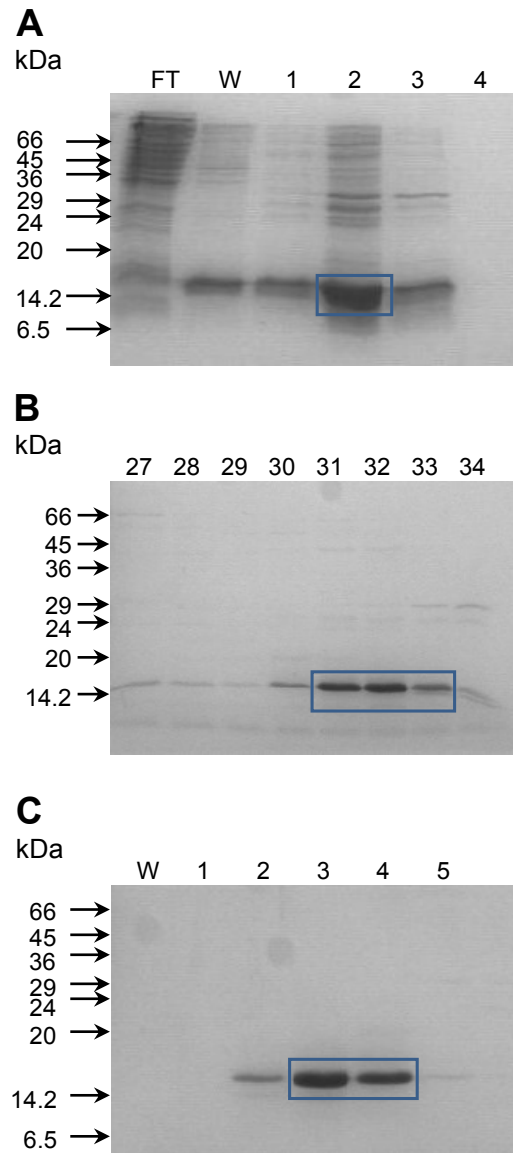


Figure 5.1. Purification of recombinant ZiaR. A. SDS-PAGE analysis of fractions eluted from a nickel affinity column loaded with soluble lysate from one 1 litre of cells overexpressing ZiaR. Fraction FT contains the flowthrough. Fraction W contains 10 column volume wash with buffer C. Fractions 1-4 were collected upon elution with buffer C with 20 mM imidazole with no PMSF. Fraction 1 is the lag fraction (see Figure 3.3) (4.5 ml), fractions 2 and 3 the peak protein elution fractions (3 and 2 ml respectively). Fraction 4 is a 2 column volume wash. B. SDS-PAGE analysis of fractions eluted from a Superdex S75 column loaded with 2 ml of fraction 2 from the nickel affinity step ('A'). Fractions are 5 ml in volume. C. SDS-PAGE analysis of fractions eluted from a heparin affinity column loaded with pooled fractions 31-33 from the size exclusion step ('B'). W contains the flowthrough and wash (with 10 column volumes of buffer B with 100 mM NaCl). Fractions 1-4 contain lag and peak elution fractions upon increasing NaCl concentration in buffer B. Fraction 4 is the peak protein containing elution fraction for buffer B with 0.4 M NaCl, whereas fraction 3 is the lag fraction for the same salt concentration ($[\text{NaCl}] = 0.3\text{-}0.4\text{ M}$). Fraction 5 is a 10 column volume wash with buffer B containing 1 M NaCl. After each purification step the boxed fractions were pooled and used in the next purification step or for experiments.

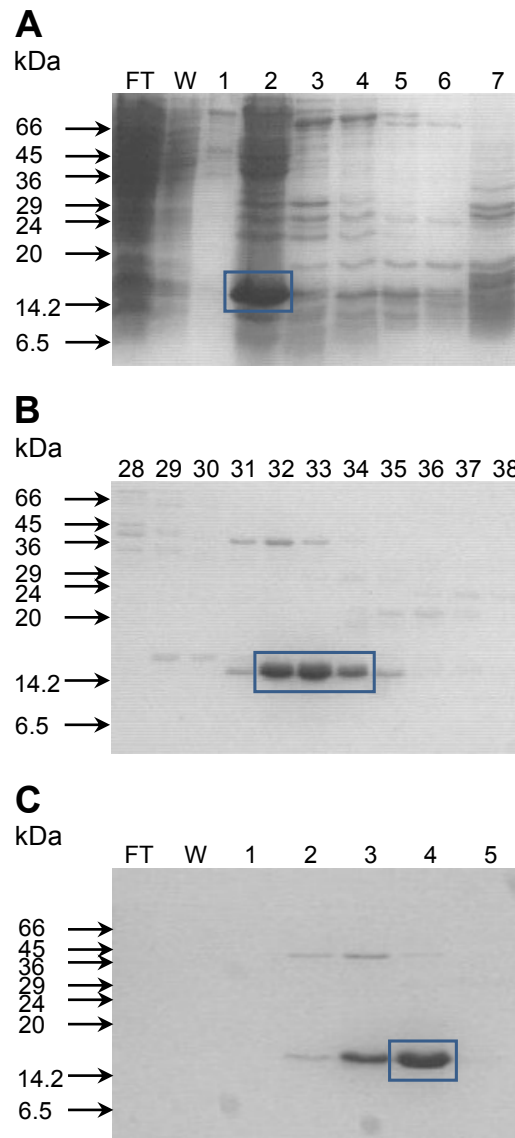


Figure 5.2. Purification of recombinant Zur. A. SDS-PAGE analysis of fractions eluted from a heparin affinity column loaded with soluble lysate from 1 litre of cells overexpressing Zur. Fraction FT contains the flowthrough. Fraction W contains 10 column volume wash with buffer B containing 100 mM NaCl and 1 mM PMSF. Fractions 1-6 (2 ml each) were collected upon elution with buffer B containing 500 mM NaCl. Fraction 7 is a 5 column volume wash with buffer B containing 500 mM NaCl. B. SDS-PAGE analysis of fractions eluted from a Superdex S75 column loaded with 2 ml of fraction 2 from the heparin affinity step ('A'). Fractions are 5 ml in volume. C. SDS-PAGE analysis of fractions eluted from a heparin affinity column loaded with pooled fractions 32-34 from the size exclusion step ('B'). FT and W contain the flowthrough and wash fractions (with 10 column volumes of buffer B with 100 mM NaCl) respectively. Fractions 1-4 contain lag (see Figure 3.3) and peak elution fractions upon increasing NaCl concentration in buffer B. Fraction 4 is the peak protein containing elution fraction upon elution with buffer B containing 0.4 M NaCl. Fraction 5 is a 10 column volume wash with buffer B containing 1 M NaCl. After each purification step the boxed fractions were pooled and used in the next purification step or for experiments.

ZiaR, Zur and CoaR was confirmed by SDS-PAGE analysis and the proteins were verified apo and reduced by ICP-MS and reaction with DTNB respectively. Zur routinely purified with approximately one molar equivalent of zinc, consistent with the presence of a structural Zn(II) site that is refractory to removal by EDTA (Tottey *et al.* 2012). CoaR gave less consistent reactivity of all thiols with DTNB although DNA- and metal-binding properties between different preparations were essentially unchanged (Patterson. 2010).

5.3 Relative Ni(II) affinities of the metalloregulators of *Synechocystis*

5.3.1 Determination of the Ni(II) affinities of ZiaR, Zur and CoaR

The Ni(II) affinities of ZiaR and Zur were determined by competition against mag-fura-2 using an experimental design similar to that described for determining the Co(II) affinity of InrS (Section 4.2.2). Ni(II) was incubated with mag-fura-2 before the addition of protein. Mag-fura-2 fluorescence was then monitored until equilibrium was reached. ZiaR and Zur have previously been shown to have two and one Ni(II) binding sites per monomer respectively (Patterson. 2010) and experiments were designed such that there was only enough Ni(II) present in the assay to fill less than one monomer site (Tables 5.1 and 5.2). Competition between mag-fura-2 and ZiaR & Zur for Ni(II) came to equilibrium rapidly (before the start of fluorescence monitoring) and resulted in partial nickel occupancy of protein and chelator allowing the Ni(II) affinities of the tightest sites of ZiaR and Zur to be calculated as $2.44(\pm 0.92) \times 10^{-8}$ M and $3.07(\pm 0.81) \times 10^{-8}$ M respectively via use of equation 2 and calibration curves produced by the titration of mag-fura-2 with Ni(II) in the absence of protein (Figures 5.3 and 5.4) (Tables 5.1 and 5.2). These calculated affinities represent the tightest site on the protein assuming the proteins are present as dimers (Figure 5.1 and 5.2) and there is negative metal binding cooperativity between sites on the proteins, which has been demonstrated to be the case for Zn(II) binding to these two proteins (Patterson. 2010).

Attempts were made to determine the affinity of mag-fura-2 for Ni(II) by competition against NTA as described for fura-2 and Co(II) (Section 4.2.2), however, minimal quenching of mag-fura-2 fluorescence was observed until Ni(II) concentrations greater than 20 μ M were reached (the concentration of NTA present in the assay) (Figure 5.5). This implies that it is necessary to saturate the metal site of NTA before any significant Ni(II) binding to mag-fura-2 is observed implying the Ni(II) affinity of NTA is

[ZiaR] ^a (μM)	6.2	6.2	7.2
[mf2] (μM)	8.4	8.4	9.64
[Ni(II)] (μM)	2.97	2.97	3.59
F _{505 nm} ^b	566.36	549.95	642.11
m ^c	-71.198	-71.198	-69.281
c ^c	680.95	680.95	808.46
[Ni(II)-ZiaR] ^b (μM)	1.36	1.13	1.19
[Ni(II)-mf2] ^b (μM)	1.61	1.84	2.4
K _{Ni} (M)	1.52x10 ⁻⁸	2.44x10 ⁻⁸	3.36x10 ⁻⁸
Average K _{Ni} (M)	2.44(±0.92 ^d)x10 ⁻⁸		

^a monomer concentration, the concentration of 'tight site' is taken to be half this value as the protein exists as a dimer. ^b equilibrium values. ^c gradient (m) and intercept (c) of the mag-fura-2 NiSO₄ titration standard curve produced concurrently with competition experiment. ^d standard deviation.

Table 5.1. Statistics for determination of ZiaR Ni(II) affinity through competition with mag-fura-2.

[Zur] ^a (μM)	6.15	6.15	6.15
[mf2] (μM)	8.8	8.8	8.8
[Ni(II)] (μM)	2.97	2.97	2.97
F _{505 nm} ^b	595.34	580.09	578
m ^c	-69.477	-69.477	-69.477
c ^c	721.28	721.28	721.28
[Ni(II)-Zur] ^b (μM)	1.16	0.94	0.91
[Ni(II)-mf2] ^b (μM)	1.81	2.03	2.06
K _{Ni} (M)	2.15x10 ⁻⁸	3.42x10 ⁻⁸	3.65x10 ⁻⁸
Average K _{Ni} (M)	3.07(±0.81 ^d)x10 ⁻⁸		

^a monomer concentration, the concentration of 'tight site' is taken to be half this value as the protein exists as a dimer. ^b equilibrium values. ^c gradient (m) and intercept (c) of mag-fura-2 NiSO₄ titration standard curve produced concurrently with competition experiment. ^d standard deviation.

Table 5.2. Statistics for the determination of Zur Ni(II) affinity through competition with mag-fura-2.

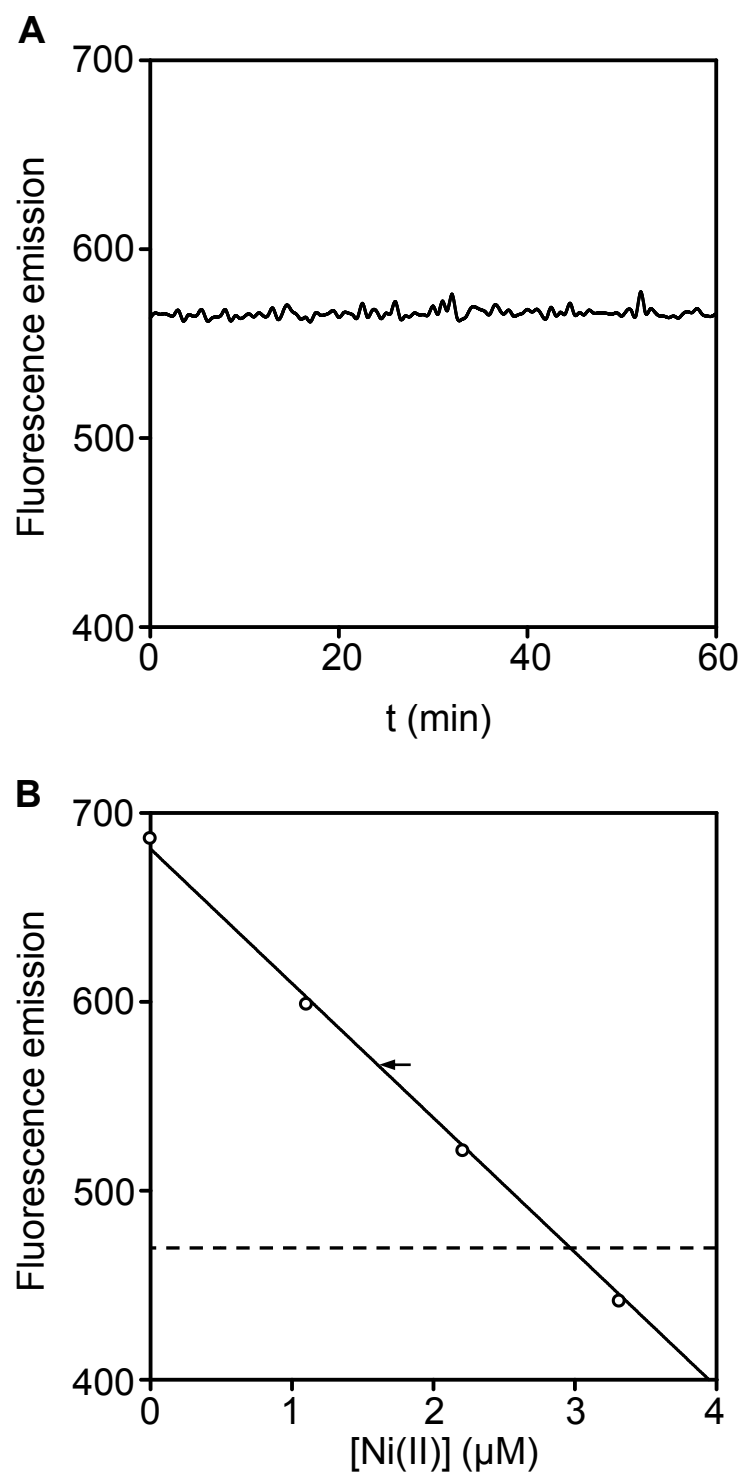


Figure 5.3. Determination of the Ni(II) affinity of ZiaR by competition with mag-fura-2. A. ZiaR ($6.2 \mu\text{M}$) was added to a solution of mag-fura-2 ($8.4 \mu\text{M}$) and NiSO_4 ($2.97 \mu\text{M}$) and fluorescence emission at 505 nm following excitation at 380 nm was monitored for 1 h. B. mag-fura-2 ($8.4 \mu\text{M}$) was titrated with NiSO_4 in the absence of protein (circles) and fluorescence emission at 505 nm following excitation at 380 nm recorded. The arrow marks the equilibrium fluorescence value of the competition between ZiaR and mag-fura-2 shown in 'A'. The dotted line represents the fluorescence value expected if mag-fura-2 completely withheld Ni(II) from ZiaR in the experiment described in 'A'.

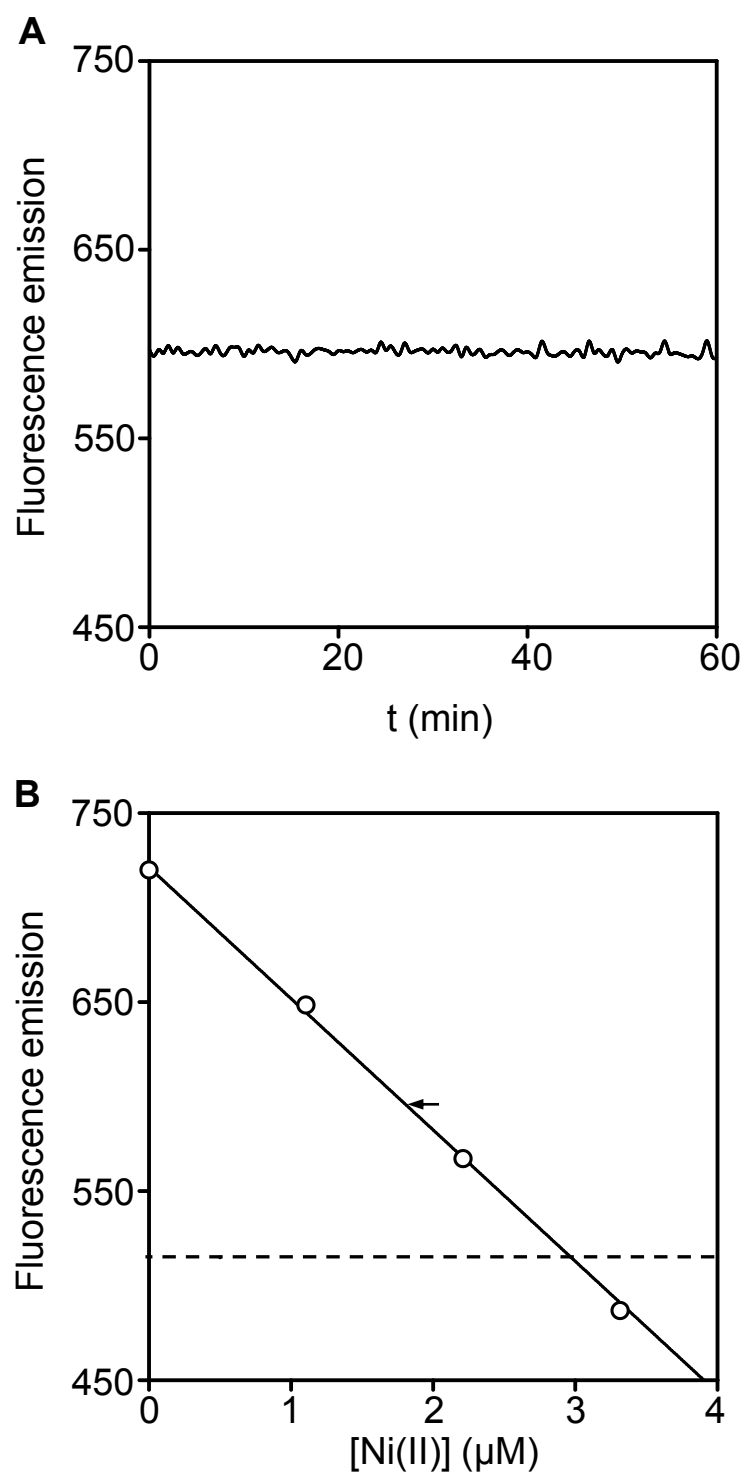


Figure 5.4. Determination of the Ni(II) affinity of Zur by competition with mag-fura-2. A. Zur ($6.15 \mu\text{M}$) was added to a solution of mag-fura-2 ($8.8 \mu\text{M}$) and NiSO_4 ($2.97 \mu\text{M}$) and fluorescence emission at 505 nm following excitation at 380 nm was monitored for 1 h. B. mag-fura-2 ($8.8 \mu\text{M}$) was titrated with NiSO_4 in the absence of protein (circles) and fluorescence emission at 505 nm following excitation at 380 nm recorded. The arrow marks the equilibrium fluorescence value of the competition between Zur and mag-fura-2 shown in 'A'. The dotted line represents the fluorescence value expected if mag-fura-2 completely withheld Ni(II) from Zur in the experiment described in 'A'.

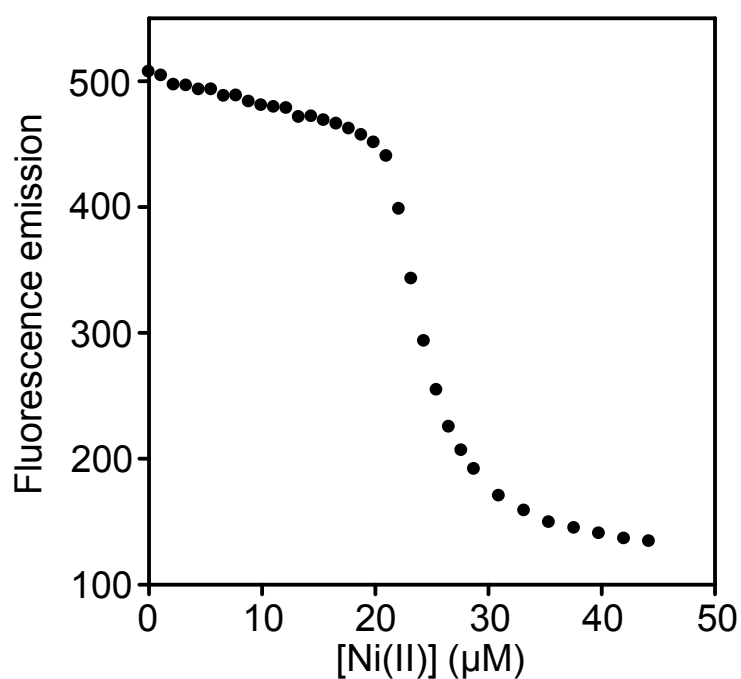


Figure 5.5. Determination of the Ni(II) affinity of mag-fura-2 by competition with NTA. NiSO₄ was titrated into a mixed solution of mf2 (5.94 μM) and NTA (20 μM). Following excitation at 360 nm fluorescence emission at 510 nm was monitored until equilibrium was reached before recording the equilibrium fluorescence emission value.

significantly tighter than that of mag-fura-2 at the pH used here (pH 7.8). NTA has been used previously to determine the Ni(II) affinity of mag-fura-2 at pH 7 (Reyes-Caballero *et al.* 2011). The Ni(II) affinity of NTA (calculated by Schwarzenbach's α -coefficient protocol (Section 2.6.7)) varies by nearly an order of magnitude between the pH values used in these two studies (1.66×10^{-9} M at pH 7 versus 2.66×10^{-10} M at pH 7.8) whereas it has been reported that the Zn(II) affinity of mag-fura-2 is independent of pH in the range pH 7-7.8, probably due to the low pKa of the carboxylate ligands (Xiao & Wedd. 2010). These observations are consistent with NTA outcompeting mag-fura-2 for Ni(II) at pH 7.8 but displaying detectable competition at pH 7 and so the association constant of mag-fura-2 with Ni(II) determined by Reyes-Caballero and co-workers at pH 7 (2×10^7 M⁻¹) was used in the calculations to determine the Ni(II) affinity of ZiaR and Zur (Tables 5.1 and 5.2).

Competition between CoaR and mag-fura-2 came slowly to equilibrium over several hours with the equilibrium fluorescence value suggesting that CoaR had completely outcompeted mag-fura-2 for Ni(II) (Figure 5.6) (the equilibrium fluorescence value in these experiments were consistently higher than the fluorescence value for apo mag-fura-2 suggesting that CoaR may have stripped a small amount of residual contaminant metal from mag-fura-2).

The experiment described above suggested that CoaR has a significantly tighter affinity for Ni(II) than mag-fura-2 and therefore CoaR was competed against NTA, a small molecule chelator with a tighter Ni(II) affinity than mag-fura-2 (Section 4.2.1). NTA has no spectral readout of occupancy with metal (Section 4.2.1) and so an alternate readout was required to monitor competition between CoaR and NTA for Ni(II). Changes in intrinsic protein fluorescence have previously been used to observe metal binding to proteins (Hitomi *et al.* 2001; VanZile *et al.* 2002b; Liu *et al.* 2008; Waldron *et al.* 2010). CoaR has an abundance of fluorescent residues (seven tyrosine and three tryptophan residues) and auto fluorescence of the protein has been shown to be quenched upon the addition of cobalt (Patterson. 2010). Addition of nickel to CoaR was also found to quench the intrinsic fluorescence of CoaR providing a readout of Ni(II) occupancy of CoaR (Figure 5.7, left panel). When this experiment was repeated in the presence of equimolar NTA it was necessary to add a concentration of nickel in excess of the concentration of NTA to observe quenching of CoaR intrinsic fluorescence (Figure 5.7, right panel). These observations imply that the Ni(II) affinity of CoaR is significantly

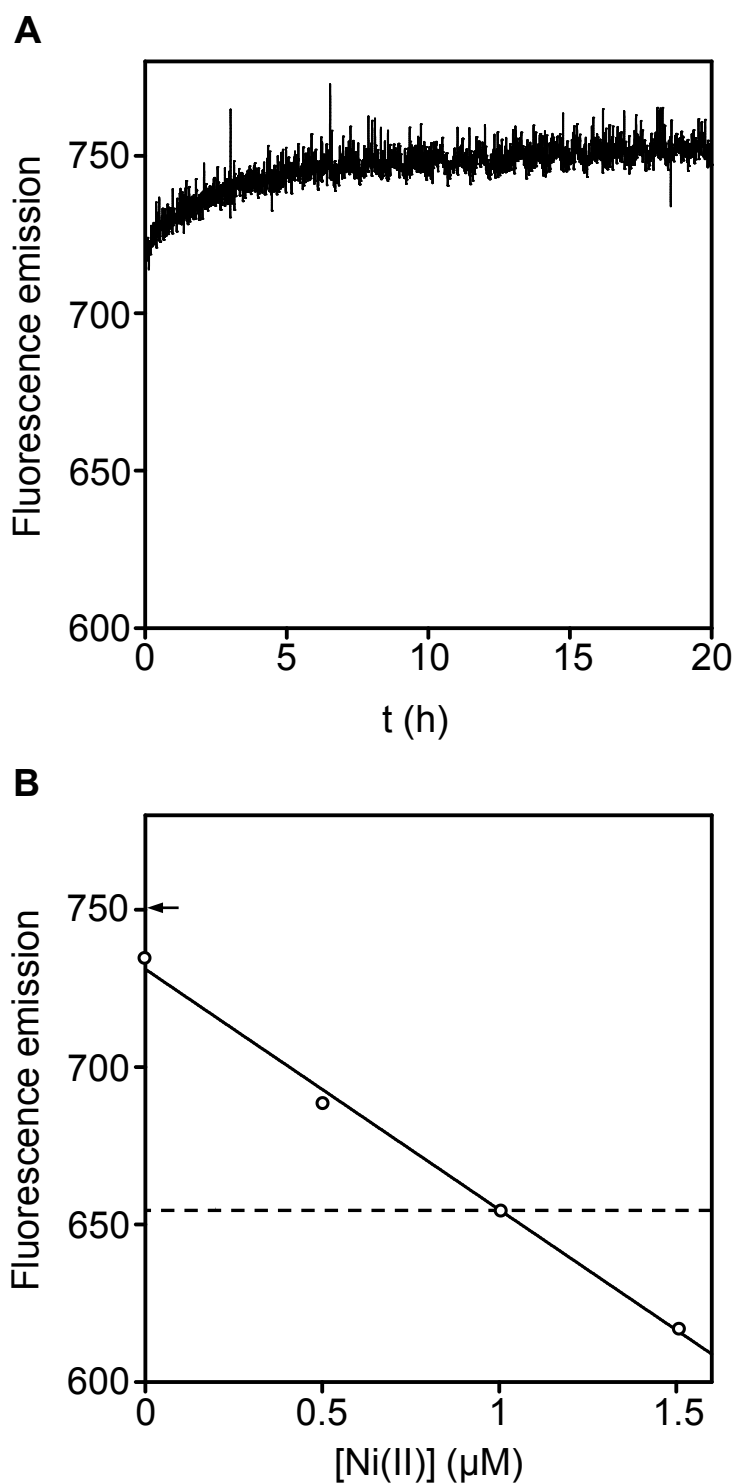


Figure 5.6. Estimation of the Ni(II) affinity of CoaR by competition with mag-fura-2. A. CoaR ($2\ \mu\text{M}$) was added to a solution of mag-fura-2 ($9.25\ \mu\text{M}$) and NiSO_4 ($1\ \mu\text{M}$) and fluorescence emission at 505 nm following excitation at 380 nm was monitored for 1 h. B. mag-fura-2 ($9.25\ \mu\text{M}$) was titrated with NiSO_4 in the absence of protein (circles) and fluorescence emission at 505 nm following excitation at 380 nm recorded. The arrow marks the equilibrium fluorescence value of the competition between CoaR and mag-fura-2 shown in 'A'. The dotted line represents the fluorescence value expected if mag-fura-2 completely withheld Ni(II) from CoaR in the experiment described in 'A'.

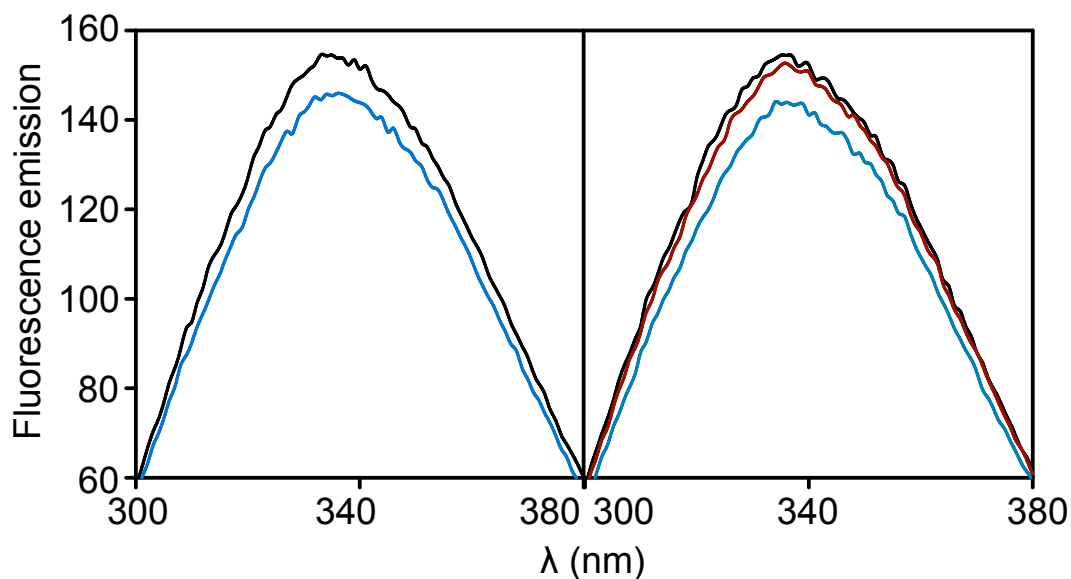


Figure 5.7. Competition with NTA to determine the Ni(II) affinity of CoaR. *Left panel*, fluorescence emission spectrum of apo-CoaR (2.5 μM) (black line) following excitation at 280 nm is quenched upon the addition of NiSO_4 (2 μM) (blue line). *Right panel*, fluorescence emission spectrum of apo-CoaR (2.5 μM) (black line) is not quenched upon the addition of a pre-incubated solution of Ni(II)-NTA (red line) to final concentrations $[\text{NTA}] = 2.5 \mu\text{M}$, $[\text{NiSO}_4] = 2 \mu\text{M}$, but is quenched to the same extent as the control experiment (*left panel*) upon addition of a further 2.5 μM NiSO_4 (blue line).

tighter than that of mag-fura-2 (5×10^{-8} M) and significantly weaker than that of NTA (2.66×10^{-10} M) placing the Ni(II) affinity of CoaR in the nanomolar range.

5.3.2 Confirmation of the relative Ni(II) affinity hierarchy of the metalloregulators of *Synechocystis*

InrS has a significantly tighter Ni(II) affinity than that of the other metalloregulators included in this study (by at least five orders of magnitude) (Sections 4.2.1 and 5.3.1). In order to validate the position of InrS as the tightest Ni(II) binder of this set of metalloregulators Zur, ZiaR and CoaR were each competed with InrS for Ni(II) in a pairwise manner. In each case the experimental design had to be optimised to best take advantage of the available spectral readouts of Ni(II) occupancy.

When Zur (which contains five tyrosine residues) is titrated with Zn(II) the intrinsic fluorescence decreases in a linear manner (Appendix Figure E1), and this fluorescence quenching is also observed on the addition of Ni(II) (Figure 5.8). InrS has no fluorescent residues and is therefore silent in fluorescence experiments. Ni(II) dependent quenching of Zur intrinsic fluorescence was alleviated upon the addition of equimolar apo-InrS to Ni(II)-Zur showing that Ni(II) completely transfers from Zur to InrS as would be predicted based on their equilibrium binding constants (Figure 5.8).

ZiaR has four tyrosine residues however upon titration of ZiaR with Ni(II) no change in protein intrinsic fluorescence is observed (Figure 5.10, *inset*). Therefore a different readout of protein Ni(II) occupancy was required. This lack of change in intrinsic protein fluorescence may be explained by the presence of two distinct metal binding sites on ZiaR. Zn(II) binding to the $\alpha 3N$ site has previously been shown to enhance intrinsic fluorescence whereas Zn(II) binding to the $\alpha 5$ site decreases intrinsic fluorescence (Patterson, 2010). ZiaR can be eluted from a heparin affinity column with 300-400 mM NaCl (Figure 5.1) whereas 800 mM NaCl is required to elute InrS (Section 3.2). This difference in heparin affinity was used to resolve the two proteins. Ni(II) was added to apo-ZiaR before the addition of equimolar apo-InrS. Following incubation the reaction mix was loaded onto a heparin affinity column before eluting at 500 mM and then 1 M NaCl. Fractions were analysed for the presence of protein by SDS-PAGE and for nickel content by ICP-MS (Figure 5.9). Nickel was found to be associated with InrS with negligible amounts retained by ZiaR, again this confirmed the rank order of affinity determined by competition with chelator.

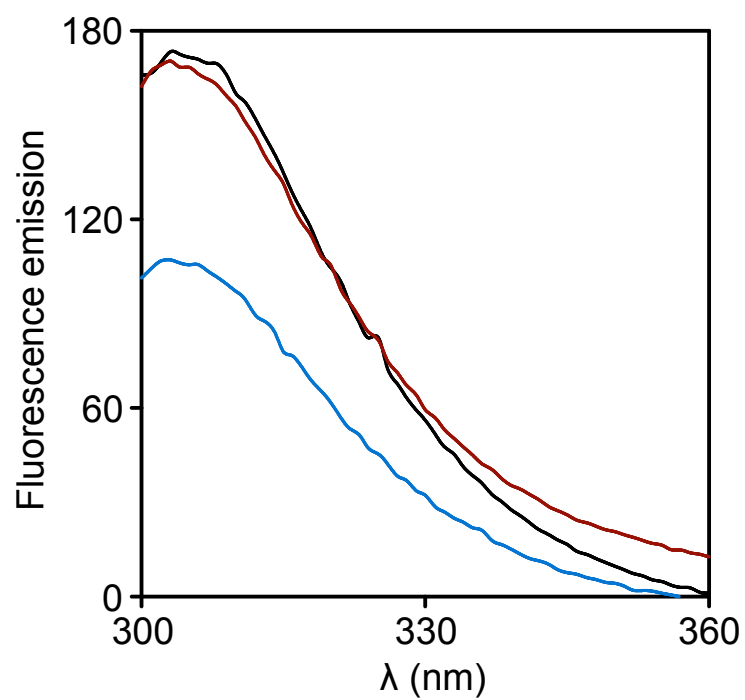


Figure 5.8. Competition between Zur and InrS for Ni(II). The fluorescence emission of Zur (10 μ M) upon excitation at 280 nm (black line) is quenched upon the addition of NiSO_4 (10 μ M) (blue line). The quenching is immediately alleviated upon addition of 10 μ M InrS (red line).

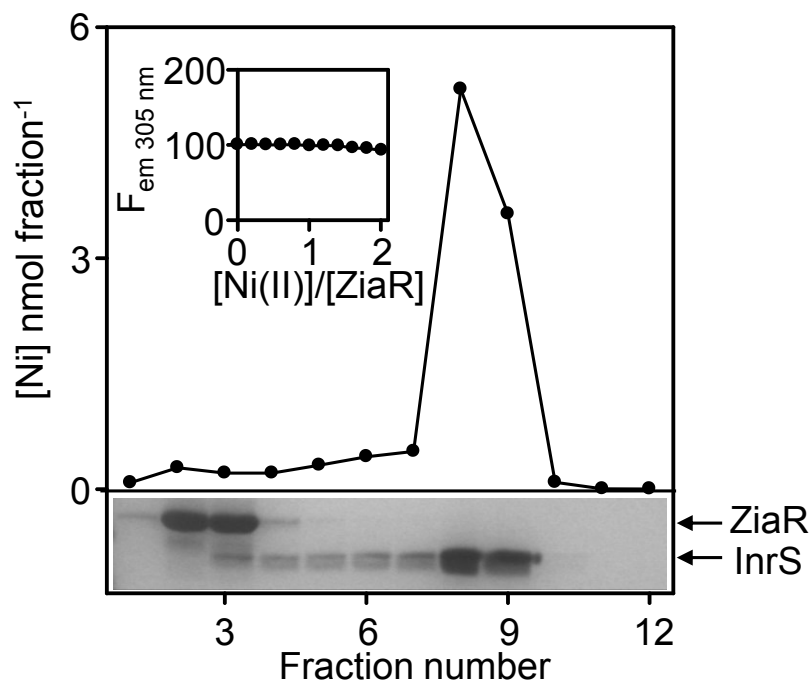


Figure 5.9. Competition between ZiaR and InrS for Ni(II). *Inset*, the intrinsic fluorescence of ZiaR upon excitation at 280 nm is not quenched on the addition of NiSO₄. *Main panel*, InrS was added to a solution of ZiaR pre-incubated with NiSO₄ to final concentrations [InrS] = 20 μ M, [ZiaR] = 20 μ M and [NiSO₄] = 9.5 μ M. Proteins were separated by heparin affinity chromatography and analysed for nickel by ICP-MS and for protein by SDS-PAGE analysis.

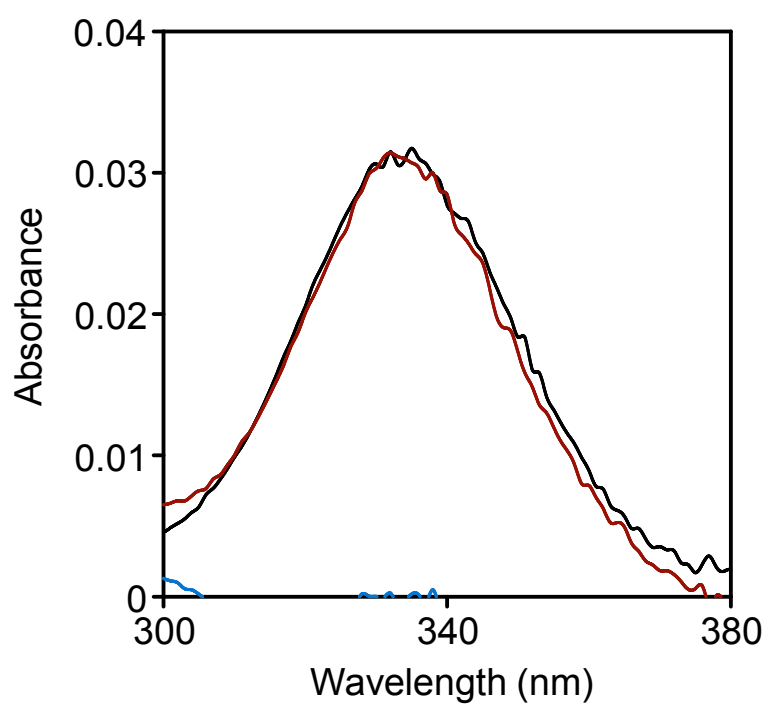


Figure 5.10. Competition between CoaR and InrS for Ni(II). Addition of NiSO_4 ($2.4 \mu\text{M}$) to CoaR ($5 \mu\text{M}$) results in negligible change in the absorbance spectrum between 300-380 nm (blue line, apo spectrum subtracted). Addition of InrS ($5 \mu\text{M}$) results in an absorbance spectra (red line) which overlays with that of $2.4 \mu\text{M}$ Ni(II)-InrS (black line).

Finally, CoaR shows Ni(II) dependent fluorescence quenching (Figure 5.7) however the alleviation of this quenching upon the addition of a chelator was found to be unreliable. For this reason the Ni(II) dependent LMCT feature of InrS (Figure 3.6) was used to assess Ni(II) occupancy of the two proteins following competition. Addition of Ni(II) to apo-CoaR results in negligible change in the absorbance spectrum between 300-380 nm (Figure 5.10). When apo-InrS is added to this mix the spectral feature generated at 333 nm is of an equivalent intensity to that obtained with an identical concentration of Ni(II)-InrS alone, again confirming complete Ni(II) transfer from CoaR to InrS.

These data show how it may be possible to overcome the limitations of the Irving-Williams series and achieve selectivity in a set of metal responsive transcriptional regulators by the sensor of a particular element having a tighter affinity for that element than the other sensors present in the cell.

5.4 Relative cobalt affinities of the metalloregulators of *Synechocystis*

The Co(II) affinities of ZiaR and Zur were determined by competition with the fluorescent chelator fura2 (Figures 5.11 and 5.12) as described for InrS in Section 4.2.2. The fluorescence values at equilibrium were used to determine the equilibrium concentrations of Co(II)-fura2 and Co(II)-protein and from this the equilibrium Co(II) binding constant of the tightest site per protein dimer was determined, ZiaR $K_{D, Co(II)} = 6.94(\pm 1.3) \times 10^{-10}$ M, Zur $K_{D, Co(II)} = 4.56(\pm 0.16) \times 10^{-10}$ M (Figures 5.11 and 5.12) (Tables 5.3 and 5.4).

Attempts were made to determine the Co(II) affinity of CoaR using the same approach however replicate experiments consistently showed that all added cobalt remained bound to fura2 (Figure 5.13) suggesting that under the conditions of the assay the Co(II) affinity of fura2 is substantially tighter than that of CoaR. Previous analysis of CoaR Co(II) dependent LMCT features suggested that CoaR binds Co(II) stoichiometrically with a binding stoichiometry of 1:1 (Patterson. 2010). As these experiments were performed with micromolar concentrations of protein the Co(II) binding affinity must be tighter than micromolar (to allow stoichiometric binding) but weaker than the Co(II) affinity of fura2 (7.03 nM (Section 4.2.2)) and is therefore estimated to lie in sub micromolar range (10^{-7} – 10^{-8} M).

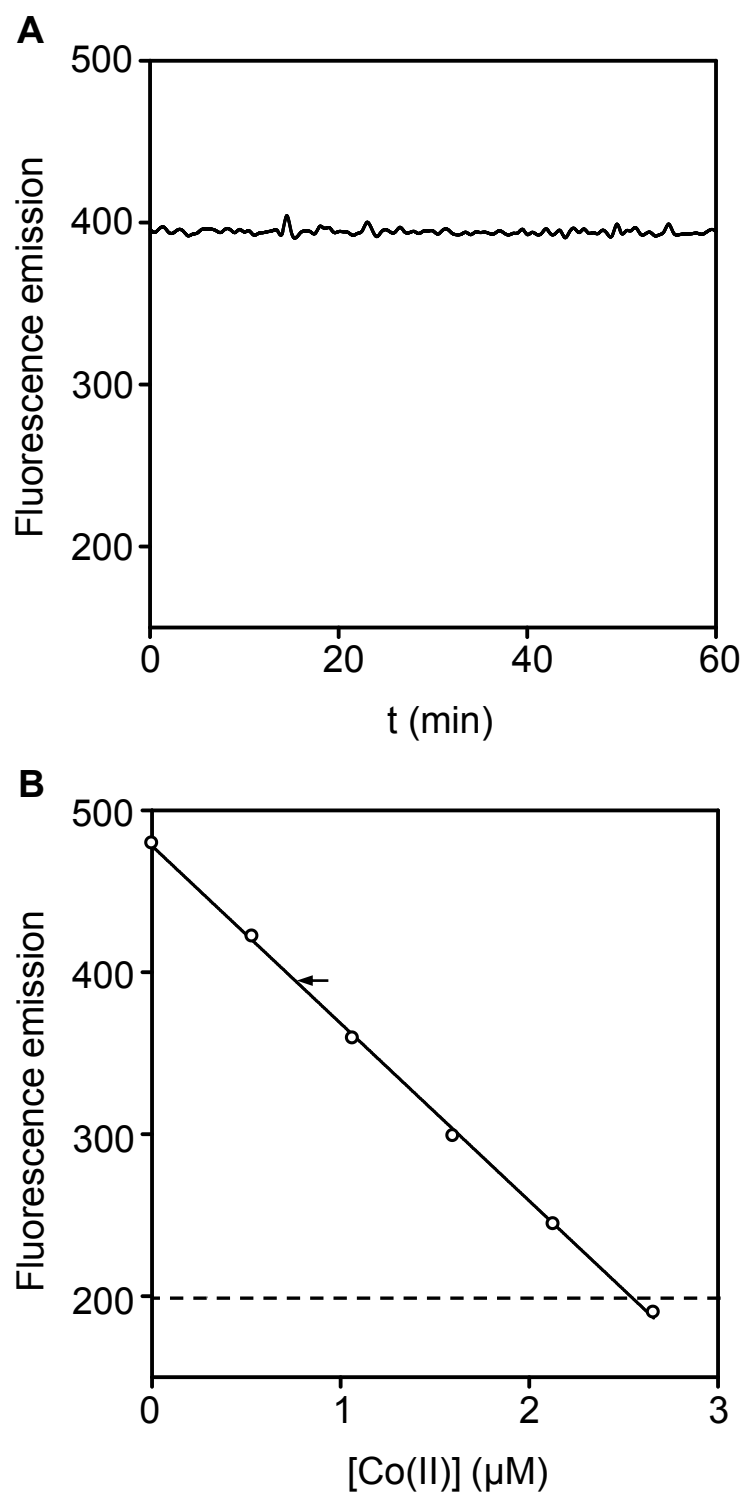


Figure 5.11. Determination of the Co(II) affinity of ZiaR by competition with fura-2. A. ZiaR ($5.2 \mu\text{M}$) was added to a solution of fura-2 ($4.5 \mu\text{M}$) and CoCl_2 ($2.55 \mu\text{M}$) and fluorescence emission at 510 nm following excitation at 360 nm was monitored for 1 h. B. fura-2 ($4.5 \mu\text{M}$) was titrated with CoCl_2 in the absence of protein (circles) and fluorescence emission at 510 nm following excitation at 360 nm recorded. The arrow marks the equilibrium fluorescence value of the competition between ZiaR and fura-2 shown in 'A'. The dotted line represents the fluorescence value expected if fura-2 completely withheld Co(II) from ZiaR in the experiment described in 'A'.

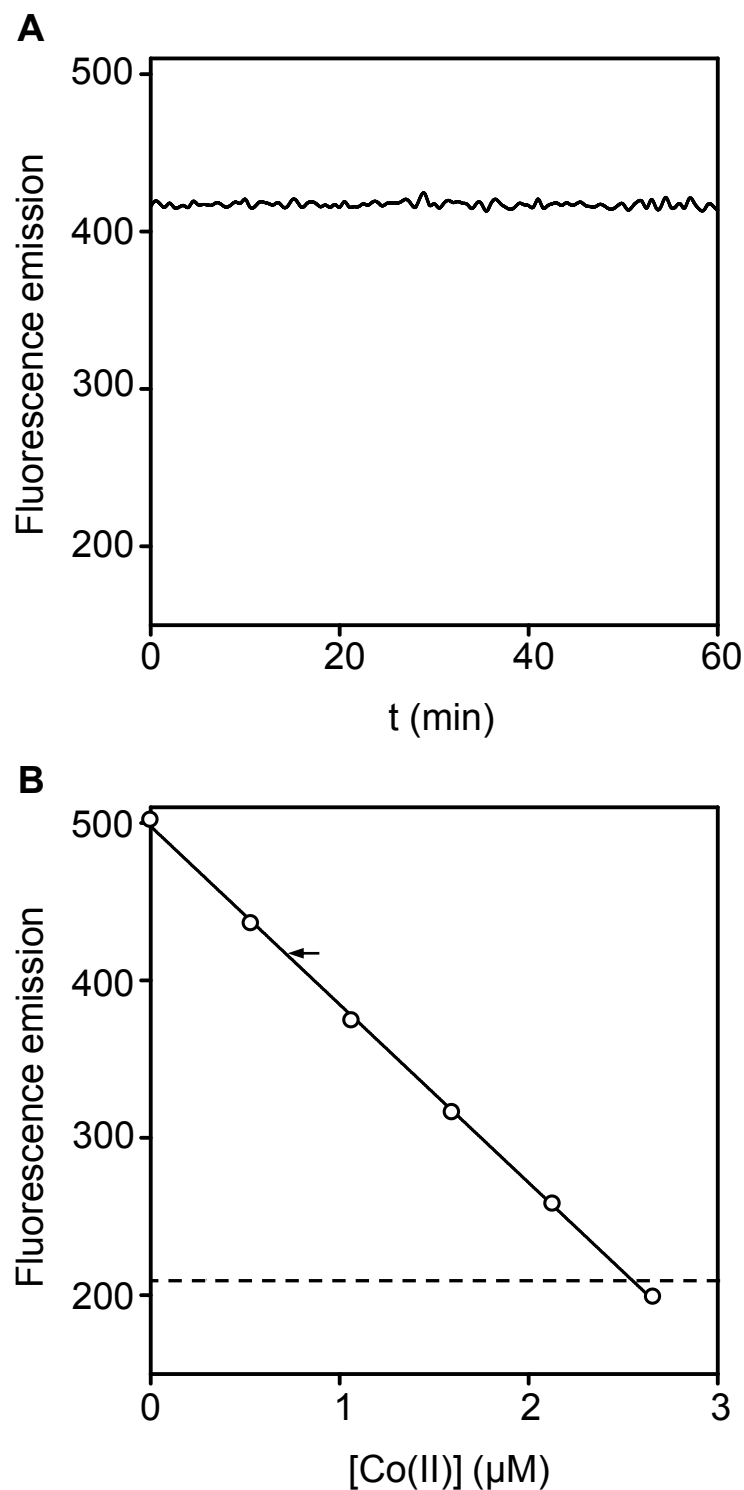


Figure 5.12. Determination of the Co(II) affinity of Zur by competition with fura-2.
 A. Zur (5.1 μM) was added to a solution of fura-2 (4.92 μM) and CoCl_2 (2.55 μM) and fluorescence emission at 510 nm following excitation at 360 nm was monitored for 1 h.
 B. fura-2 (4.92 μM) was titrated with CoCl_2 in the absence of protein (circles) and fluorescence emission at 510 nm following excitation at 360 nm recorded. The arrow marks the equilibrium fluorescence value of the competition between Zur and fura-2 shown in 'A'. The dotted line represents the fluorescence value expected if fura-2 completely withheld Co(II) from Zur in the experiment described in 'A'.

[ZiaR] ^a (μM)	5.2	5.2	5.2
[fura-2] (μM)	4.5	4.5	4.5
[Co(II)] (μM)	2.55	2.55	2.55
F _{510 nm} ^b	394.31	397.18	386.03
m ^c	-109.64	-109.64	-109.64
c ^c	478.05	478.05	478.05
[Co(II)-ZiaR] ^b (μM)	1.79	1.82	1.71
[Co(II)-fura-2] ^b (μM)	0.76	0.73	0.84
K _{Co} (M)	6.51x10 ⁻¹⁰	5.96x10 ⁻¹⁰	8.34x10 ⁻¹⁰
Average K _{Co} (M)	6.94(±1.3 ^d)x10 ⁻¹⁰		

^a monomer concentration, the concentration of “tight site” is taken to be half this value as the protein exists as a dimer. ^b equilibrium values. ^c gradient (m) and intercept (c) of fura-2 CoCl₂ titration standard curve produced concurrently with the competition experiment. ^d standard deviation.

Table 5.3. Statistics for the determination of ZiaR Co(II) affinity through competition with fura-2.

[Zur] ^a (μM)	5.1	5.1	5.1
[fura-2] (μM)	4.92	4.92	4.92
[Co(II)] (μM)	2.55	2.55	2.55
F _{510 nm} ^b	417.05	419.49	418.7
m ^c	-113.2	-113.2	-113.2
c ^c	497.88	497.88	497.88
[Co(II)-Zur] ^b (μM)	1.84	1.86	1.85
[Co(II)-fura-2] ^b (μM)	0.71	0.69	0.7
K _{Co} (M)	4.62x10 ⁻¹⁰	4.67x10 ⁻¹⁰	4.38x10 ⁻¹⁰
Average K _{Co} (M)	4.56(±0.16 ^d)x10 ⁻¹⁰		

^a monomer concentration, the concentration of “tight site” is taken to be half this value as the protein exists as a dimer. ^b equilibrium values. ^c gradient (m) and intercept (c) of fura-2 CoCl₂ titration standard curve produced concurrently with the competition experiment. ^d standard deviation.

Table 5.4. Statistics for the determination of Zur Co(II) affinity through competition with fura-2.

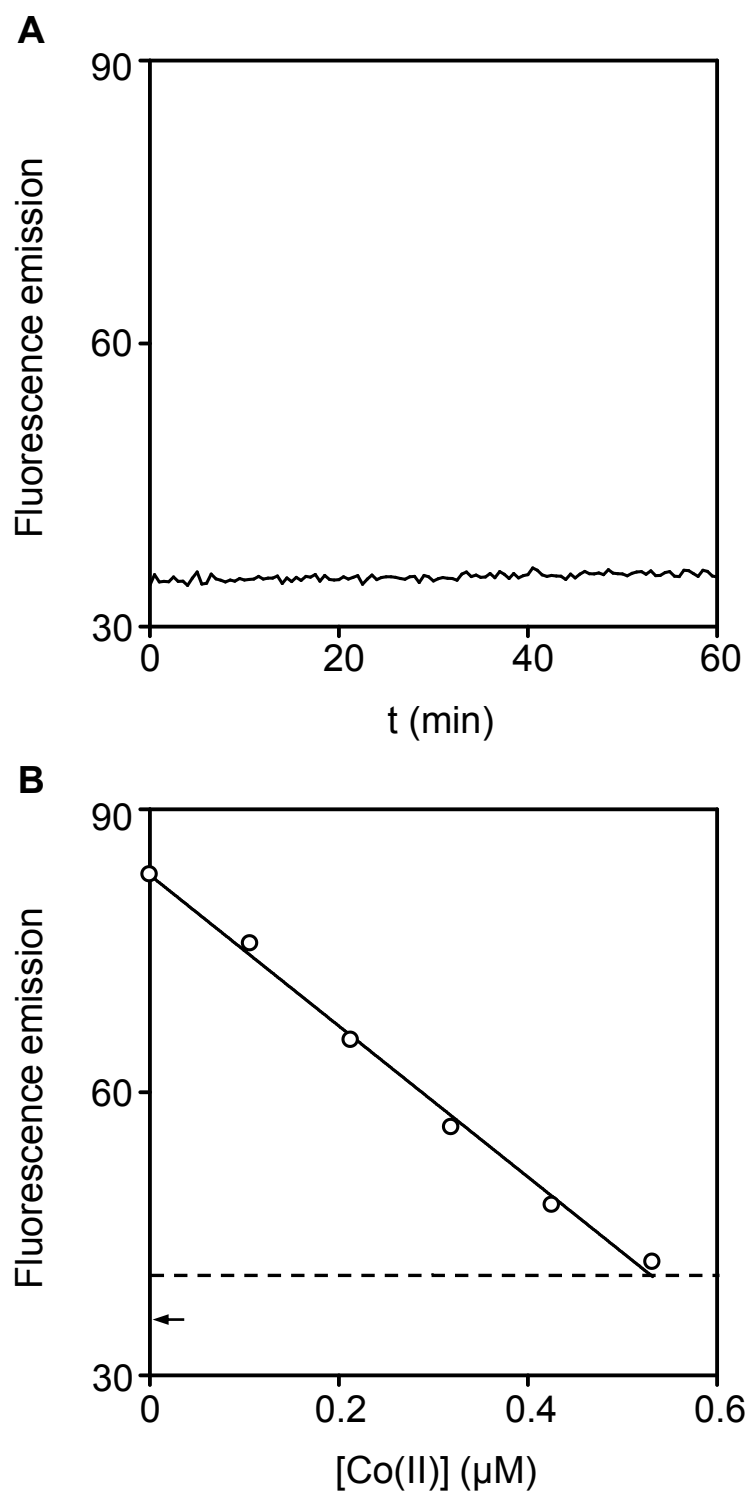


Figure 5.13. Estimation of the Co(II) affinity of CoaR by competition with fura-2. A. CoaR ($1.5 \mu\text{M}$) was added to a solution of fura-2 ($0.54 \mu\text{M}$) and CoCl_2 ($0.53 \mu\text{M}$) and fluorescence emission at 510 nm following excitation at 360 nm was monitored for 1 h . B. fura-2 ($0.54 \mu\text{M}$) was titrated with CoCl_2 in the absence of protein (circles) and fluorescence emission at 510 nm following excitation at 360 nm recorded. The arrow marks the equilibrium fluorescence value of the competition between CoaR and fura-2 shown in 'A'. The dotted line represents the fluorescence value expected if fura-2 completely withheld Co(II) from CoaR in the experiment described in 'A'.

Selectivity in Co(II) sensing in *Synechocystis* cells cannot be explained on the basis of relative affinity. InrS and CoaR, both of which appear Co(II) responsive at steady state (Appendix Figure B2A; Rutherford *et al.* 1999) have Co(II) affinities $(7.69(\pm 1.1) \times 10^{-9} \text{ M}$ and 10^{-7} – 10^{-8} M , respectively) which are weaker than ZiaR $(6.94(\pm 1.3) \times 10^{-10} \text{ M})$ and Zur $(4.56(\pm 0.16) \times 10^{-10} \text{ M})$ which are not Co(II) responsive under steady state conditions (Thelwell *et al.* 1998; Patterson. 2010). Explanations for how these unfavourable thermodynamic gradients are overcome have been sought and are discussed in Section 6.5.

5.5 Allosteric response of InrS to non *in vivo* effector metals

Under steady state conditions (48 h exposure) InrS displays an *in vivo* response to nickel and cobalt but not zinc or copper (Appendix Figure B2A). Is InrS allosterically competent to respond to zinc or copper if it were to gain access to these metals *in vivo*?

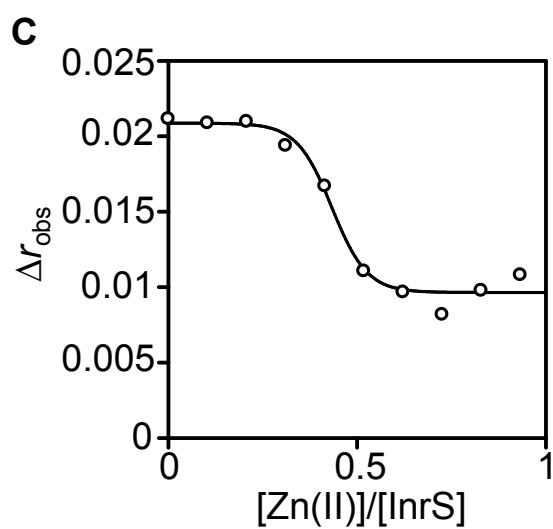
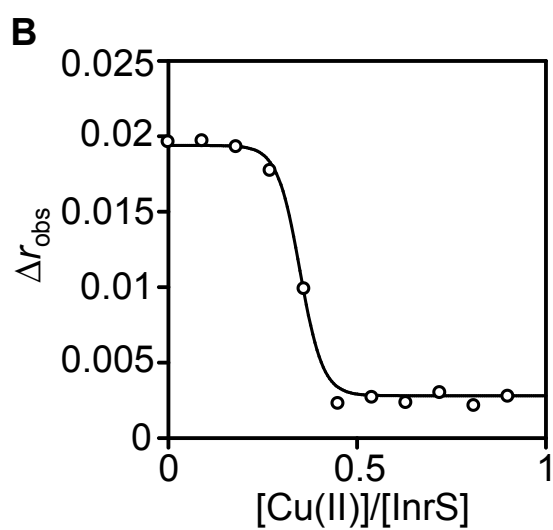
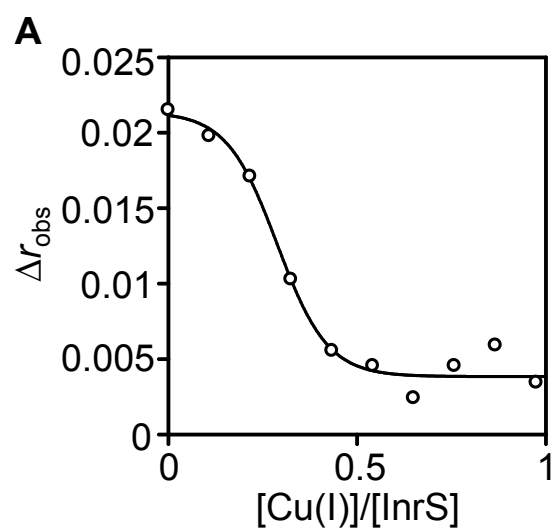
5.5.1 Disruption of InrS:DNA complexes by non-cognate metals

To assess if InrS is allosterically competent to respond to Cu(I), Cu(II) or Zn(II) pre-formed complexes of InrS and *nrsD*ProFA were titrated with these metals and complex dissociation monitored by fluorescence anisotropy (Figure 5.14). In each case the added metal was able to disrupt the pre-formed protein:DNA complex resulting in a decrease in r_{obs} (Figure 5.14). For each metal the maximal decrease in Δr_{obs} was observed following addition of 0.5 molar equivalents of metal as observed previously for Ni(II) (Figure 4.5A). For Zn(II) the decrease in Δr_{obs} was routinely less than that observed for the other metals tested.

InrS likely binds Cu(II) with square planar coordination geometry (Section 3.3.1), in a site highly similar to that used by Ni(II), so perhaps it is unsurprising that this metal is allosterically effective (Figure 5.14). In the reducing environment of the cytosol all Cu(II) is thought to be reduced to Cu(I) and therefore InrS is unlikely to encounter Cu(II) such that the ability to respond to Cu(II) is perhaps not detrimental. This observation provides another example of how access, in this case imposed by the cellular location of InrS, can help dictate selectivity.

Zn(II) is predicted to bind to the allosteric site of InrS in a tetrahedral geometry as inferred from UV-Vis spectroscopy using cobalt as a surrogate ion (Section 3.3.2). As cobalt appears to drive allostery both *in vivo* (Appendix Figure B2) and *in vitro* (Figure

Figure 5.14. Titration of pre-formed InrS:DNA complexes with Cu(I), Cu(II) and Zn(II). *nrsD*ProFA (10 nM) was pre-incubated with InrS (1 μ M) before titration with A. CuCl (confirmed to be >95 % Cu⁺), B. CuSO₄ and C. ZnSO₄. Dissociation of InrS:DNA complexes was monitored by fluorescence anisotropy. Experiments were performed anaerobically at pH 7.8.

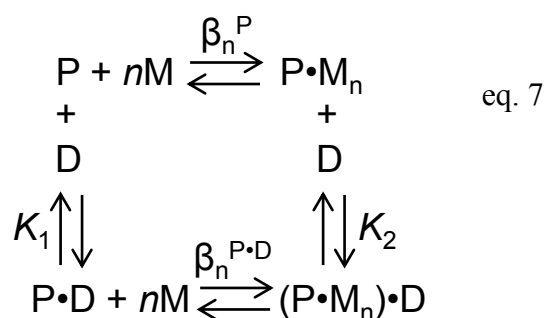


4.5B) the allosteric efficacy of Zn(II) (Figure 5.14) is once again perhaps unsurprising. Cu(I) is predicted to bind to InrS in a trigonal planar geometry (Section 3.3.3), a distinct geometry to either Ni(II) or Co(II) and so for this metal, if any, selectivity against the wrong metal could reasonably be expected to operate at the level of allostery, however Cu(I) clearly drives allostery (Figure 5.14).

The contribution of allostery to the specificity of response of de-repressors may be less important than for co-repressors or activators as any conformational change which destabilises the form with a high affinity for DNA will result in de-repression of the regulated gene (Waldron *et al.* 2009). Any change that destabilises the protein:DNA interaction will drive the protein from DNA whereas for co-repression or activation a very specific organisation of the protein may be required. This means that metal dependent de-repressors may be more susceptible to regulation by non-cognate metals than metal dependent co-repressors or metal dependent activators. The data presented here for InrS are consistent with this idea.

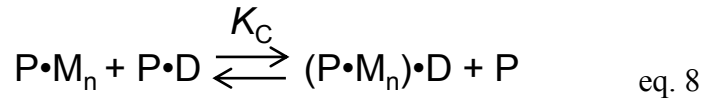
5.5.2 Allosteric coupling of InrS metal (Cu(I) or Ni(II)) binding and DNA binding

The data presented in Figures 5.14 and 4.5 show that Ni(II), Co(II), Zn(II), Cu(I) and Cu(II) are all capable of disrupting InrS-DNA interactions but provide no quantitative measure of the degree to which metal binding destabilises the interaction of InrS with DNA (the allosteric efficacy of the metal). By analogy to regulation of *B. subtilis* CsoR by Cu(I) (cognate) and Ni(II) (non-cognate) (Ma *et al.* 2009a) or *M. tuberculosis* NmtR by Ni(II) (cognate) and Zn(II) (non-cognate) (Pennella *et al.* 2003); Ni(II) may be a more potent allosteric effector than non-cognate metals. The magnitude of allosteric regulation can be described quantitatively by considering the thermodynamic cycle of ligand (DNA and metal) binding to InrS (equation 7).



Where P represents the protein assembly, M the metal ion, D the DNA, β_n is the overall stability constant for each of the metal binding events to the protein and K is the affinity of the protein for DNA (Guerra & Giedroc. 2012).

This model describes the four ‘end states’ of interaction between InrS and the two ligands (DNA and metal) ignoring intermediate states such as individual metal binding events. Another way to consider the allosteric efficacy of a metal is the degree to which metal binding weakens or increases DNA affinity. The ratio of the DNA affinity in the metallated and apo state gives the coupling constant K_C . The equilibrium described by K_C can be obtained by rearrangement of the thermodynamic cycle in equation 7 to obtain equation 8.



For metal dependent de-repressors in the presence of their cognate metal this equilibrium will lie to the left and therefore $K_C < 1$ (Giedroc & Arunkumar. 2007). K_C can be converted to free energy value using the standard thermodynamic function (equation 9).

$$\Delta G_C = -RT \ln K_C \quad \text{eq. 9}$$

Where ΔG_C represents the free energy change associated with the equilibrium shown in (equation 8), R is the molar gas constant and T the temperature at which the experiments were performed.

For $K_C < 1$ $\Delta G > 0$, the positive sign indicates that the biologically relevant ‘end states’ are $P \cdot M_n$ and $P \cdot D$ and the magnitude of the value indicates the degree to which these end states are stabilised. Therefore, by determining the DNA affinity of InrS in the apo state and various metal bound states the allosteric efficacy of different metal ions may be compared.

In order to quantitatively assess the allosteric efficacy of Cu(I) and Ni(II) binding to InrS the DNA affinity of InrS when bound to these metals was determined. *nrsD*ProFA was titrated with InrS pre-incubated with a 1.2 molar excess of either NiCl_2 or CuCl (confirmed to be $>95\% \text{ Cu}^+$ (Section 2.6.1) and the change in anisotropy monitored (Figure 5.15). The software package Dynafit (Kuzmic. 1996) was used to fit the data to

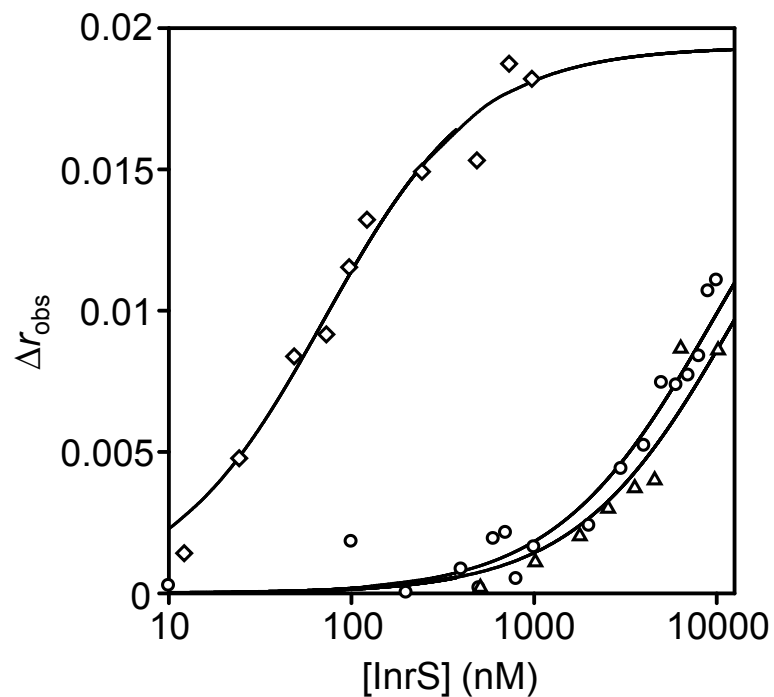


Figure 5.15. Efficacy of Ni(II) and Cu(I) at driving the InrS allosteric mechanism. Titration of *nrsD*ProFA (10nM) with either InrS in the presence of 5 mM EDTA (diamonds), Ni(II)-InrS (circles) or Cu(I)-InrS (triangles). Lines represent a fit to a 1:1 InrS tetramer:DNA model using Dynafit (Kuzmic, 1996). All titrations were performed anaerobically at pH 7.

a 1:1 tetramer:DNA (Section 4.1.1) model (Figure 5.15). As the DNA binding isotherm for Ni(II)- and Cu(I)-InrS did not saturate the $\Delta r_{\text{obs max}}$ value used in the data fitting was an average value from apo-InrS replicates. The allosteric coupling free energy for the system described in equation 8 was determined as $3.15(\pm 0.021)$ and $2.86(\pm 0.16)$ kcal mol⁻¹ for Cu(I) and Ni(II) respectively (average of two replicates for each metal). These data show that a non *in vivo* effector metal (Cu(I)) is as potent an allosteric effector as the *bona fide* effector metal (Ni(II)) (a Student's t-test reveals no statistical difference between the allosteric coupling constants for the two metals) this implies that selective recognition of Ni(II) over Cu(I) by InrS *in vivo* cannot operate at the level of allostery by analogy to *B. subtilis* CsoR (Ma *et al.* 2009a).

The estimated Zn(II) affinity of InrS at pH 7.8 (Section 5.6) means that at the lower concentrations (nanomolar) of InrS used in these DNA binding assays Zn(II) may need to be present in the buffer for the Zn(II) sites to remain saturated, especially as these assays were performed at pH 7 and (for Ni(II) at least) (Appendix Figure C2) the metal affinity of InrS has been shown to be dependent on pH. Titration of *nrsD*ProFA with Zn(II)-InrS (with 10 μ M ZnSO₄ included in the buffer) resulted in an increase in anisotropy only at higher InrS concentrations than observed with apo-InrS (i.e. Zn(II)-InrS displays a weaker DNA affinity than apo-InrS) however the Δr_{obs} value at the highest InrS concentration used in the assay was greater than that observed in apo-InrS control experiments (Appendix Figure E7). In addition the shape of the curve suggested the value would increase still higher before saturating (Appendix Figure E7). An explanation for this observation could be the formation of higher order complexes/aggregates potentially mediated by the presence of excess zinc in the buffer. Thus it was not possible to determine a ΔG_C value for Zn(II)-InrS by this method. This result is also consistent with the observation that in InrS-DNA dissociation experiments Zn(II) failed to reduce Δr_{obs} to the same degree as the other metals tested (Section 5.5.1).

5.6 Relative Zn(II) affinities of the metalloregulators of *Synechocystis*

The Zn(II) affinities of the two zinc sensors of *Synechocystis*, Zur and ZiaR, have previously been determined by competition with quin-2 (ZiaR $K_{D, \text{Zn(II)}} = 3.09(\pm 1.8) \times 10^{-13}$ and $1.91(\pm 1.1) \times 10^{-12}$ M for the first and second Zn(II) binding events respectively and Zur $K_{D, \text{Zn(II)}} = 2.18(\pm 1.9) \times 10^{-13}$ M) (Patterson. 2010) a zinc chelator used to determine the Zn(II) affinity of proteins in the picomolar range (VanZile *et al.* 2002b;

Liu *et al.* 2008). The experimental method involved titrating a mix of quin-2 and protein with zinc and monitoring Zn(II) dependent reduction in the spectral features of quin-2 (Patterson. 2010). Provided the system comes to equilibrium rapidly this experimental design can also offer an alternative way to probe the metal binding stoichiometry of a protein and can be used to calculate the metal binding affinities of multiple sites. The determination of the Zn(II) affinity of InrS was carried out using the same methodology in order to allow direct comparison of the results.

Mag-fura-2, in addition to use as a Ni(II) chelator (Section 5.4.1) (Iwig *et al.* 2008; Reyes-Caballero *et al.* 2011), is also used as a Zn(II) affinity probe (VanZile *et al.* 2000; Reyes-Caballero *et al.* 2010). Titration of mag-fura-2 with Zn(II) results in an increased intensity of a spectral feature at 325 nm and a decreased intensity of a spectral feature at 366 nm (Appendix Figure E2). Changes in both these spectral features saturate upon the addition of approximately one molar equivalent of Zn(II) consistent with a 1:1 Zn(II) binding stoichiometry (Appendix Figure E2). Upon titration of a mixed solution of InrS (10 μ M) and mag-fura-2 (16.2 μ M) with Zn(II) no change in the spectral features of mag-fura-2 are observed until a Zn(II) concentration in excess of 10 μ M has been added (Figure 5.16). At Zn(II) concentrations above 10 μ M a Zn(II) dependent change in absorbance is observed which saturates upon the addition of approximately an additional 26 μ M of Zn(II) (Figure 5.16). These data imply there are two Zn(II) binding sites per InrS monomer, one with a substantially tighter Zn(II) binding affinity than that of mag-fura-2 (2.2×10^{-8} M (Reyes-Caballero *et al.* 2010)) and one with a Zn(II) affinity close to that of mag-fura-2. Control experiments were performed to ensure these competitions reached equilibrium (Appendix Figure E3). The data was fit using Dynafit (Kuzmic. 1996) to a model describing four sites per InrS tetramer that can outcompete mag-fura-2 for Zn(II) and an additional four non-interacting sites per tetramer which compete with mag-fura-2 for Zn(II) (Figure 5.16). Through replicate experiments a mean average Zn(II) affinity for the weaker set of Zn(II) sites of InrS was obtained ($4.03(\pm 0.53) \times 10^{-8}$ M).

In order to confirm the stoichiometry of two Zn(II) atoms per InrS monomer an analogous experiment to that described in Section 3.3.2 (Figure 3.11) was carried out. InrS was applied to and eluted from a PD10 column equilibrated with buffer which had additional been supplemented with 20 μ M Zn(II) (Figure 5.17). Under these conditions InrS migrates with two molar equivalents of zinc analogous to the situation observed

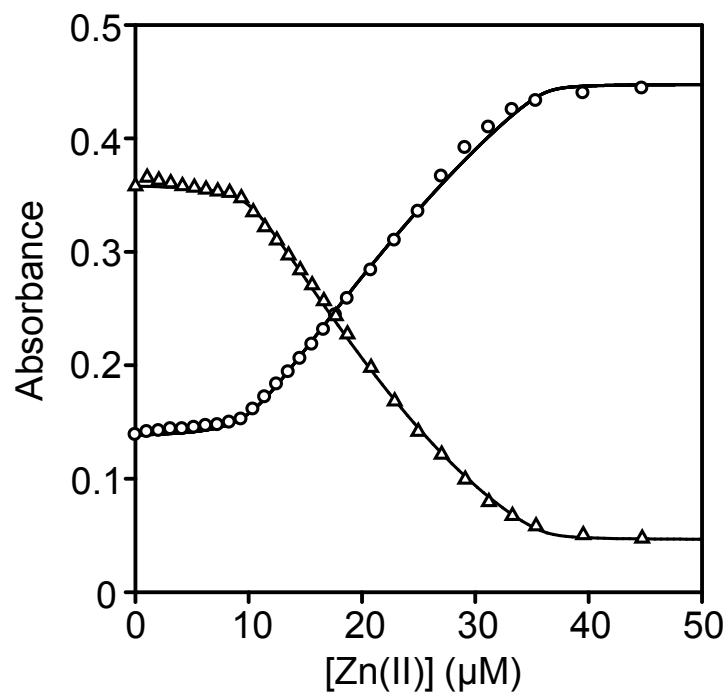


Figure 5.16. Determination of the Zn(II) binding affinity of InrS by competition with mag-fura-2. Binding isotherm of the absorbance at 325 nm (circles) and 366 nm (triangles) upon titration of a solution of InrS (10 μM) and mag-fura-2 (16.2 μM) with ZnSO₄. The lines represent a fit to a two non-interacting sites per monomer model where the Zn(II) affinity of the first site is substantially tighter than that of mag-fura-2 (Section 5.6) using Dynafit (Kuzmic. 1996).

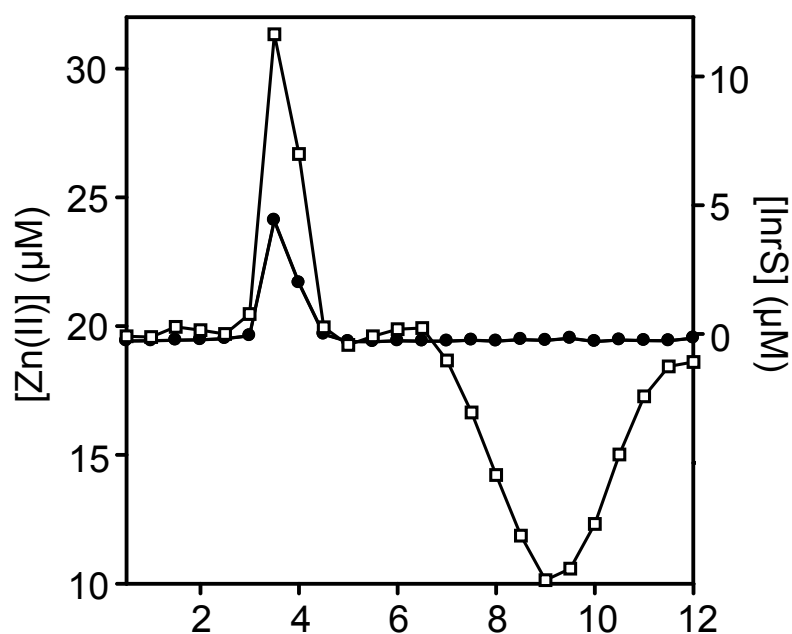


Figure 5.17. InrS migrates with approximately two equivalents of zinc by size exclusion chromatography when micromolar zinc concentrations are present in the buffer. InrS (0.5 ml at 10 μM) was applied to a Sephadex G75 matrix equilibrated in buffer additionally supplemented with 20 μM ZnSO_4 and eluted with the same buffer. Fractions (0.5 ml) were analysed for protein (filled circles, right y axis) by Bradford assay calibrated with a quantified stock of InrS and for zinc (open squares, left y axis) by ICP-MS.

with Co(II) (Figure 3.11). The site of binding for this second equivalent of Zn(II) and Co(II) is unknown although the histidine rich N-terminal extension (Figure 3.2) is a possible candidate. Histidine rich tails are found in several examples of proteins of nickel homeostasis and are suggested to aid Ni(II) acquisition or to be used for Ni(II) storage (Higgins *et al.* 2012a). Binding of super-stoichiometric concentrations of Ni(II) to InrS has not been observed in these studies however this does not preclude the possibility that Ni(II) binding to this region of the protein plays a role in Ni(II) homeostasis *in vivo*.

The Zn(II) affinity of the tighter set of sites of InrS was probed by competition with quin-2 (Figure 5.18). Zn(II) binding to quin-2 results in a decrease of an absorbance feature at 261 nm (Appendix Figure E4). This decrease saturates upon the addition of approximately one molar equivalent of Zn(II) consistent with a Zn(II) binding stoichiometry of 1:1. Titration of Zn(II) into a mixed solution of InrS and quin-2 resulted in a linear decrease in quin-2 absorbance at 261 nm which saturated upon addition of a concentration of Zn(II) approximately equal to that of quin-2 used in the experiment (Figure 5.18). Control experiments were performed to ensure these competitions reached equilibrium (Appendix Figure E5). These data suggest that the Zn(II) affinity of quin-2 (3.7×10^{-12} M (Jefferson *et al.* 1990)) is substantially tighter than either of the two sets of Zn(II) binding sites observed per InrS monomer. This places the tightest set of Zn(II) binding sites of InrS as substantially tighter than magfura-2 (2.2×10^{-8} M) but substantially weaker than quin-2 (3.7×10^{-12} M) allowing the Zn(II) affinity of the tighter set of sites of InrS to be estimated at $\sim 10^{-10}$ M.

The Zn(II) affinities ZiaR and Zur (see above (Patterson. 2010)) are more than two orders of magnitude tighter than those of InrS providing a mechanism by which zinc concentration within the cell could be buffered such that it does not interfere with cognate metal sensing by InrS.

5.7 Cu(I) affinity of InrS

There is currently no identified cytosolic copper sensor in *Synechocystis* although a plasmid borne two component system thought to detect periplasmic copper and possibly copper in the thylakoid has recently been identified (Giner-Lamia *et al.* 2012). As this sensor likely detects copper in different cellular compartments to InrS and may sense a different species of copper to that thought to be prevalent in the cytoplasm a comparison

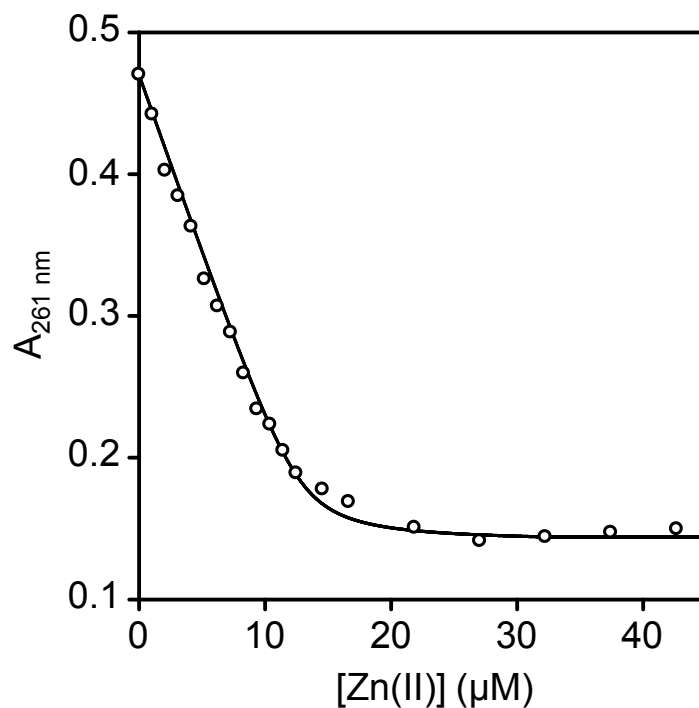


Figure 5.18. Estimation of the Zn(II) affinity of InrS by competition with quin-2. Binding isotherm of $A_{261 \text{ nm}}$ feature obtained upon titration of a solution of InrS (20 μM) and quin-2 (12.7 μM) with ZnSO_4 . The line represents a fit to a one non-interacting site per monomer model (Section 5.6) using Dynafit (Kuzmic. 1996).

of the copper affinities of these two sensors would not be relevant to understanding correct metal speciation based on relative affinity. The cytosolic copper chaperone Atx1 has recently been shown to withhold copper from binding sites for other metals (Tottey *et al.* 2012). What are the equilibrium Cu(I) binding constants of InrS and Atx1 and could Atx1 withhold Cu(I) from InrS on the basis of affinity? The Cu(I) affinity of *Synechocystis* Atx1 has been estimated to be in the range 10^{-18} - 10^{-19} M depending on the pH at which the experiment was conducted and the oligomeric status of Atx1 which can vary with Cu(I) occupancy (Badarau & Dennison. 2011). The Cu(I) affinity of InrS was estimated by titration of the Cu(I) specific chelator BCS and InrS with Cu(I) and monitoring the Cu(I) dependent change in absorbance of BCS (Figure 5.19). BCS forms a 2:1 complex with Cu(I) (Xiao *et al.* 2004). In the presence of InrS (40 μ M) the Cu(I) dependent change in absorbance of BCS (70 μ M) does not saturate until the addition of \sim 115 μ M Cu(I) suggesting that there is substantial competition of InrS with BCS for Cu(I) binding. Additionally the Cu(I) molarity required to achieve saturation suggests that InrS binds two Cu(I) per monomer as previously observed for Co(II) (Section 3.3.2) and Zn(II) (Section 5.6) (the change in absorbance would be expected to saturate upon the addition of 75 μ M Cu(I) if InrS bound one Cu(I) per monomer). Minimal change in absorbance is observed over the addition of the first 20 μ M Cu(I) suggesting the affinity of the first two sites of InrS for Cu(I) is substantially tighter than that of BCS. Consistent with this observation, when the data were subjected to data fitting using Dynafit (Kuzmic. 1996) to determine a Cu(I) affinity, the first two binding events were too tight to be modelled. The model that best described the data describes the apparent eight Cu(I) sites of InrS as pairs of sites that interact with negative cooperativity. Both the first (as mentioned above) and last pairs of Cu(I) sites were too tight and weak respectively for an affinity to be accurately determined in this assay. The affinities of the two intermediate pairs of sites were 9.9×10^{-18} M and 1.84×10^{-15} M. Control experiments were performed to ensure these competitions reached equilibrium (Appendix Figure E6). The overall stability constant of $\text{BCS}_2\text{Cu(I)}$ is 19.8 M^{-2} (Xiao *et al.* 2004) placing the Cu(I) affinity of the tighter sites of InrS at $\leq 10^{-21}$ M akin to Cu(I)-sensing CsoR from *B. subtilis* (Ma *et al.* 2009a). The equilibrium Cu(I) binding constant of the tighter sites of InrS is tighter than that of Atx1 suggesting that at equilibrium Atx1 could not withhold Cu(I) from InrS, moreover the binding of 1-2 Cu(I) atoms to an InrS tetramer is sufficient to trigger allostery (Figure 5.14) suggesting that InrS could aberrantly respond to Cu(I) *in vivo* if equilibrium were reached between InrS and Atx1. However the specific interaction of copper chaperones with their targets (Robinson &

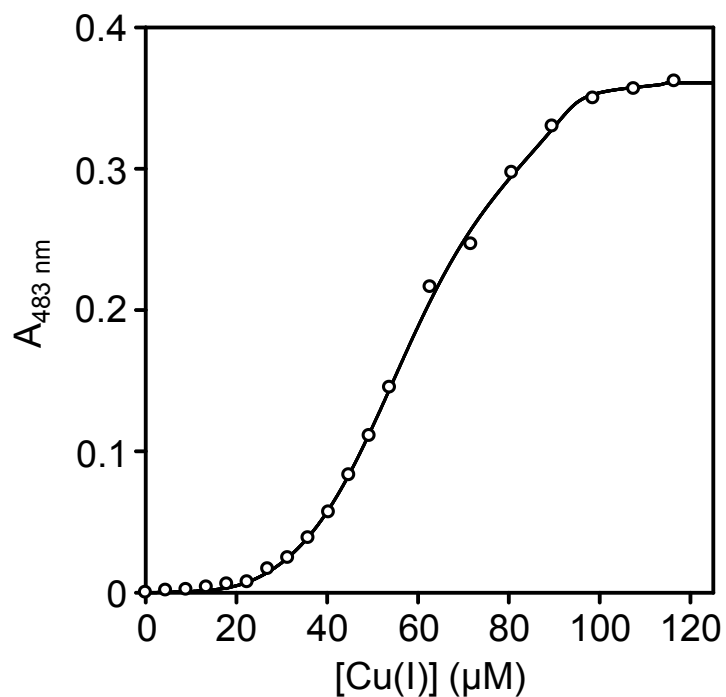


Figure 5.19. Estimation of the Cu(I) affinity of InrS by competition with BCS. Binding isotherm of $A_{483 \text{ nm}}$ feature upon titration of BCS (70 μM) and InrS (40 μM) with CuCl (confirmed to be >95 % Cu^+). The line represents a fit to a model where the eight apparent Cu(I) sites per InrS tetramer were grouped into pairs which interact with negative cooperativity (Section 5.7). Experiment conducted at pH 7.8.

Winge, 2010) will influence the kinetics of copper trafficking and therefore likely overcome limitations imposed by relative copper affinity as an equilibrium state is unlikely to be reached. The contribution of Atx1 to withholding Cu(I) from InrS is addressed in Section 6.6.

In considering the contribution of metal affinity in favour of the sensing of cognate metals and against the sensing non-cognate metals by InrS relative metal affinity across four protein families in *Synechocystis* has been addressed. This simple analysis has shown that for Ni(II) and Zn(II) but not Co(II) selective response of metalloregulators could be governed by relative affinity of a cells complement of metalloregulators. These calculated binding affinities represent metal binding preferences at thermodynamic equilibrium a state which is unlikely to exist *in vivo* as the cellular environment is in a state of constant flux, however these affinity values are a useful guide to the rank order of metal binding preference even though they are unlikely to be representative of the kinetics of *in vivo* metal transfer (discussed further in Section 6.8).

Chapter 6. Final discussion and future work

6.1 InrS is a Ni(II) sensing member of the CsoR-RcnR metalloregulatory family that regulates expression of *nrsD* a deduced major facilitator superfamily protein proposed to mediate Ni(II) export to the periplasm

InrS represents the first characterised cyanobacterial member of the CsoR-RcnR metalloregulator family. Prior to the start of this work the target of InrS regulation and the metal(s) sensed by InrS were unknown. A bioinformatics analysis coupled with EMSA approach was used to search the *Synechocystis* genome for potential InrS DNA binding sites (Section 3.4). InrS was found to form specific interactions with DNA containing a near perfect inverted repeat motif found upstream of *nrsD* (Figures 3.32-3.35 and 4.1, 4.2 & 4.4) and therefore *nrsD*, which is predicted to encode a Ni(II) exporter, represented a potential target for metalloregulation by InrS. The DNA recognition site of InrS has similarity to the DNA recognition site of copper sensing CsoR proteins and is distinct from the DNA recognition site of Ni(II)/ Co(II) sensing RcnR (Figures 3.29, 3.32 & 3.33). *nrsD* is arranged as part of an operon with the genes *nrsBAC* (Figure 3.33) and it has previously been shown by northern blot analysis that the *nrsBACD* operon is co-transcribed and is expressed in response to exogenous nickel and cobalt but not cadmium, copper, magnesium or zinc (García-Domínguez *et al.* 2000) and is under the control of the two component system NrsRS (López-Maury *et al.* 2002). These previous expression studies were conducted following a 1 h exposure to 15 μ M of each metal. The expression of *nrsB* and *nrsD* was re-examined in the course of this work following a 48 h exposure to maximum non-inhibitory concentrations of each metal to discern the steady state transcriptional response of these genes in response to physiologically equivalent concentrations of each metal. Under steady state conditions expression of *nrsB* and *nrsD* is observed in response to exogenous nickel and cobalt but not zinc or copper (Appendix Figure B2A). The identification of an InrS DNA binding site in the *nrsCD* intergenic region (Section 3.4.4) raised the possibility that *nrsD* could be expressed independently of the rest of the *nrs* operon and *vice versa*. Previous work in which independent expression of *nrsD* was not detected (García-Domínguez *et al.* 2000) but contained hints that *nrsBAC* could be regulated independently of *nrsD* is discussed in Section 3.5. The presence of a cryptic promoter in the *nrsCD* intergenic region was suggested by the PCR analysis of *nrsD* gene

expression in the Δ *inrS* strain (Appendix Figure B1) and this was confirmed by RLM-RACE experiments which showed an increase in transcript abundance corresponding to the expected size for a product initiated in the *nrsCD* intergenic region in response to nickel and cobalt treatments (Appendix Figure B2). Therefore InrS regulates the expression of *nrsD* the last gene in the *nrs* operon by binding to a cryptic promoter located in the *nrsCD* intergenic region. *nrsD* expression is regulated by the presence of exogenous nickel and cobalt but potentially only in the case of nickel does direct metal binding to InrS mediate this effect (Section 6.2).

6.2 A model of nickel homeostasis in *Synechocystis*

As previously observed (García-Domínguez *et al.* 2000) the *nrs* operon contains what are predicted to be two independent metal efflux systems. NrsD was reported as showing significant homology to the NreB protein of *Achromobacter xylosoxidans* 31A (García-Domínguez *et al.* 2000), a member of the major facilitator superfamily, which confers nickel resistance when transferred to *E. coli* (Grass *et al.* 2001). NreB and NrsD are predicted to transport Ni(II) across the cytoplasmic membrane. NrsB and NrsA display homology to the B and A components of RND metal efflux systems such as Czc of *C. metallidurans* and Cus of *E. coli* encoding the periplasmic adapter protein and cytoplasmic membrane spanning RND protein respectively (Su *et al.* 2011). It should be noted that the *nrs* operon does not encode an outer membrane channel (OMC) protein, the C component of RND systems. Interestingly, neither does the recently discovered CopBAC RND copper efflux system from *Synechocystis* (Giner-Lamia *et al.* 2012). A BLAST search of the *Synechocystis* genome with the sequence of either *E. coli* CusC or TolC as the search term returns only one significant hit (expect values of $6e^{-7}$ and $5e^{-5}$ when CusC and TolC are used as the search term respectively) the product of *slr1270*. Perhaps this OMC protein is utilized by both of these RND efflux systems and maybe the other RND proteins present in the organism, of which there are four in addition to NrsA and CopA (Slr0142, Slr2131, Slr0369, Slr0454). This is known to be the case for other OMC proteins for example TolC is known to function with an RND family protein AcrB and multiple ABC-type transporters (Janganan *et al.* 2011). The role of *nrsC*, which is predicted to encode a protein with similarity to lysozyme, is unknown.

It was noted by García-Domínguez and co-workers that strains of *Synechocystis* with insertional mutations in either *nrsA* or *nrsD* displayed distinct differences in nickel

tolerance suggesting that these two genes could be part of distinct nickel resistance systems. The discovery of a cryptic promoter in the *nrsCD* intergenic region provides a mechanism by which the expression of the two Ni(II) resistance systems can be differentially regulated to respond to Ni(II) excess in different cellular compartments (Figure 6.1). InrS could alleviate repression of *nrsD* under conditions of cytosolic Ni(II) excess without the need for expression of the rest of the *nrs* operon (Figure 6.1). Under conditions of periplasmic but not cytosolic Ni(II) excess Ni(II) will be detected by the periplasmic nickel sensor NrsS and initiate expression from the *nrsB* promoter via the response regulator NrsR (Figure 6.1). It is possible that transcripts initiated from *nrsB* may be terminated (or attenuated) upon the RNA polymerase encountering InrS bound to DNA by analogy to the actions of the *lac* repressor LacI as a transcriptional terminator as well as a de-repressor (Section 3.5) (Sellitti *et al.* 1987). This is termed ‘roadblock repression’, the advancing RNA polymerase is halted by a protein bound to DNA and, in addition to the previously given example of regulation of the *lac* operon in *E. coli*, has also been described for the regulation of nitrogen assimilation (Choi & Saier. 2005) and of branched chain amino acid biosynthesis in *B. subtilis* (Belitsky & Sonenshein. 2011). Under conditions of cytosolic and periplasmic Ni(II) excess RNA polymerase would be allowed to read through into *nrsD* at a greater frequency as well as initiate transcripts from the *nrsD* promoter (Figure 6.1). Multiple promoters within an operon additionally could confer the advantage of overcoming attenuation of transcription in a polycistronic message (Napolitano *et al.* 2013).

It was observed that the degree of induction of *nrsD* in response to exogenous nickel was less than the constitutive expression of *nrsD* in the Δ *inrS* strain (Figures B1 and B2). This has previously been observed with *L. monocytogenes* CsoR where it was shown by *lacZ* reporter gene assay that activity in a Δ *csoR* mutant was significantly greater than in the wild type strain or in a Δ *csoR* strain complemented with a plasmid expressing *csoR* under the control of its native promoter when exposed to exogenous copper (Corbett *et al.* 2011). Based on EMSA and DNase I footprinting assays it was suggested that *L. monocytogenes* CsoR retains some DNA-binding capability in the presence of copper perhaps in a different conformation to apo-CsoR which is permissive for transcription (Corbett *et al.* 2011). This explanation is consistent with results obtained for InrS which showed by EMSA that multiple InrS-DNA species may exist (Figure 3.35) and fluorescence anisotropy experiments in which it was not possible to reduce Δr_{obs} to the DNA-alone starting value upon titration of InrS:DNA complexes with both cognate and non-cognate metal ions (Figures 4.5 and 5.14).

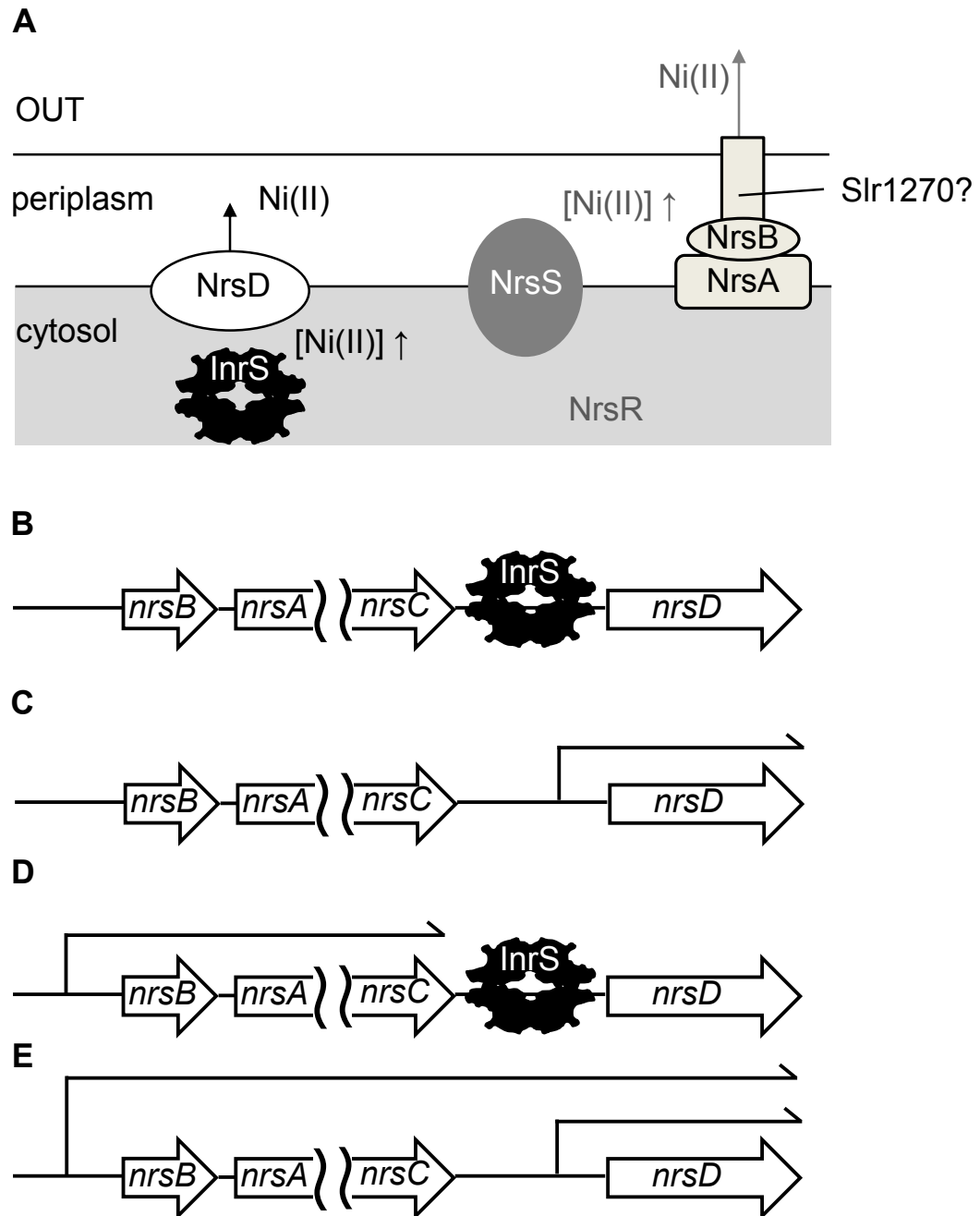


Figure 6.1. Model of Ni(II) homeostasis in *Synechocystis*. A. Excess cytosolic Ni(II) is detected by InrS which derepresses transcription of *nrsD*. NrsD pumps Ni(II) across the cytoplasmic membrane to the periplasm where excess Ni(II) is detected by NrsS which relays a signal to NrsR to activate expression from the *nrsB* promoter. NrsBA form the cytoplasmic membrane spanning RND protein and periplasmic adapter of an RND Ni(II) efflux pump. Slr1270 may serve as the outer membrane spanning component of the pump. The Nrs RND system may pump Ni(II) from the periplasm or the periplasm and cytosol. Shown below are representations of the possible transcriptional responses of the *nrs* operon to no Ni(II) stress (B), cytosolic Ni(II) stress (C), periplasmic Ni(II) stress (D) and cytosolic and periplasmic Ni(II) stress (E).

The co-expression of *nrsB* and *nrsD* raises the question of how much of the observed *nrsD* expression is due to readthrough of transcripts initiated from the *nrsB* promoter or the dislodgement of InrS-DNA complexes to expose the *nrsD* promoter. In order to address this, a mutant in which the *nrsB* promoter has been replaced with a kanamycin resistance cassette has very recently been constructed by Rafael Pernil (Figure 6.2). It is apparent that in the *nrsB* promoter mutant the level of *nrsD* transcript accumulated upon addition of exogenous nickel or cobalt is significantly lower than that in the wild type strain (Figure 6.2 and Appendix Figure B2A) suggesting that a significant amount of observed *nrsD* transcript abundance observed in response to nickel and perhaps all in response to cobalt, can be attributed to readthrough from the *nrsB* promoter or disruption of InrS-DNA complexes by RNA polymerase exposing the previously occluded *nrsD* promoter. Crucially though *nrsD* remains nickel responsive in this mutant formally showing that Ni(II) is an *in vivo* effector of InrS. Disruption of protein:DNA complexes can be influenced by multiple RNA polymerases transcribing in tandem (Epshtein & Nudler. 2003) or closely following ribosomes providing additional force to bypass the ‘roadblock’ (Proshkin *et al.* 2010). Activity of an operons upstream promoters affecting the activity of downstream promoters has been reported for a zinc responsive operon in the cyanobacterium *Anabaena* sp. Strain PCC7120 (Napolitano *et al.* 2013). Here expression from two promoters, to which Zur does not bind, is positively influenced by transcription from two upstream Zur regulated promoters (Napolitano *et al.* 2013). Further experiments with this strain should also begin to establish the relative contributions of *nrsBAC* and *nrsD* to nickel tolerance in *Synechocystis*.

6.3 The primary and secondary metal coordination spheres of InrS

6.3.1 Ni(II) coordination by InrS

Under the conditions tested InrS binds one molar equivalent of Ni(II) and based on comparison with UV-Vis spectra of structurally characterised sites Ni(II) is predicted to be coordinated in a square planar geometry (Figures 3.6 and 3.7). Structural characterisation or XAS analysis will be required to unambiguously define the coordination geometry. Three residues critical for Ni(II) binding to InrS have been conclusively identified by a mutagenesis approach coupled with UV-Vis spectroscopy (Cys53, His78, Cys82) (Section 4.3). These residues are in the equivalent positions to

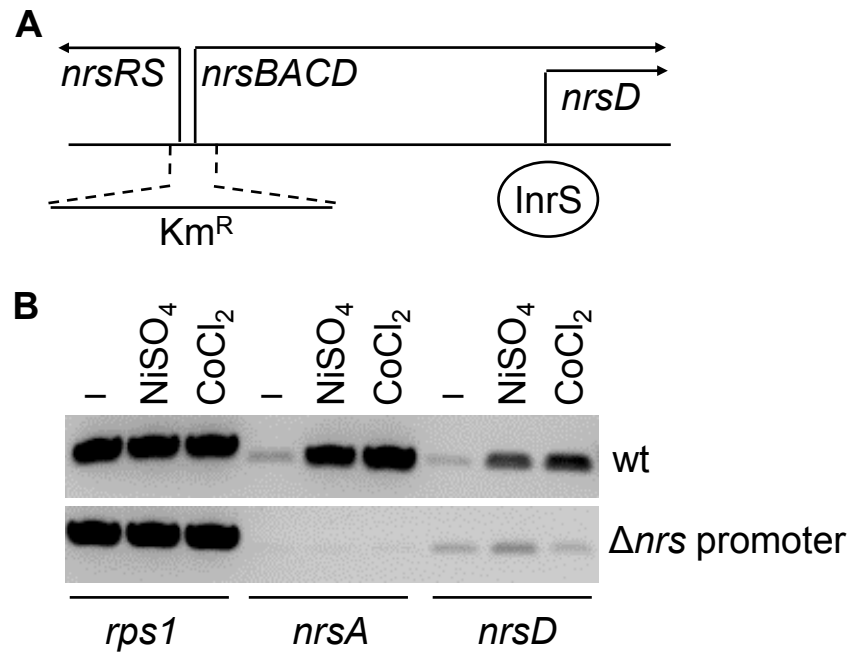


Figure 6.2. Effect of deletion of the *nrs* promoter on nickel and cobalt dependent expression from the *nrsD* promoter. A. Construction of the *nrsB* promoter mutant. Representation of the *nrs* operon indicating the relative position of the kanamycin resistance cassette which replaces the *nrs* promoter (not to scale). B. RT-PCR analysis of *nrsD*, *nrsA* and *rps1* in wild type (upper panel) and the $\Delta nrsB$ promoter mutant (lower panel) *Synechocystis* cells exposed to the maximum non-inhibitory concentration (for wild type cells) of NiSO₄ (0.5 μ M) and CoCl₂ (2 μ M) for 48 h. The maximum non-inhibitory concentration of NiSO₄ and CoCl₂ for Δnrs promoter cells remains to be determined and it is formally possible that a decreased tolerance to these metal salts in this strain may have influenced the outcome of this analysis. Construction of the Δnrs promoter mutant and RT-PCR analysis was performed by Rafael Pernil.

the Cu(I) coordinating residues of various CsoRs (Figure 3.2). The identity of any additional Ni(II) ligand(s) (which would be the fourth and final ligand if the prediction of a square planar coordination geometry is correct) are ambiguous. A His3→Leu mutation in *E. coli* RcnR causes the protein to become insensitive to nickel in a *lacZ* reporter gene assay (Iwig *et al.* 2008). This, coupled with a loss of nickel dependent UV-Vis spectral features in this mutant, led the authors to suggest that the side chain of His3 coordinated Ni(II). A more recent study, however, has shown by XAS that the nature of the nickel binding site is unchanged in an His3→Leu mutant compared with the wild type protein (Higgins *et al.* 2012b). A His3→Cys mutation recovers a modest amount of the nickel responsiveness observed in the wild type protein (~ 20 %) although again the Ni(II) site as observed by XAS is unaltered compared with the wild type protein (Higgins *et al.* 2012b). The equivalent residue in InrS (His21) can be mutated to leucine with no change in the UV-Vis spectral properties upon Ni(II) binding (Figure 4.21). This mutant is also allosterically competent to respond to nickel, as measured by fluorescence anisotropy (Figure 4.22). These data strongly suggest that this residue is not Ni(II) coordinating. However InrS His21→Glu and InrS His21→Cys mutations display tighter relative (Figure 4.25) and absolute (Appendix Figure C5) Ni(II) binding affinities than His21→Leu and, additionally, in the His21→Cys mutant a slight but perceptible red shift of the nickel dependent LMCT feature is observed (Figure 4.25). Taken together these data imply that His21, although not an obligatory Ni(II) liganding residue, is perhaps an optional ligand required to maintain a tight Ni(II) affinity or is located in the proximity of the Ni(II) binding site and is a determinant of the Ni(II) affinity of the site. This could provide an explanation for the seemingly conflicting results obtained for *E. coli* RcnR, with His3→Leu failing to gain access to nickel in the cell due to a weakened nickel affinity rather than the loss of a primary coordination sphere residue.

How does InrS His21 influence the affinity of the Ni(II) binding site? In the InrS His21 series of mutants the affinity for Ni(II) seems to correlate with the preference of Ni(II) for the donor atom supplied by the residue in position 21, but this residue does not appear to be part of the primary coordination sphere (Section 4.3.5). Perhaps His21 is involved in the loading of nickel into the binding site. Metal binding residues at or immediately preceding this position are well conserved in copper sensing CsoRs characterised to date (Figure 3.2) (with the exception of *L. monocytogenes* CsoR) suggesting that a similar role could also be played in these proteins. Additional metal binding residues are often found close to protein metal binding sites and it has been

suggested that the function of these residues is to lure non-cognate metals into non-productive coordination geometries (Waldron *et al.* 2009). Perhaps an alternative or additional function of these residues is to increase the rate with which a metal ion finds its binding site on the protein, acting to guide the metal into the site.

Given the similarity of the UV-Vis spectrum of Ni(II)-InrS (Figure 3.6) and *B. subtilis* Ni(II)-CsoR (Ma *et al.* 2009a) it may be reasonable to assume that an identical Ni(II) ligand set and coordination geometry is present in both proteins. However, the nanomolar Ni(II) affinity measured for *B. subtilis* CsoR (Ma *et al.* 2009a) is weak compared to the Ni(II) affinity of InrS (Section 4.2.1) and other proteins with square planar Ni(II) sites (picomolar and tighter) (Chivers & Sauer. 2002; Wang *et al.* 2004; Abraham *et al.* 2006). The primary coordination sphere of *E. coli* RcnR Ala2*, an insertional mutant which causes the displacement of the N-terminal amine by one residue and enforces a square planar geometry for the Ni(II) site, was found to contain two histidine residues, one cysteine residue and an open coordination position (Higgins *et al.* 2012b). Perhaps *B. subtilis* Ni(II)-CsoR has the same ligand set and this may explain the unusually weak nickel affinity of this square planar site. The ligands required for Ni(II) binding by InrS are in equivalent positions to those required for Cu(I) binding by various CsoRs (Figure 3.2). Therefore candidate residues for the fourth ligand required to complete the deduced square planar coordination sphere would need to be situated proximal to the copper binding locus identified in *M. tuberculosis* CsoR (Liu *et al.* 2007) (Figure 1.2). The histidine residues of the N-terminal extension (Figure 3.2), a region predicted to be unstructured and proximal to the metal binding locus (Figure 1.2), represent candidates for the fourth ligand. A cysteine scanning mutagenesis approach may be the best way to determine if one of these five histidine residues is in the primary coordination sphere of Ni(II)-InrS as functional substitution of one of the nearby histidine residues may occur with His→Leu mutations.

6.3.2 Co(II) coordination by InrS

InrS binds two molar equivalents of Co(II) with at least one of the Co(II) ions predicted to be bound with pseudo-tetrahedral coordination geometry (Figures 3.9-3.11). The identities of residues involved in coordination of Co(II) are less clearly defined than those involved in the coordination of Ni(II). The intensities of Co(II) dependent LMCTs suggest that two cysteine residues are involved in the coordination of Co(II) (Figure 3.10). Of the residues mutated in the course of this work (Section 4.3) only one mutation (Cys53→Ala) completely abrogated the native Co(II) coordination

environment as judged from the UV-Vis spectra (Figure 4.13). As discussed in Section 4.3, mutation of His21, His78 and Cys82 to non-coordinating residues all changed the properties of the Co(II) coordination environment but in none of these cases was Co(II) coordination lost. It will be interesting to ascertain the Co(II) binding stoichiometry of these mutant proteins. It is possible one or more of these residues are required for the second Co(II) binding event. Although the binding isotherms for the Co(II) dependent spectral properties of these mutant InrS proteins saturated at greater than one molar equivalent this could now be due to a weakened Co(II) binding affinity rather than binding a second equivalent of Co(II). The biological relevance, if any, of binding two molar equivalents of metal (also observed for Zn(II) (Figures 5.16 & 5.17) and Cu(I) (Figure 5.19) remains to be ascertained, this trait has not been reported for any other members of the CsoR-RcnR metalloregulator family.

6.3.3 Allostery in *CsoR-RcnR* proteins

Details of the allosteric network in InrS are currently sparse and are discussed here in the light of the current understanding of allostery in copper sensing CsoR proteins.

In copper sensing CsoR a triad of residues, Tyr-His-Glu in positions A, Y and B respectively, is thought to propagate the allosteric switch (Section 1.5.4). InrS lacks the Tyr residue of this triad (which is not critically required to propagate allostery (Section 1.5.4)) but retains the His and Glu residues in the appropriate positions whereas *E. coli* RcnR lacks both the Tyr and Glu (although does have an Asp immediately prior to the B position) (Figure 3.2) retaining only the His in the Y position which, however, is dispensable to Ni(II) sensing (Section 4.3). This bioinformatics analysis suggests that metal sensing may be achieved by a similar mechanism in InrS and copper sensing CsoR proteins but a different mechanism is likely employed by *E. coli* RcnR.

The role of the His residue (position Y) in the *M. tuberculosis* CsoR allosteric switch was shown in work utilising artificial histidine analogues, discussed in Section 1.5.4. Mutation of InrS His78 to leucine results in the loss of Ni(II) binding (Figure 4.17) so it is not possible to conclude from studies of this mutant if a His residue in the Y position is critical for coupling Ni(II) binding to DNA binding. Co(II) and Zn(II) binding was retained by this mutant (albeit with an alteration of the coordination environment) (Figure 4.18) however Co(II) and Zn(II) were no longer competent at dissociating complexes of this mutant form of InrS and DNA (Figure 4.20) suggesting this residue may play an important role in propagation of the allosteric response (at least for Co(II)

and Zn(II)). The essentiality of the Glu residue (position B) for the allosteric switch was also conclusively shown for *B. subtilis* CsoR and *M. tuberculosis* CsoR (Section 1.5.4) where a B position Glu→Ala mutation uncouples Cu(I)-binding from DNA-binding. Although this same effect was not observed for *L. monocytogenes* CsoR in *lacZ* reporter gene assays (Corbett *et al.* 2011), functional substitution of neighbouring acidic residues (Figure 3.2) may account for the retention of allosteric competence observed. The role of Tyr (position A) in this allosteric network was implied from the crystal structure of *M. tuberculosis* Cu(I)-CsoR (Liu *et al.* 2007). A *M. tuberculosis* CsoR Tyr35→Phe exhibits a roughly 33 % reduction in allosteric coupling free energy (Ma *et al.* 2009b) and *lacZ* reporter gene assay with a *L. monocytogenes* CsoR position B Tyr→Phe mutation resulted in an approximately 50 % reduction in β -galactosidase activity in response to exogenous copper compared with a strain harbouring the wild type protein (Corbett *et al.* 2011). These results imply that Cu(I) is capable of driving allostery in these mutants but stabilises the low DNA affinity form of the protein to a lesser extent. Alternatively in the case of *L. monocytogenes* CsoR, where experiments were performed *in vivo*, this result may suggest a weakening of the Cu(I) affinity of the protein such that it is less able to compete for Cu(I) *in vivo*. The equivalent mutation of *M. tuberculosis* CsoR weakens the Cu(I) affinity of the protein by more than an order of magnitude (Ma *et al.* 2009b), the degree to which a very tight Cu(I) affinity is required for function *in vivo* remains to be tested. Conservative mutations of the B position residue of *M. tuberculosis* CsoR Glu81 such as Glu81→Gln exhibit an approximately 50 % reduction in allosteric coupling free energy upon Cu(I) binding (Ma *et al.* 2009b). In double mutants, combining this mutation with Tyr35→Phe, the resulting reduction in the allosteric free energy of Cu(I) binding is additive of that of the two individual mutations, suggestive of no interaction between residues in the A and B positions but instead between residues in the Y & A and Y & B positions (Ma *et al.* 2009b).

A two residue allosteric network involving His78 (position Y) and Glu98 (position B) may exist in InrS. This hypothesis is consistent with the dispensable nature of a Y position Tyr (see above) and with allosteric coupling free energies of 2.86 and 3.15 kcal mol⁻¹ observed for Ni(II) and Cu(I) binding to InrS respectively, whereas the value for Cu(I) binding to *B. subtilis* CsoR is ≥ 5.4 kcal mol⁻¹ (Ma *et al.* 2009a), the lack of the additional hydrogen bond with tyrosine potentially making the allosterically inhibited form of InrS less stable than that of *B. subtilis* CsoR. Although it should be noted that an allosteric coupling free energy of 3.6 kcal mol⁻¹ has been reported for Cu(I) binding to *M. tuberculosis* CsoR (Ma *et al.* 2009b), which, of course, has the complete triad of

Tyr-His-Glu in positions A, Y and B. Experiments to identify the allosteric network of InrS are a priority for future work. Mutation of Glu98 to a residue incapable of receiving a hydrogen bond (such as alanine) should allow assessment of the role of this residue in the allosteric response, assuming the prediction of an allosteric network similar to that of CsoR is correct, it may be possible to increase the magnitude of coupling free energy by the introduction of a Tyr residue in the 'A' position of wild type InrS.

Tuning the magnitude of free energy change of ligand coupling may represent an evolutionary strategy to tune the transcriptional response in CsoR-RcnR family proteins. A requirement for prokaryotic cytoplasmic copper outside of cyanobacteria is unknown and therefore copper sensing CsoRs can be thought of primarily as defence mechanisms (Dupont *et al.* 2011). Nickel is required in *Synechocystis* and the role of InrS may be to deal with occasional nickel fluxes, for example from protein turnover rather than as a defence determinant. The larger coupling constant associated with Cu(I) binding to CsoR relative to Ni(II) (and Cu(I)) binding to InrS means an enhanced stability of the allosterically inhibited form of the regulator and therefore a greater transcriptional response of genes involved in copper resistance. The same levels of expression of *nrsD* may not be required due to the physiological relevance of nickel in *Synechocystis* in contrast to the solely toxic nature of cytosolic copper in organisms without a cytoplasmic requirement for this metal. Therefore this postulated modification of the allosteric mechanism may allow different transcriptional responses of genes that are regulated by the same family of metalloregulators.

This model does not explain why the allosteric coupling free energy for Ni(II) and Zn(II) binding to *B. subtilis* CsoR is lower than that observed for Cu(I) binding (Ma *et al.* 2009a). One postulated explanation is that Cu(I) binding destabilises physical interactions between the two tetramers bound to the promoter DNA to a greater extent than Ni(II) and Zn(II) (Ma *et al.* 2009a). As only one InrS tetramer binds to the identified DNA recognition site (Figure 4.2) this could have implications for the magnitude of coupling free energy.

A model of InrS was produced using the modelling web server SWISS-Model by threading the sequence of InrS onto the structure of *S. lividans* CsoR (Figure 6.3A). Due to the level of similarity between the two proteins being below a threshold only a monomeric model could be produced. $\alpha 3$ of the InrS model was inspected for residues whose side chains may be able to form a hydrogen bonding interaction with His78

Figure 6.3. Prediction of allosteric pathways in CsoR-RcnR proteins. A. Model of an InrS monomer created using SWISS-Model from the coordinates of the *S. lividans* CsoR crystal structure (PDB: 4ADZ) (Dwarakanath *et al.* 2012). Residues shown to be critical for Ni(II) binding are shown (His78 and Cys82). Cys53 is not shown as this residue would be provided by a symmetry related monomer for this site (see Figure 1.2). Residues Glu95 and 98 are shown to indicate how the side chains of these residues could be involved in an allosteric network with analogy to that demonstrated for *M. tuberculosis* CsoR (Figure 1.2). B. Predicted *S. lividans* CsoR Cu(I) binding site (Dwarakanath *et al.* 2012) (PDB: 4ADZ). Residues predicted to be Cu(I) ligands are shown (Cys75', His100 and Cys104) along with residues whose side chains are predicted to be involved in propagating the allosteric mechanism (Tyr74' and Glu122. Lys119 which occupies the C position (Section 6.3.3) and may be involved in propagation of an allosteric response is also shown. C. *M. tuberculosis* CsoR structure arranged to highlight the kink in $\alpha 2$ upon Cu(I) binding (PDB: 2HH7) (Liu *et al.* 2007). The side chain of Glu63 points in the opposite direction to those of Cu(I) coordinating His61 and Cys65 and is within hydrogen bonding distance (3.39 Å) of Gln76 located on $\alpha 3$ of an adjacent CsoR monomer. Individual CsoR monomers are coloured as in Figure 1.2.

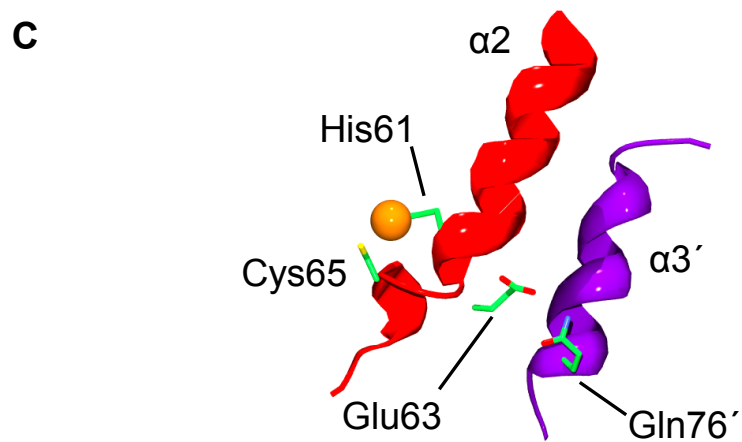
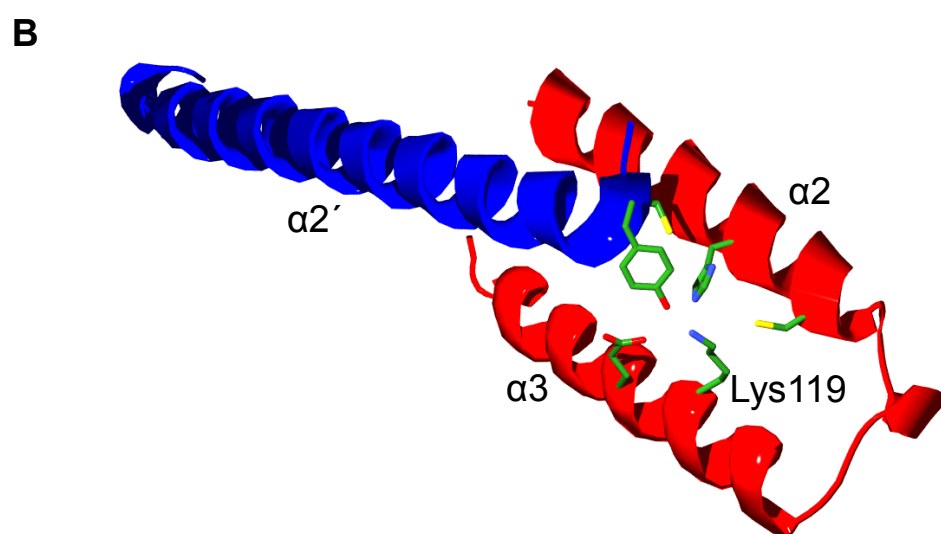
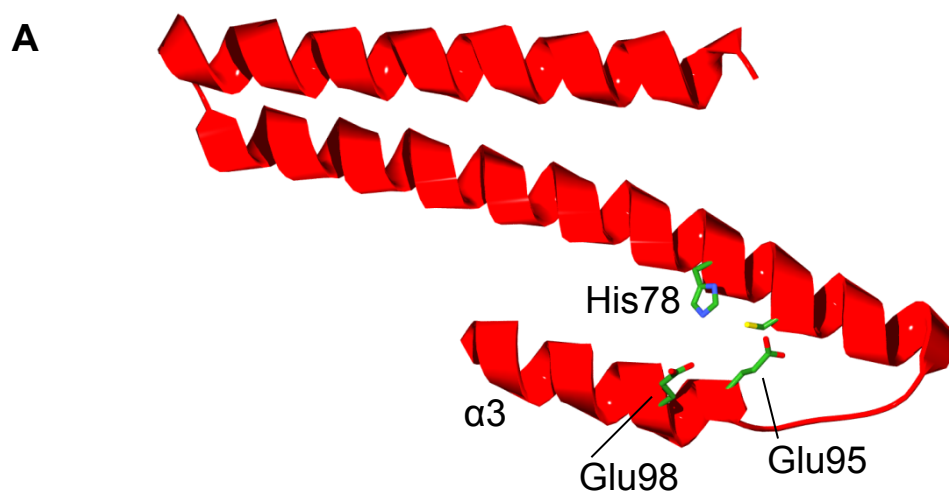


(Figure 6.3A). In addition to Glu98 the side chain of Glu95 could also plausibly form a hydrogen bond with the Nε2 face of His78 to create an allosteric hydrogen bond network with analogy to that present in copper sensing CsoR (Figure 6.3A). Inspection of an alignment of cyanobacterial InrS-like sequences (Figure 6.4) reveals conservation of a glutamate residue in this position (referred to here as position C) in all the sequences other than Gll4045. This homologue is predicted to be a copper sensor (Section 6.7) therefore bioinformatics analysis suggests that this observation may represent an alternative allosteric pathway in non-copper sensing cyanobacterial InrS homologues. Expansion of this bioinformatic analysis to include the 147 curated sequences used to seed the PFam model for the CsoR-RcnR family reveals that a sequence with Tyr in the A position always has a Glu or Asp residue in the B position and never a Glu or Asp in the C position, further supporting the possibility that this may represent an alternative allosteric pathway.

Although Glu and Asp are never represented in the C positions of sequences that have the AB motif Tyr-Glu (or Asp) other residues with side chains capable of forming hydrogen bonds are, for example in *S. lividans* CsoR a Lys residue is present in this position and inspection of the crystal structure of this protein (Dwarakanath *et al.* 2012) reveals that the orientation of the side chain of this residue could allow it to augment or buttress the hydrogen bonding allosteric network observed in *M. tuberculosis* CsoR (Figure 6.3B). Variations in this network that stabilise or de-stabilise the low DNA affinity state of the protein could tune the transcriptional response of genes regulated by this family of metalloregulators (see above).

Comparison of the crystal structures of Cu(I) bound *M. tuberculosis* (Liu *et al.* 2007) and apo *T. thermophilus* CsoR (Sakamoto *et al.* 2010) revealed the C-terminus of α2 was kinked in the copper bound protein, likely to accommodate Cu(I) binding. A similar phenomenon has now been observed by NMR upon Cu(I) binding to *Geobacillus thermodenitrificans* CsoR (Coyne III & Giedroc. 2012). Interestingly Glu63 of *M. tuberculosis* CsoR is located in this kinked region and its side chain points in the opposite direction to the copper liganding side chains of His61 and Cys65 (Figure 6.3C) which could allow an interaction with the side chain Gln76 of an adjacent protomer. Site directed mutagenesis coupled with fluorescence anisotropy to test bioinformatic predictions of potential allosteric pathways is a priority for future work.

6.4 Biological significance of coordination geometry

Two Ni(II) coordination geometries predominate in nickel responsive metalloregulators, octahedral and square planar (Iwig & Chivers. 2010). On the basis of spectral features (Figure 3.6) the Ni(II) coordination environment of InrS has tentatively been assigned as square planar although as stated earlier this awaits further experimental validation. For the purpose of this discussion a square planar assignment is assumed.

Why do InrS and *B. subtilis* CsoR bind Ni(II) with square planar geometry (Ma *et al.* 2009a) whereas *E. coli* RcnR binds Ni(II) with octahedral coordination geometry (Iwig *et al.* 2008)? The reason may simply be due to the presence of an N-terminal extension of InrS and *B. subtilis* CsoR relative to *E. coli* RcnR (Figure 3.2). *E. coli* RcnR is thought to coordinate Ni(II) using the deprotonated amine of the N-terminus and an insertional mutation extending the distance of the N-terminal amine to the metal binding site results in a square planar Ni(II) coordination geometry as revealed by UV-Vis spectroscopy and XANES analysis (Section 6.3.1). The natural N-terminal extension of InrS and *B. subtilis* CsoR makes it unlikely that either of these two proteins would exhibit a Ni(II) coordination site involving the N-terminal amine; with the available ligands a square planar geometry may be more easily adopted. Phylogenetic analysis suggests that InrS and *E. coli* RcnR share a more recent common ancestor than InrS and *B. subtilis* CsoR (Figure 6.5) suggesting that either the square planar Ni(II) coordination sites of InrS and *B. subtilis* CsoR evolved independently or that the octahedral Ni(II) binding site of *E. coli* RcnR evolved from an ancestral square planar Ni(II) binding site.

The adoption of this Ni(II) coordination geometry by InrS could have consequences for nickel homeostasis in *Synechocystis*. In *E. coli*, RcnR functions in concert with NikR to coordinate nickel homeostasis, and up-regulation of *rcnA* expression by RcnR does not occur until repression of the *nik* operon, by NikR, is maximal (Rowe *et al.* 2005; Iwig *et al.* 2006). An analogous situation exists in *E. coli* for control of zinc homeostasis by the metalloregulators Zur and ZntR (Outten & O'Halloran. 2001). NikR coordinates Ni(II) in a square planar site while RcnR does so in an octahedral site and this could provide an explanation for the coordinated control of nickel homeostasis, with the tighter binding square planar site of NikR preferentially gaining access to nickel. The presence of a square planar or octahedral site in nickel responsive metalloregulators characterised up to present has correlated with mode of action (Iwig & Chivers. 2010). Metal dependent co-repressors NikR (Schreiter *et al.* 2003; Phillips *et al.* 2008) and Nur (An *et al.* 2009) possess square planar sensory sites and metal dependent de-repressors RcnR

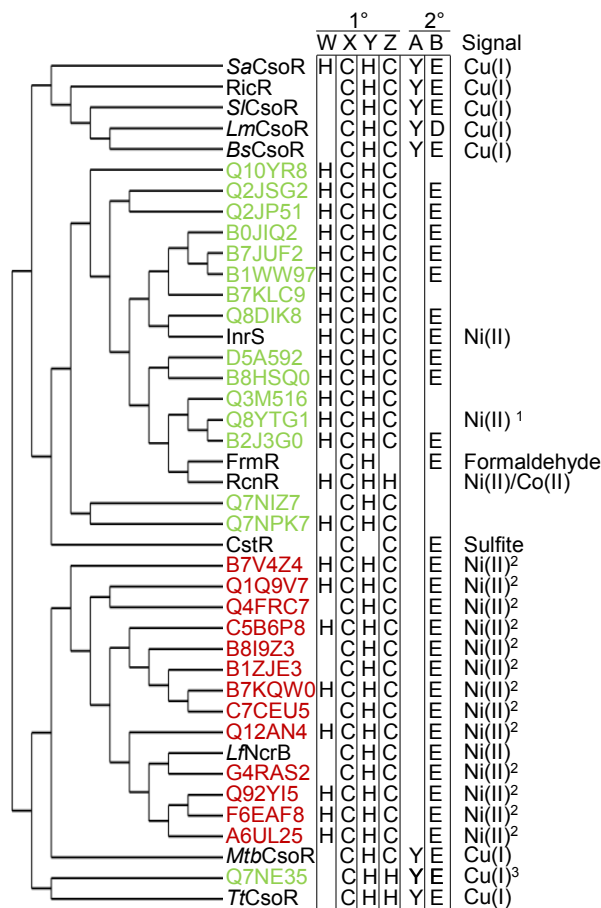


Figure 6.5. Phylogeny of selected CsoR-RcnR family proteins. Cladogram representing the relation of characterised CsoR-RcnR proteins (coloured black), cyanobacterial InrS-like proteins in organisms listed on Cyanobase (coloured green) and InrS-like proteins previously identified as being genetically proximal to genes encoding NrsD-like proteins (coloured red) (Foster *et al.* 2012). Protein sequences were aligned and the presence of a cysteine or histidine residue in the WXYZ motif positions and the presence of a tyrosine in the A position and the presence of either an aspartate or glutamate in position B noted. The known or predicted *in vivo* effectors are also listed. ¹ prediction based on the discovery of an InrS-like DNA binding site in the promoter region of an *nrsD*-like gene in this organism, ² predictions based on genetic proximity to *nrsD*-like genes, ³ prediction based on genetic proximity to a P-type ATPase and predicted copper chaperone encoding genes.

(Iwig *et al.* 2008), NmtR (Cavet *et al.* 2002; Pennella *et al.* 2003; Reyes-Caballero *et al.* 2011) and KmtR (Campbell *et al.* 2007) possess octahedral (or at least 5-coordinate in the case of KmtR) coordination geometries. The nickel coordination geometries of the unusual SrmRQ Ni(II)-dependent repressor complex (Kim *et al.* 2003) and the more recently discovered NimR, a MerR homologue, which unusually seems to act as an activator of nickel uptake in the apo state and repressor in the metal bound state (Kidd *et al.* 2011), remain to be determined. InrS departs from this established paradigm in that it is a nickel dependent de-repressor (Appendix Figure B2A, Figure 4.5 and 6.2) controlling nickel export (Appendix Figure B4A) that senses Ni(II) in a square planar site (Figure 3.6). This likely has physiological implications for the cell. Square planar sites in Ni(II) sensor proteins and Ni(II) trafficking proteins have been determined to lie in the picomolar range whereas octahedral sites have been found to have Ni(II) affinities in the nanomolar range. It may not be possible to engineer a Ni(II) site substantially tighter than that of the sensory site of InrS and therefore it is difficult to envisage Ni(II) homeostasis in *Synechocystis* being regulated in concert by analogy to nickel and zinc homeostasis in *E. coli*. Perhaps nickel acquisition in *Synechocystis* is not regulated or not directly regulated by nickel.

The identity of the nickel import system of *Synechocystis* has been inferred from bioinformatics but this remains to be confirmed experimentally (Rodionov *et al.* 2006). It will be very interesting to determine if the expression of this system is regulated by nickel or if expression is constitutive. Nickel limitation is known to be inhibitory to growth in certain cyanobacterial marine strains where it is required for nickel dependent SodN and urease activity (Dupont *et al.* 2008). Although *Synechocystis* does not contain a SodN using instead only the iron dependent SodB (Bhattacharya *et al.* 2004) it does contain a small cohort of nickel dependent enzymes (Section 1.10.1) including urease and hydrogenase. Perhaps limited availability of environmental nickel makes viable the trade-off of resources required to constitutively express the nickel import systems. Alternatively nickel import may be regulated by signals other than nickel for example the *nikABCDE* operon in *E. coli*, encoding a high affinity nickel uptake system, is known to be additionally regulated by FNR in response to anoxia (Wu *et al.* 1989) and control of nickel uptake in some marine cyanobacteria and diatoms has been shown to be regulated by nitrogen source (Price & Morel. 1991; DuPont *et al.* 2008).

6.5 Selective Ni(II) and Zn(II) sensing can be explained on the basis of relative affinity and access

The question of how sensing selectivity with regards to nickel, zinc, copper and cobalt is achieved in *Synechocystis* has been addressed in this work and possible solutions have been identified for nickel and zinc (Sections 5.3 and 5.6). All the metals tested in this study (Ni(II), Co(II), Zn(II), Cu(I), Cu(II)) were able to disrupt InrS:DNA complexes (Figures 4.5 and 5.14), suggesting allostery may be relatively unimportant in determining the correct response of InrS (Section 5.5.1). ZiaR is not allosterically competent to respond to Ni(II) and the same is predicted to be true of Zur (Patterson. 2010), however allosteric inhibition of these proteins by Ni(II) could still be problematic. Ni(II) and Zn(II) sensing was found to follow the relative affinity gradient; that is InrS has a tighter affinity for Ni(II) than the Zn(II) sensors ZiaR and Zur and the Co(II) sensor CoaR (Sections 4.2.1 and 5.3). The two Zn(II) sensors both have a tighter affinity for Zn(II) than the Ni(II) sensor InrS (Section 5.6). In addition to a relative affinity gradient between proteins InrS, ZiaR and Zur all display a binding preference for their cognate metals over non-cognate metals $\text{InrS } K_{\text{D, Ni(II)}} < K_{\text{D, Zn(II)}} < K_{\text{D, Co(II)}}$, $\text{ZiaR/ Zur } K_{\text{D, Zn(II)}} < K_{\text{D, Co(II)}} < K_{\text{D, Ni(II)}}$. Interestingly the metal binding preference of ZiaR and Zur with relation to Ni(II) and Co(II) deviates from the Irving-Williams series; this has been observed previously and it was suggested that constraints imposed by the metal binding site may be able to subvert the relative order of the Irving-Williams series (Pasternak *et al.* 2001). If the affinity of the metalloregulators defines the buffered concentration of cytosolic metal (Section 1.11) available concentrations of Zn(II) and Ni(II) will be buffered (through export (and additionally for Zn(II) the cessation of import)) such that levels do not raise high enough to populate the sensors of other metals (Figure 6.6).

The selective sensing of Co(II) by CoaR cannot operate on the basis of relative affinity (Section 5.4 and Figure 6.6). CoaR has surface exposed hydrophobic patches (Section 5.2) suggesting it might be membrane associated *in vivo* and is additionally fused to a domain with homology to precorrin isomerase, an enzyme involved in B₁₂ biosynthesis (Section 1.10.2). Enzymes in the B₁₂ biosynthesis pathway are known to be membrane associated (Maggio-Hall *et al.* 2004; Zayas *et al.* 2007) and one of the homologues of precorrin isomerase present in *Synechocystis* (Slr1467) has been shown to be membrane associated by proteomics (Mata-Cabana *et al.* 2007). Work conducted in parallel to this study revealed that residues predicted from structural modelling to bind a tetrapyrrole in

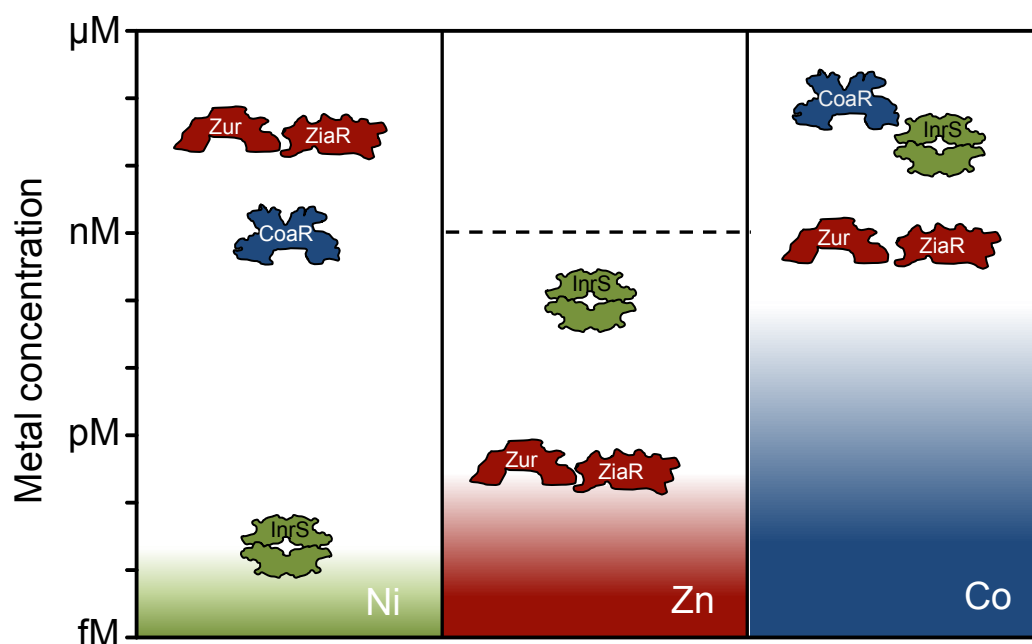


Figure 6.6. Graphical representation of the Ni(II), Zn(II) and Co(II) affinities of the metalloregulators of *Synechocystis* and the proposed buffered concentrations of Ni(II), Zn(II) and Co(II). The position of each sensor reflects the equilibrium binding affinity determined for Ni(II), Zn(II) or Co(II). The coloured fill represent the proposed buffered concentration of each element based on the Ni(II) affinity of InrS and the Zn(II) affinities of ZiaR and Zur. The buffered level shown for Co(II) is set below the Co(II) affinities of ZiaR and Zur which do not respond to Co(II) at equilibrium in spite of their competence to do so (Patterson *et al.* 2013). The dashed line in the Zn(II) Section represents the postulated buffered concentration of Zn(II) following a 1 h exposure to maximum non-inhibitory [Zn(II)] based on the work of Wang *et al* (2011). The concentration of Ni(II) is buffered such that the other sensors do not gain access to this metal. This is also the case for Zn(II) under steady state conditions but a transient rise in buffered Zn(II) concentration following exposure is predicted to allow InrS access to Zn(II).

the precorrin isomerase domain of CoaR are required for cobalt responsiveness in a *lacZ* reporter gene assay (Patterson *et al.* 2013). These results suggest that CoaR may sense a different cobalt pool to that available to the other cytosolic metalloregulators of *Synechocystis* either by virtue of its predicted membrane association or it may actually sense an intermediate in the B₁₂ pathway *in vivo* rather than cobalt directly. Alternatively the binding of a tetrapyrrole to CoaR may increase its affinity for Co(II). Investigation of cobalt sensing by CoaR highlights the importance of considering the cellular environment of a metalloregulator in its selective response. CoaR binds Ni(II) more tightly than Co(II) (Figures 5.6, 5.7 and 5.13) however the presence of InrS (which is proposed to maintain buffered Ni(II) concentrations sufficiently low that CoaR does not bind Ni(II)) in the shared cytosol provides an explanation for why Co(II) sensing by CoaR is not blocked by Ni(II). The unfavourable thermodynamic gradient for Co(II) binding between CoaR and ZiaR & Zur (Section 5.4 and Figure 6.6) highlighted the need to find alternative solutions for how cobalt homeostasis is maintained (Patterson *et al.* 2013).

Selective sensing of Co(II) by InrS cannot be explained in terms of relative affinity (Section 5.4 and Figure 6.6) however analysis of *nrsD* expression in response to cobalt in the $\Delta nrsB$ promoter mutant (Figure 6.2) suggests that the observed cobalt dependent transcriptional response of *nrsD* may be solely dependent on activity of the upstream *nrs* promoter (Section 6.2). Alternatively, given that NrsD has been reported not to contribute to cobalt tolerance *in vivo* (García-Domínguez *et al.* 2000) the response of InrS to cobalt (if indeed one exists *in vivo*) may be gratuitous. As InrS and NrsD have evolved in a common cell presumably their affinities for nickel are well matched. There would seem to be little rationale for InrS to respond to buffered nickel concentrations of $\sim 10^{-14}$ M if NrsD could not export nickel under these conditions due to a substantially weaker nickel affinity. The expression of NrsD in response to cobalt may not affect nickel homeostasis under conditions where the bioavailable concentration of nickel is not high enough to activate InrS and equally NrsD may not be competent to export cobalt. However in this latter scenario, regardless of whether the response of InrS to cobalt is gratuitous, under steady state conditions InrS appears responsive to cobalt whereas ZiaR and Zur do not despite being competent to respond to Co(II) *in vitro* (Patterson *et al.* 2013); therefore the first explanation of the apparent response of InrS to cobalt seems more likely.

The Zn(II) affinities of ZiaR and Zur are poised such that intracellular zinc levels should be buffered below the $K_{D, \text{Zn(II)}}$ of InrS (Figure 6.6) and therefore it is predicted that the actions of these two proteins will act to buffer the concentration of zinc such that InrS is effectively denied access to this metal. But what about under conditions where the intracellular zinc level may transiently rise, such as shortly after addition of exogenous zinc to cell cultures? It has been shown in *E. coli* that intracellular free Zn(II) concentrations rise transiently from picomolar to nanomolar concentrations after addition of zinc to the growth medium (Wang *et al.* 2011). If a similar situation were to occur in *Synechocystis*, following zinc exposure InrS would be predicted to aberrantly respond to zinc.

CyanoEXpress is a new database repository of *Synechocystis* microarray data (Hernandez-Prieto & Futschik. 2012). Using this website it was possible to see that in a previous study *nrsD* expression was indeed increased > 4 fold 30 min after treatment of cells with 776 μM Zn(II). This increase fell to >1.4 fold after 240 min (GEO accession: GSE3716, currently unpublished study). Longer exposure periods and an assessment of *nrsB* transcription were not included in this study.

RT-PCR was employed to determine if there is an increased abundance of *nrsD* transcripts in cells upon short term exposure to zinc (Figure 6.7). Following a 1 h exposure to maximum non-inhibitory concentrations of zinc there is an increase in the abundance of *nrsD* transcripts showing that when InrS gains access to Zn(II) *in vivo* it does indeed respond as predicted from the *in vitro* analysis (Figure 5.14) before returning to steady state at 48 h, where a response is observed only with nickel addition (Figure 6.7A). Primers specific to the *nrsCD* intergenic region were included as a control in this analysis and although a contribution to *nrsD* transcript abundance from readthrough from the *nrsB* promoter initiated transcripts is suggested, the greater abundance of *nrsD* over *nrsCD* implies InrS is aberrantly responding to zinc (Figure 6.7A). As discussed in Section 6.2, RNA polymerase transcribing from the *nrsB* promoter could dislodge InrS and expose the *nrsD* promoter to RNA polymerase. To address this issue the same analysis was carried out in the *nrs* promoter deletion strain (Figure 6.7B). Here with the effects of readthrough or InrS displacement removed a transient response of InrS to exogenous zinc addition is still observed (Figure 6.7B). Interestingly there is an elevated basal expression of *nrsD* in this strain, which is most evident in the 48 h exposure samples (Figure 6.3B). Perhaps the basal level of available nickel is higher in this strain due to the inability to express *nrsBAC*. It remains formally

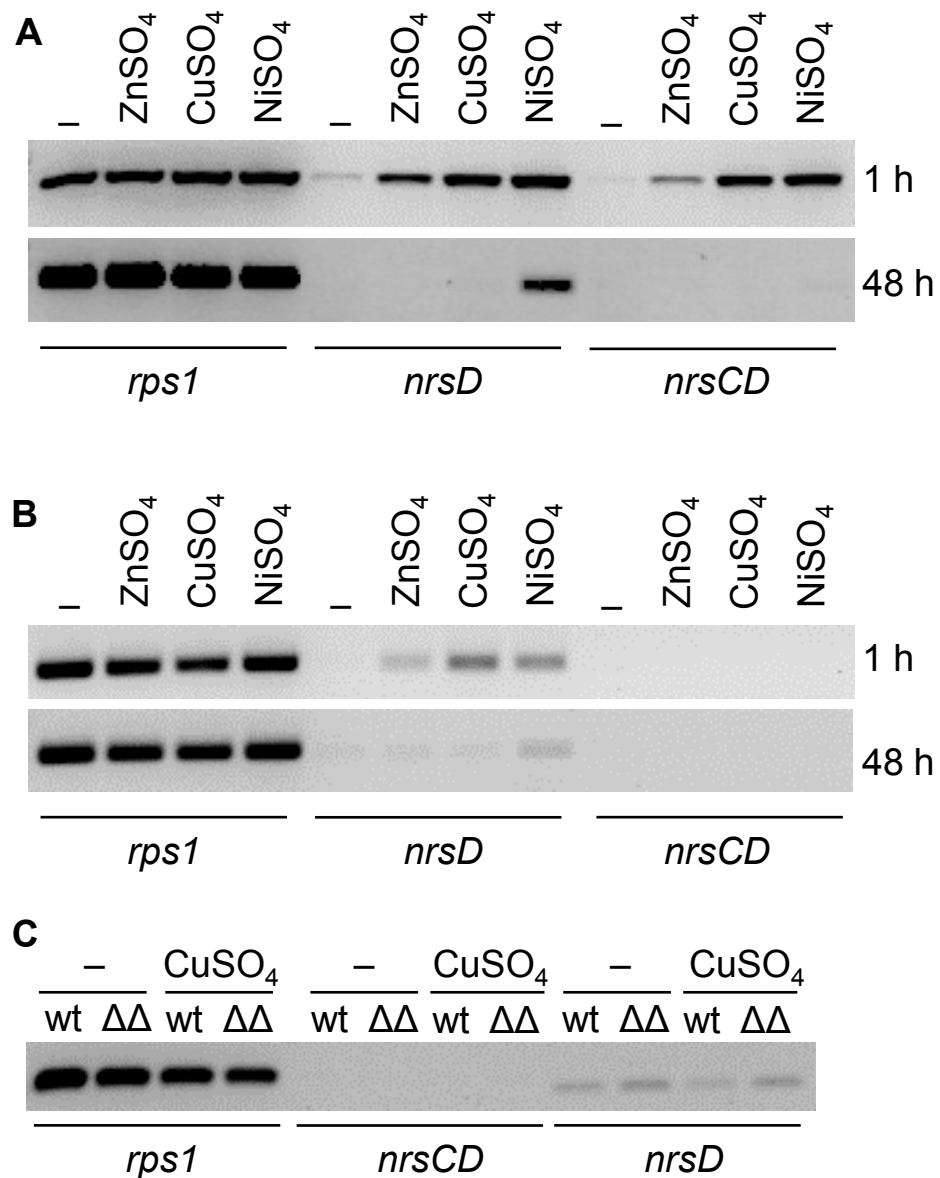


Figure 6.7. InrS responds transiently to both copper and zinc *in vivo* and Atx1 may play a subtle role in withholding copper from InrS under standard but not high copper conditions. A. RT-PCR analysis of *nrsD*, *nrsCD* (transcript spanning the *nrsCD* intergenic region) and *rps1* transcript abundance in wild type *Synechocystis* cells exposed to the maximum non-inhibitory concentration of NiSO₄ (0.5 μM), ZnSO₄ (12 μM) and CuSO₄ (1 μM) for either 1h (upper panel) or 48 h (lower panel). B. RT-PCR analysis of *nrsD*, *nrsCD* and *rps1* transcript abundance in Δ*nrs* promoter cells exposed to the maximum non-inhibitory concentration of NiSO₄, ZnSO₄ and CuSO₄ for wild type cells for either 1h (upper panel) or 48 h (lower panel). The maximum non-inhibitory concentration of NiSO₄, ZnSO₄ and CuSO₄ for Δ*nrs* promoter cells remains to be determined and it is formally possible that a decreased tolerance to these metal salts in this strain may have influenced the outcome of this analysis. C. RT-PCR analysis of *nrsD*, *nrsCD* and *rps1* transcript abundance in wild type (wt) and Δ*atx1*Δ*gshB* (ΔΔ) *Synechocystis* cells grown under standard conditions or exposed to the maximum non-inhibitory concentration of CuSO₄ for 48h. Analysis was performed by Rafael Pernil.

possible that the displacement of Ni(II) from other binding sites by Zn(II) is responsible for the apparent response of InrS to zinc.

This analysis suggests that the bioavailable levels of zinc are elevated to at least higher than 10^{-10} M (the affinity of InrS for zinc, Section 5.6) following exposure to exogenous zinc and suggests that the two zinc sensors of *Synechocystis* (along with InrS) become activated simultaneously. This is in accordance with a previous study that demonstrated a simultaneous induction of *E. coli* ZntR and Zur upon addition of high concentrations of exogenous zinc to the growth medium (Yamamoto & Ishihama. 2005b). However the activation of ZntR is quickly alleviated (Yamamoto & Ishihama. 2005b) and this is thought to be due to the intrinsic instability of ZntR to proteolytic degradation (Pruteanu *et al.* 2007). These results challenge the model of sequential activation of pairs of metalloregulators that sense the same metal in a shared cytosol as bioavailable metal concentrations rise, for example ZntR & Zur (zinc) (Outten & O'Halloran. 2001) and NikR & RcnR (nickel) (Iwig & Chivers. 2010) in *E. coli*.

The degree to which exogenous zinc treatments used in this study represent the conditions experienced by the organism in the wild is debatable. Are metalloregulators primarily responsible for maintaining metal homeostasis in response to low metal flux, for example during metalloenzyme turnover, or do sensors exist in an environment of high metal fluxes as created in laboratory experiments? The answer is perhaps that both are true and dependent on the organism and the environment inhabited. For example; copper mediated killing of bacteria in the phagosomal compartments of macrophages is thought to represent an important defence mechanism (Hodgkinson & Petris. 2012) and the survival of *Salmonella* in the macrophage has shown to be dependent on the functionality of either of the copper translocating P-type ATPase genes *copA* and *golT* (White *et al.* 2009; Osman *et al.* 2010). Both these genes are regulated by cytosolic metal sensors of the MerR family (Checa *et al.* 2007; Espariz *et al.* 2007) which presumably experience a high copper flux under these conditions. Additionally, growth rates in the wild will be slower than under laboratory conditions with many factors limiting to growth and consequently a lower metal concentration may constitute an equivalent dose.

6.6 Selectivity against Cu(I) sensing by InrS cannot currently be explained by allostery, affinity or access

InrS can bind Cu(I) very tightly (Figure 5.19) and both Cu(I) and Cu(II) are capable of driving the allosteric mechanism of InrS (Figures 5.14 and 5.15). Cu(II) is thought to be absent from the cytosol and so is predicted not to interfere with InrS function however the degree to which Cu(I) stabilises the off DNA form of InrS is equivalent to that of Ni(II) (Section 5.5.2). Given that this is the case why does InrS not function as a cytosolic copper sensor under steady state conditions? Copper availability in the cytosol of *Synechocystis* is known to be tightly controlled as a protein, MncA, with a 10,000 fold preference for Cu(I) or Cu(II) over Mn(II) is able to acquire Mn(II) in the cytosol (Tottey *et al.* 2008). Copper is not required for any cytosolic protein sites but is trafficked to the thylakoids where it is required for plastocyanin and cytochrome oxidase by the copper chaperone Atx1 (Tottey *et al.* 2002). More recently it has been shown that Atx1 plays a linked role preventing copper-mediated cellular damage by preventing mis-location of copper to sites for other metals (Tottey *et al.* 2012). A mutant deficient in *atx1* and glutathione synthase activity ($\Delta gshB$) showed hypersensitivity to elevated concentrations of exogenous copper, which was correlated with copper mis-location to the iron-sulphur clusters of the dehydratase enzyme required for branched chain amino acid biosynthesis and the Zn(II) sensory site of Zur (Tottey *et al.* 2012). It was therefore hypothesised that Atx1 may contribute to withholding Cu(I) from InrS due to a lack of specific interaction, in spite of the tighter Cu(I) affinity of InrS, and therefore contribute to selectivity against sensing of this element *in vivo*. Short term (1 h) exposure to elevated exogenous copper concentrations caused an increase in abundance of *nrsD* transcripts consistent with copper mislocating to the sensory site of InrS (Figure 6.7A) and this effect was also observed in the Δnrs promoter mutant (Figure 6.7B) showing this effect is not dependent on the activity of the *nrsB* promoter. In the $\Delta atx1 \Delta gshB$ double mutant a very subtle elevation in *nrsD* transcript is evident relative to the wild type (Figure 6.7C). This effect is not dependent on the addition of exogenous copper (Figure 6.7C). These results suggest that the copper chaperone Atx1 (and glutathione) may play a minor role in withholding copper from the sensory site of InrS under standard conditions however is unlikely to be responsible for the dramatic reduction in copper dependent *nrsD* expression between 1 and 48 h post copper addition (Figure 6.7 A and B). Given this result it remains unclear how selectivity against copper sensing by InrS is achieved in *Synechocystis* and this represents an exciting opportunity for further study.

6.7 Prediction of metals sensed by CsoR-RcnR family members on the basis of sequence

Prior to the start of this work it was postulated that the selectivity of metalloregulators of the CsoR-RcnR family could be inferred on the basis of the WXYZ motif (Section 3.1). On the basis of the WXYZ motif InrS could have been predicted to function as a copper sensor. InrS, despite displaying highly similar metal dependent spectral features to *B. subtilis* CsoR (Section 3.3) and utilising the same ligands for cognate metal binding as used by CsoR for Cu(I) binding (Section 4.3), functions as a Ni(II) sensor (Appendix Figure B2A and 6.2). Are there any sequence features that can be used to predict the selectivity of CsoR-RcnR proteins? Alignment of the cyanobacterial CsoR-RcnR homologues reveals a common XYZ motif of Cys-His-Cys other than in one case; Gll4045 (Uniprot ID: Q7NE35) which has the XYZ motif Cys-His-His (Figure 6.4). Previously Gll4045 may have been predicted to encode a Ni(II)/ Co(II) sensing RcnR-like protein and the other homologues copper sensing CsoR-like proteins. Inspection of the genomic context of *gll4045* reveals it is co-localised with a gene coding for a copper chaperone and a P-type ATPase and is therefore highly likely to encode a copper sensor. The genomic context of all other cyanobacterial homologues were examined and in no case was the gene localised with genes coding for copper chaperone or a P-type ATPase, although this does not formally rule out a function for these proteins as copper sensors. Therefore on the basis of the XYZ motif an erroneous assignment as to the function of Gll4045 would have been made. In fact the other CsoR-RcnR proteins from the same organism, Glr0048 (Uniprot ID: Q7NPK7) and Gll2035 (Uniprot ID: Q7NIZ7), would have been predicted to play the role of copper sensor. Closer inspection of the alignment reveals that Gll4045 is the only protein to have a Tyr and Glu residue in the AB positions (although over 50 % of the representatives have a Glu in the B position) (Figure 6.4). Figure 6.5 shows a phylogenetic analysis together with the known or predicted residues in the primary and secondary coordination spheres of previously characterised CsoR-RcnR family proteins along with all cyanobacterial InrS-like proteins represented in Cyanobase and InrS homologues that are encoded proximal to *nrsD*-like genes in other organisms and are therefore predicted to sense Ni(II). This analysis reveals that the originally postulated WXYZ motif of His-Cys-His-His for Ni(II)/Co(II) sensing members of the family and X-Cys-His-Cys for Cu(I) sensing members of the family is a poor predictive tool. The presence of a tyrosine residue in the A position and a residue with a carboxylic acid side chain in the B position corresponds with the known or predicted function as a Cu(I) sensor (Figure 6.5). The

identity of residues in the AB position is a better indicator as to the function of a member of the CsoR-RcnR protein family, although as shown in the course of these studies a secondary coordination sphere containing Tyr and Asp or Glu is not obligatory for a CsoR-RcnR family protein to be allosterically competent to respond to Cu(I) both *in vitro* and *in vivo* (Figures 5.14, 5.15 and 6.7).

This alignment of cyanobacterial CsoR-RcnR homologues also reveals that the presence of an N-terminal His-rich extension is a common feature of these proteins (Figure 6.4). The function of this extension remains to be discovered.

6.8 Affinities and an associative biology in the cell

The measured binding constants of many metalloregulatory proteins are very tight. There is debate as to what, for example, the zepto and femtomolar sensitivity of *E. coli* CueR (Changela *et al.* 2003) and ZntR (Hitomi *et al.* 2001; Outten & O'Halloran. 2001) mean in the context of the cell. One atom per cell is approximately a nanomolar concentration (Changela *et al.* 2003) and so the tight affinities of many metal sensors imply there are essentially no free atoms (i.e. unbound by any ligand other than water) of the element they sense. Under these conditions metal transfer between sites would be expected to be very slow. This can be illustrated by considering the example of NmtR becoming allosterically inhibited with Zn(II). Zn(II) was shown to bind more avidly to NmtR than Ni(II) as demonstrated by competitive binding chromatography experiments (Cavet *et al.* 2002). The Ni(II) affinity of tightest site of NmtR has more recently been estimated as $1.2 \times 10^{10} \text{ M}^{-1}$ (Reyes-Caballero *et al.* 2011). Although the Zn(II) affinity of NmtR has not quantitatively been determined, NmtR binds Zn(II) in an equivalent site to *S. aureus* CzcA (Pennella *et al.* 2003) where the Zn(II) affinity of the tightest site is estimated as $2.5 \times 10^{12} \text{ M}^{-1}$ (Pennella *et al.* 2006) and so it is reasonable to assume the Zn(II) affinity of NmtR may be similar to this. This difference in affinities means that under equilibrium conditions a large effective molar excess of Ni(II) over Zn(II) would be required to preferentially populate NmtR with Ni(II). However, assuming a Zn(II) on rate of $10^7 \text{ M}^{-1} \text{ s}^{-1}$ (the rate constant for Zn(II) association with a zinc finger domain peptide (Buchsbaum & Berg. 2000)) the off rate of Zn(II) from NmtR would be $4 \times 10^{-6} \text{ s}^{-1}$ giving a half time for Zn(II) dissociation of $\sim 69 \text{ h}$. In the lifetime of a cell (*M. tuberculosis* has a doubling time of 24 h (Ginsberg & Spigelman (2007)) Ni(II) would not replace Zn(II) on NmtR even if Ni(II) was present in a vast excess.

Equilibrium binding constants are a measure of exchange from free solution, however there is a view emerging that metal exchange in the cell (particularly for highly competitive metals) occurs via associative rather than dissociative exchange (Hitomi *et al.* 2001; Foster *et al.* 2012). The cellular environment is rich in organic acids plus the adventitious ligands provided by proteins, nucleic acids as well as membranes and lipids. Exchange via this polydisperse buffer (which can be thought of as metal ions ‘walking’ between metal sites gradually travelling down the affinity gradient by analogy to a protein folding free energy landscape with funnels of various depth) may act to increase the rate of metal transfer. In such a model maybe the affinity of metal sensors should be considered relative to the affinity of the polydisperse buffer. The equilibrium binding constants still serve as a useful guide of relative affinity but exchange between sites is predicted to be much faster. Ni(II) coordinated to histidine has recently been shown to be the substrate transported by the *E. coli* NikABCDE nickel uptake system (Chivers *et al.* 2012) and therefore it is reasonable to speculate that histidine coordinated Ni(II) may represent a major intracellular Ni(II) pool. SlyD increases the rate at which Ni(II) is released from HypB (both proteins implicated in the delivery of Ni(II) to hydrogenase in *E. coli*) to EDTA, decreasing the half time of Ni(II) transfer from 24 h to 73 min (Kaluarachchi *et al.* 2011) demonstrating how the kinetics of metal exchange may be enhanced in the cellular environment.

Another school of thought maintains that tight affinities of metalloregulator proteins allow them to respond rapidly when a ‘free’ metal atom becomes available i.e. when the intracellular concentration approaches nanomolar. A recent study correlated the regulatory response of *E. coli* ZntR with a rise in buffered Zn(II) concentration from picomolar to nanomolar, suggesting that *in vivo* ZntR responds to nanomolar concentrations of Zn(II) (Wang *et al.* 2012) rather than femtomolar as suggested by the equilibrium zinc binding affinity of ZntR (Hitomi *et al.* 2001; Outten & O’Halloran. 2001). In this model the sensing of metals for which equilibrium binding constants are relatively tight becomes a stochastic event; for example a free Ni(II) ion in *Synechocystis* (given a buffered Ni(II) concentration of $\sim 10^{-14}$ M) would occur only in one cell in 100,000 or 1/100,000 of the time (Foster *et al.* 2012). Data obtained in the course of these studies challenges this model. Under steady state conditions Zur and ZiaR respond to zinc (Thelwell *et al.* 1998; Tottey *et al.* 2012) but InrS does not (Appendix Figure B2A and Figure 6.7). If Zur and ZiaR responded to zinc only when free atoms of zinc were available (as the zinc concentration approached nanomolar) then InrS could reasonably be expected to also respond to zinc under steady state conditions

given its zinc binding affinity of $\sim 10^{-10}$ M (Section 5.6) and its allosteric competence to do so (Figures 5.14). Given that this is not the case these observations support a model where metals are acquired by metalloregulators via exchange with the polydisperse buffer rather than from free solution.

If metal exchange did occur via free solution the tight affinities of many metalloregulators additionally raises the question of how the transcriptional response is switched off. The simplest explanation is that the metalloregulators are turned over and new apo-protein produced however this could require a significant input of resources particularly for very abundant metalloregulators, some of which may be present on the order of thousands of molecules per cell (Section 6.9.3). Additionally ZntR has been found to be stabilised against proteolytic degradation in the zinc bound form (Pruteanu *et al.* 2007). MerD has been proposed to assist in the removal of mercury bound MerR from DNA (Section 1.7) and apo-CueR has been shown to assist in the removal of Cu(I) bound CueR from DNA (Joshi *et al.* 2012). In the absence of widespread evidence of these models, particularly outside of the MerR family of metalloregulators, metal removal via the polydisperse buffer remains a parsimonious explanation for how a metalloregulators transcriptional response is switched off.

6.9 Future work

6.9.1 Opportunities for further study based on bioinformatics results

A model for metalloregulation by Slr0240 a protein with homology to CopY/BlaI

During the course of this work opportunities for further work based on bioinformatics results have arisen. One potential avenue for further study is the possibility that Slr0240 (the CopY homologue of *Synechocystis*) may act as a metalloregulator by a novel mechanism.

A bioinformatics approach was taken to predict the likelihood of Slr0240 acting directly as a metalloregulator.

E. hirae CopY binds a Zn(II) ion in a C-terminal four cysteine residue motif and this Zn(II) ion is displaced when the copper chaperone CopZ delivers copper to CopY (Cobine *et al.* 2002a and b). The replacement of the metal coordinated by this motif regulates the action of the protein (Cobine *et al.* 2002a and b). Slr0240 lacks this C-

terminal Cys residue motif and so the mode of action of this protein must be regulated differently to CopY. CopY proteins display homology to *S. aureus* BlaI, which acts as a repressor of *blaZ* encoding a β -lactamase and thus plays a key role in β -lactam resistance in methicillin resistant *S. aureus* (MRSA) (Zhang *et al.* 2001; Portmann *et al.* 2006; Llarrull *et al.* 2009). BlaI works in conjunction with an integral membrane protein called BlaR1, which contains a cytosolic zinc-dependent metallo-endopeptidase domain on loop 3 of the four transmembrane helices (Hanique *et al.* 2004). When β -lactam is detected in the extra-cellular space, which is thought to occur through the acylation of a key serine residue (Thumanu *et al.* 2006), BlaR1 undergoes autolytic cleavage releasing the metallo-endopeptidase domain which proteolyses BlaI allowing transcription of the β -lactamase (Berzigotti *et al.* 2012; Llarrull & Mobashery. 2012). The gene immediately downstream of *slr0240*, *slr0241*, is predicted to encode an integral membrane protein with four transmembrane helices like BlaR1 with a zinc-dependent metallo-endopeptidase domain (with His-Glu-X-X-His zinc binding motif) located between helices 3 and 4 (Figure 6.8). However, the product of *slr0241* lacks the C-terminal COG2602 extracellular domain predicted to detect β -lactams in BlaR1. Excitingly, it has recently been shown that fragmentation of BlaR1 can occur in the absence of antibiotics and that the endopeptidase activity of the enzyme is metal ion dependent (Llarrull & Mobashery. 2012). Thus the mode of action of Slr0240-2041 could involve acquisition (perhaps through delivery) of Zn(II) by Slr2041 to activate its endopeptidase activity followed by proteolysis of Slr0240 by fragmented Slr0241, although the target for regulation remains unknown. As Slr0240 is unlikely to sense metals directly it was excluded from the study of relative affinity however this regulatory system represents an exciting opportunity for future work.

The role of genes genetically linked with *inrS*

Immediately downstream of *inrS* (*sll0176*) is a gene encoding a hypothetical protein predicted to function as a DNA invertase (*sll0177*). Given the proximity of this gene to *inrS* it is possible they are co-transcribed and this remains to be investigated. Upstream of *sll0176* is a small ORF (*ssl0312*) predicted to encode a 66 amino acid protein of unknown function. In a large scale analysis of protein-protein interaction in *Synechocystis* the product of *ssl0312* was the only protein observed to interact with the product of *sll0176* and *vice versa* (Sato *et al.* 2007). Of course it is possible that this observed interaction is due to the proximity of translation of these two proteins. Additionally this small protein is enriched in potential metal binding residues (3 His, 5

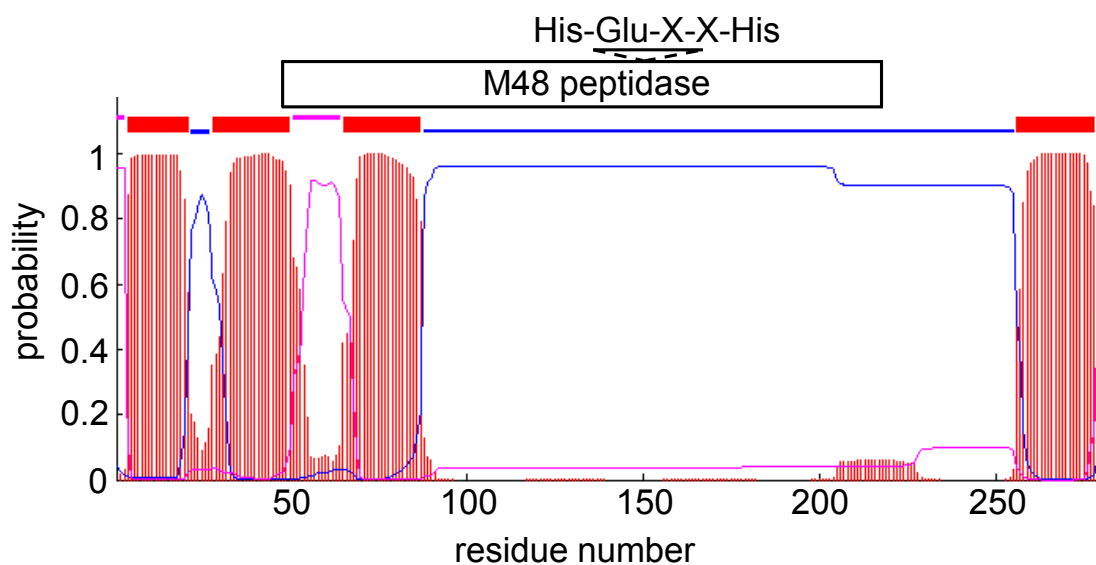


Figure 6.8. Predicted membrane topology of Slr0241. Produced using the TMHMM server V 2.0. The red line on the probability scale represents predicted transmembrane regions and the blue & pink lines on the probability scale represent regions predicted to be inside and outside the membrane respectively. The same colour scheme applies to the coloured blocks above the scale which also represent these regions. The region of the protein with homology to the M48 peptidase superfamily as predicted by the NCBI protein BLAST tool is indicated along with the position of the His-Glu-X-X-His Zn(II) binding motif.

Asp, 5 Glu) both of these observations may be consistent with the product of this small ORF playing a role in metal ion homeostasis with InrS. This small protein is poorly conserved in other bacteria. Could it play a role unique to Ni(II) homeostasis in *Synechocystis*?

6.9.2 Controlling the buffered intracellular concentration of metal ions by engineering metalloregulators in order to create useful phenotypes

The role of the NiFe hydrogenase of *Synechocystis* is not fully understood although under some conditions it is believed to act as an ‘electron valve’, dissipating the excess reducing potential of the light reactions of photosynthesis (Appel *et al.* 2000). In many cyanobacteria the activity of hydrogenase is known to be nickel limited (Xiankong *et al.* 1984; Daday *et al.* 1985; Oxelfelt *et al.* 1995; Axelsson & Lindblad. 2002). InrS regulates the expression of *nrsD* (Appendix Figures B1 & B2 and Figure 6.2) and cells constitutively expressing *nrsD* due to lack of InrS have reduced total cellular nickel quotas (Appendix Figure B4). The increased photoprotective pigment production in Δ *inrS* cells (Section 3.6) (Figure B4) is consistent with a need to dampen the light reactions of photosynthesis to cope with the reduced availability of nickel to cofactor hydrogenase. In *Helicobacter hepaticus* deletion of *nikR* results in increased activity of the nickel dependent hydrogenase and urease enzymes and this correlates with increased total cellular nickel quota but there was no change in the abundance of the urease complex suggesting this increased activity was due to additional nickel made available by an inability to repress expression of the high affinity nickel importer NikABCDE (Benoit *et al.* 2012).

The view that the affinities of metalloregulators for their cognate metal dictate the buffered concentration of that element and therefore the metal available to cofactor metalloproteins is widely held but so far remains to be formally tested experimentally (Section 1.11). Nickel homeostasis in *Synechocystis*, which is in part regulated by InrS, represents an opportunity to test this hypothesis. Nickel is only required for a few metalloproteins in *Synechocystis* (Section 1.10.1), including hydrogenase and urease, and so should provide a simple system for analysis of nickel availability. It should be possible to test the idea that the affinity of a metalloregulator determines the buffered concentration of metal available to cofactor metalloproteins by transforming *Synechocystis* with InrS variants that are allosterically competent but bind Ni(II) more weakly (such as InrS His21→Leu (Section 4.3.5)) and monitoring nickel dependent enzyme activity in these strains. It is possible that nickel export by the proteins encoded

by *nrsBAC* may compensate for the reduced expression of *nrsD* and so it may be necessary to utilise the $\Delta nrsB$ promoter (Section 6.2 and Figure 6.2) as a background strain which is solely dependent on NrsD for Ni(II) export.

Progress has been made in the development of tools for the visualisation of intracellular metal ions including fluorescent probes for measuring the buffered concentration of bioavailable metal ions (Dean *et al.* 2012). However there are few Ni(II) specific fluorescent probes for imaging intracellular Ni(II). The specific Ni(II) sensor Nickelsensor-1 has a Ni(II) affinity of 193 μM (Dodani *et al.* 2009) and would therefore not be suited for measuring bioavailable nickel in *Synechocystis* where the buffered concentration may reflect the affinity of InrS for Ni(II). Therefore a need exists for the development of specific Ni(II) chelators with a range of affinities. Genetically encoded fluorescent sensors offer advantages over small molecule sensors; by basing the metal binding domain on a metalloprotein the affinity of the sensor will be poised in a biologically relevant range. The Zn(II) sensor CAII_FP is based on carbonic anhydrase and has a Zn(II) affinity in the picomolar range (Wang *et al.* 2011). The major limitation of these sensors is obviously the inability to use them in cells where it is not trivial to express these sensors or in the diagnosis of disease. It may be possible to measure the buffered concentration of Ni(II) in mutant *Synechocystis* strains using newly developed Ni(II) probes in addition to indirectly via enzymatic activity.

There is currently interest in the development of renewable fuel sources both to curb environmental impact and to provide fuel security. Biohydrogen production by cyanobacteria offers an attractive route of being able to couple photosynthesis to hydrogen production; turning sunlight into a storable form of energy. Many challenges have been identified in the optimisation of hydrogen production using cyanobacteria such as the oxygen sensitivity of the enzyme and availability of reducing agents (Quintana *et al.* 2011). In addition the Ni(II) limitation of hydrogenase activity in many cyanobacteria suggests that availability of Ni(II) to cofactor the enzyme may be another challenge that needs to be overcome. As 41 % of enzymes require a metal ion at their catalytic centre (Andreini *et al.* 2008) the success of efforts in synthetic biology may be largely dependent on the ability to cofactor enzymes with the necessary metal ion (Waldron & Robinson. 2009). Altering the buffered concentrations of metal ions by altering the affinities of metalloregulators may represent a way to achieve this. It may also be possible to engineer different strains of *E. coli* with different buffered concentrations of different metals for the production of specific recombinant

metalloproteins. Recently it was found that the *E. coli* strain BL21(DE3) commonly used for the production of recombinant proteins has a nonsense mutation in the gene coding for the apoxia sensor FNR (Pinske *et al.* 2011). This led to complete inactivity of the four NiFe hydrogenases encoded by this strain; this inactivity could be overcome by the addition of nickel to the growth media which overcomes the inability of this strain to express the NikABCDE nickel uptake system (Pinske *et al.* 2011). Therefore the default strain for production of recombinant proteins is likely unsuitable for the production of recombinant proteins co-factored with nickel and highlights the need for considered selection of strains for the production of recombinant metalloproteins.

6.9.3 Understanding the metalloregulatory circuits of the cell

The metal affinities of a sub-set of metalloregulators from a single organism (Sections 4.2.1, 4.2.2, 5.3, 5.4 and 5.6) measured in the course of this study represent an important step in understanding the selective transcriptional response of a cell to metal stress. In order to fully understand the metalloregulatory circuits of the cell data on additional parameters will need to be collected. These will include the degree of allosteric coupling on both cognate and non-cognate metal coordination, information on the relative abundance of metal sensor proteins *in vivo* and an appreciation of metal exchange kinetics in the presence of the polydisperse buffer. With sufficient knowledge of these systems it may be possible to subvert these sensory circuits for potential applications in synthetic biology or in the design of novel antimicrobials.

It should be possible to start investigating the hypothesis that metal exchange reactions may be accelerated in the cellular environment by virtue of the polydisperse buffer. In the first instance this may involve monitoring Ni(II) exchange from EGTA to InrS in the presence of biologically relevant small molecules such as histidine. Experiments could advance to being carried out in the presence of cell lysate to provide a closer approximation of the effect of the polydisperse buffer. Computer simulations have been used to show that group 1 and 2 metals will not exchange bound water ligands for small inorganic anions but will exchange these water molecules for the negatively charged side chains of Asp and Glu residues in metalloprotein binding sites (Dudev & Lim. 2008). Given an estimate of the concentrations of the most abundant metal chelating small molecules present in the cell (such as glutathione) and their affinity for metal ions it may be possible to expand these simulations to model the effect of the polydisperse buffer on metal transfer.

Little is known about the relative abundance of metalloregulators. This is an important parameter in understanding the response of the cell to metal stress as a greater abundance of a sensor may overcome unfavourable affinity gradients through mass action. This may be particularly important for metal dependent co-repressors where metal binding to a single sensor protein will repress expression of the gene regulated. For metal dependent de-repressors where the apo form of the protein has a tighter DNA affinity the prediction is that the entire pool of sensor protein may need to be saturated for effective de-repression of the gene regulated. Likewise this may also be true for the MerR family metal dependent activators, the founder member of which, MerR, has a ~4 fold weaker affinity for DNA in the metallated form (Parkhill *et al.* 1993). However, the aforementioned increase in *E. coli* ZntR stability to proteolytic degradation upon Zn(II) binding will act to increase the pool of Zn(II)-ZntR over apo-ZntR (Pruteanu *et al.* 2007) potentially overcoming the effect of a weakened DNA affinity. The abundance of Fur molecules in *V. cholerae* (Watnick *et al.* 1997) and *E. coli* (Zheng *et al.* 1999) has been estimated by ELISA and western blot respectively as 2500-7500 molecules per cell depending on growth phase and 5,000-10,000. This estimation of abundance of Fur proteins on the order of magnitude 10^3 is greater than that observed for other prokaryotic repressor proteins such as the Trp repressor protein of *E. coli* which is present at 50-300 molecules per cell (Kelley & Yanofsky. 1982). This may reflect the large, complex nature of the Fur regulon (Litwin & Calderwood. 1994) and indeed the leucine responsive repressor protein has been shown to be present at a similar abundance and have a large regulon (Willins *et al.* 1991; Ernsting *et al.* 1993). Alternatively the abundance of Fur may represent a strategy to tune the sensitivity of regulation. In support of this idea the *B. subtilis* Zur protein has been shown to respond to a buffered zinc concentration ~7 fold lower when the protein concentration is increased 10 fold from 0.1 to 1 μ M (Ma *et al.* 2011a). It should be possible to estimate the abundance of metalloregulators by tagging the protein of interest and carrying out quantitative western blots. As many metalloregulators are autoregulatory these measurements should be carried out under conditions of metal excess and deficiency as well as under normal growth conditions. To ensure the tagged protein is functionally representative of the wild type protein the biochemical properties of the tagged protein may need to be assayed *in vitro*.

Additional facets of metal selectivity that still remain largely unexplored are metal selectivity in the periplasm both by two component sensors & by the metal binding proteins of ABC type metal importers and the selectivity of metallochaperones. A

systematic search of the Metal-MACiE database (Andreini *et al.* 2009) revealed that ~27 % of all metal sites within structurally characterised metalloenzymes are found at the end of metal delivery pathways or contain a metal ion that has been inserted into a cofactor (Figure 6.9). Understanding the selectivity at the start of these pathways may explain the correct speciation of nearly 30 % of metalloenzymes. Little is currently known about the sensing of periplasmic metal by histidine kinases let alone about selectivity. In *Pseudomonas putida* KT2440 CinS, a histidine kinase responsible for copper sensing, mutation of two conserved histidine residues predicted to be located in a periplasmic loop resulted in a ten-fold reduced copper dependent induction of the genes regulated by CinS-CinR two-component system (Quaranta *et al.* 2009). Neither of these histidine residues are conserved in NrsS or CopS from *Synechocystis* (Figure 6.10) suggesting different residues may be important for metal sensing by these proteins. Presumably differences between the two proteins must confer selectivity for either copper or nickel & cobalt. *Synechocystis* represents an excellent model in which to explore metal homeostasis in the periplasm. In addition to the histidine kinase sensors for copper and nickel & cobalt there is also a histidine kinase sensor of manganese (ManS) (Yamaguchi *et al.* 2002). There are also multiple ATP powered uptake systems for different metals (zinc, iron, manganese, nickel). Understanding what dictates the selectivity of the metal binding proteins of these systems and therefore which metals are transported into the cytosol will allow greater understanding of the correct co-factoring of metalloproteins.

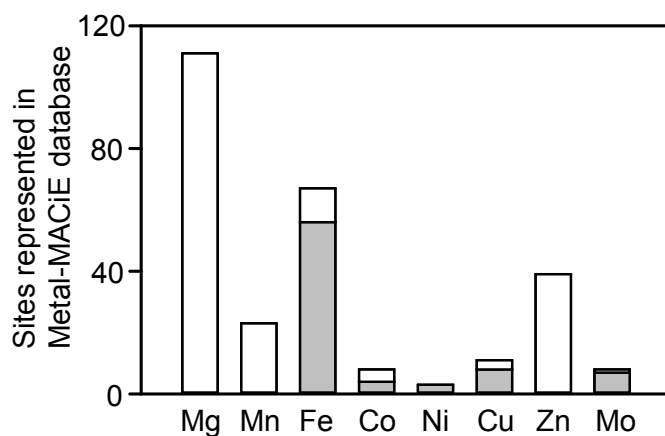


Figure 6.9. Estimation of the proportion of metalloprotein sites that are found at the end of delivery pathways. Mg, Mn, Fe, Co, Ni, Cu, Zn and Mo sites listed in the Metal-MACiE database were examined to determine the number of metal sites which lay at the end of a delivery pathway. Iron-sulphur clusters were counted as one Fe site, metal containing organic cofactors such as cobalmin and factor-430 as one site for the relevant metal, homo-clusters as one site for the relevant metal and heteroclusters as one site for each metal present i.e. a dinuclear NiFe site was counted as 1 Fe and 1 Ni site. Histograms are shaded grey to indicate sites at the end of delivery pathways and white to indicate those that are not.

```

CopS      -MQNNRFLNLSRWRLASYAGVMGLIILGLCLAVYEMTSQDHWRSLDQELTSLAGTLH-- 57
NrsS      -MNTRRLFARSRLQLAFWYALVMGGIITLLGLGVYFAIVQANWMALEREVESIAGTLH-- 57
CinS      MMRRVSLGSRRLALLFAACTATVSLGAGLLFSRASECHFVELDQQLLDSRLSLFRTQLAGV 60
          * . * : * * . . . : . * : : *

CopS      ---DGLEPLLQQPGQLEPSVKQILPNLCGLTVACPRSP--QRRHILNATQQPGYYVRFLD 112
NrsS      ---DSLEFMLPSNASPTGVLQKMLPDCLVNQPCQVNP TLIERHTLGISDRSLYYIRLFD 114
CinS      STADELQARLPALRDELHQADLALRISASNGATWFESRSGLPAAQATGLATLHAPGID 120
          * * . * . : : . . . * : . : *

CopS      LNGQLLATAG--ENPPGLAFERETTRKPLTDQKGNRYHQVSLLLK--TTTGEPWGYLK 167
NrsS      YQGNLLAFSP--NQPASLSSIFNQETWQTIHPPTGDRYRQFTTILHSAGNTDKSSWGYLEQ 172
CinS      YRSLSVPLTQAMQSPRLTLYLDITHQHFLQG-MQRLIWLTVGLSALITALLGAWAARS 179
          .. : : : .. * : : : * : * : *

CopS      VGRSLVEYDHHLHTIQG-FLVWGLPIVMIVVGGASWWLAG-LAMEPVYRSYQQIQQFTAD 225
NrsS      IGRSLAAFDAENKRILW-ILGLSFPIALGLVAFSSWGLAG-LAMRPIYQSYQQQQQFTAN 230
CinS      GLRPLRQMGQVAASVSARSLTTRLFVAQMPEELAEELASSMNAMLQRLDDAFQRLSAFSAD 239
          * . . : * : : . : : : : * : *

CopS      IAEELRTPITAIAQATLETTLNAEP-NAEETHSTLQTLKRQNYRLSHLIHDLNLLSRMDLT 284
NrsS      AAEELRSPLASLLATVEAVLRIDSSHSEINTMLHTVERQGRRLSQLITDLLLLSRLEQE 290
CinS      IAEELRTPLSNLLTHTQVTLTRPR-SLEEYREALHGNLEELQWMAQMINDMLFLAKADHG 298
          *****: : : : : * . * : : : * * : : :

CopS      TVNPTQFTLCCLNDLVEDLTEEFASLAIAGVLLSAKLDNQANIWVRGEEEQLYRLVGNL 344
NrsS      TT-AEDWRLCCLNDLVDLTFEEFLELAIAAHIDLSSDLS-SGEVYAWGNESQLYRLVSNL 348
CinS      LLVPGDAPLA-LHDEVDALLEYYAPLAEDS---DVQMLREGEAVLHGDQHMLRRALSNL 353
          . : * . * : * * : * : . : : : * : * : *

CopS      ISNAIHYTPTGGEVTVMLETDKQQAIIKVQDTGIGIASENQSRVDFRFRVDTARSRQRG 404
NrsS      IANAIQYTTAGGRVDITLTSHEQMAIITVQDTGIGIAPDQQEHI FERFVRVNRDRSRKTG 408
CinS      LDNAMRFTPAGGQIKVTLGPG--PTINVANTGLAIDPAALPRLDFRFRVDPARREGSS 410
          : * : : * : * : : * . . * . * : * : . : : * : * : *

CopS      -GAGLGLAIAQAIKQGVLTVESELGQGSFTIRLSICPPPYQSSRECTKNLT 458
NrsS      -GTGLGLAIAQVITVKHRGSLTVESALGKSLFTIQLPIFSVPVIVHS----- 454
CinS      EHAGLGLAITRSIVQAHGGCIRAECEGG-WTRFVIEFTQDR----- 450
          :*****: * . * : * . * : * . : .

```

Figure 6.10. Alignment of *Synechocystis* NrsS and CopS with *Pseudomonas putida* KT2440 CinS. The predicted membrane spanning α -helices (Quaranta *et al.* 2009) are shown as boxes above the alignment, sequence between these helices is predicted to be located on periplasmic side of the cell membrane. The two histidine residues shown to be important for copper sensing by CinS are highlighted red and boxed. The conserved histidine residue phosphorylated during signal relay is coloured blue and boxed.

References

- Abraham L. O., Li Y. & Zamble D. B. (2006) The metal- and DNA- binding activities of *Helicobacter pylori* NikR. *J. Inorg. Biochem.* 100: 1005-1014.
- Ahn B. E., Cha J., Lee E. J., Han A. R., Thompson C. J. & Roe J. H. (2006) Nur, a nickel-responsive regulator of the Fur family, regulates superoxide dismutases and nickel transport in *Streptomyces coelicolor*. *Mol. Microbiol.* 59: 1848-1858.
- Akanuma G., Nanamiya H., Natori Y., Nomura N. & Kawamura F. (2006) Liberation of zinc-containing L31 (RpmE) from ribosomes by its paralogous gene product, YtiA, in *Bacillus subtilis*. *J. Bacteriol.* 188: 2715-2720.
- Alge D. & Peschek G. A. (1993) Identification and characterization of the *ctaC* (*coxB*) gene as part of an operon encoding subunits I, II, and III of the cytochrome c oxidase (cytochrome aa3) in the cyanobacterium *Synechocystis* PCC 6803. *Biochem. Biophys. Res. Commun.* 191: 9-17.
- Althaus E. W., Outten C. E., Olson K. E., Cao H. & O'Halloran T. V. (1999) The ferric uptake regulation (Fur) repressor is a zinc metalloprotein. *Biochemistry*. 38: 6559-6569.
- Amábile-Cuevas C. F. & Demple B. (1991) Molecular characterization of the *soxRS* genes of *Escherichia coli*: two genes control a superoxide stress regulon. *Nucleic Acids Res.* 19: 4479-4484.
- An Y. J., Ahn B. E., Han A. R., Kim H. M., Chung K. M., Shin J. H., Cho Y. B., Roe J. H. & Cha S. S. (2009) Structural basis for the specialization of Nur: a nickel-specific Fur homolog, in metal sensing and DNA recognition. *Nucleic Acids Res.* 37: 3442-3451.

Anderson L.A., Palmer T., Price N. C., Bornemann S., Boxer D. H. & Pau R. N. (1997) Characterisation of the molybdenum-responsive ModE regulatory protein and its binding to the promoter region of the *modABCD* (molybdenum transport) operon of *Escherichia coli*. *Eur. J. Biochem.* 246: 119-126.

Andreini C., Bertini I., Cavallaro G., Holliday G. L. & Thornton J. M. (2008) Metal ions in biological catalysis: from enzyme databases to general principles. *J. Biol. Inorg. Chem.* 13: 1205-1218.

Andreini C., Bertini I., Cavallaro G., Holliday G. L. & Thornton J. M. (2009) Metal-MACiE: a database of metals involved in biological catalysis. *Bioinformatics.* 25: 2088-2089.

Ansari A. Z., Bradner J. E. & O'Halloran T. V. (1995) DNA-bend modulation in a repressor-to-activator switching mechanism. *Nature.* 374: 371-375.

Ansari A. Z., Chael M. L. & O'Halloran T. V. (1994) Allosteric underwinding of DNA is a critical step in positive control of transcription by Hg-MerR. *Nature.* 355: 87-89.

Appel J., Phunpruch S., Steinmüller K. & Schulz R. (2000) The bidirectional hydrogenase of *Synechocystis* sp. PCC 6803 works as an electron valve during photosynthesis. *Arch. Microbiol.* 173: 333-338.

Arnold K., Bordoli L., Kopp J. & Schwede T. (2006) The SWISS-MODEL Workspace: A web-based environment for protein structure homology modelling. *Bioinformatics.* 22: 195-201.

Aronsson A. C., Marmstal E. & Mannervik B. (1978) Glyoxalase I, a zinc metalloenzyme of mammals and yeast. *Biochem. Biophys. Res. Commun.* 81: 1235-1240.

- Arunkumar A. I., Campanello G. C. & Giedroc D. P. (2009) Solution structure of the paradigm ArsR family zinc sensor in the DNA-bound state. *Proc. Natl. Acad. Sci. USA*. 106: 18177-18182.
- Arunkumar A. I., Pennella M. A., Kong X. & Giedroc D. P. (2007) Resonance assignments of the metal sensor CzrA in the apo-, Zn²⁺- and DNA bound (42 kDa) states. *Biomol. NMR Assign.* 1: 99-101.
- Axelsson R. & Lindblad P. (2002) Transcriptional regulation of *Nostoc* hydrogenases: effects of oxygen, hydrogen, and nickel. *Appl. Environ. Microbiol.* 68: 444-447.
- Badarau A. & Dennison C. (2011) Thermodynamics of copper and zinc distribution in the cyanobacterium *Synechocystis* PCC 6803. *Proc. Natl. Acad. Sci. USA*. 108: 13007-13012.
- Bagg A. & Neilands J. B. (1985) Mapping a mutation affecting regulation of iron uptake systems in *Escherichia coli* K-12. *J. Bacteriol.* 161: 450-453.
- Bagg A. & Neilands J. B. (1987) Ferric uptake regulation protein acts as a repressor, employing iron (II) as a cofactor to bind the operator of an iron transport operon in *Escherichia coli*. *Biochemistry*. 26: 5471-5477.
- Baichoo N. & Helmann J. D. (2002) Recognition of DNA by Fur: a reinterpretation of the Fur box consensus sequence. *J. Bacteriol.* 184: 5826-5832.
- Bain D. L., Berton N., Ortega M., Baran J., Yang Q. & Catalano C. E. (2001) Biophysical characterization of the DNA binding domain of gpNu1, a viral DNA packaging protein. *J. Biol. Chem.* 276: 20175-20181.

- Baker J., Sengupta M., Jayaswal R. K. & Morrissey J. A. (2011) The *Staphylococcus aureus* CsoR regulates both chromosomal and plasmid-encoded copper resistance mechanisms. *Environ. Microbiol.* 13: 2495-2507.
- Banci L., Bertini I., Cantini F., Ciofi-Baffoni., Cavet J. S., Dennison C., Graham A. I., Harvie D. R. & Robinson N. J. (2007) NMR structural analysis of cadmium sensing by winged helix repressor CmtR. *J. Biol. Chem.* 282: 30181-30188.
- Barbosa R. L. & Benedetti C. E. (2007) BigR, a transcriptional repressor from plant-associated bacteria, regulates an operon implicated in biofilm growth. *J. Bacteriol.* 189: 6185-6194.
- Barnett J. P., Milard A., Ksibe A. Z., Scanlan D. J., Schmid R. & Blindauer C. A. (2012) Mining genomes of marine cyanobacteria for elements of zinc homeostasis. *Front. Microbiol.* 3: 142.
- Barry A. N., Otoikhian A., Bhatt S., Shinde U., Tsivkovskii R., Blackburn N. J. & Lutsenko S. (2011) The lumenal loop Met672-Pro707 of copper-transporting ATPase ATP7A binds metals and facilitates copper release from the intramembrane sites. *J. Biol. Chem.* 286: 26585-26594.
- Belitsky B. R. & Sonenshein A. L. (2011) Roadblock repression of transcription by *Bacillus subtilis* CodY. *J. Mol. Biol.* 411: 729-743.
- Bellini P. & Hemmings A. M. (2006) *In vitro* characterization of a bacterial manganese uptake regulator of the fur superfamily. *Biochemistry.* 28: 2686-2698.
- Benoit S. L., Seshadri S., Lamichane-Khadka R. & Maier R. J. (2013) *Helicobacter hepaticus* NikR controls urease and hydrogenase activities via the NikABCDE and HH0418 putative nickel import proteins. *Microbiology.* 159: 136-146.

- Bertini I., Luchinat C., Messori L. & Vařák M. (1993) A two-dimensional NMR study of Co(II)₇ rabbit liver metallothionein. *Eur. J. Biochem.* 211: 235-240.
- Berzigotti S., Benlafya K., S  pulchre J., Amoroso A. & Joris B. (2012) *Bacillus licheniformis* BlaR1 L3 loop is a zinc metalloprotease activated by self-proteolysis. *PLoS One.* 7: e36400.
- Bhattacharya J., Ghosh Dastidar K., Chatterjee A., Majee M. & Majumder A. L. (2004) *Synechocystis* Fe superoxide dismutase gene confers oxidative stress tolerance to *Escherichia coli*. *Biochem. Biophys. Res. Commun.* 316: 540-544.
- Binet M. R. & Poole R. K. (2000) Cd(II), Pb(II) and Zn(II) ions regulate expression of the metal-transporting P-type ATPase ZntA in *Escherichia coli*. *FEBS Lett.* 473: 67-70.
- Bird A. J., Gordon M., Eide D. J. & Winge D. R. (2006) Repression of ADH1 and ADH3 during zinc deficiency by Zap1-induced intergenic RNA transcripts. *EMBO J.* 25: 5726-5734.
- Borrelly G. P., Rondet S. A., Tottey S. & Robinson N. J. (2004) Chimeras of P-type ATPases and their transcriptional regulators: contributions of a cytosolic amino-terminal domain to metal specificity. *Mol. Microbiol.* 53: 217-227.
- Bradford M. M. (1976) Rapid and sensitive method for the quantitation of microgram quantities of protein utilizing the principle of protein-dye binding. *Anal. Biochem.* 72: 248-254.
- Brocklehurst K. R., Hobman J. L., Lawley B., Blank L., Marshall S. J., Brown N. L. & Morby A. P. (1999) ZntR is a Zn(II)-responsive MerR-like transcriptional regulator of *zntA* in *Escherichia coli*. *Mol. Microbiol.* 31: 893-902.

- Bsat N. & Helmann J. D. (1999) Interaction of *Bacillus subtilis* Fur (ferric uptake repressor) with the *dhb* operator *in vitro* and *in vivo*. *J. Bacteriol.* 181: 4299-4307.
- Bsat N., Herbig A., Casillas-Martinez L., Setlow P. & Helmann J. D. (1998) *Bacillus subtilis* contains multiple Fur homologues: identification of the iron uptake (Fur) and peroxide regulon (PerR) repressors. *Mol. Microbiol.* 29: 189-198.
- Buchsbaum J. C. & Berg J. M. (2000) Kinetics of metal binding by a zinc finger peptide. *Inorg. Chim. Acta.* 297: 217-219.
- Bullerjahn G. S. & Sherman L. A. (1986) Identification of a carotenoid-binding protein in the cytoplasmic membrane from the heterotrophic cyanobacterium *Synechocystis* sp. Strain PCC6714. *J. Bacteriol.* 167: 396-399.
- Busenlehner L. S., Cospier N. J., Scott R. A., Rosen B. P., Wong M. D. & Giedroc D. P. (2001) Spectroscopic properties of the metalloregulatory Cd(II) and Pb(II) sites of *S. aureus* pl258 CadC. *Biochemistry.* 40: 4426-4436.
- Busenlehner L. S., Pennella M. A. & Giedroc D. P. (2003) The SmtB/ArsR family of metalloregulatory transcriptional repressors: Structural insights into prokaryotic metal resistance. *FEMS Microbiol. Rev.* 27: 131-143.
- Busenlehner L. S., Weng T. C., Penner-Hahn J. E. & Giedroc D. P. (2002) Elucidation of primary ($\alpha 3N$) and vestigial ($\alpha 5$) heavy metal-binding sites in *Staphylococcus aureus* pl258 CadC: evolutionary implications for metal ion selectivity of ArsR/SmtB metal sensor proteins. *J. Mol. Biol.* 319: 685-701.
- Campanello G. C., Ma Z., Grossoehme N. E., Guerra A. J., Ward B. P., Dimarchi R. D., Ye Y., Dann III C. E. & Giedroc D. P. (2013) Allosteric inhibition of a zinc-sensing transcriptional repressor: insights into the allosteric repressor (ArsR) family. *J. Mol. Biol.* 425: 1143-1157.

- Campbell D. R., Chapman K. E., Waldron K. J., Tottey S., Kendall S., Cavallaro G., Andreini C., Hinds J., Stoker N. G., Robinson N. J. & Cavet J. S. (2007) Mycobacterial cells have dual nickel-cobalt sensors: sequence relationships and metal sites of metal-responsive repressors are not congruent. *J. Biol. Chem.* 282: 32298-32310.
- Cannon G. C., Heinhorst S. & Kerfeld C. A. (2010) Carboxysomal carbonic anhydrases: Structure and role in microbial CO₂ fixation. *Biochim. Biophys. Acta.* 1804: 382-392.
- Cavet J. S., Graham A. I., Meng W. & Robinson N. J. (2003) A cadmium-lead-sensing ArsR-SmtB repressor with novel sensory sites. Complementary metal discrimination by NmtR and CmtR in a common cytosol. *J. Biol. Chem.* 278: 44560-44566.
- Cavet J. S., Meng W., Pennella M. A., Appelhoff R. J., Giedroc D. P. & Robinson N. J. (2002) A nickel-cobalt-sensing ArsR-SmtB family repressor. Contributions of cytosol and effector binding sites to metal selectivity. *J. Biol. Chem.* 277: 38441-38448.
- Chakravorty D. K., Wang B., Lee C. W., Giedroc D. P. & Merz K. M. Jr. (2012) Simulations of allosteric motions in the zinc sensor CzcA. *J. Am. Chem. Soc.* 134: 3367-3376.
- Champier L., Duarte V., Michaud-Soret I. & Coves J. (2004) Characterization of the MerD protein from *Ralstonia metallidurans* CH34: a possible role in bacterial mercury resistance by switching off the induction of the *mer* operon. *Mol. Microbiol.* 52: 1475-1485.
- Chang F. M., Lauber M. A., Running W. E., Reilly J. P. & Giedroc D. P. (2011) Ratiometric pulse-chase amidation mass spectrometry as a probe of biomolecular complex formation. *Anal. Chem.* 83: 9092-9099.

- Changela A., Chen K., Xue Y., Holschen J., Outten C. E., O'Halloran T. V. & Mondragón A. (2003) Molecular basis of metal-ion selectivity and zeptomolar sensitivity by CueR. *Science*. 301: 1383-1387.
- Checa S. K., Espariz M., Audero M. E., Botta P. E., Spinelli S. V. & Soncini F. C. (2007) Bacterial sensing of and resistance to gold salts. *Mol. Microbiol.* 63: 1307-1318.
- Chen L., Keramati L. & Helmann J. D. (1995) Coordinate regulation of *Bacillus subtilis* peroxide stress genes by hydrogen peroxide and metal ions. *Proc. Natl. Acad. Sci. USA*. 92: 8190-8204.
- Chen X., Chu M. & Giedroc D. P. (2000) Spectroscopic characterization of Co(II)-, Ni(II)-, and Cd(II)- substituted wild-type and non-native retroviral-type zinc finger peptides. *J. Biol. Inorg. Chem.* 5: 93-101.
- Chivers P. T., Benanti E. L., Heil-Chapdelaine V., Iwig J. S. & Rowe J. L. (2012) Identification of Ni-(L-His)₂ as a substrate for NikABCDE-dependent nickel uptake in *Escherichia coli*. *Metallomics*. 4: 1043-1050.
- Chivers P. T. & Sauer R. T. (1999) NikR is a ribbon-helix-helix DNA-binding protein. *Protein Sci.* 8: 2494-2500.
- Chivers P. T. & Sauer R. T. (2000) Regulation of high affinity nickel uptake in bacteria. Ni²⁺-dependent interaction of NikR with wild-type and mutant operator sites. *J. Biol. Chem.* 275: 19735-19741.
- Chivers P. T. & Sauer R. T. (2002) NikR repressor: High-affinity nickel binding to the C-terminal domain regulates binding to operator DNA. *Chem. Biol.* 9: 1141-1148.

Choi S. K. & Saier M. H. Jr. (2005) Regulation of *sigL* expression by the catabolite control protein CcpA involves a roadblock mechanism in *Bacillus subtilis*: potential connection between carbon and nitrogen metabolism. *J. Bacteriol.* 187: 6856-6861.

Clugston S. L., Barnard J. F., Kinach R., Miedema D., Ruman R., Duab E. & Honek J. F. (1998) Overproduction and characterization of a dimeric non-zinc glyoxalase I from *Escherichia coli*: evidence for optimal activation by nickel ions. *Biochemistry.* 37: 8754-8763.

Cobine P. A., George G. N., Jones C. E., Wickramasinghe W. A., Solioz M. & Dameron C. T. (2002a) Copper transfer from the Cu(I) chaperone, CopZ, to the repressor, Zn(II)CopY: Metal coordination environments and protein interactions. *Biochemistry.* 41: 5822-5829.

Cobine P. A., Jones C. E. & Dameron C. T. (2002b) Role for zinc(II) in the copper(I) regulated protein CopY. *J. Inorg. Biochem.* 88: 192-196.

Cobine P. A., Wickramasinghe W. A., Harison M. D., Weber T., Solioz M. & Dameron C. T. (1999) The *Enterococcus hirae* copper chaperone CopZ delivers copper(I) to the CopY repressor. *FEBS Lett.* 445: 27-30.

Cook W. J., Kar S. J., Taylor K. B. & Hall L. M. (1998) Crystal structure of the cyanobacterial metallothionein repressor SmtB: a model for metalloregulatory proteins. *J. Mol. Biol.* 275: 337-346.

Corbett D., Schuler S., Glenn S., Andrew P. W., Cavet J. S. & Roberts I. S. (2011) The combined actions of the copper-responsive repressor CsoR and copper-metallochaperone CopZ modulate CopA-mediated copper efflux in the intracellular pathogen *Listeria monocytogenes*. *Mol. Microbiol.* 81: 457-472.

- Coyne III H. J. & Giedroc D. P. (2012) Backbone resonance assignments of the homotetrameric (48 kD) copper sensor CsoR from *Geobacillus thermodenitrificans* in the apo- and Cu(I)-bound states: insights into copper-mediated allostery. *Biomol. NMR Assign.* E-pub ahead of print.
- Daday A., Mackerras A. H. & Smith G. D. (1985) Effect of nickel on hydrogen metabolism and nitrogen fixation in the Cyanobacterium *Anabaena cylindrica*. *J. Gen. Microbiol.* 131: 231-238.
- D'Autreaux B., Touati D., Bersch B., Latour J. M. & Michaud-Soret I. (2002) Direct inhibition by nitric oxide of the transcriptional ferric uptake regulation protein via nitrosylation of the iron. *Proc. Natl. Acad. Sci. USA.* 99: 16619-16624.
- Dainty S. J., Patterson C. J., Waldron K. J. & Robinson N. J. (2010) Interaction between cyanobacterial copper chaperone Atx1 and zinc homeostasis. *J. Biol. Inorg. Chem.* 15: 77-85.
- De Pina K., Desjardin V., Mandrand-Berthelot M. A., Giordano G. & Wu L. F. (1999) Isolation and characterization of the *nikR* gene encoding a nickel-responsive regulator in *Escherichia coli*. *J. Bacteriol.* 181: 670-674.
- Dean K. M., Qui Y. & Palmer A. E. (2012) Visualizing metal ions in cells: an overview of analytical techniques, approaches, and probes. *Biochim. Biophys. ACTA.* 1823: 1406-1415.
- Delaney I., Rappuoli R. & Scarlato V. (2004) Fur functions as an activator and as a repressor of putative virulence genes in *Neisseria meningitides*. *Mol. Microbiol.* 52: 1081-1090.

- Delaney I., Spohn G., Rappuoli R. & Scarlato V. (2001) The Fur repressor controls transcription of iron-activated and –repressed genes in *Helicobacter pylori*. *Mol. Microbiol.* 42: 1297-1309.
- Dian C., Vitale S., Leonard G. A., Bahlawane C., Fauquant C., Leduc D., Muller C., de Reuse H., Michaud-Soret I. & Terradot. (2011) The structure of the *Helicobacter pylori* ferric uptake regulator Fur reveals three functional binding sites. *Mol. Microbiol.* 79: 1260-1275.
- Díaz-Mireles E., Wexler M., Sawers G. & Bellini D. (2004) The Fur-like protein Mur of *Rhizobium leguminosarum* is a Mn(2+)-responsive transcriptional regulator. *Microbiology.* 150: 1447-1456.
- Díaz-Mireles E., Wexler M., Todd J. D., Bellini D., Johnston A. W. & Sawers R. G. (2005) The manganese-responsive repressor Mur of *Rhizobium leguminosarum* is a member of the Fur-superfamily that recognises an unusual operator sequence. *Microbiology.* 151: 4071-4078.
- Diederix R. E., Farquant C., Rodrique A., Mandrand-Berthelot M. A. & Michaud-Soret I. (2008) Sub-micromolar affinity of *Escherichia coli* NikR for Ni(II). *Chem. Commun.* 21: 1813-1815.
- Dodani S. C., He Q. & Chang C. J. (2009) A turn-on fluorescent sensor for detecting nickel in living cells. *J. Am. Chem. Soc.* 131: 18020-18021.
- Dudev T. & Lim C. (2008) Metal binding affinity and selectivity in metalloproteins: insights from computational studies. *Annu. Rev. Biophys.* 37: 97-116.
- Dupont C. L., Barbeau K. & Palenik B. (2008) Ni uptake and limitation in marine *Synechococcus* strains. *Appl. Environ. Microbiol.* 74: 23-31.

- Dupont C. L., Butcher A., Valas R. E., Bourne P. E. & Caetano-Anollés G. (2010) History of biological metal utilization inferred through phylogenomic analysis of protein structures. *Proc. Natl. Acad. Sci. USA*. 107: 10567-10572.
- Dupont C. L., Grass G. & Rensing G. (2011) Copper toxicity and the origin of bacterial resistance-new insights and applications. *Metallomics*. 3: 1109-1118.
- Dupont C. L., Yang S., Palenik B. & Bourne P. E. (2006) Modern proteomes contain putative imprints of ancient shifts in trace metal geochemistry. *Proc. Natl. Acad. Sci. USA*. 103: 17822-17827.
- Dwarakanath S., Chaplin A. K., Hough M. A., Rigali S., Vigenboom E. & Worrall J. A. (2012) Response to copper stress in *Streptomyces lividans* extends beyond genes under direct control of a copper-sensitive operon repressor protein (CsoR). *J. Biol. Chem.* 287: 17833-17847.
- Eicken C., Pennella M. A., Chen X., Koshlap K. M., VanZile M. L., Sacchettini J. C. & Giedroc D. P. (2003) A metal-ligand-mediated intersubunit allosteric switch in related SmtB/ArsR zinc sensor proteins. *J. Mol. Biol.* 333: 683-695.
- Ellman G. L. (1959) Tissue sulfhydryl groups. *Arch. Biochem. Biophys.* 82: 70-77.
- Endo G. & Silver S. (1995) CadC, the transcriptional regulatory protein of the cadmium resistance protein of *Staphylococcus aureus* plasmid pl258. *J. Bacteriol.* 177: 4437-4441.
- Epshtein V. & Nudler E. (2003) Cooperation between RNA polymerase molecules in transcription elongation. *Science*. 300: 801-805.
- Ernsting B. R., Denninger J. W., Blumenthal R. M. & Matthews R. G. (1993) Regulation of the *gltBDF* operon of *Escherichia coli*: how is a leucine-insensitive

operon regulated by the leucine-responsive regulatory protein. *J. Bacteriol.* 175: 7160-7169.

Espariz M., Checa S. K., Audero M. E., Pontel L. B. & Soncini F. C. (2007) Dissecting the *Salmonella* response to copper. *Microbiology*. 153: 2989-2997.

Faulkner M. J., Ma. Z., Fuangthong M. & Helmann J. D. (2012) Derepression of the *Bacillus subtilis* PerR peroxide stress response leads to iron deficiency. *J. Bacteriol.* 194: 1226-1235.

Festa R. A., Jones M. B., Butler-Wu S., Sinsimer D., Gerads R., Bishai W. R., Peterson S. N. & Darwin K. H. (2011) A novel copper-responsive regulon in *Mycobacterium tuberculosis*. *Mol. Microbiol.* 79: 133-148.

Foster A. W., Patterson C. J., Pernil R., Hess C. R. & Robinson N. J. (2012) Cytosolic Ni(II) sensor in cyanobacterium: Nickel detection follows nickel affinity across four families of metal sensors. *J. Biol. Chem.* 287: 12142-12151.

Frantz B. & O'Halloran T. V. (1990) DNA distortion accompanies transcriptional activation by the metal-responsive gene-regulatory protein MerR. *Biochemistry*. 29: 4747-4751.

Fraústo da Silva J. J. R. & Williams R. J. P. (2002) *The Biological Chemistry of the Elements: The Inorganic Chemistry of Life*. 2nd ed. USA: Oxford University Press.

Gaballa A. & Helmann J. D. (1998) Identification of a zinc-specific metalloregulatory protein, Zur, controlling zinc transport operons in *Bacillus subtilis*. *J. Bacteriol.* 180: 5815-5821.

Gaballa A., Wang T., Ye R. W. & Helmann J. D. (2002) Functional analysis of the *Bacillus subtilis* Zur regulon. *J. Bacteriol.* 184: 6508-6514.

- Gabriel S. E. & Helmann J. D. (2009) Contributions of Zur-controlled ribosomal proteins to growth under zinc starvation conditions. *J. Bacteriol.* 191: 6116-6122.
- Gao R. & Stock A. M. (2009) Biological insights from structures of two-component proteins. *Annu. Rev. Microbiol.* 63: 133-154.
- García-Domínguez M., López-Maury L., Florencio F. J. & Reyes J. C. (2000) A gene cluster involved in metal homeostasis in the cyanobacterium *Synechocystis* sp. strain PCC 6803. *J. Bacteriol.* 182: 1507-1514.
- Gaudu P. & Weiss B. (1996) SoxR, a [2Fe-2S] transcription factor, is active only in its oxidised form. *Proc. Natl. Acad. Sci. USA.* 93: 10094-10098.
- Gavel O. Y., Bursakov S. A., Di Rocco G., Trincão J., Pickering I. J., George G. N., Calvete J. J., Shnyrov V. L., Brondino C. D., Pereira A. S., Lampreia J., Tavares P., Moura J. J. G. & Moura I. (2008) A new type of metal-binding site in cobalt- and zinc-containing adenylate kinases isolated from sulfate-reducers *Desulfovibrio gigas* and *Desulfovibrio desulfuricans* ATCC 27774. *J. Inorg. Biochem.* 102: 1380-1395.
- Ghassemian M & Straus N. A. (1996) Fur regulates the expression of the iron-stress genes in the cyanobacterium *Synechococcus* sp. Strain PCC 7942. *Microbiology.* 142: 1469-1476.
- Giedroc D. P. & Arunkumar A. I. (2007) Metal sensor proteins: nature's metalloregulated allosteric switches. *Dalton Trans.* 7: 3107-3120.
- Giner-Lamia J., López-Maury L., Reyes J. C. & Florencio F. J. (2012) The CopRS two-component system is responsible for resistance to copper in the cyanobacterium *Synechocystis* sp. PCC 6803. *Plant Physiol.* 159: 1806-1818.

- Ginsberg A. M. & Spigelman M. (2007) Challenges in tuberculosis drug research and development. *Nat. Med.* 13: 290-294.
- Godsey M. H., Baranova N. N., Neyfakh A. A. & Brennan R. G. (2001) Crystal structure of MtaN, a global multidrug transporter gene activator. *J. Biol. Chem.* 276: 47178-47184.
- Gold B., Deng H., Bryk R., Vargas D., Eliezer D., Roberts J., Jiang X. & Nathan C. (2008) Identification of a copper-binding metallothionein in pathogenic mycobacteria. *Nat. Chem. Biol.* 4: 609-616.
- Govindjee & Shevela D. (2011) Adventures with cyanobacteria: a personal perspective. *Front. Plant Sci.* 2: Article 28.
- Golynskiy M. V., Gunderson W. A., Hendrich M. P. & Cohen S. M. (2006) Metal binding studies and EPR spectroscopy of the manganese transport regulator MntR. *Biochemistry.* 45: 15359-15372
- Grass G., Fan B., Rosen B. P., Lemke K., Schlegel H. G. & Rensing C. (2001) NreB from *Achromobacter xylosoxidans* 31A is a nickel-induced transporter conferring nickel resistance. *J. Bacteriol.* 183: 2803-2807.
- Grossoehme N. E. & Giedroc D. P. (2012) Illuminating allostery in metal sensing transcriptional regulators. *Methods Mol. Biol.* 875: 165-192.
- Grossoehme N. E., Kehl-Fie T. E., Ma Z., Adams K. W., Cowart D. M., Scott R. A., Skaar E. P. & Giedroc D. P. (2011) Control of copper resistance and inorganic sulfur metabolism by paralogous regulators in *Staphylococcus aureus*. *J. Biol. Chem.* 286: 13522-13531.

- Grossoehme N. E., Spuches A. M. & Wilcox D. E. (2010) Application of isothermal titration calorimetry in bioinorganic chemistry. *J. Biol. Inorg. Chem.* 15: 1183-1191.
- Grykiewicz G., Poenie M. & Tsien R. J. (1985) A new generation of Ca²⁺ indicators with greatly improved fluorescence properties. *J. Biol. Chem.* 260: 3440-3450.
- Guedon E. & Helmann J. D. (2003) Origins of metal ion selectivity in the DtxR/MntR family of metalloregulators. *Mol. Microbiol.* 48: 495-506.
- Guerra A. J & Giedroc D. P. (2012) Metal site occupancy and allosteric switching in bacterial metal sensor proteins. *Arch. Biochem. Biophys.* 519: 210-222.
- Guex N. & Peitsch M. C. (1997) SWISS-MODEL and the Swiss-PdbViewer: An environment for comparative protein modelling. *Electrophoresis.* 18: 2714-2723.
- Guimarães B. G., Barbosa R. L., Soprano A. S., Campos B. M., de Souza T. A., Tonoli C. C., Leme A. F., Murakami M. T. & Bendetti C. E. (2011) Plant pathogenic bacteria utilize biofilm growth-associated repressor (BigR), a novel winged-helix redox switch, to control hydrogen sulphide detoxification under hypoxia. *J. Biol. Chem.* 286: 26148-26157.
- Guo J. & Giedroc D. P. (1997) Zinc site redesign in T4 gene 32 protein: Structure and stability of cobalt(II) complexes formed by the wild-type and metal ligand substitution mutants. *Biochemistry.* 36: 730-742.
- Haas C. E., Rodionov D. A., Kropat J., Malasarn D., Merchant S. S. & de Crécy-Lagard V. (2009) A subset of the diverse COG0523 family of putative metal chaperones is linked to zinc homeostasis in all kingdoms of life. *BMC Genomics.* 10: 470.
- Haas K. L. & Franz K. J. (2009) Application of metal coordination chemistry to explore and manipulate cell biology. *Chem. Rev.* 109: 4921-4960.

- Haley K. P. & Skaar E. P. (2012) A battle for iron: host sequestration and *Staphylococcus aureus* acquisition. *Microbes Infect.* 14: 217-227.
- Hall H. K. & Foster J. W. (1996) The role of *fur* in the acid tolerance response of *Salmonella typhimurium* is physiologically and genetically separable from its role in iron acquisition. *J. Bacteriol.* 178: 5683-5691.
- Hamza I., Chauhan S., Hassett R. O'Brian M. R. (1998) The bacterial Irr protein is required for coordination of heme biosynthesis with iron availability. *J. Biol. Chem.* 273: 21669-21674.
- Hanique S., Colombo M. L., Goormaghtigh E., Soumillon P., Frère J. M. & Joris B. (2004) Evidence of an intramolecular interaction between the two domains of the BlaR1 penicillin receptor during the signal transduction. *J. Biol. Chem.* 279: 14264-14272.
- Hantke K. (1981) Regulation of ferric iron transport in *Escherichia coli* K12: isolation of a constitutive mutant. *Mol. Gen. Genet.* 182: 288-292.
- Hantke K. (1987) Selection procedure for deregulated iron transport mutants (*fur*) in *Escherichia coli* K12: *fur* not only affects iron metabolism. *Mol. Gen. Genet.* 210: 135-139.
- Harvie D. R., Andreini C., Cavallaro G., Meng W., Connolly B. A., Yoshida K., Fujita Y., Harwood C. R., Radford D. S., Tottey S., Cavet J. S. & Robinson N. J. (2006) Predicting metals sensed by ArsR-SmtB repressors: allosteric interference by a non-effector metal. *Mol. Microbiol.* 59: 1341-1356.
- Heldwein E. E & Brennan R. G. (2001) Crystal structure of the transcriptional activator BmrR bound to DNA and a drug. *Nature.* 409: 378-382.
- Helm L. & Merbach A. E. (2005) Inorganic and bioinorganic solvent exchange mechanisms. *Chem. Rev.* 105: 1923-1960.

- Helmann J. D., Ballard B. T. & Walsh C. T. (1990) The MerR metalloregulatory protein binds mercuric ions as a tricoordinate, metal-bridged dimer. *Science*. 247: 946-948.
- Helmann J. D., Soonsanga S. & Gabriel S. (2007) Metalloregulators: Arbiters of metal sufficiency. In: D. H. Nies & S. Silver, ed. 2007. *Molecular Microbiology of Heavy Metals*. Springer, pp 37-71.
- Herbig A. F. & Helmann J. D. (2001) Roles of metal ions and hydrogen peroxide in modulating the interaction of *Bacillus subtilis* PerR peroxide regulon repressor with operator DNA. *Mol. Microbiol.* 41: 849-859.
- Hernandez-Prieto M. A. & Futschik M. E. (2012) CyanoEXpress: a web database for exploration and visualisation of the integrated transcriptome of cyanobacterium *Synechocystis* sp. PCC6803. *Bioinformatics*. 8: 634-638.
- Herring C. D. & Blattner F. R. (2004) Global transcriptional effects of a suppressor tRNA and the inactivation of the regulator *frmR*. *J. Bacteriol.* 186: 6714-6720.
- Higgins K. A., Carr C. E. & Maroney M. J. (2012a) Specific metal recognition in nickel trafficking. *Biochemistry*. 51: 7816-7832.
- Higgins K. A., Chivers P. T. & Maroney M. J. (2012b) Role of the N-terminus in determining metal-specific responses in the *E. coli* Ni- and Co-responsive metalloregulator, RcnR. *J. Am. Chem. Soc.* 134: 7081-7093.
- Higgins K. A., Hu H. Q., Chivers P. T. & Maroney M. J. (2013) Effects of select histidine to cysteine mutations on transcriptional regulation by *Escherichia coli* RcnR. *Biochemistry*. 52: 84-97.
- Hitomi Y., Outten C. E. & O'Halloran T. V. (2001) Extreme zinc-binding thermodynamics of the metal sensor/regulator protein, ZntR. *J. Am. Chem. Soc.* 123: 8614-8615.

- Hobman J. L., Wilkie J. & Brown N. L. (2005) A design for life: prokaryotic metal-binding MerR family regulators. *Biometals*. 18: 429-436.
- Hobman J. L., Yamamoto K. & Oshima T. (2007) Transcriptomic responses of bacterial cells to sublethal metal ion stress. In: D. H. Nies & S. Silver, ed. 2007. *Molecular Microbiology of Heavy Metals*. Springer, pp 73-115.
- Hodgkinson V. & Petris M. J. (2012) Copper homeostasis at the host-pathogen interface. *J. Biol. Chem.* 287: 13549-13555.
- Holm R. H., Kennepohl P. & Solomon E. I. (1996) Structural and functional aspects of metal sites in biology. *Chem. Rev.* 96: 2239-2314.
- Huckle J. W., Morby A. P., Turner J. S. & Robinson N. J. (1993) Isolation of a prokaryotic metallothionein locus and analysis of transcriptional control by trace metal ions. *Mol. Microbiol.* 7: 177-187.
- Huyen N. T. T., Eiamphungporn W., Mäder U., Liebeke M., Lalk M., Hecker M., Helmann J. D. & Hantelmann H. (2009) Genome-wide responses to carbonyl electrophiles in *Bacillus subtilis*: control of the thiol-dependent formaldehyde dehydrogenase AdhA and cysteine proteinase YraA by the MerR-family regulator YraB (AdhR). *Mol. Microbiol.* 71: 876-894.
- Irving H. & Williams R. J. P. (1948) Order of stability of metal complexes. *Nature*. 162: 746-747.
- Iwig J. S. & Chivers P. T. (2010) Coordinating intracellular nickel-metal-site structure-function relationships and the NikR and RcnR repressors. *Nat. Prod. Rep.* 27: 658-667.
- Iwig J. S. & Chivers P. T. (2009) DNA recognition and wrapping by *Escherichia coli* RcnR. *J. Mol. Biol.* 393: 514-526.
- Iwig J.S., Leitch S., Herbst R.W., Maroney M.J. & Chivers P.T. (2008) Ni(II) and Co(II) sensing by *Escherichia coli* RcnR. *J. Am. Chem. Soc.* 130: 7592-7606.

- Iwig J.S., Rowe J.L. & Chivers P.T. (2006) Nickel homeostasis in *Escherichia coli* – the *rcnR-rcnA* efflux pathway and its linkage to NikR function. *Mol. Microbiol.* 62: 252-262.
- Jacquamet L., Aberdam D., Adrait A., Hazemann J. L., Latour J. M. & Michaud-Soret I. (1998) X-ray absorption spectroscopy of a new zinc site in the Fur protein from *Escherichia coli*. *Biochemistry.* 37: 2564-2571.
- Janganan T. K., Zhang L., Bavro V. N., Matak-Vinkovic D., Barrera N. P., Burton M. F., Steel P. G., Robinson C. V., Borges-Walmsley M. I. & Walmsley A. R. (2011) Opening of the outer membrane protein channel in tripartite efflux pumps is induced by interaction with the membrane fusion partner. *J. Biol. Chem.* 286: 5484-5493.
- Jefferson J. R., Hunt J. B. & Ginsburg A. (1990) Characterization of indo-1 and quin-2 as spectroscopic probes for Zn^{2+} -protein interactions. *Anal. Biochem.* 187: 328-336.
- Joshi C. P., Panda D., Martell D. J., Andoy N. M., Chen T. Y., Helmann J. D. & Chen P. (2012) Direct substitution and assisted dissociation pathways for turning off transcription by a MerR-family metalloregulator. *Proc. Natl. Acad. Sci.* 109: 15121-15126.
- Kaluarachchi H., Zhang J. W. & Zamble D. B. (2011) *Escherichia coli* SlyD, more than a Ni(II) reservoir. *Biochemistry.* 50: 10761-10763.
- Kanamaru K., Kashiwagi S. & Mizuno T. (1994) A copper-transporting P-type ATPase found in the thylakoid membrane of the cyanobacterium *Synechococcus* species PCC7942. *Mol. Microbiol.* 13: 369-377.
- Kar S. R., Adams A. C., Lebowitz J., Taylor K. B. & Hall L. M. (1997) The cyanobacterial repressor SmtB is predominantly a dimer and binds two Zn^{2+} ions per subunit. *Biochemistry.* 36: 15343-15348.

- Kaur P. & Rosen B. P. (1992) Plasmid-encoded resistance to arsenic and antimony. *Plasmid*. 27: 29-40.
- Kelley R. L. & Yanofsky C. (1982) Trp aporepressor production is controlled by autogenous regulation and inefficient translation. *Proc. Natl. Acad. Sci. USA*. 79: 3120-3124.
- Kelly S. M., Jess T. J. & Price N. C. (2005) How to study proteins by circular dichroism. *Biochim. Biophys. ACTA*. 1751: 119-139.
- Keren N., Aurora R. & Pakrasi H. B. (2004) Critical roles of bacterioferritins in iron storage and proliferation of cyanobacteria. *Plant Physiol*. 135: 1666-1673.
- Keren N., Kidd M. J., Penner-Hahn J. E. & Pakrasi H. B. (2002) A light-dependent mechanism for massive accumulation of manganese in the photosynthetic bacterium *Synechocystis* sp. PCC6803. *Biochemistry*. 41: 15085-15092.
- Keyer K. & Imlay J. A. (1996) Superoxide accelerates DNA damage by elevating free-iron levels. *Proc. Natl. Acad. Sci. USA*. 93: 13635-13640.
- Kobayashi M., Ishizuka T., Katayama M., Kanehisa M., Bhattacharyya-Pakrasi M., Pakrasi H. B. & Ikeuchi M. (2004) Response to oxidative stress involves a novel peroxiredoxin gene in the unicellular cyanobacterium *Synechocystis* sp. PCC 6803. *Plant Cell Physiol*. 45: 290-299.
- Kidd S. P., Djoko K. Y., Ng J., Argente M. P., Jennings M. P. & McEwan A. G. (2011) A novel nickel responsive MerR-like regulator, NimR, from *Haemophilus influenza*. *Metallomics*. 3: 1009-1018.

- Kidd S. P., Potter A. J., Apicella M. A., Jennings M. P. & McEwan A. G. (2005) NmlR of *Neisseria gonorrhoeae*: a novel redox responsive transcription factor from the MerR family. *Mol. Microbiol.* 57: 1676-1689.
- Kim J. S., Kang S. O. & Lee J. K. (2003) The protein complex composed of nickel-binding SrnQ and DNA binding motif-bearing SrnR of *Streptomyces griseus* represses *sodF* transcription in the presence of nickel. *J. Biol. Chem.* 278: 18455-18463.
- Kloosterman T. G., van der Kooi-Pol M. M., Bijlsma J. J. & Kuipers O. P. (2007) The novel transcriptional regulator SczA mediates protection against Zn²⁺ stress by activation of the Zn²⁺-resistance gene *czcD* in *Streptococcus pneumoniae*. *Mol. Microbiol.* 65: 1049-1063.
- Krissinel E. & Henrick K. (2007) Inference of molecular assemblies from crystalline state. *J. Mol. Biol.* 372: 774-797.
- Krizek B. A., Merkle D. L. & Berg J. M. (1993) Ligand variation and metal ion binding specificity in zinc finger peptides. *Inorg. Chem.* 32: 937-940.
- Kunert A., Vinnemeier J., Erdmann N. & Hagemann M. (2003) Repression by Fur is not the main mechanism controlling the iron-inducible *isiAB* operon in the cyanobacteria *Synechocystis* sp. PCC6803. *FEMS Microbiol. Lett.* 227: 255-262.
- Kuroda M., Hayashi H. & Ohta T. (1999) Chromosome-determined zinc-responsible operon *czr* in *Staphylococcus aureus* strain 912. *Microbiol. Immunol.* 43: 115-125.
- Kuzmic P. (1996) Program DYNAFIT for the analysis of enzyme kinetic data: Application to HIV proteinase. *Anal. Biochem.* 237: 260-273.
- Lane T. W. & Morel F. M. (2000) A biological function for cadmium in marine diatoms. *Proc. Natl. Acad. Sci. USA.* 97: 4627-4631.

- Lam M. S., Litwin C. M., Carroll P. A. & Calderwood S. B. (1994) *Vibrio cholerae fur* mutations associated with loss of repressor activity: implications for the structural-functional relationships of *fur*. *J. Bacteriol.* 176: 5108-5115.
- Lee C. W., Chakravorty D. K., Chang F. M., Reyes-Caballero H., Ye Y., Merz K. M. Jr. & Giedroc D. P. (2012) Solution structure of *Mycobacterium tuberculosis* NmtR in the apo state: insights into Ni(II)-mediated allostery. *Biochemistry.* 51: 2619-2629.
- Lee J. W. & Helmann J. D. (2006a) Biochemical characterization of the structural Zn²⁺ site in the *Bacillus subtilis* peroxide sensor PerR. *J. Biol. Chem.* 281: 23567-23578.
- Lee J. W. & Helmann J. D. (2006b) The PerR transcription factor senses H₂O₂ by metal-catalysed histidine oxidation. *Nature.* 440: 363-367.
- Lee J. W. & Helmann J. D. (2007) Functional specialization within the Fur family of metalloregulators. *Biometals.* 20: 485-499.
- Leitch S., Bradley M. J., Rowe J. L., Chivers P. T. & Maroney M. J. (2007) Nickel-specific response in the transcriptional regulator, *Escherichia coli* NikR. *J. Am. Chem. Soc.* 129: 5085-5095.
- Lewin A. C., Doughty P. A., Flegg L., Moore G. R. & Spiro S. (2002) The ferric uptake regulator of *Pseudomonas aeruginosa* has no essential cysteine residues and does not contain a structural zinc ion. *Microbiology.* 148: 2449-2456.
- Li H., Singh A. K., McIntyre L. M. & Sherman L. A. (2004) Differential gene expression in response to hydrogen peroxide and the putative PerR regulon of *Synechocystis* sp. Strain PCC6803. *J. Bacteriol.* 186: 3331-3345.
- Li Y. & Zamble D. B. (2009) Nickel homeostasis and nickel regulation: An overview. *Chem. Rev.* 109: 4617-4643.

- Li Z. & Dimple B. (1994) SoxS, an activator of superoxide stress genes in *Escherichia coli*. Purification and interaction with DNA. *J. Biol. Chem.* 269: 18371-18377.
- Litwin C. M. & Calderwood S. B. (1994) Analysis of the complexity of gene regulation by Fur in *Vibrio cholerae*. *J. Bacteriol.* 176: 240-248.
- Liu T., Chen X., Ma Z., Shokes J., Hemmingsen L., Scott R. A. & Giedroc D. P. (2008) A Cu^I-sensing ArsR family metal sensor protein with a relaxed metal selectivity profile. *Biochemistry.* 47: 10564-10575.
- Liu T., Nakashima S., Hirose K., Shibasaki M., Katsuhara M., Ezaki B., Giedroc D. P. & Kasamo K. (2004) A novel cyanobacterial SmtB/ArsR family repressor regulates the expression of a CPx-ATPase and a metallothionein in response to both Cu(I)/Ag(I) and Zn(II)/Cd(II). *J. Biol. Chem.* 279: 17810-17818.
- Liu T., Ramesh A., Ma Z., Ward S. K., Zhang L., George G. N., Talaat A. M., Sacchettini J. C. & Giedroc D. P. (2007) CsoR is a novel *Mycobacterium tuberculosis* copper-sensing transcriptional regulator. *Nat. Chem. Biol.* 3: 60-68.
- Llarrull L. I., Fischer J. F. & Mobashery S. (2009) Molecular basis and phenotype of methicillin resistance in *Staphylococcus aureus* and insights into new beta-lactams that meet the challenge. *Antimicrob. Agents Chemother.* 53: 4051-4063.
- Llarrull L. I. & Mobashery S. (2012) Dissection of the events in resistance to β -lactam antibiotics mediated by the protein BlaR1 from *Staphylococcus aureus*. *Biochemistry.* 51: 4642-4649.
- López-Maury L., Florencio F. J. & Reyes J. C. (2003) Arsenic sensing and resistance system in the cyanobacterium *Synechocystis* sp. Strain PCC6803. *J. Bacteriol.* 185: 5363-5371.

- López-Maury L., García-Domínguez M., Florencio F. J. & Reyes J. C. (2002) A two-component signal transduction system involved in nickel sensing in the cyanobacterium *Synechocystis* sp. PCC 6803. *Mol. Microbiol.* 43: 247-256.
- Lu Y., Roe J. A., Bender C. J., Peisach J., Banci L., Bertini I., Gralla E. B. & Valentine J. S. (1996) New type 2 copper-cysteinate proteins. Copper site histidine-to-cysteine mutants of yeast copper-zinc superoxide dismutase. *Inorg. Chem.* 35: 1692-1700.
- Luque I. & Forchhammer K. (2008) Nitrogen assimilation and C/N balance sensing. In: Herrero A. & Flores E., Eds. *The Cyanobacteria: Molecular Biology, Genetics and Evolution*. Caister Academic Press: Norfolk. UK. pp 335-382.
- Ma Z., Cowart D. M., Scott R. A. & Giedroc D. P. (2009a) Molecular insights into the metal selectivity of the copper(I)-sensing repressor CsoR from *Bacillus subtilis*. *Biochemistry*. 48: 3325-3334.
- Ma Z., Cowart D.M., Ward B.P., Arnold R.J., DiMarchi R.D., Zhang L., George G.N., Scott R.A. & Giedroc D.P. (2009b) Unnatural amino acid substitution as a probe of the allosteric coupling pathway in a mycobacterial Cu(I) sensor. *J. Am. Chem. Soc.* 131:18044-18045.
- Ma Z., Faulkner M. J. & Helmann J. D. (2012) Origins of specificity and cross-talk in metal ion sensing by *Bacillus subtilis* Fur. *Mol. Microbiol.* 86: 1144-1155.
- Ma Z., Gabriel S. E. & Helmann J. D. (2011a) Sequential binding and sensing of zinc by *Bacillus subtilis* Zur. *Nucleic Acids Res.* 39: 9130-9138.
- Ma Z., Jacobsen F. E. & Giedroc D. P. (2009c) Coordination chemistry of bacterial metal transport and sensing. *Chem. Rev.* 109: 4644-4681.

- Ma Z., Lee J. W. & Helmann J. D. (2011b) Identification of altered function alleles that affect *Bacillus subtilis* PerR metal ion selectivity. *Nucleic Acids Res.* 39: 5036-5044.
- Maciag A., Dainese E., Rodriguez G. M., Milano A., Prowedi R., Pasca M. R., Smith I., Palù G., Riccardi G. & Manganelli R. (2007) Global analysis of the *Mycobacterium tuberculosis* Zur (FurB) regulon. *J. Bacteriol.* 189: 730-740.
- Macomber L., Elsey S. P. & Hausinger R. P. (2011) Fructose-1,6-bisphosphate aldolase (class II) is the primary site of nickel toxicity in *Escherichia coli*. *Mol. Microbiol.* 82: 1291-1300.
- Macomber L. & Hausinger R. P. (2011) Mechanisms of nickel toxicity in microorganisms. *Metallomics.* 3: 1153-1162.
- Macomber L. & Imlay J. A. (2009) The iron-sulfur clusters of dehydratases are primary targets intracellular targets of copper toxicity. *Proc. Natl. Acad. Sci. USA.* 106: 8344-8349.
- Maggio-Hall L. A., Claas K. R. & Escalante-Semerena J. C. (2004) The last step in coenzyme B₁₂ synthesis is localized to the cell membrane in bacteria and archaea. *Microbiology.* 150: 1385-1395.
- Magyar J. S., Weng T., Stern C. M., Dye D. F., Rous B. W., Payne J. C., Bridgewater B. M., Mijovilovich A., Parkin G., Zaleski J. M., Penner-Hahn J. E. & Godwin H. A. (2005) Reexamination of lead(II) coordination preferences in sulphur-rich sites: Implications for a critical mechanism of lead poisoning. *J. Am. Chem. Soc.* 127: 9495-9505.
- Massé E. & Arguin M. (2005) Ironing out the problem: new mechanisms of iron homeostasis. *Trends Biochem. Sci.* 30: 462-468.

- Massé E., Escorcia F. E. & Gottesman S. (2003) Coupled degradation of a small regulatory RNA and its mRNA targets in *Escherichia coli*. *Genes Dev.* 17: 2374-2383.
- Massé E & Gottesman S. (2002) A small RNA regulates the expression of genes involved in iron metabolism in *Escherichia coli*. *Proc. Natl. Acad. Sci. USA.* 99: 4620-4625.
- Massé E., Vanderpool C. K. & Gottesman S. (2005) Effect of RyB small RNA on global iron use in *Escherichia coli*. *J. Bacteriol.* 187: 6962-6971.
- Mata-Cabana A., Florencio F. J. & Lindahl M. (2007) Membrane proteins from the cyanobacterium *Synechocystis* sp.PCC6803 interacting with thioredoxin. *Proteomics.* 7: 3953-3963.
- McIntosh C. L., Germer F., Schulz R., Appel J. & Jones A. K. (2011) The [NiFe]-hydrogenase of the cyanobacterium *Synechocystis* sp. PCC6803 works bidirectionally with a bias to H₂ production. *J. Am. Chem. Soc.* 133: 11308-11319.
- McNicholas P. M., Rech S. A. & Gunsalus R. P. (1997) Characterisation of the ModE DNA-binding sites in the control regions of *modABCD* and *moaABCD* of *Escherichia coli*. *Mol. Microbiol.* 23: 515-524.
- Merchant S. S. & Helmann J. D. (2012) Elemental economy: microbial strategies for optimizing growth in the face of nutrient limitation. *Adv. Microb. Physiol.* 60: 91-210.
- Mills S. A. & Marletta M. A. (2005) Metal binding characteristics and role of iron oxidation in the ferric uptake regulator from *Escherichia coli*. *Biochemistry.* 44: 13553-13559.
- Mitschke J., Georg J., Scholz I., Sharma C. M., Dienst D., Bantscheff J., Voss B., Steglich C., Wilde A., Vogel J. & Hess W. R. (2011) An experimentally anchored map

- of transcriptional start sites in the model cyanobacterium *Synechocystis* sp. PCC6803. *Proc. Natl. Acad. Sci. U. S. A.* 108: 2124-2129.
- Moore C. M., Nakano M. M., Wang T., Ye R. W. & Helmann J. D. (2004) Response of *Bacillus subtilis* to nitric oxide and nitrosating agent sodium nitroprusside. *J. Bacteriol.* 186: 4655-4664.
- Morby A. P., Turner J. S., Huckle J. W. & Robinson N. J. (1993) SmtB is a metal-dependent repressor of the cyanobacterial metallothionein gene *smtA*: identification of a Zn inhibited DNA-protein complex. *Nucleic Acids Res.* 21: 921-925.
- Mukhopadhyay A., Kladova A. V., Bursakov S. A., Gavel O. Y., Calvete J. J., Shnyrov V. L., Moura I., Moura J. J., Romão M. J. & Trincão J. (2011) Crystal structure of the zinc-, cobalt-, and iron-containing adenylate kinase from *Desulfovibrio gigas*: a novel metal-containing adenylate kinase from Gram-negative bacteria. *J. Biol. Inorg. Chem.* 16: 51-61.
- Munier-Lehmann H., Burlacu-Miron S., Craescu C. T., Mantsch H. H. & Schultz C. P. (1999) A new subfamily of short bacterial adenylate kinases with the *Mycobacterium tuberculosis* enzyme as a model: A predictive and experimental study. *Proteins.* 36: 238-248.
- Nakamura Y., Kaneko T., Hirosawa M., Miyajima N. & Tabata S. (1998) Cyanobase, a www database containing the complete nucleotide sequence of the genome of *Synechocystis* sp. strain PCC6803. *Nucleic Acids Res.* 26: 63-67.
- Nakao M., Okamoto S., Kohara M., Fujishiro T., Fujisawa T., Sato S., Tabata S., Kaneko T. & Nakamura Y. (2010) Cyanobase: the cyanobacteria genome database update 2010. *Nucleic Acids Res.* 38: D379-381.

Napolitano M., Rubio M. Á., Santamaría-Gómez J., Olmedo-Verd E., Robinson N. J. & Luque I. (2012) Characterization of the response to zinc deficiency in the cyanobacterium *Anabaena* sp. Strain PCC 7120. *J. Bacteriol.* 194: 2426-2436.

Napolitano M., Rubio M. Á., Camargo S. & Luque I. (2013) Regulation of internal promoters in a zinc-responsive operon is influenced by transcription from upstream promoters. *J. Bacteriol.* 195: 1285-1293.

Nichols J. & Rajagopalan K. V. (2002) *Escherichia coli* MoeA and MogA. Function in metal incorporation step of molybdenum cofactor biosynthesis. *J. Biol. Chem.* 277: 24995-25000.

Nunoshiba T., Hidalgo E., Amábile-Cuevas C. F. & Dimple B. (1993) Two-stage control of an oxidative stress regulon: the *Escherichia coli* SoxR protein triggers redox-inducible expression of the *soxS* regulatory gene. *J. Bacteriol.* 174: 6054-6060.

Odermatt A. & Solioz M. (1995) Two trans-acting metalloregulatory proteins controlling expression of the copper-ATPases of *Enterococcus hirae*. *J. Biol. Chem.* 270: 4349-4354.

Ogawa T., Bao D. H., Katoh H., Shibata M., Pakrasi H. B. & Bhattacharyya-Pakrasi M. (2002) A two-component signal transduction pathway regulates manganese homeostasis in *Synechocystis* 6803, a photosynthetic organism. *J. Biol. Chem.* 277: 28981-28986.

Osman D. & Cavet J. S. (2010) Bacterial metal-sensing proteins exemplified by ArsR-SmtB family repressors. *Nat. Prod. Rep.* 27: 668-680.

Osman D., Patterson C. J., Bailey K., Fisher K., Robinson N. J., Rigby S. E. & Cavet J. S. (2013) The copper supply pathway to a *Salmonella* Cu, Zn-superoxide dismutase (SodCII) involves P(1) (B) -type ATPase copper efflux and periplasmic CueP. *Mol. Microbiol.* 87: 466-477.

- Osman D., Waldron K. J., Denton H., Taylor C. M., Mastroeni P., Robinson N. J. & Cavet J. S. (2010) Copper homeostasis in *Salmonella* is atypical and copper-CueP is a major periplasmic metal complex. *J. Biol. Chem.* 285: 25259-25268.
- Outten C. E. & O'Halloran T. V. (2001) Femtomolar sensitivity of proteins controlling zinc homeostasis. *Science*. 292: 2488-2492.
- Outten C. E., Tobin D. A., Penner-Hahn J. E. & O'Halloran T. V. (2001) Characterization of the metal receptor sites in *Escherichia coli* Zur, an ultrasensitive zinc(II) metalloregulatory protein. *Biochemistry*. 40: 10417-10423.
- Oxelfelt F., Tamagnini P., Salema R. & Lindblad P. (1995) Hydrogen uptake in *Nostoc* strain PCC73102- effects of nickel, hydrogen, carbon and nitrogen. *Plant Physiol. Biochem.* 33: 617-623.
- Pakrasi H. B., Ogawa T. & Bhattacharya-Pakrasi M. (2002) Transport of metals: a key process in oxygenic photosynthesis. *Biochem. Soc. Trans.* 30: 768-770.
- Panina E. M., Mironov A. A. & Gelfand M. S. (2003) Comparative genomics of bacterial zinc regulons: enhanced ion transport, pathogenesis, and rearrangement of ribosomal proteins. *Proc. Natl. Acad. Sci. USA*. 100: 9912-9917.
- Parkhill J., Ansari A. Z., Wright J. G., Brown N. L. & O'Halloran T. V. (1993) Construction and characterization of a mercury-independent MerR activator (MerRAC): transcriptional activation in the absence of Hg(II) is accompanied by DNA distortion. *EMBO J.* 12: 413-421.
- Parkhill J. & Brown N. L. (1990) Site-specific insertion and deletion mutants in the *mer* promoter-operator region of Tn501- 19 bp spacer is essential for normal induction of the promoter by MerR. *Nucleic Acids Res.* 18: 5157-5162.

- Pasternak A., Kaplan J., Lear J. D. Degrado W. F. (2001) Proton and metal ion-dependent assembly of a model diiron protein. *Protein Sci.* 10: 958-969.
- Patterson C. J. (2010) *In vitro* and *in vivo* responses of CoaR, ZiaR and Zur (Trans-family metal-sensing). PhD Thesis. Newcastle University.
- Patterson C. J., Pernil R., Dainty S. J., Chakrabarti B., Henry C. E., Money V. A., Foster A. W. & Robinson N. J. (2013) Co(II)-detection does not follow $K_{\text{Co(II)}}$ gradient: Channeling in Co(II)-sensing. *Metallomics.* 5: 352-362.
- Patzer S. I. & Hantke K. (1998) The ZnuABC high-affinity zinc uptake system and its regulator Zur in *Escherichia coli*. *Mol. Microbiol.* 28: 1199-1210.
- Patzer S. I. & Hantke K. (2000) The zinc-responsive regulator Zur and its control of the *znu* gene cluster encoding the ZnuABC zinc uptake system in *Escherichia coli*. *J. Biol. Chem.* 275: 24321-24332.
- Payne J. C., ter Horst M. A. & Godwin H. A. (1999) Lead fingers: Pb^{2+} binding to structural zinc-binding domains determined by monitoring lead-thiolate charge-transfer bands. *J. Am. Chem. Soc.* 121: 6850-6855.
- Peers G. & Price N. M. (2006) Copper-containing plastocyanin used for electron transport by an oceanic diatom. *Nature.* 441: 341-344.
- Pennella M. A., Arunkumar A. I. & Giedroc D. P. (2006) Individual metal ligands play distinct functional roles in the zinc sensor *Staphylococcus aureus* CztA. *J. Mol. Biol.* 356: 1124-1136.
- Pennella M. A., Shokes J. E., Cospers N. J., Scott R. A. & Giedroc D. P. (2003) Structural elements of metal selectivity in metal sensor proteins. *Proc. Natl. Acad. Sci. U. S. A.* 100: 3713-3718.

- Permina E. A., Kasakov A. E., Kalinina O. V. & Gelfand M. S. (2006) Comparative genomics of regulation of heavy metal resistance in eubacteria. *BMC Microbiol.* 6: 49.
- Petersen C. & Møller L. B. (2000) Control of copper homeostasis in *Escherichia coli* by a P-type ATPase, CopA, and a MerR-like transcriptional activator, CopR. *Gene.* 261: 289-298.
- Phillips C. M., Schreiter E. R., Guo Y., Wang S. S., Zamble D. B. & Drennan C. L. (2008) Structural basis of the metal specificity for nickel regulatory protein NikR. *Biochemistry.* 47: 1938-1946.
- Pinske C., Bönn M., Krüger S., Lindenstrauss U. & Sawers R. G. (2011) Metabolic deficiencies revealed in the biotechnologically important model bacterium *Escherichia coli* BL21(DE3). *PLoS One.* 6: e22830.
- Pohl E., Haller J. C., Mijovilovich A., Meyer-Klaucke W., Garman E. & Vasil M. L. (2003) Architecture of a protein central to iron homeostasis: crystal structure and spectroscopic analysis of the ferric uptake regulator. *Mol. Microbiol.* 47: 903-915.
- Portmann R., Poulsen K. R., Wimmer R. & Solioz M. (2006) CopY-like copper inducible repressors are putative 'winged helix' proteins. *Biometals.* 19: 61-70.
- Potter A. J., Kidd S. P., McEwan A. G. & Paton J. C. (2010) The MerR/NmlR family transcription factor of *Streptococcus pneumoniae* responds to carbonyl stress and modulates hydrogen peroxide production. *J. Bacteriol.* 192: 4063-4066.
- Price N. M. & Morel F. M. M. (1991) Colimitation of phytoplankton growth by nickel and nitrogen. *Limnol. Oceanogr.* 36: 1071-1077.

- Proshkin S., Rahmouni A. R., Mironov A. & Nudler E. (2010) Cooperation between translating ribosomes and RNA polymerase in transcription elongation. *Science*. 328: 504-508.
- Pruteanu M., Neher S. B. & Baker T. A. (2007) Ligand-controlled proteolysis of the *Escherichia coli* transcriptional regulator ZntR. *J. Bacteriol.* 189: 3017-3025.
- Qi Z., Hamza I. & O'Brian M. R. (1999) Heme is an effector molecule for iron-dependent degradation of the bacterial iron response regulator (Irr) protein. *Proc. Natl. Acad. Sci. USA*. 96: 13056-13061.
- Qi Z. & O'Brian M. R. (2002) Interaction between bacterial iron response regulator and ferrochelatase mediates genetic control of heme biosynthesis. *Mol. Cell*. 9: 155-162.
- Quaranta D., McEvoy M. M. & Rensing C. (2009) Site-directed mutagenesis identifies a molecular switch involved in copper sensing by the histidine kinase CinS in *Pseudomonas putida* KT2440. *J. Bacteriol.* 191: 5304-5311.
- Quintana N., Van der Kooy F., Van de Rhee M. D., Voshol G. P. & Verpoorte R. (2011) Renewable energy from Cyanobacteria: energy production optimization by metabolic pathway engineering. *Appl. Microbiol. Biotechnol.* 91: 471-490.
- Raimunda D., González-Guerrero M., Leeber B. W. 3rd. Argüello J. M. (2012) The transport mechanism of bacterial Cu⁺-ATPases: distinct efflux rates adapted to different function. *Biometals*. 24: 467-475.
- Ranquet C., Ollagnier-de-Choudens S., Loiseau L., Barras F. & Fontecave M. (2007) Cobalt stress in *Escherichia coli*. The effect on the iron-sulfur proteins. *J. Biol. Chem.* 282: 30442-30451.

- Rensing C., Mitra B. & Rosen B. P. (1997) The *zntA* gene of *Escherichia coli* encodes a Zn(II)-translocating P-type ATPase. *Proc. Natl. Acad. Sci. USA*. 94: 14326-14331.
- Rensing C., Sun Y., Mitra B. & Rosen B. P. (1998) Pb(II)-translocating P-type ATPases. *J. Biol. Chem.* 179: 2769-2771.
- Reyes-Caballero H., Guerra A. J., Jacobsen F. E., Kazmierczak K. M., Cowart D., Koppolu U. M., Scott R. A., Winkler M. E. & Giedroc D. P. (2010) The metalloregulatory zinc site in *Streptococcus pneumoniae* AdcR, a zinc-activated MarR family repressor. *J. Mol. Biol.* 403: 197-216.
- Reyes-Caballero H., Lee C. W. & Giedroc D. P. (2011) Mycobacterium tuberculosis NmtR harbors a nickel sensing site with parallels to Escherichia coli RcnR. *Biochemistry*. 50: 7941-7952.
- Richardson A. R., Dunman P. M. & Fang F. C. (2006) The nitrosative stress response of *Staphylococcus aureus* is required for resistance to innate immunity. *Mol. Microbiol.* 61: 927-939.
- Riddles P. W., Blakeley R. L. & Zerner B. (1979) Ellman's reagent: 5,5'-Dithio-bis-(2-nitrobenzoic acid), a re-examination. *Anal. Biochem.* 94: 75-81.
- Robinson N. J. (2007) A more discerning zinc exporter. *Nat. Chem. Biol.* 3: 692-693.
- Robinson N. J. & Winge D. R. (2010) Copper metallochaperones. *Annu. Rev. Biochem.* 79: 537-562.
- Rodionov D. A., Hebbeln P., Gelfand M. S. & Eitinger T. (2006) Comparative and functional genomic analysis of prokaryotic nickel and cobalt uptake transporters: evidence for a novel group of ATP-binding cassette transporters. *J. Bacteriol.* 188: 317-327.

- Rodrique A., Effantin G. & Mandrand-Berthelot M. A. (2005) Identification of *rcnA* (*yohM*), a nickel and cobalt resistance gene in *Escherichia coli*. *J. Bacteriol.* 187: 2912-2916.
- Rowe J. L., Starnes G. L. & Chivers P. T. (2005) Complex transcriptional control links NikABCDE-dependent nickel transport with hydrogenase expression in *Escherichia coli*. *J. Bacteriol.* 187: 6317-6323.
- Rutherford J. C., Cavet J. S. & Robinson N. J. (1999) Cobalt-dependant transcriptional switching by a dual-effector MerR-like protein regulates a cobalt-exporting variant CPx-type ATPase. *J. Biol. Chem.* 274: 25827-25832.
- Saint-Jean A. P., Phillips K. R., Creighton D. J. & Stone M. J. (1998) Active monomeric and dimeric forms of *Pseudomonas putida* glyoxalase I: evidence for 3D domain swapping. *Biochemistry.* 37: 10345-10353.
- Sakamoto K., Agari Y., Agari K., Kuramitsu S. & Shinkai A. (2010) Structural and functional characterisation of the transcriptional repressor CsoR from *Thermus thermophiles* HB8. *Microbiology.* 156: 1993-2005.
- Sambrook J. & Russell D. (2001) *Molecular Cloning: A Laboratory Manual*. 3rd ed. Cold Spring Harbour Press, USA.
- Sato S., Shimoda Y., Muraki A., Kohara M., Nakamura Y. & Tabata S. (2007) A large scale protein-protein interaction analysis in *Synechocystis* sp. PCC6803. *DNA Res.* 14: 207-216.
- Schmitt M. P., Twiddy E. M. & Holmes R. K. (1992) Purification and characterization of the diphtheria toxin repressor. *Proc. Natl. Acad. Sci. USA.* 89: 7576-7580.

- Schreiter E. R., Sintchak M. D., Guo Y., Chivers P. T., Sauer R. T. & Drennan C. L. (2003) Crystal structure of the nickel-responsive transcription factor NikR. *Nat. Struct. Biol.* 10: 794-799.
- Schröder J., Jochmann N., Rodionov D. A. & Tauch A. (2010) The Zur regulon of *Corynebacterium glutamicum* ATCC 13032. *BMC Genomics*. 11: 12.
- Schultz S. C., Shields G. C. & Steitz T. A. (1991) Crystal structure of a CAP-DNA complex: the DNA is bent by 90 degrees. *Science*. 253: 1001-1007.
- Schwartz C. J., Giel J. L., Patschkowski T., Luther C., Ruzicka F. J., Beinert H. & Kiley P. J. (2001) IscR, an Fe-S cluster-containing transcription factor, represses expression of *Escherichia coli* genes encoding Fe-S cluster assembly proteins. *Proc. Natl. Acad. Sci. USA*. 98: 14895-14900.
- Schwarz G., Mendel R. R. & Ribbe M. W. (2009) Molybdenum cofactors, enzymes and pathways. *Nature*. 460: 839-847.
- Sellitti M. A., Pavco P. A. & Steege D. A. (1987) *lac* repressor blocks *in vivo* transcription of *lac* control region DNA. *Proc. Natl. Acad. Sci. USA*. 84: 3199-3203.
- Shewchuk L. M., Verdine G. L. & Walsh C. T. (1989) Transcriptional switching by the metalloregulatory MerR protein: initial characterization of the DNA and mercury(II) binding activities. *Biochemistry*. 28: 2331-2339.
- Shi W., Dong J., Scott R. A., Ksenzenko M. Y. & Rosen B. P. (1996) The role of arsenic-thiol interactions in metalloregulation of the *ars* operon. *J. Biol. Chem.* 271: 9291-9297.
- Shi W., Wu J. & Rosen B. P. (1994) Identification of a putative metal binding site in a new family of metalloregulatory proteins. *J. Biol. Chem.* 269: 19826-19829.

- Shin J. H., Jung H. J., An Y. J., Cho Y. B., Cha S. S. & Roe J. H. (2011) Graded response of zinc-responsive genes through two regulatory zinc-binding sites in Zur. *Proc. Natl. Acad. Sci. USA*. 108: 5045-5050.
- Shin J. H., Oh S. Y., Kim S. J. & Roe J. H. (2007) The zinc-responsive regulator Zur controls a zinc uptake system and some ribosomal proteins in *Streptomyces coelicolor* A3(2). *J. Bacteriol.* 189: 4070-4077.
- Smaldone G. T. & Helmann J. D. (2007) CsoR regulates the copper efflux operon *copZA* in *Bacillus subtilis*. *Microbiology*. 153: 4123-4128.
- Spiering M. M., Ringe D., Murphy J. R. & Marletta M. A. (2003) Metal stoichiometry and functional studies of the diphtheria toxin repressor. *Proc. Natl. Acad. Sci. USA*. 100: 3808-3813.
- Sridhar J., Sabarinathan R., Gunasekaran P. & Sekar K. (2012) Comparative genomics reveals 'novel' Fur regulated sRNAs and coding genes in diverse proteobacteria. *Gene*. 516: 335-344.
- Stoyanov J. V. & Brown N. L. (2003) The *Escherichia coli* copper-responsive *copA* promoter is activated by gold. *J. Biol. Chem.* 278: 1407-1410.
- Stoyanov J. V., Hobman J. L. & Brown N. L. (2001) CueR (YBBI) of *Escherichia coli* is a MerR family regulator controlling expression of the copper exporter CopA. *Mol. Microbiol.* 39: 502-511.
- Su C. C., Long F. & Yu E. W. (2011) The Cus efflux system removes toxic ions via a methionine shuttle. *Protein Sci.* 20: 6-18.
- Summers A. O. (1992) Untwist and shout: a heavy metal-responsive transcriptional regulator. *J. Bacteriol.* 174: 3097-3101.

Suttisansanee U. & Honek J. F. (2011) Bacterial glyoxalase enzymes. *Semin. Cell Dev. Biol.* 22: 285-292.

Tanioka Y., Yabuta Y., Yamaji R., Shigeoka S., Nakano Y., Watanabe F. & Inui H. (2009) Occurance of pseudovitamin B12 and its possible function as a cofactor of cobalamin-dependent methionine synthase in a cyanobacterium *Synechocystis* sp. PCC6803. *J. Nutr. Sci. Vitaminol. (Tokyo)*. 55: 518-521.

Tao X. & Murphy J. R. (1992) Binding of the metalloregulatory protein DtxR to the diphtheria *tox* operator requires a divalent heavy metal ion and protects the palindromic sequence from DNaseI digestion. *J. Biol. Chem.* 267: 21761-21764.

Thelwell C., Robinson N.J. & Turner-Cavet J.S. (1998) An SmtB-like repressor from *Synechocystis* PCC 6803 regulates a zinc exporter. *Proc. Natl. Acad. Sci. USA*. 95: 10728-33.

Thumanu K., Cha J., Fischer J. F., Perrins R., Mobashery S. & Wharton C. (2006) Discrete steps in sensing beta-lactam antibiotics by the BlaR1 protein of the methicillin-resistant *Staphylococcus aureus* bacterium. *Proc. Natl. Acad. Sci. USA*. 103: 10630-10635.

Tottey S., Harvie D. R. & Robinson N. J. (2005) Understanding how cells allocate metals using metal sensors and metallochaperones. *Acc. Chem. Res.* 38: 775-783.

Tottey S., Patterson C. J., Banci L., Bertini I., Felli I. C., Pavelkova A., Dainty S. J., Pernil R., Waldron K. J., Foster A. W. & Robinson N. J. (2012) A cyanobacterial metallochaperone inhibits deleterious side effects of copper. *Proc. Natl. Acad. Sci. USA*. 109: 95-100.

- Tottey S., Rich P. R., Rondet S. A. & Robinson N. J. (2001) Two Menkes-type ATPases supply copper for photosynthesis in *Synechocystis* PCC 6803. *J. Biol. Chem.* 276: 19999-20004.
- Tottey S., Rondet S. A., Borrelly G. P., Robinson P. J., Rich P. R. & Robinson N. J. (2002) A copper metallochaperone for photosynthesis and respiration reveals metal-specific targets, interaction with an importer, and alternative sites for copper acquisition. *J. Biol. Chem.* 277: 5490-5497.
- Tottey S., Waldron K. J., Firbank S. J., Reale B., Bessant C., Sato K., Cheek T. R., Gray J., Banfield M. J., Dennison C. & Robinson N. J. (2008) Protein-folding location can regulate manganese-binding versus copper- or zinc-binding. *Nature*. 455: 1138-1142.
- Turner J. S., Glands P. D., Samson A. C. & Robinson N. J. (1996) Zn^{2+} -sensing by the cyanobacterial metallothionein repressor SmtB: different motifs mediate metal-induced protein-DNA dissociation. *Nucleic Acids Res.* 24: 3714-3721.
- Valladares A., Montesinos M. L., Herrero A. & Flores E. (2002) An ABC-type, high-affinity urea permease identified in cyanobacteria. *Mol. Microbiol.* 43: 703-715.
- VanZile M. L., Chen X. & Giedroc D. P. (2002a) Allosteric negative regulation of *smt* O/P binding of the zinc sensor, SmtB, by metal ions: A coupled equilibrium analysis. *Biochemistry*. 41: 9776-9786.
- VanZile M. L., Chen X. & Giedroc D. P. (2002b) Structural characterization of distinct $\alpha 5N$ and $\alpha 3$ metal sites in the cyanobacterial zinc sensor SmtB. *Biochemistry*. 41: 9765-9775.
- VanZile M. L., Cosper N. J., Scott R. A. & Giedroc D. P. (2000) The zinc metalloregulatory protein *Synechococcus* PCC7942 SmtB binds a single zinc ion per

- monomer with high affinity in a tetrahedral coordination geometry. *Biochemistry*. 39: 11818-11829.
- Vašák M. & Kägi J. H. R. (1981) Metal thiolate clusters in cobalt(II)-metallothionein. *Proc. Natl. Acad. Sci. USA*. 78: 6709-6713.
- Vavilin D. V. & Vermaas W. F. J. (2002) Regulation of tetrapyrrole biosynthetic pathway leading to heme and chlorophyll in plants and cyanobacteria. *Physiol. Plant*. 115: 9-24.
- Waldron K. J., Firbank S. J., Dainty S. J., Pérez-Rama M., Tottey S. & Robinson N. J. (2010) Structure and metal loading of a soluble periplasm cuproprotein. *J. Biol. Chem*. 285: 32504-32511.
- Waldron K. J. & Robinson N. J. (2009) How do bacterial cells ensure that metalloproteins get the correct metal? *Nat. Rev. Microbiol*. 6: 25-35.
- Waldron K. J., Rutherford J. C., Ford D. & Robinson N. J. (2009) Metalloproteins and metal sensing. *Nature*. 460: 823-830.
- Wang D., Hosteen O. & Fierke C. A. (2012) ZntR-mediated transcription of *zntA* responds to nanomolar intracellular free zinc. *J. Inorg. Biochem*. 111: 173-181.
- Wang D., Hurst T. K., Thompson R. B. & Fierke C. A. (2011) Genetically encoded ratiometric biosensors to measure intracellular exchangeable zinc in *Escherichia coli*. *J. Biomed. Opt*. 16: 087011.
- Wang S. C., Dias V. A., Bloom S. L. & Zamble D. B. (2004) Selectivity of metal binding and metal-induced stability of *Escherichia coli* NikR. *Biochemistry*. 43: 10018-10028.
- Wang Y., Hemmingsen L. & Giedroc D. P. (2005) Structural and functional characterization of *Mycobacterium tuberculosis* CmtR, a Pb^{II}/Cd^{II}-sensing SmtB/ArsR metalloregulatory repressor. *Biochemistry*. 44: 8976-8988.

- Wang Y., Kendall J., Cavet J. S. & Giedroc D. P. (2010) Elucidation of the functional metal binding profile of a Cd^{II}/Pb^{II} sensor CmtR^{Sc} from *Streptomyces coelicolor*. *Biochemistry*. 49: 6617-6626.
- Watanabe S., Kita A., Kobayashi K. & Miki K. (2008) Crystal structure of the [2Fe-2S] oxidative-stress sensor SoxR bound to DNA. *Proc. Natl. Acad. Sci. USA*. 105: 4121-4126.
- Waterman M. S. & Eggert M. (1987) A new algorithm for best sequence alignments with application to tRNA-rRNA comparisons. *J. Mol. Biol.* 197: 723-728.
- Watnick P. I., Eto T., Takahashi H. & Calderwood S. B. (1997) Purification of *Vibrio cholera* Fur and estimation of its intracellular abundance by antibody sandwich enzyme-linked immunosorbent assay. *J. Bacteriol.* 179: 243-247.
- Watton S. P., Wright J. G., MacDonnell F. M., Bryson J. W., Sabat M. & O'Halloran T. V. (1990) Trigonal mercuric complex of an aliphatic thiolate: A spectroscopic and structural model for the receptor site in the Hg(II) biosensor MerR. *J. Am. Chem. Soc.* 112: 2824-2826.
- White C., Lee J., Kambe T., Fritsche K. & Petris M. J. (2009) A role for the ATP7A copper-transporting ATPase in macrophage bactericidal activity. *J. Biol. Chem.* 284: 33949-33956.
- Williams S. G., Attridge S. R. & Manning P. A. (1993) The transcriptional activator HlyU of *Vibrio cholerae*: nucleotide sequence and role in virulence gene expression. *Mol. Microbiol.* 9: 751-760.
- Williams S. G. & Manning P. A. (1991) Transcription of the *Vibrio cholerae* haemolysin gene, *hlyA*, and cloning of a positive regulatory locus, *hlyU*. *Mol. Microbiol.* 5: 2031-2038.

- Willins D. A., Ryan C. W., Platko J. V. & Calvo J. M. (1991) Characterization of Lrp, an *Escherichia coli* regulatory protein that mediates a global response to leucine. *J. Biol. Chem.* 266: 10768-10774.
- Wilson A., Ajlani G., Verbavatz J. M., Vass I., Kerfeld C. A. & Kirilovsky D. (2006) A soluble carotenoid protein involved in phycobilisome related energy dissipation in cyanobacteria. *Plant Cell.* 18: 992-1007.
- Wu J. & Rosen B. P. (1993) Metalloregulated expression of the *ars* operon. *J. Biol. Chem.* 268: 52-8.
- Wu J. & Weiss B. (1991) Two divergently transcribed genes, *soxR* and *soxS*, control a superoxide response regulon of *Escherichia coli*. *J. Bacteriol.* 173: 2864-2871.
- Wu L. F., Mandrand-Berthelot M. A., Waugh R., Edmonds C. J., Holt S. E. & Boxer D. H. (1989) Nickel deficiency gives rise to the defective hydrogenase phenotype of *hydC* and *fnr* mutants in *Escherichia coli*. *Mol. Microbiol.* 3: 1709-1718.
- Wu Q. & Vermaas W. F. (1995) Light-dependent chlorophyll *a* biosynthesis upon *chlL* deletion in wild-type and photosystem I-less strains of the cyanobacterium *Synechocystis* sp. PCC 6803. *Plant Mol. Biol.* 29: 933-945.
- Wu Y. P. & Krogmann D. W. (1997) The orange carotenoid protein of *Synechocystis* PCC 6803. *Biochim. Biophys. Acta.* 1322: 1-7.
- Xiankong Z., Tabita R. & vanBaalen C. (1984) Nickel control of hydrogen production and uptake in *Anabaena* spp. Strains CA and 1F. *J. Gen. Microbiol.* 130: 1815-1818.
- Xiao Z., Brose J., Schimo S., Ackland S. M., La Fontaine S. & Wedd A. G. (2011) Unification of the copper(I) binding affinities of the metallo-chaperones Atx1, Atox1, and related proteins: detection probes and affinity standards. *J. Biol. Chem.* 286: 11047-11055.
- Xiao Z., Loughlin F., George G. N., Howlett G. J. & Wedd A. G. (2004) C-terminal domain of the membrane copper transporter Ctr1 from *Saccharomyces cerevisiae* binds

four Cu(I) ions as a cuprous-thiolate polynuclear cluster: sub-femtomolar Cu(I) affinity of three proteins involved in copper trafficking. *J. Am. Chem. Soc.* 126: 3081-3090.

Xiao Z. & Wedd A. G. (2010) The challenges of determining metal-protein affinities. *Nat. Prod. Rep.* 27: 768-789.

Yamaguchi K., Suzuki I., Yamamoto H., Lyukevich A., Bodrova I., Los D. A., Piven I., Zinchenko V., Kanehisa M. & Murata N. (2002) A two-component Mn^{2+} -sensing system negatively regulates expression of the *mntCAB* operon in *Synechocystis*. *Plant Cell*. 14: 2901-2913.

Yamamoto K. & Ishihama A. (2005a) Transcriptional response of *Escherichia coli* to external copper. *Mol. Microbiol.* 56: 215-227.

Yamamoto K. & Ishihama A. (2005b) Transcriptional response of *Escherichia coli* to external zinc. *J. Bacteriol.* 187: 6333-6340.

Ye J., Kandegedara A., Martin P. & Rosen B. P. (2005) Crystal structure of the *Staphylococcus aureus* pl258 CadC Cd(II)/Pb(II)/Zn(II)-responsive repressor. *J. Bacteriol.* 187: 4214-4221.

Zambelli B., Bellucci M., Danielli A., Scarlato V. & Ciurli S. (2007) The Ni^{2+} binding properties of *Helicobacter pylori* NikR. *Chem. Commun.* 21: 3649-3651.

Zayas C. L., Claas K. R. & Escalante-Semerena J. C. (2007) The CbiB protein of *Salmonella enterica* is an integral membrane protein involved in the last step of the *de novo* corrin ring biosynthetic pathway. *J. Bacteriol.* 189: 7697-7708.

Zhang H. Z., Hackbarth C. J., Chansky K. M. & Chambers H. F. (2001) A proteolytic transmembrane signalling pathway and resistance to beta-lactams in staphylococci. *Science*. 291: 1962-1965.

Zhang L., McSpadden B., Pakrasi H. B. & Whitmarsh J. (1992) Copper-mediated regulation of cytochrome c533 and plastocyanin in the cyanobacterium *Synechocystis* 6803. *J. Biol. Chem.* 267: 19054-19059.

Zheng M., Doan B., Schneider T. D. & Storz G. (1999) OxyR and SoxRS regulation of *fur*. *J. Bacteriol.* 181: 4639-4643.

Zhu T., Tian J., Zhang S., Wu N. & Fan Y. (2011) Identification of the transcriptional regulator NcrB in the nickel resistance determinant of *Leptospirillum ferriphilum* UBK03. *PLoS One*. 6: e17367.

Appendix A

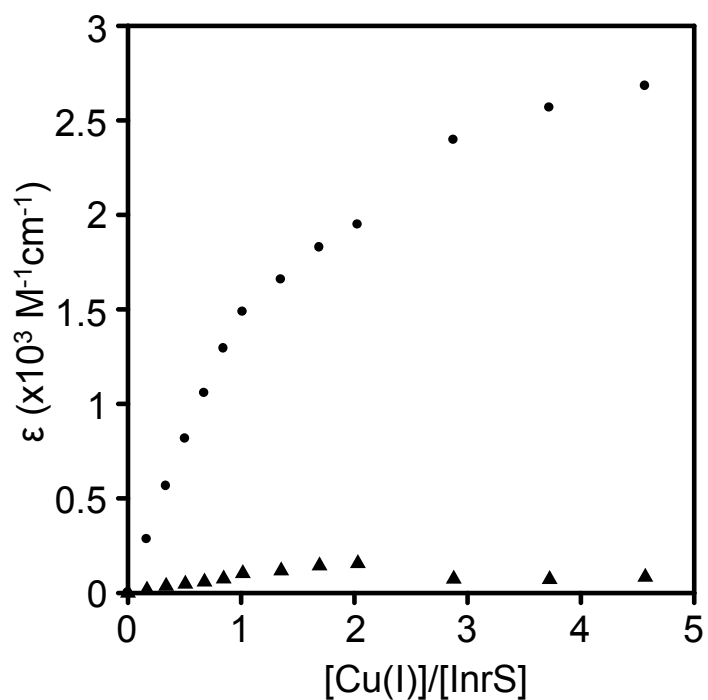


Figure A1. Apo-subtracted Cu(I)-dependent spectral features of InrS. Binding isotherm depicting spectral features of InrS (10 μM) at 240 nm (circles) and (435 nm) upon titration with CuCl (confirmed to be >95 % Cu^+).

GGCTGGTAGAACTGGTTTGGTAAATGACCTGTGACTATCCATCAATT
GAAGGCATTGGCAAGATGGAAACCTTCCAGAAGGAACGGGAATGCTG
GTTCGATCGCTAATTCTGGACAGGATAACAAAACCAGTTGGTAATGT
GGAAAAAGCTGTCTCCATGTCATTTGGACTGATGCCCTGTTTACTTT
ATTAAACCCACCAATGGTTCAACTTTCCCCGACCC

Figure A2. The promoter region of *ctaA* lacks a GC-rich tract. Nucleotide coding sequence of the start of *ctaA* and 200 nucleotides upstream of the translational start codon (highlighted in red box). A GC-rich tract analogous to that in the promoter regions of *petE* and *pacS* is not observed.

Appendix B

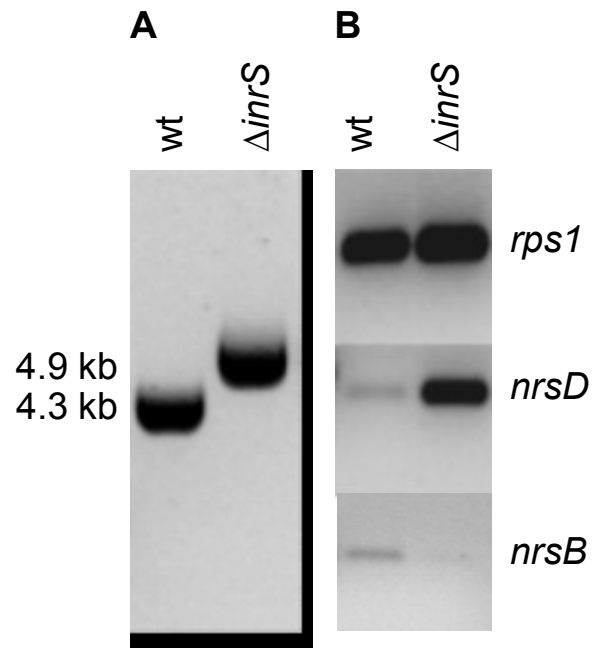


Figure B1. PCR analysis of $\Delta inrS$ mutant. A. PCR amplification of *inrS* flanking regions from wild type and $\Delta inrS$ cells confirming integration of the *inrS* disrupting chloramphenicol resistance cassette and segregation to all chromosomes in $\Delta inrS$. B. RT-PCR analysis of *nrsD*, *nrsB* and *rps1* transcript abundance in wild type and $\Delta inrS$ cells. (Data collected by Rafael Pernil).

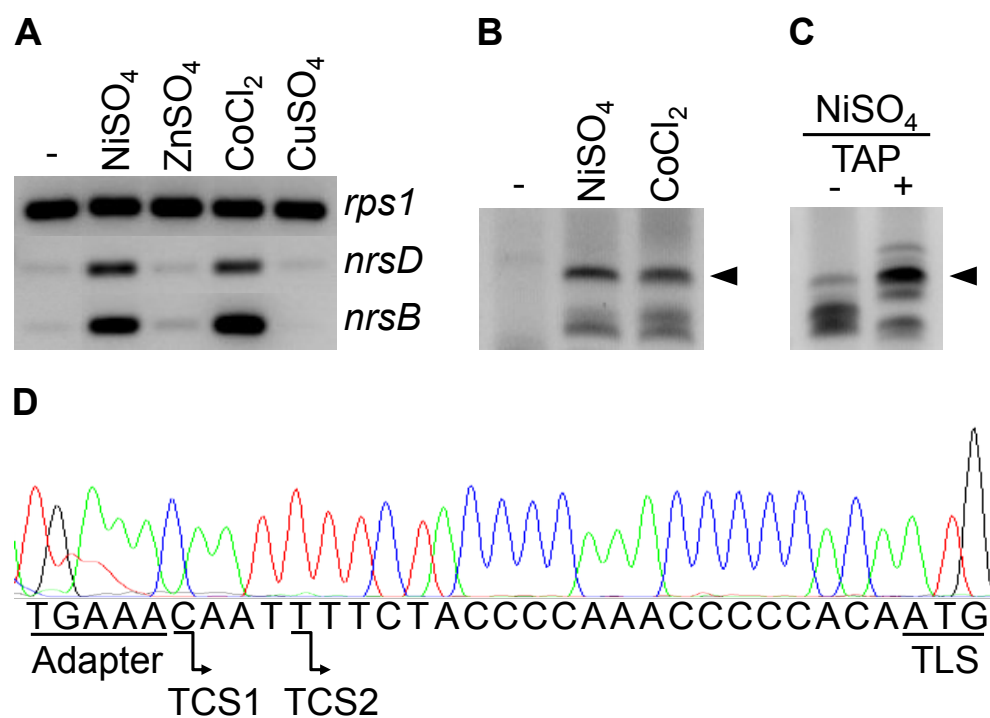


Figure B2. The *nrsD* promoter is responsive to nickel and cobalt but not copper or zinc at steady state. A. RT-PCR analysis of *nrsD*, *nrsB* and *rps1* transcript abundance in wild type cells exposed to maximum non-inhibitory concentrations of NiSO₄ (0.5 μ M), ZnSO₄ (12 μ M), CoCl₂ (2 μ M), and CuSO₄ (1 μ M) for 48 h. B. RLM-RACE experiment performed using RNA extracted from cells grown in BG11 or BG11 supplemented with maximum non-inhibitory concentrations of NiSO₄ and CoCl₂. The indicated products are the expected size (~400 bp) for transcripts originating from an *nrsD* promoter. C. Separate RLM-RACE experiment with RNA from NiSO₄ exposed cells (maximum non-inhibitory concentration) in which tobacco pyrophosphatase treatment has been omitted from a control sample. The ~ 400 bp product increases in a TAP dependent manner confirming the presence of tri-phosphate capped transcript. D. The ~ 400 bp products were cloned and sequenced. The 3' end of the adapter is indicated along with the transcriptional start site (TCS) and the predicted translational start site (TLS). A separate RLM-RACE experiment identified a second TCS 4 bp downstream of the first identified. (Data collected by Rafael Pernil).

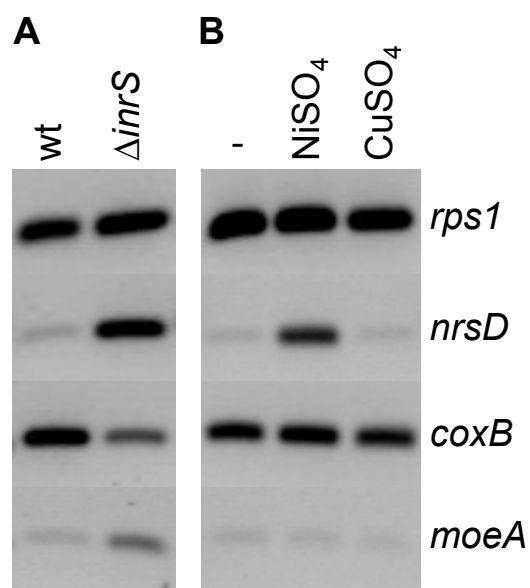


Figure B3. Transcriptional responses of *coxB* and *moeA*. A. RT-PCR analysis of *coxB* and *moeA* transcript abundance in $\Delta inrS$ and wild type cells. *rps1* and *nrsD* were included as controls. B. RT-PCR analysis of *coxB* and *moeA* transcript abundance in $\Delta inrS$ cells exposed to maximum non-inhibitory concentrations of NiSO₄ (0.5 μ M) and CuSO₄ (1 μ M) for 48 h. (Data collected by Rafael Pernil).

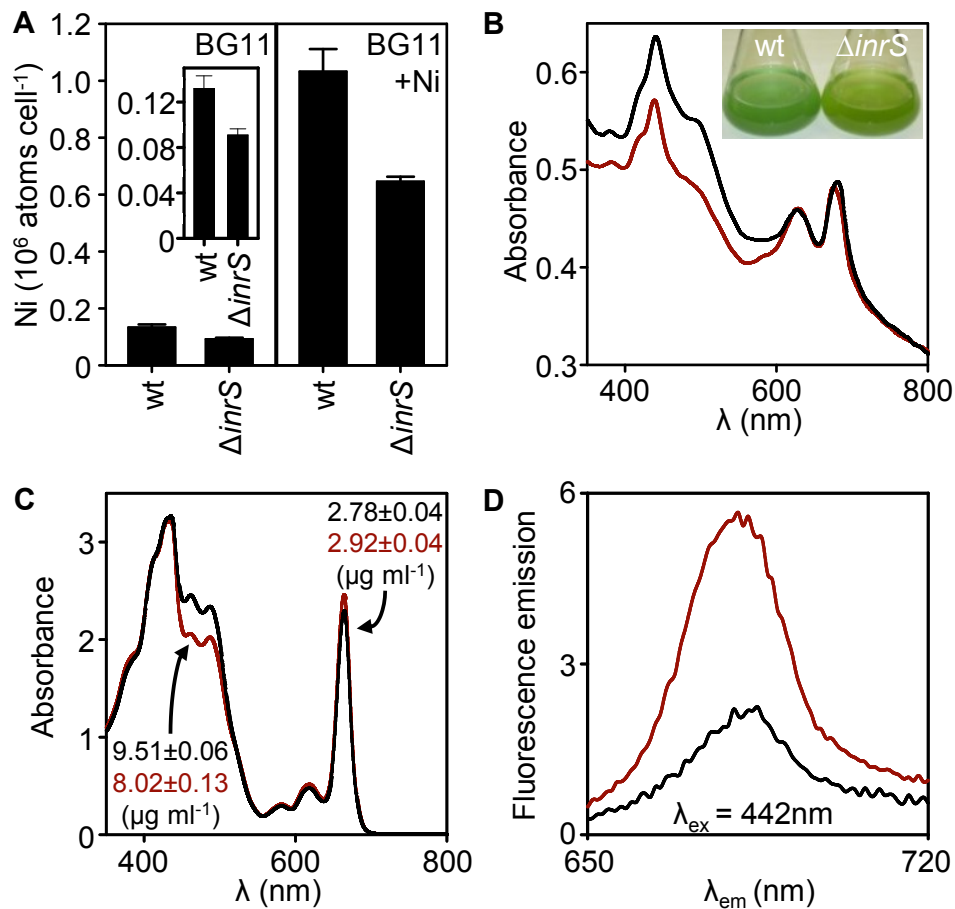


Figure B4. Nickel-homeostasis and pigments are altered in the $\Delta inrS$ strain. A. Whole cell nickel content of wild type and $\Delta inrS$ cells cultured in standard BG11 (left and inset) or exposed to maximum non-inhibitory concentrations of NiSO_4 (0.5 μM) (right) measured by ICP-MS. Cells were digested overnight in 65 % ultra pure HNO_3 prior to ICP-MS analysis. Cells were counted using a Casy Cell Counter TT (Innovatis). B. Visible absorption spectra of wild type (red line) and $\Delta inrS$ (black line) cells normalized to $\text{OD}_{800 \text{ nm}} = 0.3$. Inset, cultures of wild type and $\Delta inrS$ *Synechocystis* normalised to $\text{OD}_{800 \text{ nm}} = 0.3$. C. Visible absorption spectra of *N,N*-dimethylformamide-extracted pigments from wild type (red line) and $\Delta inrS$ (black line) cells with mean concentration (shown with standard deviation) of carotenoids derived from absorbance at 461 nm and chlorophyll *a* derived from absorbance at 664 nm for wild type (red line) and $\Delta inrS$ cells (black line). D. Chlorophyll *a* fluorescence emission of cultures used in 'B' following excitation at 442 nm. Wild type = red line, $\Delta inrS$ = black line. (Data in part C was collected Rafael Pernil, the data in part A and B was collected Rafael Pernil and the author and the data in part D was collected by the author).

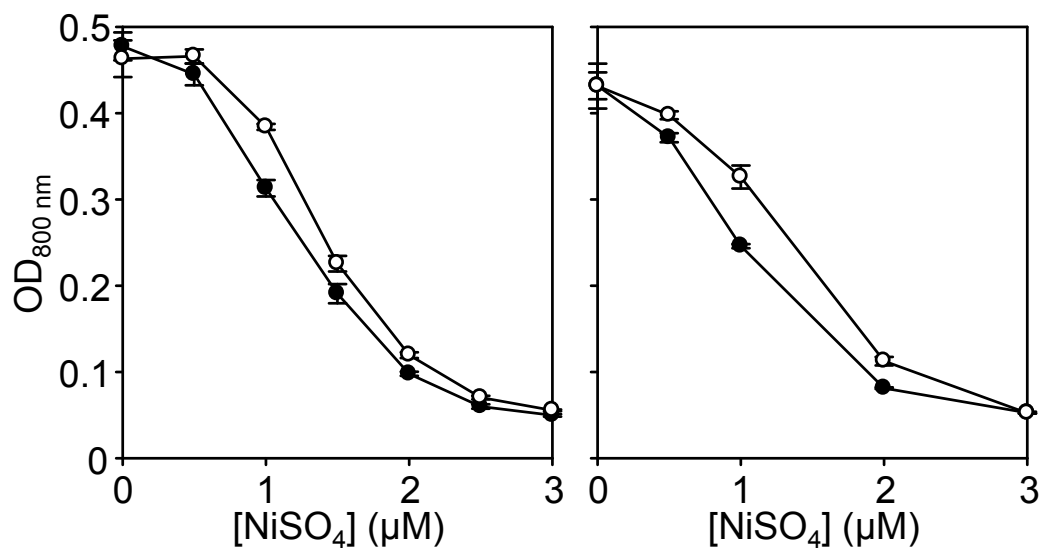


Figure B5. $\Delta inrS$ shows a slight but reproducible increase in Ni(II) tolerance. Two independent experiments (each performed in triplicate) showing optical density of wild type (closed circles) and $\Delta inrS$ (open circles) cells exposed to a range of concentrations of NiSO₄ for 72 h following normalisation of culture OD_{800 nm} to 0.02 at $t = 0$. All values are means of three replicates with standard deviation shown. (Data collected by Rafael Pernil).

Appendix C

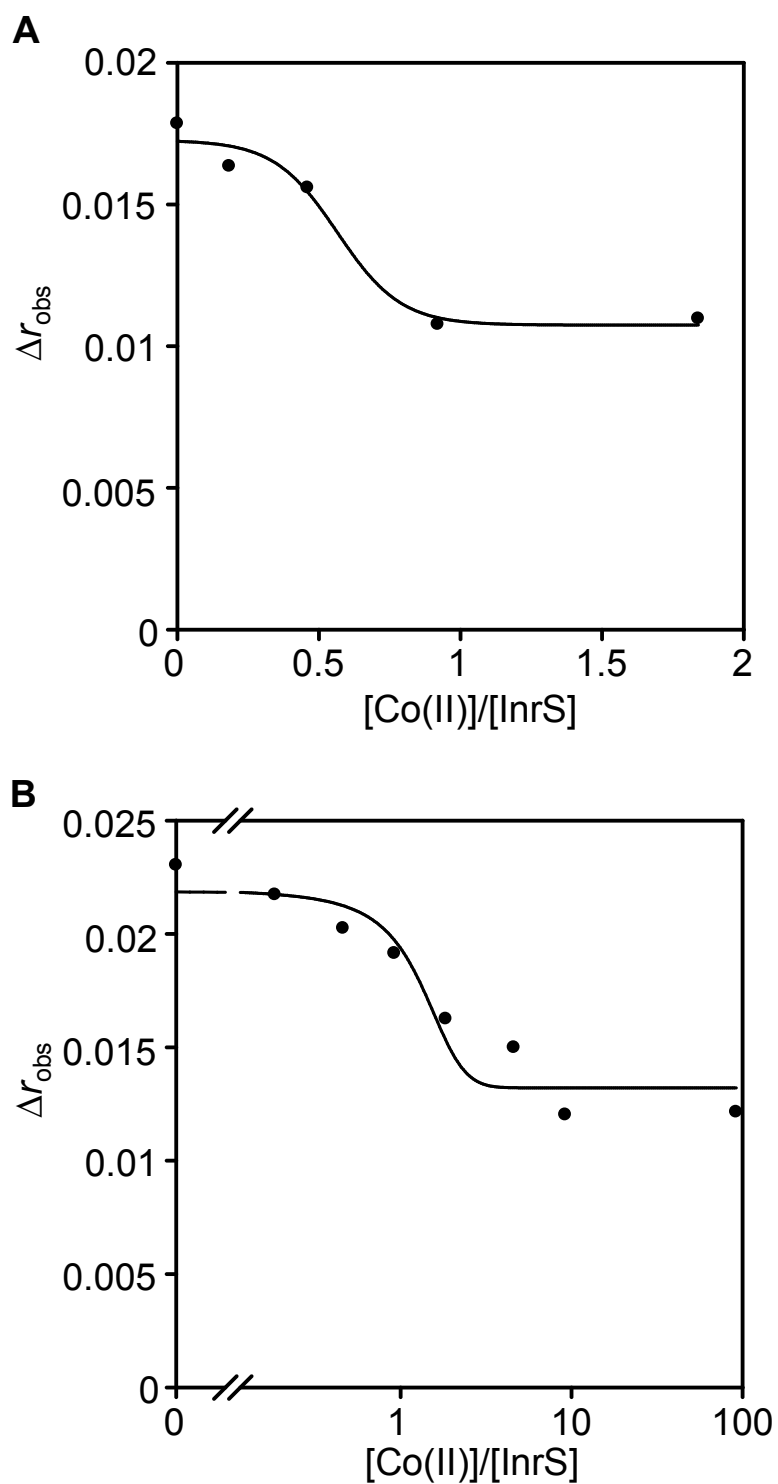


Figure C1. Titration of pre-formed InrS:DNA complexes with CoCl_2 . A. *nrsD*ProFA (10 nM) was pre-incubated with InrS (1 μM) before titration with CoCl_2 . Dissociation of InrS:DNA complexes was monitored by fluorescence anisotropy. Performed anaerobically at pH 7.8. B. As 'A' but performed at pH 7.

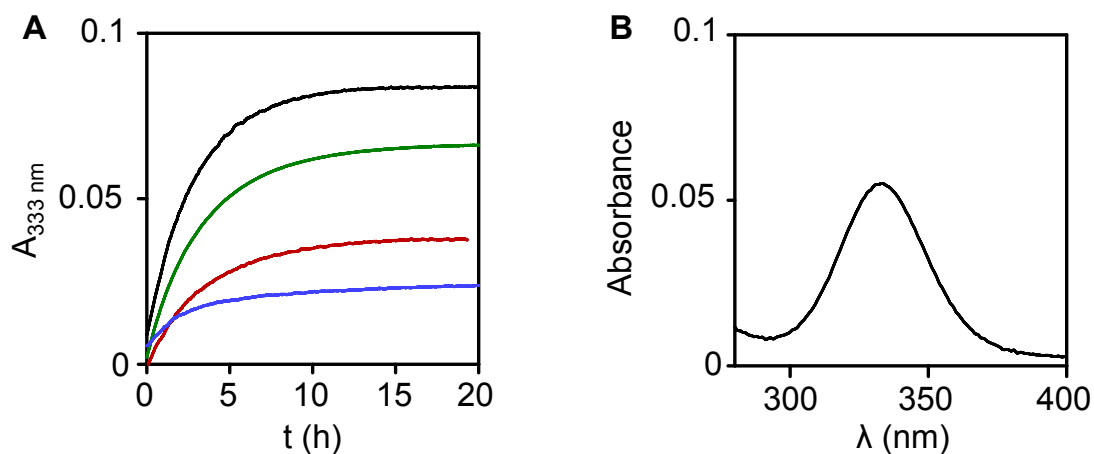


Figure C2. Determination of the Ni(II) affinity of InrS at pH 7 by competition with EGTA. A. NiCl_2 was incubated for 10 min with various excess concentrations of EGTA before addition to a solution of InrS (20 μM). The concentration of NiCl_2 upon addition of the EGTA-Ni(II) mix was 4.85 μM in each experiment and the concentration of EGTA 400 μM (black line), 1 mM (green line), 2 mM (red line) and 4 mM (blue line). Upon addition of the EGTA-Ni(II) mix the change in absorbance at 333 nm which reports on Ni(II) binding to InrS was monitored. B. An analogous experiment to those described in 'A' were carried out at final $[\text{EGTA}] = 1.4 \text{ mM}$. This competition was allowed to come to equilibrium for 20 h before recording the spectrum and equilibrium $A_{333 \text{ nm}}$ value. The equilibrium $A_{333 \text{ nm}}$ values for these experiments were used with the extinction coefficient of Ni(II)-InrS at $A_{333 \text{ nm}}$ (Table 4.3) to determine the equilibrium concentration of Ni(II)-InrS and the Ni(II) affinity of InrS was determined as described in Section 4.2.1.

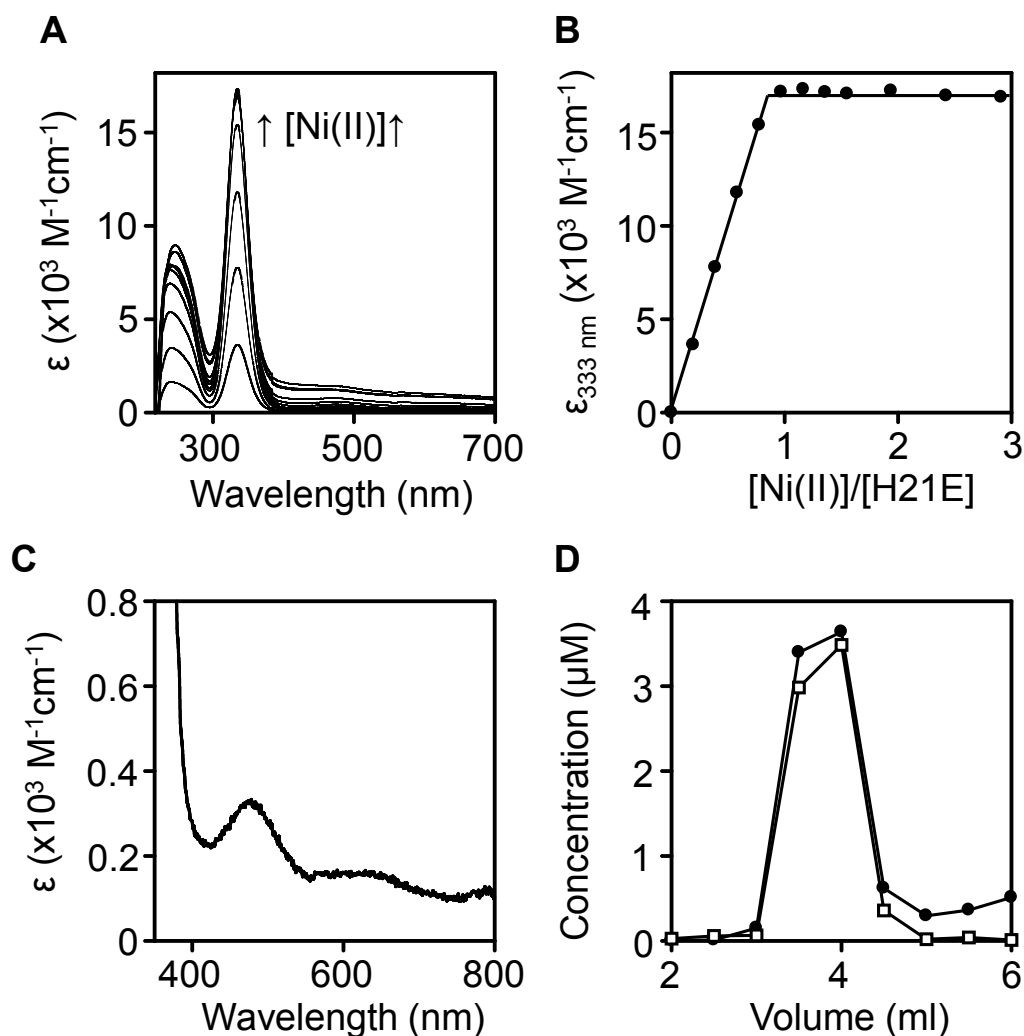


Figure C3. Ni(II) binding properties of InrS His21→Glu. A. Apo-subtracted UV-Vis difference spectra of InrS His21→Glu (10 μM) upon titration with NiCl_2 . B. Binding isotherm depicting the nickel dependent spectral feature at 333 nm in 'A'. C. Enlargement of the InrS UV-Vis spectrum upon addition of 1 molar equivalent of NiCl_2 to highlight the small peak with an absorbance maxima of ~ 480 nm, characteristic of Ni(II) bound in a square planar geometry. D. InrS His21→Glu migrates with one molar equivalent of nickel by size exclusion chromatography. Following the titration of InrS His21→Glu with NiCl_2 shown in 'A' an aliquot (0.5 ml) was applied to and eluted from a PD10 column. Fractions (0.5 ml) were analysed for protein (filled circles) by Bradford assay calibrated against a quantified stock of InrS His21→Glu and nickel (open squares) by ICP-MS. All experiments were performed anaerobically at pH 7.

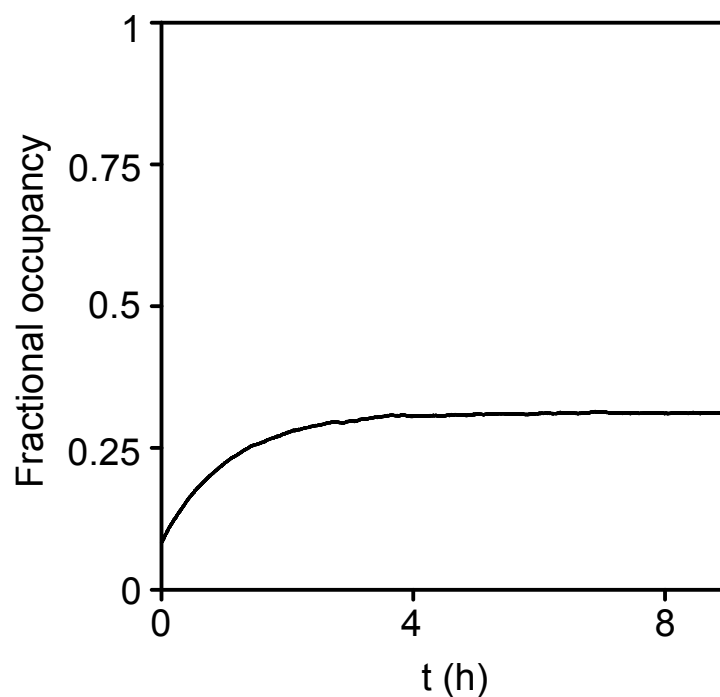
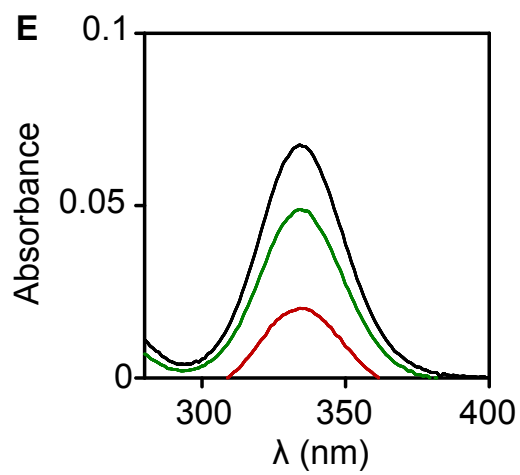
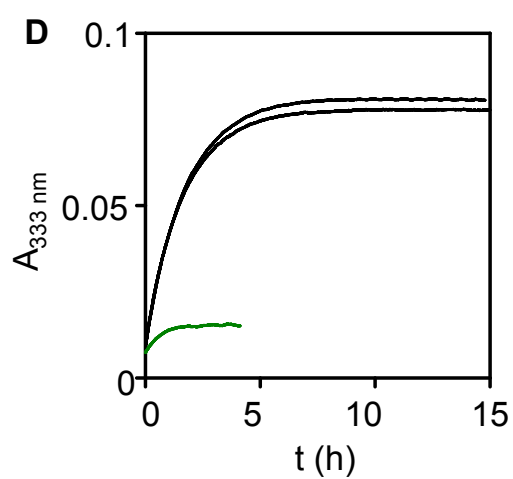
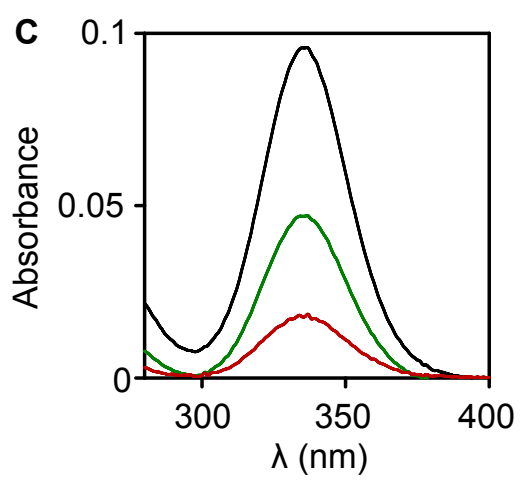
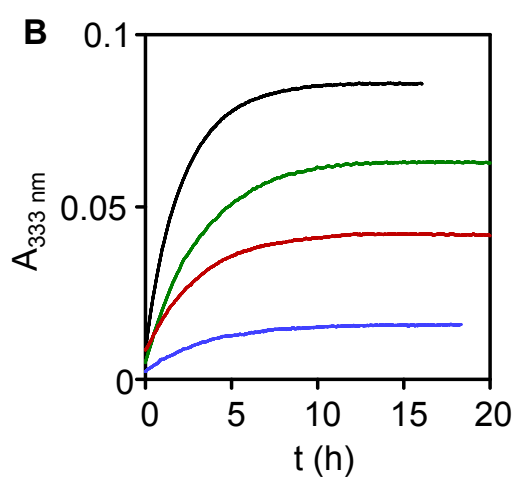
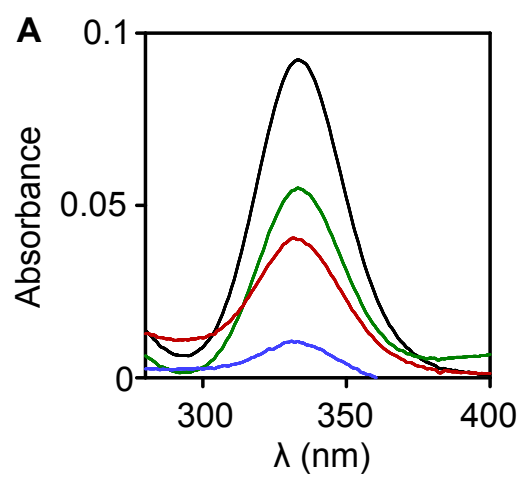


Figure C4. Relative affinity of InrS H21E for Ni(II). Competition between InrS His21→Glu (20 μ M) and EGTA (100 μ M) for NiCl₂ (4.85 μ M) carried out as described in Section 4.2.1 for wild type InrS. The fractional occupancy of the tightest site with Ni(II) was determined using the $\epsilon_{333 \text{ nm}}$ for Ni(II)-InrS His21→Glu determined from UV-Vis titrations of InrS His21→Glu with NiCl₂ (Appendix Figure C3 and Table 4.3).

Figure C5. Determination of the Ni(II) affinity of InrS His21 mutant variants at pH 7 by competition with EGTA. A. NiCl₂ was incubated for 10 min with various excess concentrations of EGTA before addition to a solution of InrS His21→Leu (20 μM). The concentration of NiCl₂ upon addition of the EGTA-Ni(II) mix was 4.85 μM in each experiment and the concentration of EGTA 20 μM (black line), 50 μM (green line), 70 μM (red line) and 150 μM (blue line). These competitions were allowed to come to equilibrium for 20 h before recording the spectrum and equilibrium A_{333 nm} value. B. NiCl₂ was incubated for 10 min with various excess concentrations of EGTA before addition to a solution of InrS His21→Cys (20 μM). The concentration of NiCl₂ upon addition of the EGTA-Ni(II) mix was 4.85 μM in each experiment and the concentration of EGTA 70 μM (black line), 150 μM (green line), 300 μM (red line) and 500 μM (blue line). Upon addition of the EGTA-Ni(II) mix the change in absorbance at 333 nm which reports on Ni(II) binding to InrS was monitored. C. Analogous experiments to those described in 'B' were carried out at final [EGTA] = 50 μM (black line), 200 μM (green line) and 400 μM (red line). These competitions were allowed to come to equilibrium for 20 h before recording the spectrum and equilibrium A_{333 nm} value. D. NiCl₂ was incubated for 10 min with various excess concentrations of EGTA before addition to a solution of InrS His21→Glu (20 μM). The concentration of NiCl₂ upon addition of the EGTA-Ni(II) mix was 4.85 μM in each experiment and the concentration of EGTA 40 μM (black line, 2 replicates) and 200 μM (green line). E. Analogous experiments to those described in 'D' were carried out at final [EGTA] = 50 μM (black line), 70 μM (green line) and 130 μM (red line). These competitions were allowed to come to equilibrium for 20 h before recording the spectrum and equilibrium A_{333 nm} value. The equilibrium A_{333 nm} values for these experiments were used with the extinction coefficients of Ni(II)-InrS His 21 variants at A_{333 nm} (Table 4.3) to determine the equilibrium concentration of Ni(II)-InrS His21 variants and the Ni(II) affinity of the InrS His21 variants was determined as described in Section 4.2.1. The A_{333 nm} values of InrS His21→Leu, Cys and Glu from competition with 100 μM EGTA (Figure 4.25 and Appendix Figure C4) were also used in these calculations. Ni(II) affinities were found to be InrS His21→Leu $K_{D, Ni(II)} = 6.73(\pm 5.0) \times 10^{-11}$ M, InrS His21→Cys $K_{D, Ni(II)} = 1.10(\pm 0.97) \times 10^{-11}$ M, InrS His21→Glu $K_{D, Ni(II)} = 2.65(\pm 2.5) \times 10^{-11}$ M.



Appendix D

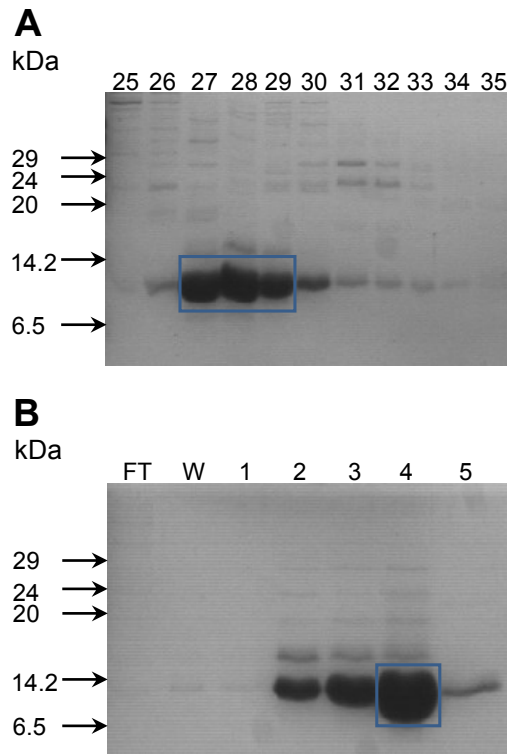


Figure D1. Purification of recombinant InrS Cys53→Ala. A. SDS-PAGE analysis of fractions eluted from a Superdex S75 column loaded with 2 ml of peak fraction from the nickel affinity step. Fractions are 5 ml in volume. B. SDS-PAGE analysis of fractions eluted from a heparin affinity column loaded with pooled fractions 27-29 from the size exclusion step ('A'). FT and W contain the flowthrough and wash (with 10 column volumes of buffer B) respectively. Fractions 1-4 contain lag and peak elution fractions upon increasing NaCl concentration in buffer B. Fraction 4 is the peak elution fraction for buffer B with 0.8 M NaCl. Fraction 5 is a 10 column volume wash with buffer B containing 1 M NaCl. The boxed bands represent protein taken to the next purification step or used in experiments.

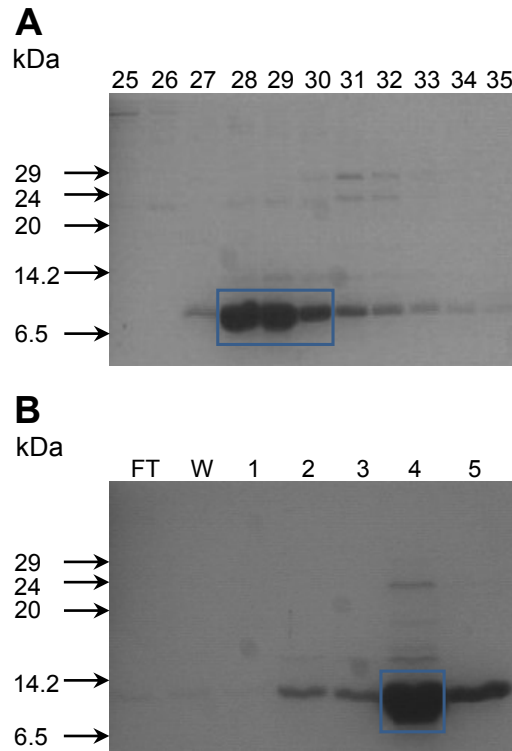


Figure D2. Purification of recombinant InrS Cys82→Ala. A. SDS-PAGE analysis of fractions eluted from a Superdex S75 column loaded with 2 ml of peak fraction from the nickel affinity step. Fractions are 5 ml in volume. B. SDS-PAGE analysis of fractions eluted from a heparin affinity column loaded with pooled fractions 28-30 from the size exclusion step ('A'). FT and W contain the flowthrough and wash (with 10 column volumes of buffer B) respectively. Fractions 1-4 contain lag and peak elution fractions upon increasing NaCl concentration in buffer B. Fraction 4 is the peak elution fraction for buffer B with 0.8 M NaCl. Fraction 5 is a 10 column volume wash with buffer B containing 1 M NaCl. The boxed bands represent protein taken to the next purification step or used in experiments.

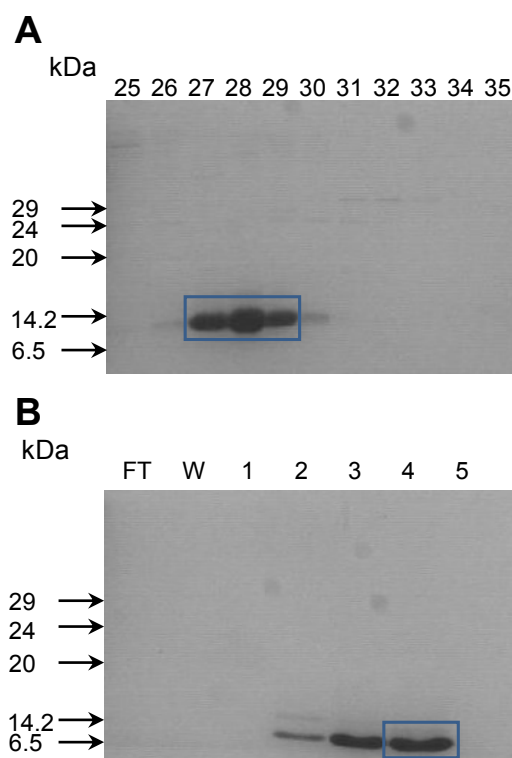


Figure D3. Purification of recombinant InrS His78→Leu. A. SDS-PAGE analysis of fractions eluted from a Superdex S75 column loaded with 2 ml of peak fraction from the nickel affinity step. Fractions are 5 ml in volume. B. SDS-PAGE analysis of fractions eluted from a heparin affinity column loaded with pooled fractions 27-29 from the size exclusion step ('A'). FT and W contain the flowthrough and wash (with 10 column volumes of buffer B) respectively. Fractions 1-4 contain lag and peak elution fractions upon increasing NaCl concentration in buffer B. Fraction 4 is the peak elution fraction for buffer B with 0.8 M NaCl. Fraction 5 is a 10 column volume wash with buffer B containing 1 M NaCl. The boxed bands represent protein taken to the next purification step or used in experiments.

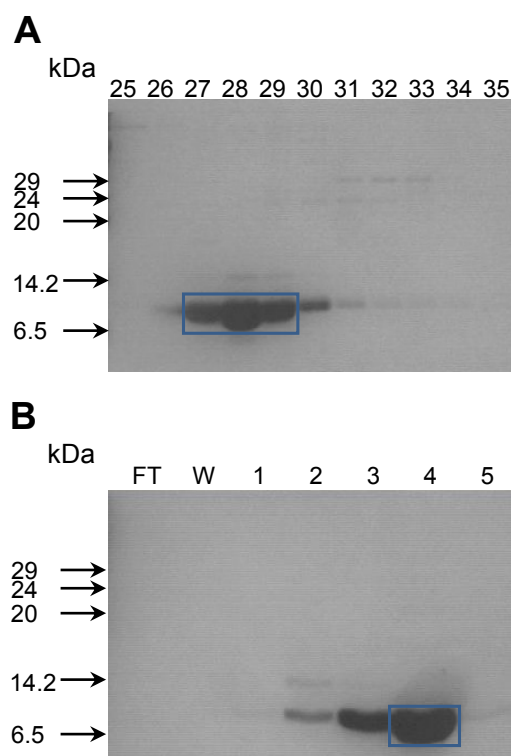


Figure D4. Purification of recombinant InrS His21→Leu. A. SDS-PAGE analysis of fractions eluted from a Superdex S75 column loaded with 2 ml of peak fraction from the nickel affinity step. Fractions are 5 ml in volume. B. SDS-PAGE analysis of fractions eluted from a heparin affinity column loaded with pooled fractions 27-29 from the size exclusion step ('A'). FT and W contain the flowthrough and wash (with 10 column volumes of buffer B) respectively. Fractions 1-4 contain lag and peak elution fractions upon increasing NaCl concentration in buffer B. Fraction 4 is the peak elution fraction for buffer B with 0.8 M NaCl. Fraction 5 is a 10 column volume wash with buffer B containing 1 M NaCl. The boxed bands represent protein taken to the next purification step or used in experiments.

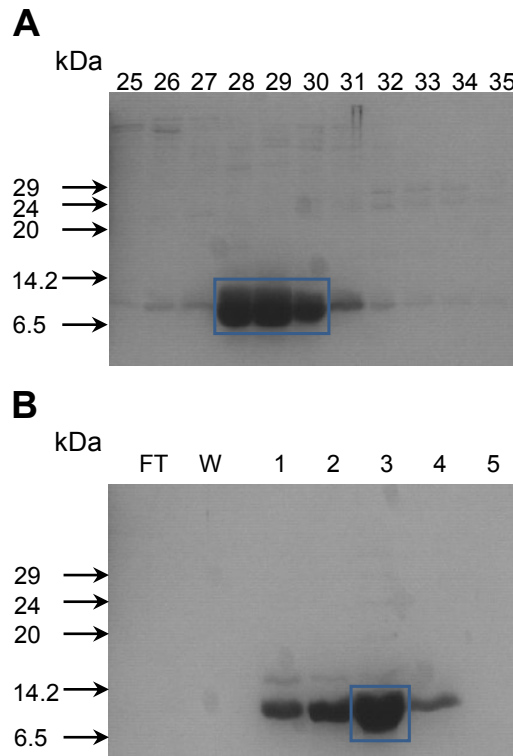


Figure D5. Purification of recombinant InrS His21→Cys. A. SDS-PAGE analysis of fractions eluted from a Superdex S75 column loaded with 2 ml of peak fraction from the nickel affinity step. Fractions are 5 ml in volume. B. SDS-PAGE analysis of fractions eluted from a heparin affinity column loaded with pooled fractions 27-29 from the size exclusion step ('A'). FT and W contain the flowthrough and wash (with 10 column volumes of buffer B) respectively. Fractions 1-4 contain lag and peak elution fractions upon increasing NaCl concentration in buffer B. Fraction 4 is the peak elution fraction for buffer B with 0.8 M NaCl. Fraction 5 is a 10 column volume wash with buffer B containing 1 M NaCl. The boxed bands represent protein taken to the next purification step or used in experiments.

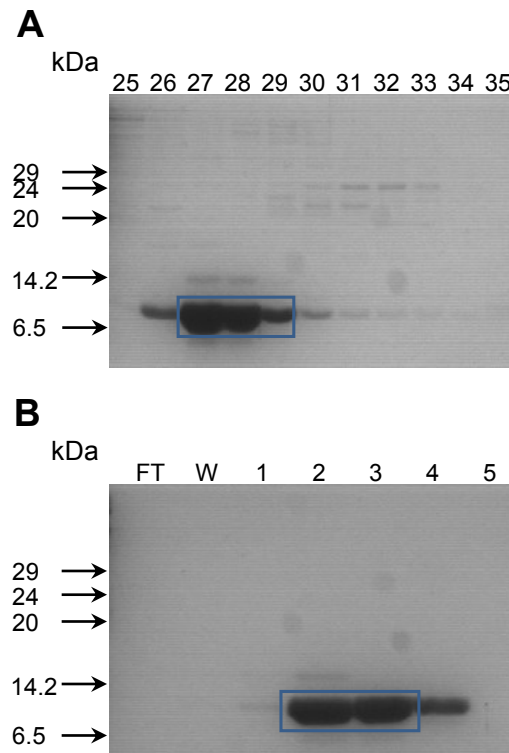


Figure D6. Purification of recombinant InrS His21→Glu. A. SDS-PAGE analysis of fractions eluted from a Superdex S75 column loaded with 2 ml of peak fraction from the nickel affinity step. Fractions are 5 ml in volume. B. SDS-PAGE analysis of fractions eluted from a heparin affinity column loaded with pooled fractions 27-29 from the size exclusion step ('A'). FT and W contain the flowthrough and wash (with 10 column volumes of buffer B) respectively. Fractions 1-4 contain lag and peak elution fractions upon increasing NaCl concentration in buffer B. Fraction 2 is the peak elution fraction for buffer B with 0.5 M NaCl and fraction 3 is the lag elution fraction for buffer B containing 800 mM NaCl ([NaCl] = 500-800 mM). Fraction 5 is a 10 column volume wash with buffer B containing 1 M NaCl. The boxed bands represent protein taken to the next purification step or used in experiments.

Appendix E

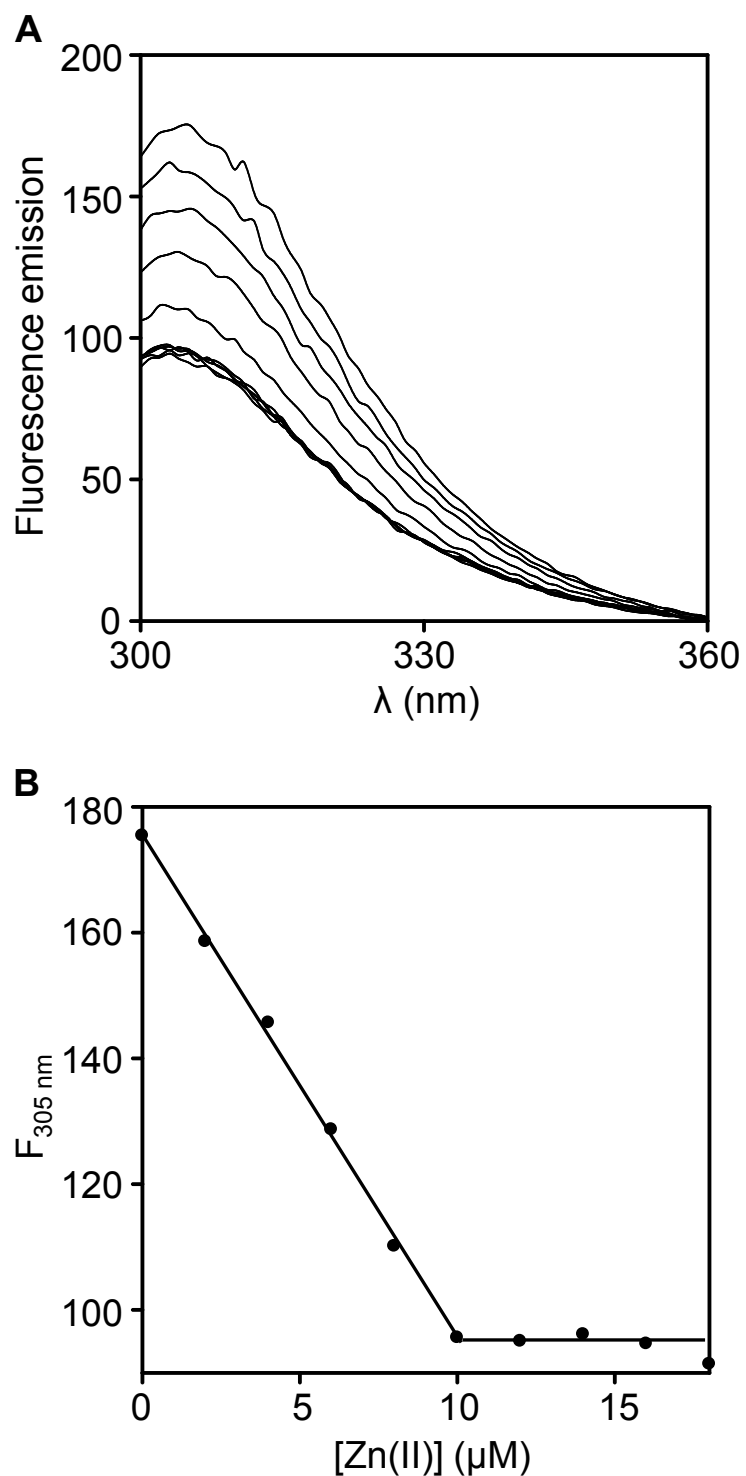


Figure E1. Zur intrinsic fluorescence quenching upon Zn(II) binding. A. Fluorescence emission spectra of Zur (10 μM) upon excitation at 280 nm following titration with ZnSO_4 . B. Binding isotherm depicting the decrease of fluorescence emission feature at 305 nm observed in 'A'.

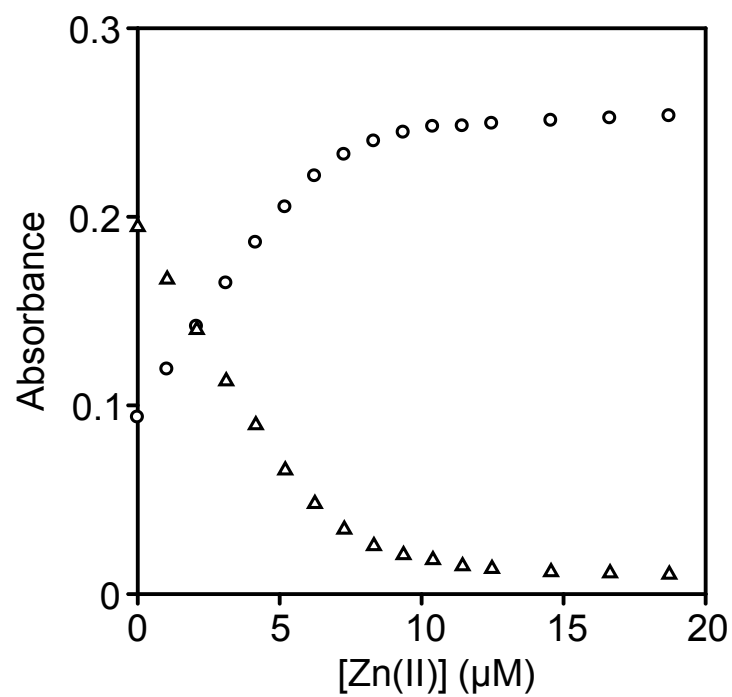


Figure E2. 1:1 Zn(II) binding stoichiometry of mag-fura-2. Binding isotherms of mag-fura-2 (8.8 μM) spectral features at 325 nm (circles) and 366 nm (triangles) upon titration with ZnSO₄. Experiment conducted at pH 7.8.

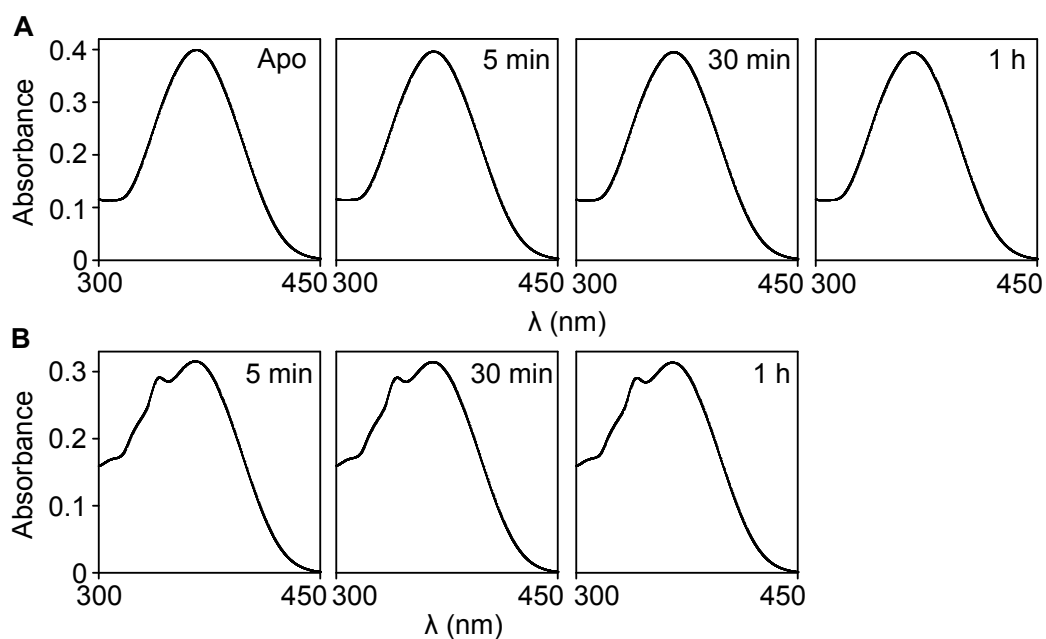


Figure E3. Zn(II) partitioning between InrS and mag-fura-2 reaches equilibrium within 5 min of Zn(II) addition. A. ZnSO₄ (5.2 μM) was added to a solution of InrS (10 μM) and mag-fura-2 (18 μM) and the UV-Vis spectra recorded before addition and 5, 30 and 60 min post-addition. B. A further 10.4 μM ZnSO₄ was added to the solution described in ‘A’ and the spectra recorded at the same time intervals. The spectra 5 min post Zn(II) addition can be overlaid with the spectra recorded at later time points for binding events to both the tight (‘A’) and weak (‘B’) zinc binding sites on InrS. Experiment conducted at pH 7.8.

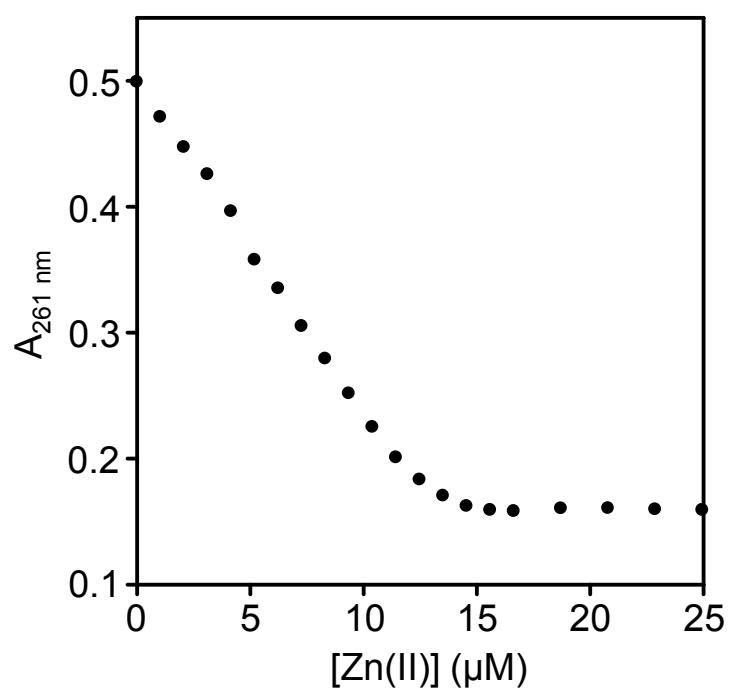


Figure E4. 1:1 Zn(II) binding stoichiometry of quin-2. Binding isotherm of quin-2 (13.5 μM) spectral feature at 261 nm upon titration with ZnSO₄. Experiment conducted at pH 7.8.

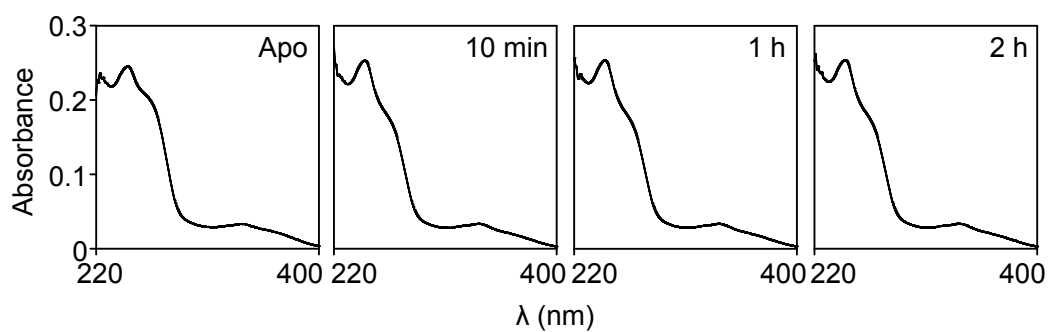


Figure E5. Zn(II) partitioning between InrS and quin-2 reaches equilibrium within 10 min of Zn(II) addition. ZnSO₄ (3.12 μ M) was added to a solution of InrS (20 μ M) and quin-2 (5.54 μ M) and the spectra recorded before addition and 10, 60 and 120 min post-addition. The spectrum 10 min post zinc addition can be overlaid with the spectra recorded at later time points. Experiment conducted at pH 7.8.

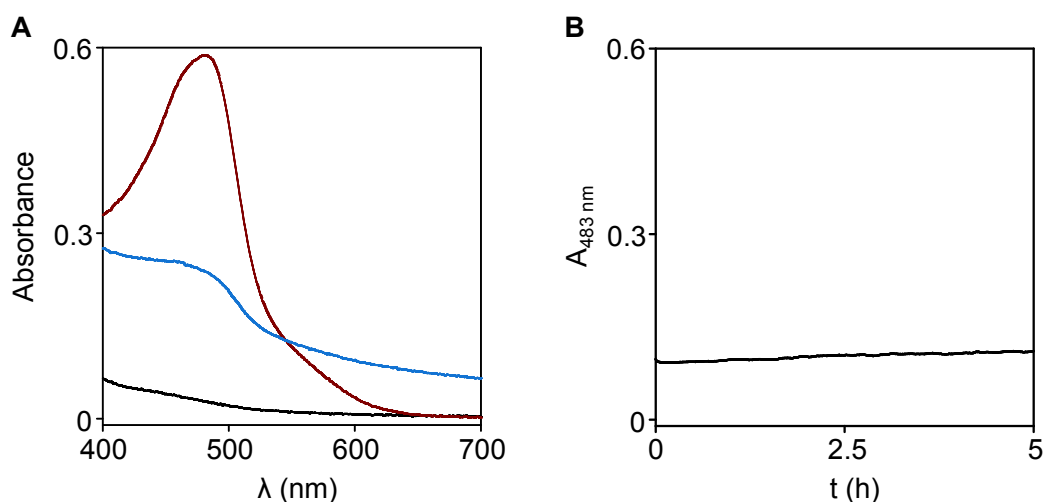


Figure E6. Cu(I) partitioning between InrS and BCS reaches equilibrium rapidly.

A. The absorbance spectrum of BCS (17.5 μM) was recorded (black line) before the addition of CuCl (4 μM) (verified as >95 % Cu^+) (red line) followed by the addition of InrS (10 μM) (blue line). All spectra were recorded immediately following addition and mixing. Some precipitation was visible upon addition of InrS, evident as non-specific light scatter at $A_{700 \text{ nm}}$. The decrease in absorbance at 483 nm shows Cu(I) has transferred rapidly from BCS to InrS, the transfer appears to be ~50 % although this is likely to be an underestimation due to non-specific light scatter. B. CuCl (verified as >95 % Cu^+) was added to a solution of InrS and BCS (all concentrations as in 'A') and the absorbance at 483 nm was monitored. Negligible change in $A_{483 \text{ nm}}$ is observed over 5 h. These data show that Cu(I) bound to BCS can rapidly partition to InrS and that the final equilibrium position of competition between InrS and BCS for Cu(I) is rapidly established when Cu(I) is added to a solution of both molecules.

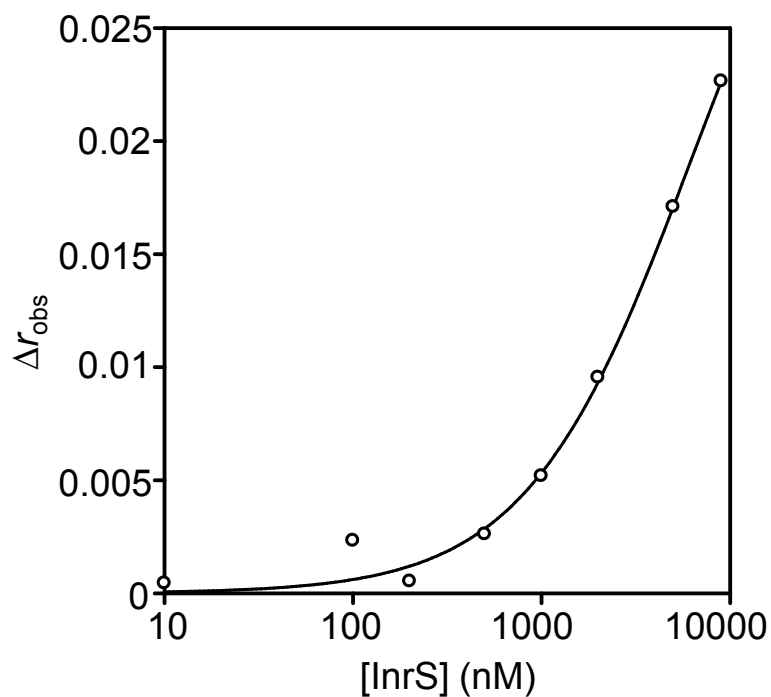


Figure E7. Titration of fluorescently labelled *nrsD*ProFA with Zn(II) loaded InrS. InrS was incubated with a 1.2 molar excess of ZnSO₄ then used to titrate *nrsD*ProFA. 10 μ M ZnSO₄ was added to the buffer to ensure the metal binding sites were saturated. Titration performed anaerobically at pH 7.